INFORMATION TO USERS

This manuscript has been reproduced from the microfilm master. UMI films the text directly from the original or copy submitted. Thus, some thesis and dissertation copies are in typewriter face, while others may be from any type of computer printer.

The quality of this reproduction is dependent upon the quality of the copy submitted. Broken or indistinct print, colored or poor quality illustrations and photographs, print bleedthrough, substandard margins, and improper alignment can adversely affect reproduction.

In the unlikely event that the author did not send UMI a complete manuscript and there are missing pages, these will be noted. Also, if unauthorized copyright material had to be removed, a note will indicate the deletion.

Oversize materials (e.g., maps, drawings, charts) are reproduced by sectioning the original, beginning at the upper left-hand corner and continuing from left to right in equal sections with small overlaps. Each original is also photographed in one exposure and is included in reduced form at the back of the book.

Photographs included in the original manuscript have been reproduced xerographically in this copy. Higher quality 6" x 9" black and white photographic prints are available for any photographs or illustrations appearing in this copy for an additional charge. Contact UMI directly to order.

UMI

A Bell & Howell Information Company
300 North Zeeb Road, Ann Arbor MI 48106-1346 USA
313/761-4700 800/521-0600

BARYON NUMBER AND INDIVIDUAL LEPTON NUMBER VIOLATION IN SUPERSYMMETRIC SO(10) GRAND UNIFICATION THEORIES

DISSERTATION

Presented in Partial Fulfillment of the Requirements for

the Degree Doctor of Philosophy in the

Graduate School of The Ohio State University

By

Vincent Alfred Lucas, B.S.

* * * * *

The Ohio State University

1997

Dissertation Committee:

Dr. Stuart Raby, Adviser

Dr. Richard Kass

Dr. Junko Shigemitsu

Dr. Alan van Heuvelen

Approved by

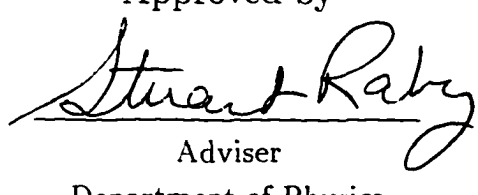

Adviser

Department of Physics

UMI Number: 9801738

UMI Microform 9801738
Copyright 1997, by UMI Company. All rights reserved.

This microform edition is protected against unauthorized
copying under Title 17, United States Code.

UMI
300 North Zeeb Road
Ann Arbor, MI 48103

ABSTRACT

Baryon and individual lepton number violation are studied in the context of several SO(10) supersymmetric [SUSY] grand unification theories [GUTs] that successfully fit experimental fermion mass and mixing angle data. We show that when predictions for proton decay (a test of baryon number conservation) and one-loop GUT scale threshold corrections to gauge couplings are considered together, they form a significant constraint on the GUT symmetry-breaking sector of the theory. We then construct a model with a GUT symmetry-breaking sector consistent with this constraint. We explicitly calculate baryon number-violating nucleon decay in this model and show that the results are consistent with experimental bounds. We find that the branching ratios obtained from this realistic SO(10) SUSY GUT differ significantly from the predictions obtained from "generic" SU(5) SUSY GUTS. Thus nucleon decay branching ratios, when observed, can be used to test theories of fermion masses.

We then calculate individual lepton number-violating processes in this model. Individual lepton number violation occurs as the result of non-universality in the SUSY breaking terms at the GUT scale. This non-universality is induced, in part, as the result of renormalization group running between the Planck and GUT scales. We additionally find, however, that non-universality may be induced in the SUSY breaking trilinear parameters purely as the result of the renormalization group boundary conditions at the GUT scale. For our model, the non-universality resulting from

renormalization group boundary conditions allows a partial cancellation that would not otherwise occur between terms in the formulas for rates of individual lepton number violation. As a result, rates of individual lepton number violation are smaller in certain regions of parameter space than they otherwise would be. We find that rates of individual lepton number violation consistent with experiment can be obtained with an electron sneutrino mass as low as 800 GeV.

ACKNOWLEDGMENTS

I would like to express my deep gratitude to Dr. Stuart Raby for his guidance in my research at Ohio State. His ideas for research and suggestions for improvements have been a tremendous help in the creation of this work. Without his collaboration, this thesis would not have been possible.

I would also like to thank Dr. Tomáš Blažek for sharing with me the results of his global χ^2 analysis of the models discussed in this thesis, while his work was still in its preliminary stages; and for many useful discussions on the subject of supersymmetry.

VITA

September 9, 1971	Born – Euclid, Ohio
1992	Teaching associate
December, 1992	B.S. Mathematics and physics, Ohio State University
1993	Departmental fellowship
1994	Graduate teaching associate
1994-6	Graduate research associate

PUBLICATIONS

Research Publications

V. Lucas and S. Raby, "GUT Scale Threshold Corrections in a Complete Supersymmetric SO(10) Model: $\alpha_s(M_Z)$ Versus Proton Lifetime". *Phys. Rev.* **D54** 2261 (1996)

V. Lucas and S. Raby, "Nucleon Decay in a Realistic SO(10) SUSY GUT", *Phys. Rev.* **D55** 6986 (1997)

FIELDS OF STUDY

Major Field: Physics

TABLE OF CONTENTS

Page

Abstract ii

Acknowledgments iv

Vita v

List of Tables x

List of Figures xiii

Chapters:

1. Introduction 1

2. Review of the ADHRS effective operator search 6

   2.1 Grand Unification and Supersymmetry 6
   2.2 SO(10) 9
   2.3 Effective fermion mass generating operators and the hierarchy of fermion masses 11
   2.4 Summary of ADHRS 12
   2.5 Questions not answered by ADHRS 16

3. Construction of the model 21

   3.1 Introduction 21
   3.2 One loop threshold corrections at M_G. 25
      3.2.1 Formula for ϵ_3 in a general SO(10) theory 26
      3.2.2 The dependence of ϵ_3 on the Higgs sector 28
      3.2.3 An Example : ϵ_3 in the Hall-Raby model 30

3.3 A complete SO(10) SUSY GUT 31
3.3.1 The GUT symmetry breaking and Higgs sectors 31
3.3.2 Fermion mass sector 35
3.3.3 Symmetries 38
3.4 Upper bound for $\tilde{M}_t$ in model 4(c) based on naturalness 39
3.5 Conclusions for Chapter 3 40
3.6 Proof of equation 3.8 41
3.7 U(1) symmetries and the dependence of ϵ_3 on GUT scale vevs . . . 43

4. Calculation of rates of baryon number violating nucleon decay 49

4.1 The low energy effective operators generating nucleon decay, and their renormalization 51
4.2 Nucleon decay formulas 53
4.2.1 Gluino diagrams 53
4.2.2 Chargino diagrams 56
4.2.3 Neutralino contribution 58
4.3 Numerical procedure and results 58
4.4 Discussion of the results 63
4.4.1 Overall Rates 63
4.4.2 LLRR vs. LLLL Operators 77
4.4.3 $p \to \pi^+\overline{\nu}$ vs. $p \to K^+\overline{\nu}$ 81
4.4.4 "Generic" SU(5) vs Large tan β SO(10) models 82
4.4.5 Sensitivity to "22" Clebsch 84
4.4.6 Gluino vs. Chargino contributions 85
4.4.7 Proton decay from gauge boson exchange 85
4.5 Conclusions for Chapter 4 86
4.6 Why $|V_{td}|$ increases when the $\mathcal{O}_{13}$ is included in model 4(c) 88

5. Individual lepton number violation 91

5.1 Introduction 91
5.2 Model 4(c), RG running above the GUT scale, and boundary conditions at the GUT scale 97
5.2.1 Model 4(c) 97
5.2.2 Renormalization group equation running above the GUT scale 105
5.2.3 GUT scale RGE boundary conditions 107
5.2.4 Non-universality assumptions for m_{H_u} and m_{H_d} coming from D-term splittings and radiative electroweak symmetry breaking requirements 115
5.3 Formulas for $e_j \to e_i\gamma$ and the electron and muon dipole moments in terms of low energy parameters 118

5.4 Numerical procedure 121
5.5 Results 125
5.5.1 $Br(\mu \to e\gamma)$ vs. $m_{\tilde{\nu}_e}$, $m_{1/2}(M_{GUT})$, μ, and A_τ 125
5.5.2 Dependence on ζ_1, ζ_2, λ_{N_1}, and λ_{N_2} 131
5.5.3 Dependence on γ 144
5.5.4 Branching ratios for $\tau \to e\gamma$, $\tau \to \mu\gamma$, and the electron and muon dipole moments 147
5.5.5 Affect of non-universality of GUT scale boundary conditions for A_B 149
5.6 Conclusions for Chapter 5 153

Appendices:

A. Review of the MSSM 158

A.1 Particle content 158
A.2 Lagrangian 158
A.3 Electroweak symmetry breaking 161
A.4 Mass terms 162
A.4.1 Chargino, neutralino masses 162
A.4.2 Squark and slepton masses 163

B. Feynman vertices 165

C. Review of SO(10) 169

C.1 The fundamental representation 170
C.2 SU(5)×U(1) subgroup of SO(10) 171
C.3 45 and 54 representations 173
C.4 The spinor representation 176
C.5 Clifford algebras 180

D. Formulas for nucleon decay in terms of chiral Lagrangian factors 186

E. Mass matrices and effective determinants for model 4(c) 188

F. Renormalization group equations between the Planck and GUT scales . . 191

G. Planck scale renormalization group boundary conditions for the scalar masses 199

Bibliography 201

LIST OF TABLES

Table		Page
3.1	Notation used for states in different charge sectors	27
3.2	U(1) and R charges of the new model	34
4.1	y Clebsches for each version of model 4	52
4.2	u Clebsches for models 4(a) through (c)	52
4.3	Table of all gluino-dressed four fermion operators relevant to nucleon decay	55
4.4	Partial mean lifetime for proton decaying into kaon plus anti-neutrino and ratios of the rates of proton decay into various decay products versus rate of decay into kaon plus anti-neutrino for various values of the GUT scale parameters, when the $\mathcal{O}_{13}$ operator is included.	64
4.5	Partial mean lifetime for neutron decaying into kaon plus anti-neutrino and ratios of the rates of proton decay into various decay products versus rate of decay into kaon plus anti-neutrino for various values of the GUT scale parameters, when the $\mathcal{O}_{13}$ operator is included.	64
4.6	Ratios of the rate of proton decay that would occur if chargino diagrams contributed only versus total proton decay rate for the three most dominant decay modes, for various values of the GUT scale parameters, when the $\mathcal{O}_{13}$ operator is included.	65
4.7	Ratios of the rate of neutron decay that would occur if chargino diagrams contributed only versus total neutron decay rate, for various values of the GUT scale parameters, when the $\mathcal{O}_{13}$ operator is included.	65

4.8 Ratios of the rate of proton decay that would occur if gluino diagrams contributed only versus total proton decay rate for the three most dominant decay modes, for various values of the GUT scale parameters, when the $\mathcal{O}_{13}$ operator is included. 66

4.9 Ratios of the rate of neutron decay that would occur if gluino diagrams contributed only versus total neutron decay rate for various values of the GUT scale parameters, when the $\mathcal{O}_{13}$ operator is included. 66

4.10 Ratios of the rate of proton decay that would occur if LLLL operators contributed only versus the rate of proton decay that would occur if LLRR operators contributed only, for each of the three anti-neutrino generations, for various values of the GUT scale parameters, when the $\mathcal{O}_{13}$ operator is included. 67

4.11 Ratios of partial decay rates for $p \to K^+\overline{\nu}$, which compare the importance of the LLLL and LLRR operators for each generation of anti-neutrino versus contribution of the LLRR operator of the third generation anti-neutrino for various values of the GUT scale parameters, when the $\mathcal{O}_{13}$ operator is included. 67

4.12 Ratios of partial decay rates for $p \to \pi^+\overline{\nu}$, which compare the importance of the LLLL and LLRR operators for each generation of anti-neutrino versus contribution of the LLRR operator of the third generation anti-neutrino for various values of the GUT scale parameters, when the $\mathcal{O}_{13}$ operator is included. 68

4.13 Values of the GUT scale parameters used in Tables 4.4 through 4.12. All dimensions in GeV units. 68

4.14 Partial mean lifetime for proton decaying into kaon plus anti-neutrino and ratios of the rates of proton decay into various decay products versus rate of decay into kaon plus anti-neutrino for various values of the GUT scale parameters, when the $\mathcal{O}_{13}$ operator is not included. For all entries, $\beta = -\alpha$. 69

4.15 Partial mean lifetime for neutron decaying into kaon plus anti-neutrino and ratios of the rates of neutron decay into various decay products versus rate of decay into kaon plus anti-neutrino for various values of the GUT scale parameters, when the $\mathcal{O}_{13}$ operator is not included. For all entries, $\beta = -\alpha$. 70

4.16 Ratios of the rate of proton decay that would occur if chargino diagrams contributed only versus total proton decay rate for the three most dominant decay modes, for various values of the GUT scale parameters, when the $\mathcal{O}_{13}$ operator is not included. 71

4.17 Ratios of the rate of neutron decay that would occur if chargino diagrams contributed only versus total neutron decay rate for various values of the GUT scale parameters, when the $\mathcal{O}_{13}$ operator is not included. 72

4.18 Ratios of the rate of proton decay that would occur if LLLL operators contributed only versus the rate of proton decay that would occur if LLRR operators contributed only, for each of the three anti-neutrino generations, for various values of the GUT scale parameters, when the $\mathcal{O}_{13}$ operator is not included. 73

4.19 Ratios of partial decay rates for $p \to K^+\overline{\nu}$, which compare the importance of the LLLL and LLRR operators for each generation of anti-neutrino versus contribution of the LLRR operator of the third generation anti-neutrino for various values of the GUT scale parameters, when the $\mathcal{O}_{13}$ operator is not included. 74

4.20 Ratios of partial decay rates for $p \to \pi^+\overline{\nu}$, which compare the importance of the LLLL and LLRR operators for each generation of anti-neutrino versus contribution of the LLRR operator of the third generation anti-neutrino for various values of the GUT scale parameters, when the $\mathcal{O}_{13}$ operator is not included. 75

4.21 Values of the GUT scale parameters used in Tables 4.14 through 4.20. All dimensions in GeV units. 76

4.22 Current experimental lower bounds on the various partial lifetimes of the nucleons [2] 77

5.1 Default values used for the parameters. All quantities in GeV units. . 123

A.1 Particle content of the MSSM 159

G.1 Table showing the assignments of matter fields to E(6) representations. 200

LIST OF FIGURES

Figure		Page
3.1	Supergraphs showing baryon number violation mediated by color triplet Higgs exchanges.	24
3.2	Supergraphs representing the generation of effective fermion mass operators $\mathcal{O}_{33}$, $\mathcal{O}_{23}$, $\mathcal{O}_{22}$, and $\mathcal{O}_{12}$ for model 4(c).	36
3.3	Supergraph representing the generation of new effective fermion mass operator $\mathcal{O}_{13}$ for model 4(c).	37
4.1	The one-loop gluino diagrams contributing to $C_{ijkl}^{(ud)(d\nu)[G]}$	55
4.2	Results of the global χ^2 analysis of Blazek, et al. for model 4(c), plotted in the m_0 - $m_{1/2}$ plane for μ = 80 GeV, 160 GeV, and 240 GeV. The solid, double-dashed-dotted, and dotted lines represent contour lines of constant χ^2, with χ^2/d.o.f. = 2,1, and $\frac{1}{2}$, respectively. Points I,II, and III(1,2), at which we present nucleon decay results for model 4(c), are also shown in the figure.	61
4.3	Feynman diagram that gives the dominant contribution to $C_{1jk3}^{(\overline{ud})(d\nu)}$.	79
5.1	One loop chargino Feynman diagram contributing to $e_j \to e_i\gamma$. (Fermions in diagram are Dirac fermions.)	92
5.2	One loop neutralino Feynman diagram contributing to $e_j \to e_i\gamma$. (Fermions in diagram are Dirac fermions.)	93
5.3	Feynman diagrams which will give rise to large mass splittings between the first and second generations of sleptons if the Yukawa couplings at the vertices are $\mathcal{O}(1)$.	101

5.4 Radiatively generated SUSY breaking multilinear terms. All fields in the diagrams are scalars. 105

5.5 Feynman diagrams entering the calculation of the one loop RGEs above the GUT scale. The lines in the wavefunction renormalization diagrams represent superfields. In all other diagrams, solid and dashed lines represent scalar and fermionic fields, respectively. 109

5.6 Feynman diagrams contributing to $\tilde{\mathcal{O}}_{23}$. All fields in the diagrams are scalar fields. 112

5.7 Several Feynman diagrams which are enhanced by large $\tan\beta$. Not all diagrams enhanced by large $\tan\beta$ are shown. 120

5.8 Contour plot of $Br(\mu \to e\gamma)$ in the $m_{\tilde{\nu}_e}$ - $m_{1/2}(M_{GUT})$ plane, with 4 contours per order of magnitude. The gray line shows the experimental upper bound. The gray region denotes a region of parameter space where $m_0 < 700$ GeV. 126

5.9 Contour plot of $Br(\mu \to e\gamma)$ in the $m_{\tilde{\nu}_e}$ - μ plane, with 4 contours per order of magnitude. The gray line shows the experimental upper bound. 127

5.10 Contour plot of $Br(\mu \to e\gamma)$ in the $m_{\tilde{\nu}_e}$ - A_τ plane, with 2 contours per order of magnitude. The gray line shows the experimental upper bound. 127

5.11 Plot of $(\overline{m}_L^2)_{12}(M_Z)/GeV^2$ in the complex plane as $\overline{A}_0$ is varied from -1 TeV to 1 TeV, when $m_{\tilde{\nu}_e} = 1$ TeV. The gray points represent points at which $\overline{A}_0$ is a multiple of 250 GeV. The lower-rightmost point is $\overline{A}_0 = -1$ TeV and the upper-leftmost point is $\overline{A}_0 = 1$ TeV. 131

5.12 Plot of $(\overline{m}_L^2)_{13}(M_Z)/GeV^2$ in the complex plane as $\overline{A}_0$ is varied from -1 TeV to 1 TeV, when $m_{\tilde{\nu}_e} = 1$ TeV. The gray points represent points at which $\overline{A}_0$ is a multiple of 250 GeV. The lower-rightmost point is $\overline{A}_0 = -1$ TeV and the upper-leftmost point is $\overline{A}_0 = 1$ TeV. 132

5.13 Plot of $(\overline{m}_L^2)_{23}(M_Z)/GeV^2$ in the complex plane as $\overline{A}_0$ is varied from -1 TeV to 1 TeV, when $m_{\tilde{\nu}_e} = 1$ TeV. The gray points represent points at which $\overline{A}_0$ is a multiple of 250 GeV. The lower-leftmost point is $\overline{A}_0 = -1$ TeV. 132

5.14 Plot of $1000 M_W^2 [X_{L_j}]_1$ and $1000 M_W^2 [X_{L_j}]_3$ in the complex plane, where M_W is the W boson mass, as $\overline{A}_0$ is varied from -1 TeV to 1 TeV, when $m_{\tilde{\nu}_e}$=1 TeV. The gray points represent points at which $\overline{A}_0$ is a multiple of 250 GeV. The longer line is $[X_{L_j}]_1$ and the shorter is $[X_{L_j}]_3$. The upper-rightmost point of $[X_{L_j}]_1$ is $\overline{A}_0 = -1$ TeV and the lower-leftmost point is $\overline{A}_0 = 1$ TeV. The lower-leftmost point of $[X_{L_j}]_3$ is $\overline{A}_0 = -1$ TeV. 133

5.15 Contour plot of $Br(\mu \to e\gamma)$ in the $A_\tau - \zeta_1$ plane, with 2 contours per order of magnitude. The gray line shows the experimental upper bound. 137

5.16 Contour plot of x_2 in the $A_\tau - \zeta_1$ plane. 138

5.17 Contour plot of x_3 in the $A_\tau - \zeta_1$ plane. 138

5.18 Sketch illustrating the effect changing x_3 has on the X_{L_j}. $[X_{L_j}]_1$ and $[-X_{L_j}]_3$ are sketched in the complex plane. This sketch corresponds to fig. 5.14, except that $[-X_{L_j}]_3$ is sketched instead of $[X_{L_j}]_3$. The distance between two points of equal $\overline{A}_0$ on these two lines represents $|X_{L_j}|$. The dashed line represents the old $[-X_{L_j}]_3$ and the solid line represents the $[-X_{L_j}]_3$ when x_3 is increased. The hash marks and the circles on the $[X_{L_j}]_1$ and the old $[-X_{L_j}]_3$ lines represent points where $\overline{A}_0$ is a multiple of 250 GeV. The crosses represent how those points on $[-X_{L_j}]_3$ change as x_3 is increased. The length of the dashed line extending from $[X_{L_j}]_1$ to the old $[-X_{L_j}]_3$ line represents the old minimum of $|X_{L_j}|$ with respect to $\overline{A}_0$ and the length of the solid line extending from $[X_{L_j}]_1$ to the new $[-X_{L_j}]_3$ represents how that minimum changes as x_3 increases. 139

5.19 Contour plot of $Br(\mu \to e\gamma)$ in the $A_\tau - \zeta_2$ plane, with 2 contours per order of magnitude. The gray line shows the experimental upper bound. 141

5.20 Contour plot of x_2 in the $A_\tau - \zeta_2$ plane. 142

5.21 Contour plot of x_3 in the $A_\tau - \zeta_2$ plane. 142

5.22 Sketch illustrating the effect changing x_2 has on the X_{L_j}. $[X_{L_j}]_1$ and $[-X_{L_j}]_3$ are sketched in the complex plane for various values of x_2. The distance between two points of equal $\overline{A}_0$ on these two lines represents $|X_{L_j}|$. The hash marks and the circles on the $[X_{L_j}]_1$ and the $[-X_{L_j}]_3$ lines represent points where $\overline{A}_0$ is a multiple of 250 GeV. The length of the dashed lines extending from $[X_{L_j}]_1$ to the $[-X_{L_j}]_3$ line represents the minimum of $|X_{L_j}|$ with respect to $\overline{A}_0$ for various values of x_2. . . 143

5.23 Contour plot of $Br(\mu \to e\gamma)$ in the A_τ - λ plane, with 5 contours per order of magnitude, where $\lambda = \lambda_{N_1} = \lambda_{N_2}$. The gray line shows the experimental upper bound. 145

5.24 Contour plot of x_2 in the A_τ - λ plane, where $\lambda = \lambda_{N_1} = \lambda_{N_2}$. 145

5.25 Contour plot of x_3 in the A_τ - λ plane, where $\lambda = \lambda_{N_1} = \lambda_{N_2}$ 146

5.26 Contour plot of $Br(\mu \to e\gamma)$ in the A_τ - γ plane, with 2 contours per order of magnitude. The gray line shows the experimental upper bound. ($m_{\tilde{\nu}_e}$=1 TeV.) 147

5.27 Contour plot of $Br(\mu \to e\gamma)$ in the A_τ - γ plane, with 2 contours per order of magnitude and $m_{\tilde{\nu}_e} = 3$ TeV. The gray line shows the experimental upper bound. 148

5.28 Plot of γ versus the relative mass splittings of $m^2_{16_2}$, $m^2_{16_1}$, and $m^2_{\psi_1}$ with respect to $m^2_{16_1}$ at M_{GUT}, with $m_{\tilde{\nu}_e}$=3 TeV. The upper, middle, and bottom lines represent $[m^2_{\psi_1} - m^2_{16_1}]/m^2_{16_1}$, $[m^2_{16_2} - m^2_{16_1}]/m^2_{16_1}$, and $[m^2_{16_3} - m^2_{16_1}]/m^2_{16_1}$, respectively. The thickness in the lines represents how much the relative mass splitting varies as A_τ is varied from -200 GeV to 200 GeV. The mass splitting for $m^2_{\psi_2}$ is not shown because $m^2_{\psi_2} \approx m^2_{\psi_1}$. 148

5.29 Contour plot of $Br(\tau \to e\gamma)$ in the $m_{\tilde{\nu}_e}$ - $m_{1/2}(M_{GUT})$ plane, with 2 contours per order of magnitude. The gray region denotes a region of parameter space where $m_0 < 700$ GeV. 149

5.30 Contour plot of $Br(\tau \to \mu\gamma)$ in the $m_{\tilde{\nu}_e}$ - $m_{1/2}(M_{GUT})$ plane, with 2 contours per order of magnitude. The gray region denotes a region of parameter space where $m_0 < 700$ GeV. 150

5.31 Contour plot of $d_e/(e \text{ cm})$ in the $m_{\tilde{\nu}_e}$ - $m_{1/2}(M_{GUT})$ plane, with 2 contours per order of magnitude. The gray region denotes a region of parameter space where $m_0 < 700$ GeV. 150

5.32 Contour plot of $d_\mu/(e \text{ cm})$ in the $m_{\tilde{\nu}_e}$ - $m_{1/2}(M_{GUT})$ plane, with 2 contours per order of magnitude. The gray region denotes a region of parameter space where $m_0 < 700$ GeV. 151

5.33 Contour plot of $Br(\mu \to e\gamma)$ in the $m_{\tilde{\nu}_e}$ - $m_{1/2}(M_{GUT})$ plane, using the (incorrect) universal GUT scale boundary condition eqn. (5.50), with 4 contours per order of magnitude. The gray line shows the experimental upper bound. The gray region denotes a region of parameter space where $m_0 < 700$ GeV. 152

5.34 Contour plot of $Br(\mu \to e\gamma)$ in the $m_{\tilde{\nu}_e}$ - A_τ plane, using the (incorrect) universal GUT scale boundary condition eqn. (5.50), with 2 contours per order of magnitude. 153

B.1 Feynman vertices relevant to calculations of baryon number and individual lepton number violating processes. 165

C.1 Feynman diagram contributing to the wavefunction renormalization for ψ_1. 184

C.2 Feynman diagram contributing to the wavefunction renormalization for 10_1. 185

CHAPTER 1

INTRODUCTION

For nearly three decades, the Standard Model [SM] [1] has stood as a remarkable success, withstanding thousands of experimental tests. However, the Standard Model does not include gravity, and therefore, there must be physics beyond the Standard Model. In addition to gravity, one of the most compelling clues for physics beyond the Standard Model is the observed hierarchy of fermion masses and mixing angles. For all fermions in the same representation of the Standard Model gauge group, the mass of the third generation fermion is much greater than the mass of the second which is much greater than the mass of the first. [2] The Kobayashi-Maskawa [KM] matrix elements V_{KM} exhibit a similar hierarchy. Namely, $|(V_{KM})_{us}| >> |(V_{KM})_{cb}| >> |(V_{KM})_{td}|$. [2] Yet, according to the Standard Model, this observed pattern in the fermion masses and mixing angles is a pure coincidence. The Standard Model contains 13 independent parameters in the fermionic sector: 9 fermion masses and 4 independent KM matrix parameters. According to the Standard Model, these 13 independent parameters, by accident, happen to be arranged so that there is the observed hierarchy in the fermion masses and mixing angles. It seems rather unlikely that the observed orderly, hierarchical pattern of fermion masses

and mixing angles could be a sheer accident, as the Standard Model suggests. Accordingly, numerous theorists have searched for a theory more fundamental than the Standard Model which would be able to explain this Standard Model "coincidence."

In addition to gravity and the fermion mass hierarchy, there are a variety of other questions that theorists hope that a more fundamental theory would be able to answer. For example, why is electric charge quantized? Why are there three gauge couplings and three generations of fermions? Why do the gauge couplings have the relative strengths that they do? Why are fermions assigned into the SM gauge group representations that they are assigned? How is it possible that the Higgs mass can be of order the electroweak scale when the natural scale for the Higgs mass should be the Planck scale, due to radiative corrections to the Higgs mass?

In the mid-seventies, Georgi and Glashow made a major advance towards the formulation of a theory that could answer some of these questions by showing how the three gauge couplings of the Standard Model could be related to each other in terms of one gauge coupling of a more fundamental theory. [3] In their model, the SU(3) $\times$ SU(2) $\times$ U(1) gauge group of the Standard Model is the low energy remnant of a more fundamental, unified gauge group, SU(5). The SU(5) gauge group is spontaneously broken at very high energies ($\approx 10^{14}$ GeV), down to the Standard Model gauge group. The three gauge couplings of the Standard Model are thus functions of the unified gauge coupling and the scale at which the unified gauge group is broken. [4] These relations can be inverted to obtain a prediction for the strong coupling constant g_3 in terms of the electroweak coupling constants g_1 and g_2. This prediction is consistent with what the experimental measurements for g_1, g_2, and g_3 were at that time. The model has the additional features that it (1) explains the

quantization of electric charge, (2) explains how fermions are assigned the Standard Model gauge group representations they are assigned and why only certain gauge group representations appear in the Standard Model but not others, and (3) relates the masses of the down-type quarks to the masses of the leptons. Because of these very attractive features, Georgi and Glashow's idea of using a simple Lie group gauge symmetry to unify the three gauge couplings of the Standard Model has been the subject of much theoretical work towards models of physics beyond the Standard Model.

However, the results of experimental searches for violations of conservation laws of the Standard Model provide very tight constraints on any theory of physics beyond the Standard Model. The conservation laws of the Standard Model have been tested in numerous experiments in the hopes of finding physics beyond the Standard Model, but, so far, no violation of any Standard Model conservation law has been found. This is a potential problem for Grand Unification Theories [GUTs] because baryon number and lepton number are conserved in the Standard Model but are not conserved in GUTs. [5] Furthermore, individual lepton number (i.e., electron, muon, and tau lepton number) are conserved in the Standard Model but are generally not conserved in supersymmetric [SUSY] GUTs. [6, 7, 8] Experimental bounds on processes predicted to occur in SUSY GUTs which violate these conservation laws are extremely tight. For example, the partial lifetime of the proton decaying into a kaon plus antineutrino (a test of baryon and lepton number violation), one of the most dominant proton decay modes in SUSY GUTs, is experimentally constrained to be greater than 10^{32} years — roughly 10^{22} times the age of the universe. [2] Similarly, experimental tests for $\mu \rightarrow e\gamma$, a test of electron and muon number violation, show

that if $\mu \rightarrow e\gamma$ occurs at all, it must occur at a rate of less than once in 20 billion muon decays. [2]

In this thesis, baryon and individual lepton number non-conservation are studied in the context of several phenomenologically successful SO(10) SUSY GUTs. In particular, the models that baryon and individual lepton number violation will be explored in are extensions of the SO(10) effective operator models of Anderson et al. [9] (ADHRS). These models have the features that:

1. They are predictive theories for fermion masses and mixing angles: All the parameters in the fermionic sector of the Standard Model are explained in terms of just seven fundamental parameters.

2. They are "natural" in the sense that (a) There are no couplings that are inexplicably small in comparison to the other couplings in the theory. In particular, the hierarchy of fermion masses is explained in terms of ratios of several vacuum expectation values. (b) There is no fine tuning of the parameters. (c) There are no superpotential terms consistent with the symmetries of the theory which were inexplicably not included in the theory.

3. The models are in excellent agreement with the low energy experimental data.

In Chapter 2, we review the effective operator models of ADHRS, discussing the assumptions, motivations for, and theoretical underpinnings of the ADHRS effective operator search. In Chapter 3, we discuss how to extend the effective operator models of ADHRS, which are effective theories valid only up to the scale of Grand Unification, to more complete theories, valid up to the Planck or string scale. This is necessary because, as will be discussed later, it is necessary to extend the ADHRS theories to

theories valid up to around the Planck or string scales in order to calculate rates of baryon and individual lepton number violating processes. As we will see, there is an intimate connection between the rates of proton decay and the form of SO(10) breaking sector of the superpotential in any SO(10) SUSY GUT meeting the naturalness requirements specified above, which is sufficient to rule out numerous candidate models. In Chapter 4, the rates of various baryon number violating nucleon decay processes are calculated and compared with experiment for the models constructed in Chapter 3. In Chapter 5, individual lepton number violation is studied in the context of model 4(c) of Chapter 3. In Chapters 4 and 5, we also compare our results with results for other SUSY GUTs explored by other authors, and, where possible, extend our results to more general conclusions applicable to other models than those constructed in this thesis.

CHAPTER 2

REVIEW OF THE ADHRS EFFECTIVE OPERATOR SEARCH

At its heart, ADHRS relies on SO(10) grand unification, supersymmetry, and effective operators — all of which are important tools in modern model building of physics beyond the Standard Model. We therefore begin our review of ADHRS by motivating each of these ingredients.

2.1 Grand Unification and Supersymmetry

The virtues of Grand Unification have already been discussed. In summary, Grand Unification

1. reduces the number of fundamental parameters in the theory by one by relating the strong coupling constant g_3 to the electroweak coupling constants g_1 and g_2;

2. explains the quantization of electric charge;

3. explains the assignment of quarks and leptons to their respective Standard Model gauge group representations; and

4. relates the masses of the down-type quarks to the masses of the charged leptons. hence providing a starting point for work on a theory of fermion masses.

However, experimental measurements for the Standard Model gauge coupling constants have improved considerably since Georgi and Glashow's original work on Grand Unification. It is now known that, in fact, if Standard Model gauge coupling renormalization group evolution is used, the gauge couplings do *not* converge. In fact, Georgi and Glashow's model predicts a value of the strong coupling constant about eight standard deviations from the current experimental value.

On the other hand, when supersymmetry is added to the theory, the supersymmetric partners of the Standard Model particles modify the β functions for the gauge coupling constants in a way such that the coupling constants *do* converge. [10] The precise convergence of the gauge coupling constants that occurs when SUSY is included is considered the most compelling evidence for SUSY to date.

An additional reason for using supersymmetry with Grand Unification is that SUSY can provide a solution to the gauge hierarchy problem. [11] The gauge hierarchy problem stems from the fact that the mass squared of the Higgs doublet(s) receive radiative corrections proportional to the scale of Grand Unification squared. As a result, the natural scale for the masses of the Higgs doublet(s) and their vacuum expectation values [vevs] is the scale of Grand Unification. In order to have the Higgs mass and vacuum expectation value at the electroweak scale, there must be an order by order cancellation of the radiative corrections to the Higgs doublet masses, requiring a fine tuning of the parameters in the theory to an accuracy of one part of 10^{26}.

However, supersymmetry provides a solution to this problem. It can be shown that various radiative corrections that generally appear in field theories do not appear in a supersymmetric field theory. [12] This is because radiative corrections involving bosonic loops cancel those involving fermionic loops in certain contexts in a supersymmetric theory so that the radiative corrections are not as severe as they would otherwise be. In particular, in a supersymmetric theory, the quadratic divergences which would give the Higgs doublets mass corrections proportional to the mass of the GUT scale squared, no longer appear. Hence, if the Higgs doublets get tree-level masses of order the electroweak scale, their masses will remain of order the electroweak scale in a supersymmetric theory.

In any realistic theory, supersymmetry obviously needs to be broken. Nevertheless, SUSY can be broken in such a way that the cancellation of divergences characteristic of a SUSY theory still holds. [13] When SUSY is broken in this way, SUSY is said to be "softly" broken. When SUSY is softly broken, the Higgs doublets squared masses receive corrections proportional to the scale of SUSY breaking squared (instead of the scale of Grand Unification). [14] Hence, in order for SUSY to provide a solution to the gauge hierarchy problem, SUSY must be broken at a scale not too far away from the electroweak scale. Although what constitutes fine tuning is inherently something that cannot be given a precise definition, it is generally agreed that the scale of SUSY breaking can be no greater than around a few TeV unless there is excessive fine tuning.[1] Similarly, in order for SUSY to be useful in altering the β functions of the gauge couplings so they converge, the scale of SUSY breaking cannot be too far above

[1]In addition, in order for the mechanism of electroweak symmetry breaking used in the Minimal Supersymmetric extension of the Standard Model to work without fine tuning, the scale of SUSY breaking can not be too far from the electroweak scale, as a result of tree level relations imposed on the SUSY breaking parameters by electroweak symmetry breaking.[15]

the electroweak scale. This requirement is met when the scale of SUSY breaking is no greater than a few TeV.

Supersymmetric Grand Unification thus proceeds as follows. Below the Planck scale, there exists a "complete" supersymmetric theory, with a unified gauge coupling. At the scale of Grand Unification, the GUT gauge group is spontaneously broken to the Standard Model gauge group. Below the GUT scale, the Minimal Supersymmetric extension of the Standard Model [MSSM] is valid as an effective low energy field theory. The MSSM and the notation used throughout this thesis associated with the MSSM are reviewed in Appendix A. Between the Grand Unification scale and the scale of SUSY breaking, there is a "GUT desert" — once all the SUSY partners are discovered near the SUSY breaking scale, there are no new particles and no new physics to be discovered until the GUT scale. Below the electroweak/SUSY breaking scale, SUSY partners decouple from the theory, so that physics can be treated in terms of a $SU(3)_{color} \times U(1)_{E.M.}$ theory, which basically behaves the same way as the effective $SU(3)_{color} \times U(1)_{E.M.}$ theory valid below the electroweak scale found in the Standard Model.

2.2 SO(10)

There are several reasons for choosing SO(10) as the Grand Unification gauge group. [29]

1. It is the smallest group in which all of the fermions of a single generation fit into a single irreducible representation — the 16. Moreover, the 16 representation introduces into the theory only one additional state not found in the Standard Model. This additional state can be associated with the right-handed neutrino.

Moreover there are experimental and theoretical reasons why it may be desirable to introduce a right-handed neutrino into the theory. The right-handed neutrino can be used in a see-saw mechanism to give left-handed neutrinos a small, non-zero mass. [16] This may be desirable because there is indirect astrophysical evidence suggesting that Standard Model neutrinos have a small non-zero mass. [17] By contrast, in groups larger than SO(10), the representation corresponding to Standard Model fermions introduce into the theory a variety of undesirable, exotic particles not corresponding to anything in the Standard Model.

2. Similarly, both Higgs doublets of the MSSM fit into a single representation of SO(10), the 10 representation.

3. Because the up-type quarks of each generation are in the same representation as the down-type quark and lepton of the same generation, it is possible to relate the masses of the up-type quarks to the masses of both the down-type quarks and the leptons. Hence, use of SO(10) can increase the predictivity of the model being built by further decreasing the number of parameters in mass generating sector for Standard Model fermions.

4. In contrast to SU(5), SO(10) SUSY GUTs provide a simple solution to the doublet-triplet splitting problem. The doublet-triplet splitting problem is the problem of understanding why the Higgs doublets in the 5 and $\bar{5}$ representations of SU(5), (10 representation of SO(10)), get masses of order the electroweak scale, while the Higgs color triplets in the same representation get masses around the order of the GUT scale. The Higgs color triplets are required to get masses

of around the order of the GUT scale in order to adequately suppress baryon-number violating processes mediated by the Higgs color triplets. In simple SU(5) models, the tree level splitting of the doublets and triplets can only be accomplished with an excessive amount of fine tuning. On the other hand, in SO(10), an adjoint getting a vev in the $B-L$ direction can be used to give a tree level mass of order the GUT scale to the Higgs color triplets, while not giving mass to the Higgs doublets, hence providing a solution of the doublet-triplet splitting problem. [18] A specific implementation of this solution will be further elaborated on in Chapter 3.

2.3 Effective fermion mass generating operators and the hierarchy of fermion masses

ADHRS expresses the sector of its models which generate fermion masses and mixing angles for the first and second generation fermions in terms of a set of non-renormalizable effective operators, valid below the GUT scale. Such effective operators could be obtained from a more complete theory, valid up to the Planck scale, by integrating out at the Planck scale superheavy fields getting masses at the Planck scale. They could also be generated by integrating out superheavy fields at an intermediate M_{10} between the Planck and GUT scales at which SO(10) is spontaneously broken down to SU(5). In particular, ADHRS uses effective fermion mass generating operators of the form

$$\mathcal{O}_{ij} = 16_i \; \mathcal{A} \; 10 \; \mathcal{A}' \; 16_j \tag{2.1}$$

where

$$\mathcal{A} = \frac{45_1 \ldots 45_n (\mathcal{S}_G)_1 \ldots (\mathcal{S}_G)_N}{\langle (45_X)_1 \rangle \ldots \langle (45_X)_k \rangle \langle (\mathcal{S}_M)_1 \rangle \ldots \langle (\mathcal{S}_M)_{N+n-k} \rangle}$$

$$\mathcal{A}' = \frac{45_{n+1} \ldots 45_m (\mathcal{S}_G)_{N+1} \ldots (\mathcal{S}_G)_M}{\langle (45_X)_{k+1} \rangle \ldots \langle (45_X)_l \rangle \langle (\mathcal{S}_M)_{N+n-k+1} \rangle \ldots \langle (\mathcal{S}_M)_{M+m-l} \rangle}$$

and where 16_i and 16_j are 16s containing the ith and jth generation of Standard Model fermions: $45_1 \ldots 45_m$ are adjoints fields getting vevs of order the GUT scale M_{GUT}: $(45_X)_1 \ldots (45_X)_l$ are adjoints getting vevs of order M_{10} in the X (SU(5) invariant) direction: $(\mathcal{S}_G)_1 \ldots (\mathcal{S}_G)_M$ are SO(10) singlets getting vevs of order M_{GUT}: and $(\mathcal{S}_M)_1 \ldots (\mathcal{S}_M)_{M+m-l}$ are singlets getting vevs of order the Planck scale M_{Planck}. Note that when the 45s and $\mathcal{S}_G$s get vevs of order M_{GUT}, this operator contributes to the i, j entries of the Yukawa matrices in the effective theory below M_{GUT}. That contribution is suppressed by $(M_{GUT}/M_{10})^l (M_{GUT}/M_{Planck})^{m+M-l}$.

One of the principle motivations for using such an effective operator approach is that it can be used to explain the hierarchy of fermion masses. [19] The masses of fermions getting mass via non-renormalizable operators are suppressed by powers of M_{GUT}/M_{Planck} and/or M_{GUT}/M_{10}. This suppression provides a mechanism for naturally suppressing the masses of the lighter fermion generations. If the model uses effective operators with appropriate suppression factors, the hierarchy of Standard Model fermion masses can be produced without any Yukawa coupling in the complete theory valid up to the Planck scale being inexplicably small in comparison to the other Yukawa couplings.

2.4 Summary of ADHRS

The ADHRS operator search addressed the issue of what sets of effective operators need to be present in the effective theory below the GUT scale in order to have a model with fermion masses and mixing angles consistent with experiment. The models obtained by this search are models only of physics in an effective theory

below the GUT scale — no attempt was made in ADHRS to construct a model for physics above the GUT scale which would generate the effective operators found in any of the ADHRS models.[2] Specifically, ADHRS searched for all possible sets of effective operators that could explain fermion masses and mixing angles when certain assumptions are made. These assumptions are:

1. SO(10) SUSY Grand Unification

2. Below the GUT scale, the effective theory is the MSSM, with a GUT desert between the GUT and electroweak scales.

3. The three generations of Standard Model fermions are contained in three 16 representations of SO(10), and the Higgs doublets are in a single 10 representation of SO(10).

4. All dimensionless couplings are of order unity. This implies that only the third generation of fermions can get its mass via dimension four operators.

5. The first and second generations of Standard Model fermions get masses via higher dimension operators of the form given by eqn. 2.1.

6. Each of the adjoints can get vevs in only one of four directions — the SU(5) invariant direction X; the hypercharge direction Y; the B-L direction; or the T_{3_R} direction, which is perpendicular to the B-L direction.

7. Threshold corrections are negligible.

8. Maximal predictivity: Fermion masses and mixing angles are described using the smallest number of effective operators necessary. This means each of

[2]ADHRS did however describe in an appendix how one might try to construct such a theory.

the models contain only four fermion mass generating operators, three being required to give non-zero mass to all Standard Model fermions and a fourth necessary to have CP violation.

ADHRS found that the operators could be in two textures: the "22" texture in which the set of effective operators were of the generic form $\{\mathcal{O}_{33}, \mathcal{O}_{23}, \mathcal{O}_{22}, \mathcal{O}_{12}\}$, where $\mathcal{O}_{33}, \ldots, \mathcal{O}_{12}$ are some set operators of the form given in 2.1; and the "23" texture in which the set of effective operators were of the generic form $\{\mathcal{O}_{33}, \mathcal{O}_{23}, \mathcal{O}_{23}', \mathcal{O}_{12}\}$.

Under assumptions (3) and (4), there is only one possible choice for $\mathcal{O}_{33}$.

$$\mathcal{O}_{33} = 16_3\ 10\ 16_3.$$

Moreover, the operator search found that only one $\mathcal{O}_{12}$ operator was possible.

$$\mathcal{O}_{12} = 16_1\ (\frac{\tilde{A}}{\mathcal{S}_M})^3\ 10_1\ (\frac{\tilde{A}}{\mathcal{S}_M})^3\ 16_2$$

where $\tilde{A}$ is an adjoint getting a vev in the X direction.

In the 22 texture, there were 54 possible combinations of operators found. There were six choices for the $\mathcal{O}_{22}$ operator:

$$\mathcal{O}_{22} =$$

$$\begin{aligned}
(a) \quad & 16_2\ \frac{\tilde{A}}{\mathcal{S}_M}\ 10_1 \frac{A_1}{\tilde{A}} 16_2 \\
(b) \quad & 16_2\ \frac{\mathcal{S}_G}{\tilde{A}}\ 10_1\ \frac{A_1}{\mathcal{S}_M}\ 16_2 \\
(c) \quad & 16_2\ \frac{\tilde{A}}{\mathcal{S}_M}\ 10_1\ \frac{A_1}{\mathcal{S}_M}\ 16_2 \\
(d) \quad & 16_2\ 10_1\ \frac{A_1}{\tilde{A}}\ 16_2 \\
(e) \quad & 16_2\ 10_1\ \frac{\tilde{A}\ A_1}{\mathcal{S}_M{}^2}\ 16_2 \\
(f) \quad & 16_2\ 10_1\ \frac{A_1 \mathcal{S}_G}{\tilde{A}^2}\ 16_2
\end{aligned}$$

where A_1, A_2, and $\tilde{A}$ are 45s which get vevs in the B-L, hypercharge, and X (SU(5) invariant) directions, respectively. However, each of the six choices of $\mathcal{O}_{22}$ operator give the same Clebsch relations between up-type quark, down-type quark, and charged lepton matrices, and hence are not distinguishable in terms of their predictions for fermion masses and mixing angles.

There were nine choices for $\mathcal{O}_{23}$:

$$\mathcal{O}_{23} =$$

$$\begin{aligned}
&(1.)\quad 16_2\ \frac{A_2}{S_M}\ 10_1\ \frac{S_G}{\tilde{A}}\ 16_3\\
&(2.)\quad 16_2\ \frac{A_2}{S_M}\ 10_1\ \frac{A_1}{\tilde{A}}\ 16_3\\
&(3.)\quad 16_2\ \frac{A_2}{\tilde{A}}\ 10_1\ \frac{S_G}{\tilde{A}}\ 16_3\\
&(4.)\quad 16_2\ \frac{A_2}{\tilde{A}}\ 10_1\ \frac{A_1}{\tilde{A}}\ 16_3\\
&(5.)\quad 16_2\ \frac{A_2}{S_M}\ 10_1\ \frac{A_2}{\tilde{A}}\ 16_3\\
&(6.)\quad 16_2\ \frac{A_2}{\tilde{A}}\ 10_1\ \frac{A_2}{\tilde{A}}\ 16_3\\
&(7.)\quad 16_2\ 10_1\ \frac{S_G{}^2}{\tilde{A}^2}\ 16_3\\
&(8.)\quad 16_2\ 10_1\ \frac{S_G A_1}{\tilde{A}^2}\ 16_3\\
&(9.)\quad 16_2\ 10_1\ \frac{A_1^2}{\tilde{A}^2}\ 16_3
\end{aligned} \tag{2.2}$$

The models are labeled 1-9, corresponding to the choice of $\mathcal{O}_{23}$ operator for that model.[3]

[3]Because each of six choices for $\mathcal{O}_{22}$ operator give the same predictions for fermion masses and mixing angles, models which are the same except for the choice of $\mathcal{O}_{22}$ operator are referred to as being the same model in ADHRS.

The Yukawa sector is parameterized by five real parameters — four corresponding to the magnitudes of the Yukawa coefficients multiplying each of the four effective operators, and one corresponding to the one physically relevant phase in the Yukawa sector. At the GUT scale, using phase rotations to remove physically irrelevant phases, these effective operators generate the following Yukawa matrices.

$$Y_u = \begin{pmatrix} 0 & C & 0 \\ C & 0 & x'_u B \\ 0 & x_u B & A \end{pmatrix}$$

$$Y_d = \begin{pmatrix} 0 & -27C & 0 \\ -27C & Ee^{i\phi} & x'_d B \\ 0 & x_d B & A \end{pmatrix}$$

$$Y_e = \begin{pmatrix} 0 & -27C & 0 \\ -27C & 3Ee^{i\phi} & x'_e B \\ 0 & x_e B & A \end{pmatrix}$$

where A, B, C, D, E and ϕ are the parameters of the Yukawa sector, and x_u, x'_u, x_d, x'_d, x_e, and x'_e are Clebsch coefficients which depend on the choice of the $\mathcal{O}_{23}$ operator.

The ADHRS analysis of these models concluded that models 4, 6, and 9 give the best fits to low energy data for fermion masses and mixing angles, and that those three models fit the low energy data reasonably well.

ADHRS also found three models in the 23 texture which fit the low energy data well. However, those models were disfavored because they required modest fine-tuning.

2.5 Questions not answered by ADHRS

ADHRS was a remarkable achievement. ADHRS was able to fit fermion mass and mixing angle data surprisingly well using the smallest number of effective operators possible. Yet, there were many questions left unanswered by ADHRS:

1. **How would the fits of the models change if corrections due to SUSY particles are explicitly included in the analysis?** In ADHRS, the only effects of the SUSY particles that were expressly considered in the numeric calculations were the effects the SUSY particles have on the β functions for the gauge and Yukawa couplings. However, the SUSY particles have a variety of other effects. Most significantly, there are threshold corrections to the down-type quark and charged lepton masses, and to the KM matrix elements proportional to $\tan\beta$. [20, 21, 22] These corrections can be several tens of percent depending on the SUSY particle spectrum. These corrections were assumed to be small in ADHRS (assumption no. 7), and ADHRS argued that there was a region of SUSY parameter space in which these corrections could be neglected. However, allowing larger threshold corrections could potentially improve the fit of some of the models to the experimental data, or could change which of the nine models best fits the data.

2. **How do threshold corrections at the GUT scale change the predictions of the models?** In addition to the threshold corrections due to SUSY particles, there are threshold corrections at the GUT scale due to the effects of superheavy particles that must be integrated out at the GUT scale. [23] These threshold corrections can affect a variety of things, including the gauge couplings and the top, bottom, and tau Yukawa couplings. However, unlike the SUSY threshold corrections, these corrections cannot be computed without a model valid above the GUT scale.

3. **Why only four dominant operators?** The assumption that there are only four dominant effective operators was put in by hand. ADHRS gives no understanding of why there should be only four dominant effective operators. It was argued that the existence of just four dominant operators might be the result of some family symmetries in a more complete theory, valid beyond the GUT scale, from which the ADHRS effective operators were generated. However, an explicit implementation of this idea was not given.

4. **What about corrections due to subdominant effective operators?** In any complete theory, valid beyond the GUT scale, from which the ADHRS operators might be derived, the four effective operators of any ADHRS model will be just the most dominant effective operators in an expansion in powers of M_{GUT}/M_{10} and/or M_{GUT}/M_{Planck}. There will be an infinite sum of subdominant operators suppressed by powers of M_{GUT}/M_{10} and/or M_{GUT}/M_{Planck}. ADHRS did not explicitly include the effects of these operators in their numeric calculations, but estimated that the correction to the predictions of the models due to these corrections would be about 10%.

5. **How is SO(10) gauge symmetry breaking achieved? How is it guaranteed that the vevs of the adjoints can only be in the four directions specified in ADHRS assumption no. 6?**

6. **How is doublet-triplet splitting achieved?**

7. **What about baryon number violation and lepton flavor violation?** In any SUSY GUT, baryon number and lepton flavor violation are guaranteed to occur. However, neither can be computed in the context of the ADHRS models,

because the ADHRS effective operator models are valid only up to the GUT scale, but baryon number and lepton flavor violation can only be computed if one has a theory valid above the GUT scale. Constraints from baryon number and lepton flavor violating processes may be particularly compelling because of the $\tan\beta$ dependence of rates of baryon number and lepton flavor violating processes. The rates of baryon number violating processes are proportional to $\tan^2\beta$. Because of top-bottom-tau Yukawa unification, the ADHRS models necessarily require large $\tan\beta$. Namely, $\tan\beta \approx m_t/m_b \approx 50$. Since the rates of several baryon number violating decays predicted by low[4] $\tan\beta$ minimal SUSY SU(5) GUTs are near their experimental limits [24], a naive extrapolation of these results to ADHRS suggests that ADHRS is ruled out. Similarly, the rates of lepton flavor violating processes have terms proportional to $\tan^2\beta$. If the results of studies of individual lepton flavor violation in the context of a low $\tan\beta$, minimal SO(10) SUSY GUT are naively extrapolated to large $\tan\beta$[8], they also suggest that the ADHRS models may be ruled out, unless the sleptons are unnaturally heavy.

8. **What is the origin of supersymmetry breaking?**

9. **How shall the ADHRS models be extended to include gravity?**

Question 1 was recently addressed by a global χ^2 analysis of the ADHRS models in [25], which expressly included the effects of the SUSY threshold corrections. That χ^2 analysis fitted 20 low energy observables, including experimental measurements for the gauge couplings; fermion masses and mixing angles; and $b \to s\gamma$. It found

[4] I.e. $\tan\beta \approx 1$

that model 4 by far gave the best fit. It further found that the best, global χ^2 fit gives a fit in which all the low energy observables agree to within 2σ of their experimental values and that most observables agree to within 1σ.

In order to answer questions 2 to 7, we need to have a model for physics up to the Planck scale. Finding such a model will be the focus of the next chapter of this thesis. Namely, we will give a more complete theory, valid up to the Planck scale, which reproduces the low energy effective operators of model 4(c) of ADHRS, when superheavy fields are integrated out of the theory. Model 4 was chosen because it is the model which gives the best fit, according to [25]. This model will answer questions 3, 5, and 6, and will give a framework in which one can answer questions 2, 4, and 7. In that chapter, we also partially answer question 2 by calculating one loop threshold corrections at the GUT scale to the gauge couplings. We show that when these one loop threshold corrections are combined with order of magnitude estimates for baryon number violating processes, they form a major constraint of the SO(10) symmetry breaking sector of the theory. The remaining chapters are devoted to answering question number 7. The remaining questions (2, 4, 8, and 9) are subjects for future research.

CHAPTER 3

CONSTRUCTION OF THE MODEL

3.1 Introduction

In this chapter, we construct a model valid up to the Planck scale, which is designed to generate the low energy effective operators of model 4(c) of ADHRS. This model will be "natural" in the sense described in Chapter 1. In addition, we will argue in the chapter, via order of magnitude estimates, that this model gives rates for baryon number violating nucleon decay consistent with the experimental bounds, and explicitly calculate the rates of decay in the next chapter.

This work builds on many of the ideas of Hall and Raby in [26]. In that work, a model, valid up to the Planck scale, was constructed which reproduces the low energy effective operators of ADHRS model 6(a). Their model contains an SO(10) symmetry breaking sector; a Higgs sector which ensures doublet-triplet splitting; and a neutrino sector for giving sufficiently large masses to the right-handed neutrinos. It also contains a variety of U(1), R, and discrete symmetries which ensure that the four operators of ADHRS model 6(a), and *no others*, are the dominant effective operators. Our analysis differs significantly from theirs, however, in that they did not analyze the

effects of constraints coming from the relationship between baryon number violating nucleon decay rates and the prediction for the strong coupling constant.

The Hall-Raby model uses the Dimopoulos-Wilczek mechanism for doublet-triplet splitting. Specifically, the Higgs sector of the theory giving doublet-triplet splitting is

$$W_{d-t} = 10_1\ A_1\ 10_2 + S_*\ 10_2^2 \tag{3.1}$$

where A_1 is an adjoint getting a vev in the $B-L$ direction and S_* is a singlet. The 10_1 contains the massless[5] Higgs doublets of the MSSM. When A_1 and S_* get vevs. the relevant portions of the doublet and triplet mass matrices. M_d and M_t, will be

$$\begin{aligned} M_d &= \begin{array}{c} \\ 10_1 \\ 10_2 \end{array} \begin{array}{c} \begin{array}{cc} 10_1 & 10_2 \end{array} \\ \begin{pmatrix} 0 & 0 \\ 0 & S_* \end{pmatrix} \end{array}, \\ M_t &= \begin{array}{c} \\ 10_1 \\ 10_2 \end{array} \begin{array}{c} \begin{array}{cc} 10_1 & 10_2 \end{array} \\ \begin{pmatrix} 0 & a_1 \\ -a_1 & S_* \end{pmatrix} \end{array}. \end{aligned} \tag{3.2}$$

where a_1 is the coefficient of the vev of A_1. As can be seen, the doublets of the 10_1 will be massless, while the triplets of both 10_1 and 10_2 are massive.

In SUSY GUTs, the dominant contribution to proton decay comes from the exchange of color triplet Higgses. [28] Specifically, color triplet Higgs exchanges result in effective dimension 5 baryon number violating operators $(Qc_{qq}Q)(Qc_{ql}L)$ and $(\overline{U}c_{ud}\overline{D})(\overline{U}c_{ue}\overline{E})$, where c_{qq}, c_{ql}, c_{ud}, and c_{ue} are 3×3 model-dependent, flavor matrices. [33, 27] Figure 3.1 shows the supergraphs with produce these operators. In a model in which the Higgs doublets are contained in a single 10 representation, 10_1,

[5] "Massless" in this context means that any mass is many, many orders of magnitude below the GUT scale.

the rate of proton decay due to these effective operators will be inversely proportional to the square of an effective color triplet Higgs mass $\tilde{M}_t$. The inverse of this mass is equal to the $10_1, 10_1$ entry of the inverse of the color triplet mass matrix. I.e. $\tilde{M}_t^{-1} = (M_t^{-1})_{11}$.

In order to get a preliminary, order of magnitude estimate of how big $\tilde{M}_t$ needs to be in order to adequately suppress proton decay, we consider the analyses of proton decay in minimal SU(5) models. Those analyses find that proton decay rates are near their experimental bounds when $\tilde{M}_t \approx 10^{17}$ GeV. [24] However, the c_{ud} and c_{ql} matrices they use are much smaller than the c_{ud} and c_{ql} matrices for the ADHRS models. This is because the minimal SU(5) models also use low $\tan\beta$ in order to suppress proton decay. When $\tan\beta$ is small, the entries in the Y_d and Y_e matrices are suppressed by roughly $\tan\beta \times (m_b/m_t) \approx 1/50$. Since, the Y_d and Y_e matrices come from the same SU(5) coupling term that the c_{ud} and c_{ql} matrices come from — the $\overline{\mathbf{5}}\ \mathbf{10}\ \overline{\mathbf{5}}$ coupling — this means that c_{ud} and c_{ql} will also be suppressed by $\approx 1/50$. Accordingly, the effective dimension 5 baryon number violating operators resulting from color triplet Higgs exchanges are also suppressed by $\approx 1/50$ in comparison with what they would be for a large $\tan\beta$ model. Therefore, since the ADHRS models use large $\tan\beta$ ($\tan\beta \approx 50$), $\tilde{M}_t$ should be roughly at least two orders of magnitude greater than what it is in the minimal SU(5) models, i.e. $\tilde{M}_t = O(10^{19}$ GeV).

For the Hall-Raby model, $\tilde{M}_t = a_1^2/S_*$. It would naively seem that proton decay could be suppressed to arbitrarily small amounts by making S_* arbitrarily small. However, this is not the case because S_* affects the prediction for α_s through GUT scale threshold corrections to the gauge couplings.

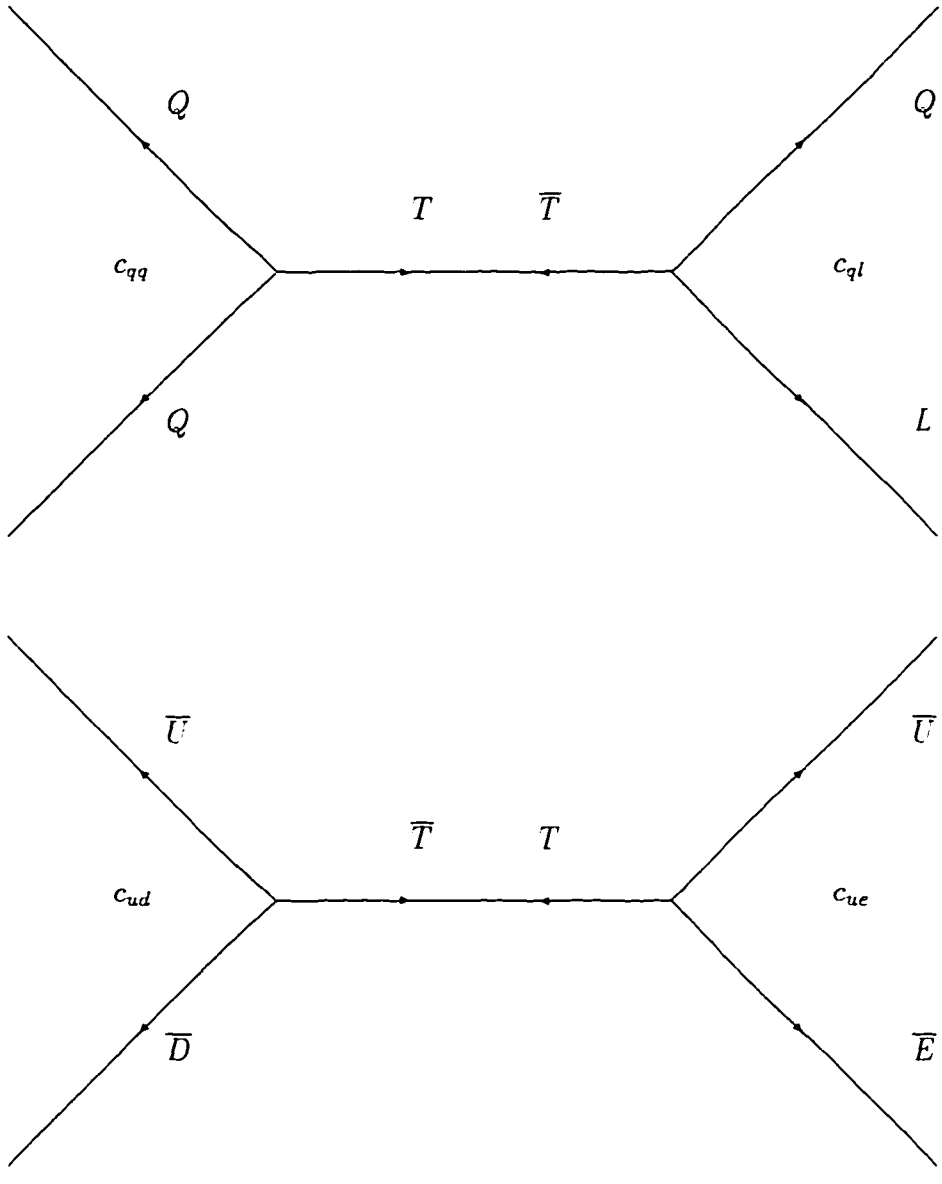

Figure 3.1: Supergraphs showing baryon number violation mediated by color triplet Higgs exchanges.

On the other hand, the Hall-Raby model contains a large number of additional superheavy states associated with the GUT symmetry breaking sector of the theory, which also affect the prediction for α_s through GUT scale threshold corrections. The spectrum of masses for these states depends on six independent GUT scale vevs, which serve as additional parameters for the model. Hence, it would seem *a priori* that one should readily be able to adjust the spectrum of states in the GUT symmetry breaking sector of the theory so that the effect of the threshold corrections due to having S_* small is canceled by the effect due to the other states.

Surprisingly however, we show in this chapter that this is not the case. In fact, rather remarkably, it is typical in a theory with a large number of family symmetries that the dependence of the threshold corrections to α_s on GUT scale vevs almost drops out completely. Hence, constraints due to proton decay are much more stringent that one would at first think they would be. In fact, we show that the Hall-Raby model is entirely ruled out as a result of these constraints. We then construct a new GUT symmetry sector which is consistent with α_s and proton decay constraints.

3.2 One loop threshold corrections at M_G.

One loop threshold corrections at M_G for gauge couplings are given by [23]

$$\alpha_i^{-1}(M_G) = \alpha_G^{-1} - \Delta_i \tag{3.3}$$

where Δ_i is the leading log threshold correction to α_i. Furthermore,

$$\Delta_i = \frac{1}{2\pi} \sum_{\zeta} b_i^{\zeta} \log \left| \frac{M_\zeta}{M_G} \right| \tag{3.4}$$

where the sum is over all superheavy particles and b_i^ζ is the contribution the superheavy particle ζ would make to the beta function coefficient b_i if the particle were not integrated out at M_G.

At one loop the definition of the GUT scale is somewhat arbitrary. In order to avoid large logarithms it must certainly be at the geometric mean of the heavy masses: otherwise we are free to choose its value. A particularly convenient choice is to define M_G as the scale where the two gauge couplings, α_i, $i = 1, 2$, meet. At this point $\Delta_1 = \Delta_2$ and we define

$$\tilde{\alpha}_G \equiv \alpha_1(M_G) = \alpha_2(M_G). \tag{3.5}$$

Then define

$$\epsilon_3 \equiv (\alpha_3(M_G) - \tilde{\alpha}_G)/\tilde{\alpha}_G, \tag{3.6}$$

i.e. the relative shift in α_3 at M_G. In general, a value of $\epsilon_3 \sim -(2-3\%)$ is needed to obtain $\alpha_s \sim 0.12$.

3.2.1 Formula for ϵ_3 in a general SO(10) theory

We consider a general SO(10) SUSY GUT that contains only the SO(10) states[6] —

$$(n_{16}+3)\,\mathbf{16} + n_{16}\,\bar{\mathbf{16}} + n_{10}\,\mathbf{10} + n_{45}\,\mathbf{45} + n_{54}\,\mathbf{54} + n_1\,\mathbf{1} \tag{3.7}$$

with $n_{16}, n_{10}, n_{45}, n_{54}, n_1$ specific, model-dependent integers. These states can be decomposed into their SU(3) × SU(2) × U(1) content by first considering the decomposition to SU(5) [see Appendix C] and then the rest of the way [31].

[6]This feature is consistent with a stringy origin to such a model[30].

$SU(3) \times SU(2) \times U(1)$ representation	name	appears in $SU(5)$ representation
$(8,1,0)$	g	24
$(1,3,0)$	w	24
$(3,2,-\frac{5}{3})$; $(\overline{3},2,\frac{5}{3})$	$x;\overline{x}$	24
$(3,1,\frac{4}{3})$; $(\overline{3},1,-\frac{4}{3})$	$u;\overline{u}$	$\overline{10}$; 10
$(1,1,-2)$; $(1,1,2)$	$e;\overline{e}$	$\overline{10}$; 10
$(3,2,\frac{1}{3})$; $(\overline{3},2,-\frac{1}{3})$	$q;\overline{q}$	10, 15; $\overline{10}$, $\overline{15}$
$(6,1,-\frac{4}{3})$; $(\overline{6},1,\frac{4}{3})$	$s;\overline{s}$	15; $\overline{15}$
$(1,3,2)$; $(1,3,-2)$	$\sigma,\overline{\sigma}$	15; $\overline{15}$
$(3,1,-\frac{2}{3})$; $(\overline{3},1,\frac{2}{3})$	$t;\overline{t}$	5; $\overline{5}$
$(1,2,1)$; $(1,2,-1)$	$d;\overline{d}$	5; $\overline{5}$

Table 3.1: Notation used for states in different charge sectors

In section 3.6, we derive a general formula for ϵ_3 in this case given by the expression (valid to lowest order in $\tilde{\alpha}_G$)

$$\epsilon_3 = \frac{\tilde{\alpha}_G}{2\pi}\sum_\gamma[(b_3^\gamma - b_2^\gamma) - \frac{1}{2}(b_2^\gamma - b_1^\gamma)]\log\left|\det'\frac{M_\gamma}{M_G}\right| \tag{3.8}$$

where

$$\det' M_\gamma = \begin{cases} \det M_\gamma & \text{if} \quad \gamma = t,g,w,s,\sigma \\ \frac{\det M_\gamma}{(M_{gaugino}^\gamma)^4} & \text{if} \quad \gamma = q,u,e,x \\ \det M_d' & \text{if} \quad \gamma = d \end{cases} \tag{3.9}$$

where M_d' is defined as the doublet mass matrix M_d with the massless Higgs doublets projected out.[7] Note, ϵ_3 only depends on the number of states in the theory through the mass matrices M_γ in each charge sector γ. Moreover, the effective determinants, defined above, explicitly take into account the special contributions of vector multiplets to the threshold corrections.

Putting in the values of b_i^γ for $i = 1,2,3$ into eqn. (3.8) we find

[7]Our notation for the states discussed above is found in table 3.1.

$$\epsilon_3 = \frac{\tilde{\alpha}_G}{\pi}\Big(\frac{3}{2}\log\Big|\det'\frac{M_g}{M_G}\Big| - \frac{3}{2}\log\Big|\det'\frac{M_w}{M_G}\Big|$$
$$+\frac{33}{10}\log\Big|\det'\frac{M_s}{M_G}\Big| - \frac{21}{10}\log\Big|\det'\frac{M_\sigma}{M_G}\Big| + \frac{9}{10}\log\Big|\det'\frac{M_u}{M_G}\Big| + \frac{3}{10}\log\Big|\det'\frac{M_e}{M_G}\Big|$$
$$-\frac{6}{5}\log\Big|\det'\frac{M_q}{M_G}\Big| - \frac{3}{5}\log\Big|\det'\frac{M_d}{M_G}\Big| + \frac{3}{5}\log\Big|\det'\frac{M_t}{M_G}\Big|\Big). \qquad (3.10)$$

The dominant contribution to ϵ_3 comes from the GUT symmetry breaking and electroweak Higgs sectors with superspace potential $W_{sym\ breaking}$ and W_{Higgs}, respectively. An additional small contribution comes from the fermion mass sector. These sectors are by reasons of "naturalness" necessarily invariant under several U(1) symmetries (including an R symmetry). In section 3.7, we show that these symmetries impose stringent constraints on the form of ϵ_3. In brief, ϵ_3 is implicitly a function of the vacuum expectation values [vevs] of fields in the symmetry breaking sector. These vevs transform under the U(1) and R symmetries. As a consequence of the invariance, we find

$$\epsilon_3 = f(\zeta_1, \ldots, \zeta_m) + \frac{3\tilde{\alpha}_G}{5\pi}\log\left|\frac{\det\bar{M}_t}{M_G \det\bar{M}'_d}\right| + \cdots \qquad (3.11)$$

where the first term represents the contributions from $W_{sym\ breaking}$. It is only a function of U(1) and R invariant products of powers of vevs $\{\zeta_i\}$. The second term, coming from the Higgs sector, is discussed further in the next section and the ellipsis refers to the small additional contribution arising from the fermion mass sector. Note, $\bar{M}_t$, $\bar{M}'_d$ only include those states, from 5s and $\bar{5}$s of SU(5) contained in $W_{sym\ breaking}$ and W_{Higgs}, *which mix with the Higgs sector* (see the next section).

3.2.2 The dependence of ϵ_3 on the Higgs sector

We assume the Higgs sector includes any number of **10**s with, for simplicity, only one of these, say $\mathbf{10}_1$, coupling to light fermions. We also include the doublet-triplet

splitting mechanism introduced by Dimopoulos-Wilczek [18]. Accordingly, the terms in the superspace potential relevant for doublet - triplet splitting are of the form

$$W_{d-t} = \bar{5}_2 \left[a_1 \frac{3}{2} (B - L)\right] 5_1 - \bar{5}_1 \left[a_1 \frac{3}{2} (B - L)\right] 5_2 + \sum_{i,j \geq 2} M_{ij}\, \bar{5}_i\, 5_j \qquad (3.12)$$

where $a_1 \frac{3}{2} (B - L)$ is the vev of the field A_1 in the 45 dimensional representation and $(B - L)$ is the [Baryon - Lepton number] charge matrix (see eqn. (3.16)). Thus, since the doublets in $5_1, \bar{5}_1 \subset 10_1$ have zero $B - L$, they remain massless. [Note, some of the $\bar{5}_i, 5_j$ states may come from 16 and $\overline{16}$ representations, respectively, in $W_{sym\ breaking}$. We include, however, only those states which mix with 10_1.] Note, this superpotential is simply a generalization of the superpotential of eqn. 3.1. With this superpotential, we have $\tilde{M}'_d \equiv M[d]$, and the triplet mass matrix, $\tilde{M}_t$, with non-vanishing determinant, includes the terms which mix states in 10_1 with $\bar{5}_i$, 5_j, for $i, j \geq 2$ and the sub-matrix $M[t]$, where the matrix $M[d]$, ($M[t]$) is given by M with Clebsches appropriate for doublets (triplets).

Proton decay in this model is mediated by the Higgses in 10_1. Hence, the coefficient of the resulting effective dimension 5 baryon violating operators is

$$(M_t^{-1})_{11} \equiv \frac{\det M[t]}{\det \tilde{M}_t} = \frac{\det \tilde{M}'_d}{\det \tilde{M}_t} \times g$$

where $g \equiv \frac{\det M[t]}{\det M[d]}$. We show, in section 3.7, that $g = g(\zeta_1, \cdots, \zeta_m)$ is a holomorphic function of the set of U(1) and R invariant products of powers of vevs. If we now define the effective triplet mass by $\tilde{M}_t^{-1} \equiv (M_t^{-1})_{11}$, we obtain the final form for the factor in eqn. (3.11) - $\frac{\det \tilde{M}_t}{\det \tilde{M}'_d} = \tilde{M}_t\, g(\zeta_1, \cdots, \zeta_m)$. As a consequence, eqn. (3.11) becomes

$$\epsilon_3 = F(\zeta_1, \ldots, \zeta_m) + \frac{3\tilde{\alpha}_G}{5\pi} \log \left| \frac{\tilde{M}_t}{M_G} \right| + \cdots \qquad (3.13)$$

where f and g are absorbed in the function F. We thus find that suppressing the proton decay rate by increasing the ratio $\frac{\tilde{M}_t}{M_G}$ has the effect of increasing the value of ϵ_3 and consequently increasing the value of α_s.[8]

3.2.3 An Example : ϵ_3 in the Hall-Raby model

As an example, for the Hall-Raby model, there is only one independent invariant ratio of the GUT scale vevs given by $\zeta = \frac{v\bar{v}}{a_1 a_2}$. In principle, ϵ_3 could depend on an arbitrary function $f(\zeta)$. However, when we put the effective determinants for this model in equation (3.10) we find

$$\epsilon_3 = \frac{3\,\tilde{\alpha}_G}{5\pi}\left\{21\,\log(2) + \log\left|\frac{\tilde{M}_t}{M_G}\right|\right\}. \tag{3.14}$$

Remarkably, all dependence of ϵ_3 on the GUT scale vevs has dropped out except for the dependence on $\tilde{M}_t$. Unfortunately, the large positive constant that appears in the expression means that in order to get ϵ_3 negative, the proton's lifetime would be many orders of magnitude lower than the experimental bound. In addition, changing the Yukawa coupling coefficients of the terms of $W_{sym\,breaking}$ cannot cure this problem. For the most part, changing the Yukawa coupling constants of one of the terms of $W_{sym\,breaking}$ has the result of multiplying the effective determinants of the mass matrices M_γ in eqn. (3.8), for states γ in a complete SU(5) multiplet, all by the same amount. Thus, this multiplicative factor has no effect on ϵ_3. Hence, as a consequence of (3.14), we find that the symmetry breaking sector of the Hall-Raby model is ruled out by the dual constraints coming from the low energy measurement of α_s and the proton lifetime.

[8]This observation in the context of minimal SU(5), where in that case $\tilde{M}_t$ is the color triplet Higgs mass, was discussed earlier by Hisano et al.[24].

Is it possible to find a symmetry breaking sector which has all the U(1) symmetries required for the naturalness of the theory and is consistent with the constraints of α_s and τ_p? In the next section we describe a new SO(10) SUSY GUT which satisfies all our criteria. In fact it may contain the minimal symmetry breaking sector consistent with the requirements of (1) obtaining the effective fermion mass operators of ADHRS, (2) "naturalness," and (3) retaining only those states at energies below M_G, which either have trivial SM charge or are contained in the MSSM.

3.3 A complete SO(10) SUSY GUT

3.3.1 The GUT symmetry breaking and Higgs sectors

For this model,

$$\begin{aligned} W_{sym\ breaking} = \ & \tfrac{1}{M} A_1'(A_1^3 + \mathcal{S}_3 S A_1 + \mathcal{S}_4 A_1 A_2) \\ & + A_2(\Psi\overline{\Psi} + \mathcal{S}_1 \tilde{A}) + S\tilde{A}^2 \\ & + S'(S\mathcal{S}_2 + A_1\tilde{A}) + \mathcal{S}_3 S'^2 \end{aligned} \tag{3.15}$$

where the fields $\{A_1,\ A_2,\ \tilde{A},\ A_1'\}$, $\{S,\ S'\}$, Ψ, $\bar{\Psi}$, $\{\mathcal{S}_1, \cdots, \mathcal{S}_4\}$ are in the 45, 54, 16, $\bar{16}$ and 1 representations, respectively. [Note, traces and contractions of indices are implicit.] The supersymmetric minimization condition $\frac{\partial W}{\partial A_1'} = 0$ gives four discrete choices for the direction of the vev of A_1. We will assume that nature chooses the $B - L$ direction. The second term gives $\tilde{A}$ a vev in the X direction, A_2 a vev in the Y direction, and Ψ and $\overline{\Psi}$ vevs in the right-handed neutrino-like direction (see eqn. (3.16) below). The third and fourth terms, and the $\mathcal{S}_4$ subterm of the first term, were added to give mass to all non-MSSM fields which are not in a singlet representation of the standard model gauge group. The last term was added in accordance with our "naturalness" criterion, namely that the theory should be the most general one

consistent with the symmetries. The term $\mathcal{S}_3 S'^2$ is consistent with the U(1) and R symmetries of the symmetry breaking sector of the theory that will be discussed below, and we are aware of no other additional symmetry that might exclude this term. Therefore the term must be included.

The above vevs are given by

$$\langle A_1 \rangle = a_1 \begin{pmatrix} 1 & & & & \\ & 1 & & & \\ & & 1 & & \\ & & & 0 & \\ & & & & 0 \end{pmatrix} \otimes \eta \equiv a_1 \frac{3}{2}(B-L) \tag{3.16}$$

$$\langle A_2 \rangle = a_2 \begin{pmatrix} 1 & & & & \\ & 1 & & & \\ & & 1 & & \\ & & & -3/2 & \\ & & & & -3/2 \end{pmatrix} \otimes \eta \equiv a_2 \frac{3}{2} Y$$

$$\langle \tilde{A} \rangle = \tilde{a} \begin{pmatrix} 1 & & & & \\ & 1 & & & \\ & & 1 & & \\ & & & 1 & \\ & & & & 1 \end{pmatrix} \otimes \eta \equiv \tilde{a} \frac{1}{2} X$$

$$\langle S \rangle = s \begin{pmatrix} 1 & & & & \\ & 1 & & & \\ & & 1 & & \\ & & & -3/2 & \\ & & & & -3/2 \end{pmatrix} \otimes \mathbf{1}$$

$$\langle \Psi \rangle = v \ |\text{SU(5) singlet}\rangle$$

$$\langle \overline{\Psi} \rangle = \overline{v} \ |\text{SU(5) singlet}\rangle$$

where

$$\eta = \begin{pmatrix} 0 & -i \\ i & 0 \end{pmatrix} , \mathbf{1} = \begin{pmatrix} 1 & 0 \\ 0 & 1 \end{pmatrix} .$$

The vacuum minimization conditions are explicitly

$$a_1^2 = -s\mathcal{S}_3, \qquad \mathcal{S}_1\tilde{a} = \frac{1}{4}v\overline{v} \tag{3.17}$$

$$s\mathcal{S}_2 + \frac{2}{5}a_1\tilde{a} = 0, \qquad a_2\mathcal{S}_1 + 2s\tilde{a} = 0$$

Using these equations, the set $\{a_1, a_2, \tilde{a}, v, \overline{v}, \mathcal{S}_4\}$ form a complete set of independent variables.

Two caveats -

• Note at tree level the GUT symmetry breaking vevs are undetermined since the potential in these directions are both supersymmetric and flat. We will not discuss the process for fixing these vevs in this thesis. That analysis must necessarily include supersymmetry breaking effects as well as supergravity and radiative corrections.

• We do not describe the source of supersymmetry breaking in this thesis. Soft SUSY breaking operators are included at the GUT scale and renormalized down to the weak scale when making any comparison with the low energy data.

The same doublet-triplet splitting mechanism that was used in the Hall-Raby model can be used in this model. Accordingly, the Higgs sector of the Lagrangian is given by

$$L_{Higgs} = [10_1 A_1 10_2 + \mathcal{S}_5 10_2^2|_F + \frac{1}{M}[z^* 10_1^2|_D \tag{3.18}$$

where the first term is W_{Higgs} and the second generates a μ term when the F component of the hidden sector field z gets a vev of order $10^{10} GeV$. We then obtain $\mu = \langle F_z \rangle / M$.

U(1) and R symmetries of $W_{sym\,breaking}$ and ϵ_3

$W_{sym\,breaking}$ has a [U(1)]$^4\times$ R symmetry as is summarized in table 3.2. Up to arbitrary Yukawa coupling coefficients assumed to be of $O(1)$, $W_{sym\,breaking}$ is the most

field	U(1) charge	field	U(1) charge
A_1	$(1,0,0,0,0)$	A_1'	$(-3,0,0,0,0)$
A_2	$(0,1,0,0,0)$	$\tilde{A}$	$(0,0,1,0,0)$
S	$(0,0,-2,0,0)$	S'	$(-1,0,-1,0,0)$
Ψ	$(0,-1,0,1,0)$	$\bar{\Psi}$	$(0,0,0,-1,0)$
$\mathcal{S}_1$	$(0,-1,-1,0,0)$	$\mathcal{S}_2$	$(1,0,3,0,0)$
$\mathcal{S}_3$	$(2,0,2,0,0)$	$\mathcal{S}_4$	$(2,-1,0,0,0)$
$\mathcal{S}_5$	$(2,0,0,0,-4)$	16_3	$(0,0,0,0,1)$
16_2	$(-1,-1,2,0,1)$	16_1	$(-2,-5,7,0,1)$
10_1	$(0,0,0,0,-2)$	10_2	$(-1,0,0,0,2)$
z	$(0,0,0,0,-4)$	N_3	$(0,0,0,1,-1)$
N_2	$(1,1,-2,1,-1)$	N_1	$(2,5,-7,1,-1)$

All fields, except A_1' and z, have R charge 1. A_1' (z) has R charge 0 (2). The superpotential has R charge 3. The first 4 charges listed above contribute to states in the GUT symmetry breaking sector.

Table 3.2: U(1) and R charges of the new model

general superspace potential consistent with these symmetries. Using $a_1, a_2, \tilde{a}, v, \bar{v}$, and $\mathcal{S}_4$ as independent variables, the only invariant under a $[\mathrm{U}(1)]^4 \times \mathrm{R}$ rotation of the vevs is $\zeta = \frac{a_1^4}{a_2^2 \mathcal{S}_4^2}$. After evaluating ϵ_3 explicitly using equation (3.10) we obtain

$$\epsilon_3 = \frac{3\tilde{\alpha}_G}{10\pi}\left\{2\ \log\frac{256}{243} - \log\left|\frac{(1-25\zeta)^4}{(1-\zeta)}\right| + 2\log\left|\frac{\tilde{M}_t}{M_G}\right|\right\}. \tag{3.19}$$

The explicit mass matrices used in evaluating ϵ_3 are contained in Appendix E.

Before we can check whether the experimental measurement of $\alpha_s(M_Z)$ in this model is consistent with the non-observation of proton decay, we must discuss the fermion mass sector of the theory. The proton lifetime and branching ratios depend crucially on the couplings of the color triplet Higgses to fermions. In a theory of fermion masses, these couplings are related to the Yukawa couplings of fermions to Higgs doublets, *but they are not identical.* For example, the dimension 5 operators

responsible for proton decay are given by

$$\frac{1}{M_t}\,\mathbf{Q}\frac{1}{2}c_{qq}\mathbf{Q}\;\mathbf{Q}c_{ql}\mathbf{L} \tag{3.20}$$

$$\frac{1}{M_t}\,\bar{\mathbf{u}}c_{ue}\bar{\mathbf{e}}\;\bar{\mathbf{u}}c_{ud}\bar{\mathbf{d}}$$

where c_{qq}, c_{ql}, c_{ue} and c_{ud} are 3×3 complex matrices. The matrices c_{qq} and Y_u, the up quark Yukawa matrix, contain the same independent parameters but the SO(10) Clebsches are different.

3.3.2 Fermion mass sector

The superspace potential for the complete theory above the GUT scale which reproduces model 4(c) of ADHRS is given by (see fig. 3.2)

$$\begin{aligned} W_{fermion} = \quad & 16_3 10_1 16_3 + \bar{\Psi}_1 A_1 16_3 + \quad \bar{\Psi}_1 \tilde{A} \Psi_1 + \Psi_1 10_1 \Psi_2 \\ & + \bar{\Psi}_2 \tilde{A} \Psi_2 + \bar{\Psi}_2 A_2 16_2 + \quad \bar{\Psi}_3 A_1 16_2 \\ & + \Psi_3 10_1 \Psi_4 + \quad S_M \sum_{a=3}^{9} (\bar{\Psi}_a \Psi_a) \\ & + \bar{\Psi}_4 \tilde{A} 16_2 + \bar{\Psi}_5 \tilde{A} \Psi_4 + \quad \bar{\Psi}_6 \tilde{A} \Psi_5 \\ & + \Psi_6 10_1 \Psi_7 + \bar{\Psi}_7 \tilde{A} \Psi_8 + \quad \bar{\Psi}_8 \tilde{A} \Psi_9 + \bar{\Psi}_9 \tilde{A} 16_1 \end{aligned} \tag{3.21}$$

This superpotential is consistent with the symmetries discussed previously with the addition of one new U(1) given in table 3.2. However it is not the most general fermion sector consistent with these symmetries. In fact *one and only one* new operator must be added

$$\bar{\Psi}_6 A_2 16_3. \tag{3.22}$$

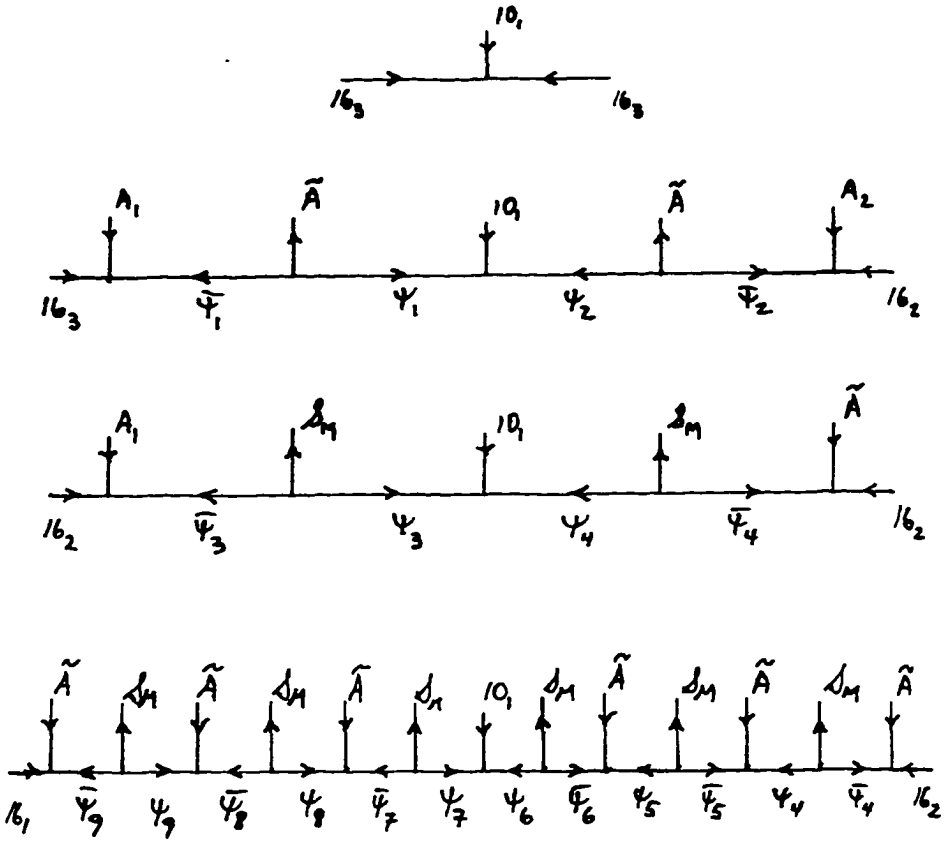

Figure 3.2: Supergraphs representing the generation of effective fermion mass operators $\mathcal{O}_{33}$, $\mathcal{O}_{23}$, $\mathcal{O}_{22}$, and $\mathcal{O}_{12}$ for model 4(c).

It is easy to see that this operator leads to one new effective operator at the GUT scale when heavy states are integrated out (see fig. 3.3). The new operator is

$$\mathcal{O}_{13} = 16_1 \left(\frac{\bar{A}}{S_M}\right)^3 10_1 \left(\frac{A_2}{S_M}\right) 16_3 \quad . \tag{3.23}$$

The complete model 4(c) is thus defined with this new operator and includes the operators of ADHRS model 4(c) plus the operator in eqn. (3.23).

Notice that a different choice of 22 operator will result in a different U(1) symmetry and thus by "naturalness," a distinct theory. In particular, we have checked that for

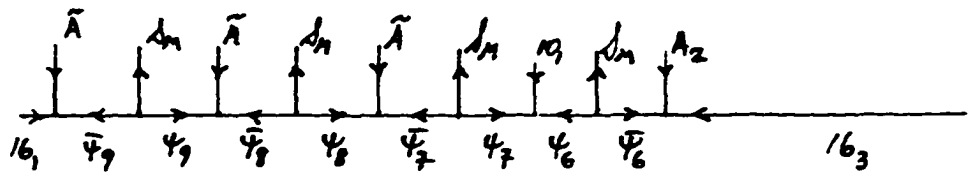

Figure 3.3: Supergraph representing the generation of new effective fermion mass operator $\mathcal{O}_{13}$ for model 4(c).

model 4(b) there are no new effective fermion mass operators generated, while for model 4(a) the new 13 operator

$$O_{13} = \quad 16_1 \left(\frac{\bar{A}}{S_M}\right)^3 \; 10_1 \left(\frac{\bar{A}A_2}{S_M^2}\right) 16_3 \tag{3.24}$$

is needed.

Finally, we note that the global χ^2 analysis of [25] also considered what effect including the additional $\mathcal{O}_{13}$ operator for models 4(a) and 4(c) has on the fits. That analysis concluded that an additional operator such as the 13 operator in eqn. (3.23) is absolutely necessary to fit the data. Model 4(c) (with the $\mathcal{O}_{13}$ operator) works best by far. The fit of model 4(c) to the low energy data agrees to better than 1σ for all observables considered in [25].

Additional threshold corrections at M_G

The dominant effective operators at the scale M_G are obtained by integrating out states with mass greater than M_G. Higher order corrections to these operators are also obtained. These typically lead to $O(10\%)$ corrections to the leading terms in the Yukawa matrices. Of course the terms in the Yukawa matrices will also receive corrections at one loop. We have neglected these corrections in the following analysis.

Neutrino masses

For completeness we include a minimal neutrino mass sector

$$W_{neutrino} = \bar{\Psi} \sum_{i=1}^{3} 16_i \, N_i \tag{3.25}$$

where the states N_i, $i = 1, \cdots, 3$ are SO(10) singlets. This term has the effect of giving GUT scale Dirac masses to the right-handed neutrinos in the 16's. Thus, the SM left-handed neutrinos are absolutely massless in this theory.

If necessary, left-handed neutrinos can be given masses as described in [26]. However, in order to do so we must either break one linear combination of the U(1)s or introduce additional SO(10) singlets. In either case, we must then check for "naturalness" and add any operator allowed by the symmetries of the theory.

3.3.3 Symmetries

This theory has 5 global U(1) symmetries and a global continuous R symmetry. The charges of most of the states are given in table 3.2. The charges of the other states can easily be derived. We have checked our theory for "naturalness." We find that only 3 additional operators need to be added to the superpotential -

$$\bar{\Psi}_2 A_1' \Psi_1 \mathcal{S}_2, \quad \bar{\Psi}_2 A_1' 16_3 \mathcal{S}_3, \quad \bar{\Psi}_5 A_1' \Psi_3 \mathcal{S}_3.$$

These three operators have no direct effect on any observable properties since the vev of A_1' vanishes. With the inclusion of these three operators the total superspace potential for model 4(c) is "natural" (i.e. no additional operators consistent with these symmetries are allowed) *for all possible powers of the fields.* In addition the theory has a matter reflection symmetry (see Dimopoulos and Georgi, ref. [27]) which forbids dimension 4 baryon or lepton number violating operators.

Some problems, however, remain to be solved in our model. Given the states and symmetries, we find that $f_{\alpha\beta}$, the coefficient of the general gauge kinetic term, is trivial in this model. Thus we have not explicitly included the sector of the theory which generates gaugino masses once SUSY is broken. In addition, the U(1) symmetries of the theory are not sufficient to significantly constrain the Kahler potential. For example, terms such as

$$\frac{1}{M^2}\,\Psi_4^{\dagger}\,\mathcal{S}_M^{\dagger}\,\tilde{A}\,16_2$$

are allowed which mix light generations with heavy states. This term (and others like it) is allowed since it already appears in the structure of the Feynman diagrams of fig. 3.2. These off diagonal terms in the Kahler potential can affect fermion mass operators as well as introduce flavor changing neutral current processes at low energies[32]. When deriving the effective theory at M_G we have implicitly assumed that the Kahler potential is universal for all 16s in the theory.

3.4 Upper bound for $\tilde{M}_t$ in model 4(c) based on naturalness

In order to adequately suppress proton decay, we can try taking the effective Higgs triplet mass, $\tilde{M}_t = a_1^2/\mathcal{S}_5 = 4 \times 10^{19} GeV$ with $a_1 = M_G \approx 2 \times 10^{16} GeV$ and $\mathcal{S}_5 = 10^{13} GeV$. This corresponds to light Higgs doublets with mass $10^{13} GeV$.

We have evaluated the expression for ϵ_3 including the additional states with GUT scale masses contained in the fermion mass sector of the theory. These typically shift the value of ϵ_3 by a small amount in the positive direction. We find that for typical values of a_1, a_2, and $\mathcal{S}_4$ around the GUT scale, we can obtain ϵ_3 negative for $\tilde{M}_t$ of order 10^{19} GeV. For example, with $a_1 = 2a_2 = 2\mathcal{S}_4 = \frac{a}{3} = M_G$ we have $\zeta = 16$ and

$\epsilon_3 \approx -0.030$, which includes a positive contribution of 0.005 from the fermion mass sector.

However, is it natural to have such light Higgs doublets? Are we populating the GUT desert? To address this question we should compare the Higgs doublet mass with the spectrum of masses for states in the symmetry breaking sector of the theory. These in fact range from $10^{13} - 10^{20} GeV$. Thus we have taken the doublet mass to lie at the lower bound of this GUT scale spectrum. This seems to be the only natural criteria for setting an upper bound on $\tilde{M}_t$.

By contrast, in order to have $\tilde{M}_t$ much bigger than 10^{19} GeV, there would need to be a supermassive electroweak doublet in the GUT desert with mass many orders of magnitude lower than the GUT scale itself and at least an order of magnitude lighter than any other particle getting mass around the GUT scale. It therefore seems unnatural to have $\tilde{M}_t$ much bigger than 10^{19} GeV.

Comparing our naturalness upper bound with the preliminary estimate for how big $\tilde{M}_t$ needs to be, given in the introduction to this chapter, we see that this value of $\tilde{M}_t$ might adequately suppress proton decay. The value of $\tilde{M}_t$ is not so small that the model is obviously ruled out, as was the case with the Hall-Raby model. However, it is not so big that one can conclude that proton decay is adequately suppressed without doing a detailed calculation. In the next chapter, we will do such a detailed calculation.

3.5 Conclusions for Chapter 3

We have presented a new complete SO(10) SUSY GUT. This theory has several interesting features. The superspace potential is "natural" to all orders in the fields. It

contains what may possibly be the minimal GUT symmetry breaking sector necessary to obtain the desired adjoint vevs consistent with (1) "naturalness" and (2) fermion masses.

We have also shown that one loop GUT scale threshold corrections are a significant constraint on the GUT symmetry breaking sector of the theory. This constraint, for example, is sufficient to rule out the model of [26]. The one loop threshold corrections relate the prediction for $\alpha_s(M_Z)$ to the proton lifetime.

It would be presumptuous of us to conclude without discussing some of the open questions. We have not discussed the origin of SUSY breaking nor how it feeds into the visible sector with the one exception of the μ term which we have nominally considered. We also do not discuss what determines the GUT vevs. At tree level, in the globally supersymmetric theory considered here and neglecting SUSY breaking, these are flat directions of the potential. Finally, and perhaps most seriously, the symmetries discussed in this chapter do not significantly constrain the Kahler potential. Flavor mixing in the Kahler potential could lead to dangerous flavor changing neutral current processes. We have *assumed* the trivial universal Kahler potential in our analysis.

3.6 Proof of equation 3.8

We define the GUT scale M_G as the point where $\tilde{\alpha}_G \equiv \alpha_1(M_G) = \alpha_2(M_G)$. This means that $\Delta_1(M_G) = \Delta_2(M_G)$. We then define the relative shift in $\alpha_3(M_G)$ by

$$\begin{aligned} \epsilon_3 &\equiv (\alpha_3(M_G) - \tilde{\alpha}_G)/\tilde{\alpha}_G \\ &= \alpha_3(M_G)\,(\Delta_3 - \Delta_1|_{M_G}) \end{aligned} \tag{3.26}$$

We then have

$$\Delta_3 - \Delta_1|_{M_G} = \frac{1}{2\pi}(\sum_\gamma (b_3^\gamma - b_1^\gamma)\log|\det' M_\gamma| - \sum_\gamma (b_3^\gamma - b_1^\gamma) n_\gamma \log M_G) \qquad (3.27)$$

where n_γ = the mass dimension of $\det' M_\gamma$ and $\det' M_\gamma$ is defined in eqn. (3.9), except for $\det' M_d$ where it will be convenient to define $\tilde{M}_d$ by $\det \tilde{M}_d = M_G \det M_d'$, and $\det' M_d = \det \tilde{M}_d$. This redefinition does not affect eqn. (3.8). Note, the matrix $\tilde{M}_d$ is defined such that $n_t = n_d$.

In addition,

$$\Delta_1|_{M_G} = \Delta_2|_{M_G}$$

which implies

$$\sum_\gamma (b_1^\gamma - b_2^\gamma)\log|\det' M_\gamma| = (\sum_\gamma (b_1^\gamma - b_2^\gamma) n_\gamma)\log M_G \qquad (3.28)$$

Substituting for $\log M_G$ we obtain

$$\begin{aligned} \epsilon_3 &\approx \frac{\tilde{\alpha}_G}{2\pi}\{\sum_\gamma (b_3^\gamma - b_1^\gamma)\log|\det' M_\gamma| - \frac{\sum_\gamma (b_3^\gamma - b_1^\gamma) n_\gamma}{\sum_\gamma (b_1^\gamma - b_2^\gamma) n_\gamma} \sum_\gamma (b_1^\gamma - b_2^\gamma)\log|\det' M_\gamma|\} \\ &= \frac{1}{2\pi}\frac{1}{c_{12}}\sum_\gamma (b_1^\gamma c_{23} + b_2^\gamma c_{31} + b_3^\gamma c_{12})\log|\det' M_\gamma| \qquad (3.29) \end{aligned}$$

where $c_{ij} = \sum_\gamma (b_i^\gamma - b_j^\gamma) n_\gamma$. To evaluate the c_{ij}s, define n_{54}, n_{45} and n_{10} to be the number of 54, 45, and 10 representations in the theory, respectively, and n_{16} and $n_{\overline{16}}$ to be the number of supermassive 16 and $\overline{16}$ representations, respectively. For any SO(10) model built with only 1, 10, 16, $\overline{16}$, 45, and 54 representations and one pair of light Higgs doublets, we have

$$\begin{aligned} n_{16} &= n_{\overline{16}} \\ n_g = n_w &= n_{45} + n_{54} \\ n_x &= n_{45} + n_{54} - 3 \\ n_u = n_e &= n_{45} + n_{16} - 3 \\ n_s = n_\sigma &= n_{54} \\ n_q &= n_{45} + n_{54} + n_{16} - 3 \\ n_d = n_t &= n_{10} + n_{16} \end{aligned}$$

Evaluating c_{23} explicitly

$$\begin{aligned} c_{23} &= (4n_s + 3n_q + 2n_w + 3n_x + n_d) - (5n_s + 2n_q + n_u + 3n_g + 2n_x + n_t) \\ &= \{4(n_{54}) + 3(n_{54} + n_{45} + n_{16} - 3) + 2(n_{54} + n_{45}) + \\ &\quad 3(n_{54} + n_{45} - 3) + (n_{10} + n_{16}) \\ &\quad -[5(n_{54}) + 2(n_{54} + n_{45} + n_{16} - 3) + (n_{45} + n_{16} - 3) + 3(n_{54} + n_{45}) + \\ &\quad 2(n_{54} + n_{45} - 3) + (n_{10} + n_{16})]\} \\ &= -3 \end{aligned} \tag{3.30}$$

Similarly

$$c_{31} = 9 \tag{3.31}$$

$$c_{12} = -6$$

Thus, the c_{ij}s are completely independent of the number of fields in any theory built with 1s, 10s, 16s, $\overline{16}$s, 45s, and 54s. Plugging eqns. (3.30) and (3.31) into eqn. (3.29), eqn. (3.8) readily follows.

3.7 U(1) symmetries and the dependence of ϵ_3 on GUT scale vevs

In this section we prove that the contribution to ϵ_3 from the GUT symmetry breaking sector is only a function of U(1) and R invariant products of powers of vevs. The proof relies on two facts:

1. the effective determinants of mass matrices are holomorphic functions of the symmetry breaking vevs, and

2. the effective determinants have simple phase rotations under U(1) and R symmetry transformations.

Note, since the effective determinants are independent of the conjugates of vevs, the U(1) and R invariance of ϵ_3 is very restrictive.

We first discuss the case for mass matrices which do *not* include vector multiplets, followed immediately by the case for mass matrices including vector multiplets. Note, in the first case the mass matrices themselves are, by construction, holomorphic functions of vevs. This is however not true for the latter case which is why it requires a separate discussion.

Consider a general superspace potential $W(\Phi_1, \Phi_2, \ldots, \Phi_N)$ whose superfields rotate under a U(1) symmetry as

$$\Phi_j \xrightarrow{\theta} e^{iQ_j\theta}\Phi_j$$

By defining the shifted fields $\hat{\Phi}_i \equiv \Phi_i - \langle\Phi_i\rangle$ and expanding the superspace potential about $\langle\Phi\rangle$ we can find the fermion mass matrices.

$$W(\hat{\Phi}_1 + \langle\Phi_1\rangle, \ldots) = \ldots + \sum_\gamma \psi_\gamma m_\gamma(\langle\Phi_1\rangle, \langle\Phi_2\rangle, \ldots)\psi_\gamma + \ldots \tag{3.32}$$

Now consider what would happen if the superfields received a different vacuum expectation value,

$$\langle\Phi_j\rangle^{\text{new}} = e^{iQ_j\theta}\langle\Phi_j\rangle^{\text{old}}$$

Under this change, the mass matrices would change.

$$W(\hat{\Phi}_1 + e^{iQ_1\theta}\langle\Phi_1\rangle, \ldots) = \ldots + \sum_\gamma \psi_\gamma m_\gamma^\theta \psi_\gamma + \ldots \tag{3.33}$$

where

$$m_\gamma^\theta \equiv m_\gamma(e^{iQ_1\theta}\langle\Phi_1\rangle, e^{iQ_2\theta}\langle\Phi_2\rangle, \ldots)$$

However, if we rotate the shifted fields $\hat{\Phi}_j$ by $e^{iQ_j\theta}$, the superspace potential will be invariant under the combined rotation of $\hat{\Phi}$ and $\langle\Phi\rangle$.

$$
\begin{aligned}
& W(e^{iQ_1\theta}\hat{\Phi}_1 + e^{iQ_1\theta}\langle\Phi_1\rangle, \ldots, e^{iQ_N\theta}\hat{\Phi}_N + e^{iQ_N\theta}\langle\Phi_N\rangle) \\
& = \ldots + \textstyle\sum_\gamma \psi_\gamma \begin{pmatrix} e^{iQ_1\theta} & & \\ & e^{iQ_2\theta} & \\ & & \ddots \end{pmatrix} m_\gamma^\theta \begin{pmatrix} e^{iQ_1\theta} & & \\ & e^{iQ_2\theta} & \\ & & \ddots \end{pmatrix} \psi_\gamma + \ldots \qquad (3.34) \\
& = W(\hat{\Phi}_1 + \langle\Phi_1\rangle, \ldots, \hat{\Phi}_N + \langle\Phi_N\rangle) \\
& = \ldots + \textstyle\sum_\gamma \psi_\gamma \, m_\gamma \, \psi_\gamma + \ldots
\end{aligned}
$$

Therefore, m_γ^θ rotates in a very simple way.

$$
m_\gamma^\theta = \begin{pmatrix} e^{-iQ_1\theta} & & \\ & e^{-iQ_2\theta} & \\ & & \ddots \end{pmatrix} m_\gamma \begin{pmatrix} e^{-iQ_1\theta} & & \\ & e^{-iQ_2\theta} & \\ & & \ddots \end{pmatrix} \qquad (3.35)
$$

Thus,

$$
\det m_\gamma^\theta = e^{-2i\theta\sum Q} \det m_\gamma \qquad (3.36)
$$

where the sum is over all fields that have columns in the mass matrix.

Similar arguments can show that under an R symmetry rotation, $\langle\Phi\rangle \to e^{iQ\theta}\langle\Phi\rangle$, m_γ^θ is equal to

$$
e^{iQ_W\theta} \begin{pmatrix} e^{-iQ_1\theta} & & \\ & e^{-iQ_2\theta} & \\ & & \ddots \end{pmatrix} m_\gamma \begin{pmatrix} e^{-iQ_1\theta} & & \\ & e^{-iQ_2\theta} & \\ & & \ddots \end{pmatrix} \qquad (3.37)
$$

where Q_W is the charge of the superspace potential under the R symmetry. Therefore,

$$
\det m_\gamma^\theta = e^{iQ_W N\theta - 2i\theta\sum Q} \det m_\gamma \qquad (3.38)
$$

where $N = \dim m_\gamma$.

The situation is a bit more complicated for mass matrices which receive contributions from vector multiplets. The proof that the determinants and hence the effective determinants have simple phase rotations under the U(1) and R symmetry transformations can readily be extended to these mass matrices. However, since the entries in

the gaugino-chiral fermion mixing rows are actually the complex conjugates of vevs. the determinants of these matrices are not holomorphic. However, in the following we prove that the *effective determinants* of these mass matrices, which include vector multiplets, *are* in fact holomorphic functions of the vevs.

Since the would-be Goldstone fermion states are perpendicular to the massive chiral fermion states, any mass matrix containing gaugino-chiral fermion mixing can be written in the form

$$\begin{pmatrix} 0 & x_1^* & x_2^* & x_3^* & \cdots & x_N^* \\ \overline{x}_1^* & c_{11} & c_{12} & c_{13} & \cdots & c_{1N} \\ \overline{x}_2^* & c_{21} & c_{12} & c_{23} & \cdots & c_{2N} \\ \overline{x}_3^* & c_{31} & c_{12} & c_{33} & \cdots & c_{3N} \\ \vdots & \vdots & \vdots & \vdots & \ddots & \vdots \\ \overline{x}_N^* & c_{N1} & c_{N2} & c_{N3} & \cdots & c_{NN} \end{pmatrix} \tag{3.39}$$

with $\sum_j c_{ij} x_j = 0$ for all i, $\sum_i c_{ij} \bar{x}_i = 0$ for all j, and the c_{ij}s, xs, and $\overline{x}$s are functions of the vevs but not of their conjugates. The rows and columns of the mass matrix can be rearranged so that x_N and $\overline{x}_N$ are not zero. However, the determinant of this matrix can be reduced by elementary row and column operations. Namely, by adding to the last column the second column multiplied by $\frac{x_1}{x_N}$ plus the third column multiplied by $\frac{x_2}{x_N}$, and so forth, the determinant of the mass matrix becomes

$$\begin{vmatrix} 0 & x_1^* & x_2^* & \cdots & x_{N-1}^* & x_N^* + \frac{x_1^* x_1}{x_N} + \ldots + \frac{x_{N-1}^* x_{N-1}}{x_N} \\ \overline{x}_1^* & c_{11} & c_{12} & \cdots & c_{1,N-1} & 0 \\ \overline{x}_2^* & c_{21} & c_{12} & \cdots & c_{2,N-1} & 0 \\ \overline{x}_3^* & c_{31} & c_{12} & \cdots & c_{3,N-1} & 0 \\ \vdots & \vdots & \vdots & \ddots & \vdots & \vdots \\ \overline{x}_N^* & c_{N1} & c_{N2} & \cdots & c_{N,N-1} & 0 \end{vmatrix}$$

Doing the analogous operation on the rows, the determinant becomes

$$\begin{vmatrix} 0 & x_1^* & x_2^* & \cdots & x_{N-1}^* & \frac{1}{x_N} \sum_k^N x_k^* x_k \\ \overline{x}_1^* & c_{11} & c_{12} & \cdots & c_{1,N-1} & 0 \\ \overline{x}_2^* & c_{21} & c_{12} & \cdots & c_{2,N-1} & 0 \\ \vdots & \vdots & \vdots & \ddots & \vdots & \vdots \\ \overline{x}_{N-1}^* & c_{N-1,1} & c_{N-1,2} & \cdots & c_{N-1,N-1} & 0 \\ \frac{1}{\overline{x}_N} \sum_k^N \overline{x}_k^* \overline{x}_k & 0 & 0 & \cdots & 0 & 0 \end{vmatrix}$$

Thus, the determinant is equal to

$$\begin{vmatrix} \frac{\sum_k^N x_k^* x_k}{x_N} & \frac{\sum_k^N \overline{x}_k^* \overline{x}_k}{\overline{x}_N} \\ c_{11} & \cdots & c_{1,N-1} \\ \vdots & \ddots & \vdots \\ c_{N-1,1} & \cdots & c_{N-1,N-1} \end{vmatrix} \tag{3.40}$$

$$= (\sum_k^N x_k^* x_k)(\sum_k^N \overline{x}_k^* \overline{x}_k) f(\text{vevs})$$

where f is a holomorphic function of the vevs. By setting $\overline{v} = v$, $\overline{x}_i$ will equal x_i for all i and the mass of the vector multiplet is $\sqrt{\sum_k^N x_k^* x_k}$. Therefore, the determinant is equal to $M^4_{vector\ multiplet}$ times f and the effective determinant is just the function f. Note, $M_{vector\ multiplet}$ is thus always canceled from the denominator of the effective determinant (eqn. 3.8) and no conjugates of vevs can appear in the effective determinant. Thus, the effective determinants for mass matrices containing gauginos are holomorphic functions of the vevs; just as those discussed earlier for mass matrices which do not have gaugino-chiral fermion mixing entries.

These simple transformation properties of the mass matrices, under U(1) rotations of the vevs, have significant consequences for the form of ϵ_3. Consider the following expression entering ϵ_3 (see eqn. 3.10) —

$$\frac{3}{2}\log\det'\frac{M_g}{M_G} - \frac{3}{2}\log\det'\frac{M_w}{M_G} + \frac{33}{10}\log\det'\frac{M_s}{M_G} - \frac{21}{10}\log\det'\frac{M_\sigma}{M_G} \tag{3.41}$$

$$+\frac{9}{10}\log\det'\frac{M_u}{M_G} + \frac{3}{10}\log\det'\frac{M_e}{M_G} - \frac{6}{5}\log\det'\frac{M_q}{M_G}$$

It is now easy to show that it is invariant under the U(1) and R symmetries. Namely, the U(1) charge of the determinant of M_w (eqn. 3.36) is equal to the charge of the determinant of M_g which is equal to -2 times the sum of U(1) charges of all fields in the 24 representation of SU(5). Therefore, the U(1) rotation of det M_g will cancel the rotation of det M_w in expression, eqn. (3.41). In addition, we note that the

U(1) charges of the effective determinants of $\{M_s, M_\sigma\}$, $\{M_u, M_e\}$, and M_q equal -1 times the sum of U(1) charges of all fields in the {15 and $\overline{15}$}; {10 and $\overline{10}$}, and {10, 15, $\overline{10}$ and $\overline{15}$} representations of SU(5), respectively. Therefore, the U(1) rotation of $\det' M_q$ is canceled by the rotations of the effective determinants of M_u, M_e, M_s, and M_σ in expression, eqn. (3.41). Similar arguments show that the expression in eqn. (3.41) is invariant under an R symmetry rotation. Thus finally we arrive at the conclusion that the expression in eqn. (3.41) is invariant under the U(1) and R symmetries of $W_{sym.breaking}$ for any superspace potential built with 1, 10, 16, $\overline{16}$, 45, and 54 representations of SO(10). Moreover, since expression, eqn. (3.41), is holomorphic, the contribution of the GUT symmetry breaking sector to ϵ_3 is only a function of U(1) and R invariant products of powers of vevs.

The same is not true for the contributions from either the Higgs or fermion mass sectors. This is because both the Higgs and fermion mass sectors contain massless states that must be projected out of the mass matrices before the effective determinants are taken. After this projection, the determinants of the resulting mass matrices are no longer holomorphic functions of the vevs. Nevertheless for the Higgs sector we can prove a similar but limited result, namely, that $g \equiv \frac{\det M[t]}{\det M[d]} = g(\zeta_1, \cdots, \zeta_m)$; i.e., g is a function of U(1) invariants only. By eqns. (3.36) and (3.38), we see that $\det M[t]$ and $\det M[d]$ transform in the same way under the U(1) and R symmetries; therefore the ratio is invariant.

CHAPTER 4

CALCULATION OF RATES OF BARYON NUMBER VIOLATING NUCLEON DECAY

In the previous chapter, we saw that the nucleon decay amplitude is directly proportional to the inverse of an effective color triplet Higgs mass $\tilde{M}_t$ (resulting from effective dimension 5 baryon number violating operators) multiplied by a product of the Yukawa couplings of this color triplet Higgs to quarks and leptons. Thus, obtaining a theoretical prediction for nucleon decay rates depends critically on two factors:

1. obtaining bounds on the effective color triplet mass, and

2. predictions for the relevant Yukawa couplings.

   The nucleon decay branching ratios are sensitive to these color triplet Higgs-quark-quark and Higgs-quark-lepton Yukawa couplings. These couplings are completely determined in any *predictive theory* of fermion masses and mixing angles, but they are typically **NOT** identical to the Yukawa couplings responsible for quark and lepton masses.

In addition, one must take these effective dimension 5 operators and renormalize them from M_{GUT} to M_Z. Then, at the weak scale, effective dimension 6 operators

are obtained by closing the squark and/or slepton lines into a loop via chargino or gluino exchanges. Hence the decay rate depends sensitively on soft SUSY breaking parameters. Finally the effective dimension 6 operators are renormalized from M_Z to the nucleon mass and then an effective chiral Lagrangian analysis is used to obtain lifetimes and branching ratios.

In this chapter, we present the details of our calculations of the nucleon decay rates for model 4(c), which includes the additional "13" mass operator. Our main results for the predictions of the proton and neutron decay rates and branching ratios in model 4(c) are found in Tables 4.4, 4.5, and 4.13.

In addition we have studied the sensitivity of our predictions to different factors. We have compared the predictions for our model 4(c) to those of models 4(a) through (f) of ADHRS. This tests the sensitivity of the predicted branching ratios to the quality of the fit for fermion masses and mixing angles. We find that branching ratios can differ by factors as large as 10.

We have also compared the predictions of our models with those of small $\tan\beta$ minimal SUSY SU(5) GUTs. We find that some results in the large $\tan\beta$ regime are qualitatively different than for small $\tan\beta$. For example, certain dimension 6 operators with the chiral structure[9] LLRR tend to dominate over their LLLL counterparts for $\mu(M_Z)/m_{1/2} > 1$. In this limit, the ratio τ_p/τ_n, for example, is sensitive to the quality of the fermion mass fit and is substantially larger than what it is in small $\tan\beta$ SUSY GUTs.

[9]LLLL, LLRR, and RRRR refer to four-fermion operators pairing four left-handed Weyl fermions, pairing two left handed Weyl fermions and the conjugates of two right-handed Weyl fermions, and pairing the conjugates of four right-handed Weyl fermions, respectively. Specific examples of each type of four-fermion operator can be found in Table 4.3, infra.

Finally we discuss the sensitivity of our predictions to neglecting either the gluino or chargino exchange diagrams. We find both contributions to be significant.

The chapter is organized as follows — in sections 4.1, 4.2, and 4.3 we discuss the calculational ingredients. Namely, in section 4.1, we discuss physics from M_{GUT} to M_Z; in section 4.2, SUSY loops at M_Z and the resulting dimension 6 baryon violating operators: and in section 4.3, the physics from M_Z to the nucleon mass and a summary of the numerical procedure and our results. In section 4.4, we discuss our results and the aforementioned sensitivities to different factors.

4.1 The low energy effective operators generating nucleon decay, and their renormalization

At low energies, the $\mathcal{O}_{33}$, $\mathcal{O}_{23}$, $\mathcal{O}_{22}$, $\mathcal{O}_{12}$, and $\mathcal{O}_{13}$ operators of model 4(c) produce effective operators which generate the fermion masses and which are responsible for baryon-number violating nucleon decay.

$$\mathcal{O}_{33} + \mathcal{O}_{23} + \mathcal{O}_{22} + \mathcal{O}_{12} + \mathcal{O}_{13}$$

$$\Longrightarrow$$

$$H_u Q Y_u \overline{U} + H_d Q Y_d \overline{D} + H_d L Y_e \overline{E} + Q \tfrac{1}{2} c_{qq} Q T + Q c_{ql} L \overline{T} + \overline{U} c_{ud} \overline{D} \overline{T} + \overline{U} c_{ue} \overline{E} T$$

$$\Longrightarrow$$

$$H_u Q Y_u \overline{U} + H_d Q Y_d \overline{D} + H_d L Y_e \overline{E} + \tfrac{1}{\tilde{M}_t} Q \tfrac{1}{2} c_{qq} Q \; Q c_{ql} L + \tfrac{1}{\tilde{M}_t} \overline{U} c_{ud} \overline{D} \; \overline{U} c_{ue} \overline{E}$$

with T and $\overline{T}$ being the color triplet Higgses from 10_1. At the GUT scale,

$$Y_u = \begin{pmatrix} 0 & C & u_u D e^{i\delta} \\ C & 0 & -\frac{1}{3}B \\ u'_u D e^{i\delta} & -\frac{4}{3}B & A \end{pmatrix}$$

$$Y_d = \begin{pmatrix} 0 & -27C & u_d D e^{i\delta} \\ -27C & E e^{i\phi} & \frac{1}{9}B \\ u'_d D e^{i\delta} & -\frac{2}{9}B & A \end{pmatrix}$$

model	y_{qq}	y_{ql}	y_{ud}	y_{ue}
a	$-3/4$	$3/4$	$-5/4$	$-3/4$
b	$-3/2$	$5/2$	$1/2$	$-3/2$
c	$-1/2$	$3/2$	$-1/2$	$-1/2$
d	$3/2$	$3/2$	$-1/2$	$3/2$
e	$1/2$	$5/2$	$1/2$	$1/2$
f	$9/4$	$3/4$	$-5/4$	$9/4$

Table 4.1: y Clebsches for each version of model 4

model	u_u	u'_u	u_d	u'_d	u_e	u'_e	u_{qq}	u_{ql}	u'_{ql}	u_{ud}	u'_{ud}	u_{ue}	u'_{ue}
a	$-4/3$	$1/3$	-2	-9	-54	3	$1/3$	3	-9	-2	36	2	$-4/3$
b	0	0	0	0	0	0	0	0	0	0	0	0	0
c	$-4/3$	$1/3$	$2/3$	-9	-54	-1	$1/3$	-1	-9	$2/3$	36	2	$-4/3$

Table 4.2: u Clebsches for models 4(a) through (c)

$$
\begin{aligned}
Y_e &= \begin{pmatrix} 0 & -27C & u_e De^{i\delta} \\ -27C & 3Ee^{i\phi} & B \\ u'_e De^{i\delta} & 2B & A \end{pmatrix} \\
c_{qq} &= \begin{pmatrix} 0 & C & u_{qq} De^{i\delta} \\ C & y_{qq} Ee^{i\phi} & \frac{1}{3}B \\ u_{qq} De^{i\delta} & \frac{1}{3}B & A \end{pmatrix} \\
c_{ql} &= \begin{pmatrix} 0 & -27C & u_{ql} De^{i\delta} \\ -27C & y_{ql} Ee^{i\phi} & \frac{1}{3}B \\ u'_{ql} De^{i\delta} & \frac{1}{3}B & A \end{pmatrix} \\
c_{ud} &= \begin{pmatrix} 0 & -27C & u_{ud} De^{i\delta} \\ -27C & y_{ud} Ee^{i\phi} & -\frac{4}{9}B \\ u'_{ud} De^{i\delta} & \frac{2}{9}B & A \end{pmatrix} \\
c_{ue} &= \begin{pmatrix} 0 & C & u_{ue} De^{i\delta} \\ C & y_{ue} Ee^{i\phi} & -4B \\ u'_{ue} De^{i\delta} & -2B & A \end{pmatrix}
\end{aligned}
\tag{4.1}
$$

with the values of the Clebsches given in Tables 4.1 and 4.2.

Note that in a predictive theory for fermion masses, there are no arbitrary phases in the Yukawa matrices.[10] The two possible phases in model 4c are fixed when fitting fermion masses and mixing angles.

These matrices need to be renormalized from the GUT scale to the electroweak scale. Due to the no-renormalization theorems of supersymmetry, only wavefunction renormalizations enter into the calculation of the renormalization group equations of these matrices. The RGEs for the matrices are

$$\begin{aligned}
\frac{dc_{qq}}{dt} &= \frac{1}{16\pi^2}[(Y_u Y_u^\dagger + Y_d Y_d^\dagger)c_{qq} + c_{qq}(Y_u Y_u^\dagger + Y_d Y_d^\dagger)^T \\
&\quad -(\frac{16}{3}g_3^2 + 3g_2^2 + \frac{1}{15}g_1^2)c_{qq}] \\
\frac{dc_{ql}}{dt} &= \frac{1}{16\pi^2}[(Y_u Y_u^\dagger + Y_d Y_d^\dagger)c_{ql} + c_{ql}(Y_e Y_e^\dagger)^T \\
&\quad -(\frac{8}{3}g_3^2 + 3g_2^2 + \frac{1}{3}g_1^2)c_{ql}] \\
\frac{dc_{ud}}{dt} &= \frac{1}{16\pi^2}[2(Y_u^\dagger Y_u)^T c_{ud} + 2c_{ud}Y_d^\dagger Y_d - (\frac{16}{3}g_3^2 + \frac{2}{3}g_1^2)c_{ud}] \\
\frac{dc_{ue}}{dt} &= \frac{1}{16\pi^2}[2(Y_u^\dagger Y_u)^T c_{ue} + 2c_{ue}Y_e^\dagger Y_e - (\frac{8}{3}g_3^2 + \frac{26}{15}g_1^2)c_{ue}]
\end{aligned} \tag{4.2}$$

with $t = \log(\mu/M_Z)$.

4.2 Nucleon decay formulas

4.2.1 Gluino diagrams

Figure 4.1 shows the two diagrams which contribute to the four-fermion operator $C_{ijkl}^{(ud)(d\nu)[G]}(u_i^\alpha d_j^\beta)(d_k^\gamma \nu_l)\epsilon_{\alpha\beta\gamma}$. Calculating these two diagrams, we find

$$C_{ijkl}^{(ud)(d\nu)[G]} = \tfrac{4}{3}\tfrac{1}{16\pi^2 M_t}g_3^2\{\Gamma_{U,L\,\lambda i}\Gamma^*_{U,L\,\lambda i'}\Gamma_{D,L\,\rho j}\Gamma^*_{D,L\,\rho j'}\hat{c}_{qq}{}^{i'[j'}\hat{c}_{ql}{}^{k]l}m_{\tilde{g}}I(\tilde{g},\tilde{u}_\lambda,\tilde{d}_\rho)-$$

[10]This is in contrast to the generic, minimal SU(5) model in which no assumptions are made about the form of the Yukawa matrices other than those imposed by the SU(5) symmetry. When no assumptions are made about the form of the Yukawa matrices in a minimal SU(5) model, there are two arbitrary phases in the Yukawa sector which do not enter into fermion masses and mixing angles but which do enter into nucleon decay. See, e.g., ref. [43] and [24]. Because of the form of the Yukawa matrices in our model, there are no such arbitrary phases.

$$\Gamma_{D,L\,\rho j}\Gamma^{*}_{D,L\,\rho j'}\Gamma_{D,L\,\sigma k}\Gamma^{*}_{D,L\,\sigma k'}\hat{c}_{qq}{}^{i[j'}\hat{c}_{ql}{}^{k']l}m_{\tilde{g}}I(\tilde{g},\tilde{d}_{\rho},\tilde{d}_{\sigma})\}$$

where α, β, and γ are color indices, i, i', j, j', k, and l are fermion flavor indices, ρ and λ are squark flavor indices, $\hat{c}_{qq} = S_u c^R_{qq} S^T_d$, $\hat{c}_{ql} = S_d c^R_{ql} S^T_e$ with c^R_{qq} and c^R_{ql} being c_{qq} and c_{ql}, respectively, renormalized to M_Z, and

$$I(a,b,c) = \frac{m_a^2 \log m_a^2}{(m_a^2 - m_b^2)(m_a^2 - m_c^2)} + \frac{m_b^2 \log m_b^2}{(m_b^2 - m_c^2)(m_b^2 - m_a^2)} + \frac{m_c^2 \log m_c^2}{(m_c^2 - m_a^2)(m_c^2 - m_b^2)}$$

where m_a equals the mass of particle a, etc.[11] All other notation follows that given in Appendix A.

By similar calculations, we can construct the remaining four-fermion operators listed in Table 4.3. Note, we also use Table 4.3 to define our notation for these four-fermion operators. The C_{ijkl}s for these operators are

$$C^{(ud)(ue)[G]}_{ijkl} = -\tfrac{4}{3}\tfrac{1}{16\pi^2\tilde{M}_t}g_3^2\{\Gamma_{U,L\,\lambda i}\Gamma^{*}_{U,L\,\lambda i'}\Gamma_{D,L\,\rho j}\Gamma^{*}_{D,L\,\rho j'}\hat{c}_{qq}{}^{[i'j'}\check{c}_{ql}{}^{k]l}m_{\tilde{g}}I(\tilde{g},\tilde{u}_{\lambda},\tilde{d}_{\rho}) -$$

$$\Gamma_{U,L\,\lambda i}\Gamma^{*}_{U,L\,\lambda i'}\Gamma_{U,L\,\sigma k}\Gamma^{*}_{U,L\,\sigma k'}\hat{c}_{qq}{}^{[i'j}\check{c}_{ql}{}^{k']l}m_{\tilde{g}}I(\tilde{g},\tilde{u}_{\lambda},\tilde{u}_{\sigma})\}$$

$$C^{(\overline{dd})(u\nu)[G]}_{ijkl} = \frac{4}{3}\frac{1}{16\pi^2\tilde{M}_t}g_3^2\Gamma_{D,R\,\rho j}\Gamma^{*}_{D,L\,\rho j'}\Gamma_{D,R\,\sigma k}\Gamma^{*}_{D,L\,\sigma k'}\hat{c}_{qq}{}^{i[j'}\check{c}_{ql}{}^{k']l}m_{\tilde{g}}I(\tilde{g},\tilde{d}_{\rho},\tilde{d}_{\sigma})$$

$$C^{(\overline{ud})(d\nu)[G]}_{ijkl} = \frac{4}{3}\frac{1}{16\pi^2\tilde{M}_t}g_3^2\Gamma_{U,R\,\lambda i}\Gamma^{*}_{U,L\,\lambda i'}\Gamma_{D,R\,\rho j}\Gamma^{*}_{D,L\,\rho j'}\hat{c}_{qq}{}^{i[j'}\check{c}_{ql}{}^{k]l}m_{\tilde{g}}I(\tilde{g},\tilde{u}_{\lambda},\tilde{d}_{\rho})$$

$$C^{(\overline{ud})(ue)[G]}_{ijkl} = -\frac{4}{3}\frac{1}{16\pi^2\tilde{M}_t}g_3^2\Gamma_{U,R\,\lambda i}\Gamma^{*}_{U,L\,\lambda i'}\Gamma_{D,R\,\rho j}\Gamma^{*}_{D,L\,\rho j'}\hat{c}_{qq}{}^{[i'j'}\check{c}_{ql}{}^{k]l}m_{\tilde{g}}I(\tilde{g},\tilde{u}_{\lambda},\tilde{d}_{\rho})$$

$$C^{(ud)(\overline{ue})[G]}_{ijkl} = -\frac{4}{3}\frac{1}{16\pi^2\tilde{M}_t}g_3^2\Gamma_{U,L\,\lambda i}\Gamma^{*}_{U,R\,\lambda i'}\Gamma_{D,L\,\rho j}\Gamma^{*}_{D,R\,\rho j'}\hat{c}^{*}_{ud}{}^{[i'j'}\hat{c}^{*}_{ue}{}^{k]l}m_{\tilde{g}}I(\tilde{g},\tilde{u}_{\lambda},\tilde{d}_{\rho})$$

$$C^{(\overline{ud})(\overline{ue})[G]}_{ijkl} = -\tfrac{4}{3}\tfrac{1}{16\pi^2\tilde{M}_t}g_3^2\{\Gamma_{U,R\,\lambda i}\Gamma^{*}_{U,R\,\lambda i'}\Gamma_{D,R\,\rho j}\Gamma^{*}_{D,R\,\rho j'}\hat{c}^{*}_{ud}{}^{[i'j'}\hat{c}^{*}_{ue}{}^{k]l}m_{\tilde{g}}I(\tilde{g},\tilde{u}_{\lambda},\tilde{d}_{\rho}) -$$

$$\Gamma_{U,R\,\lambda i}\Gamma^{*}_{U,R\,\lambda i'}\Gamma_{U,R\,\sigma k}\Gamma^{*}_{U,R\,\sigma k'}\hat{c}^{*}_{ud}{}^{[i'j}\hat{c}^{*}_{ue}{}^{k']l}m_{\tilde{g}}I(\tilde{g},\tilde{u}_{\lambda},\tilde{u}_{\sigma})\}$$

where $\check{c}_{ql} = S_u c^R_{ql} S^T_e$, $\hat{c}_{ud} = T^T_u c^R_{ud} T_d$, and $\hat{c}_{ue} = T^T_u c^R_{ue} T_e$ with c^R_{ud} and c^R_{ue} being c_{ud} and c_{ue}, respectively, renormalized to M_Z.

[11] We use a notation for antisymmetrization on tensor indices in which $A_{i[jkl]mn}$ is equal to $A_{ijklmn} - A_{iljkmn}$, and so forth.

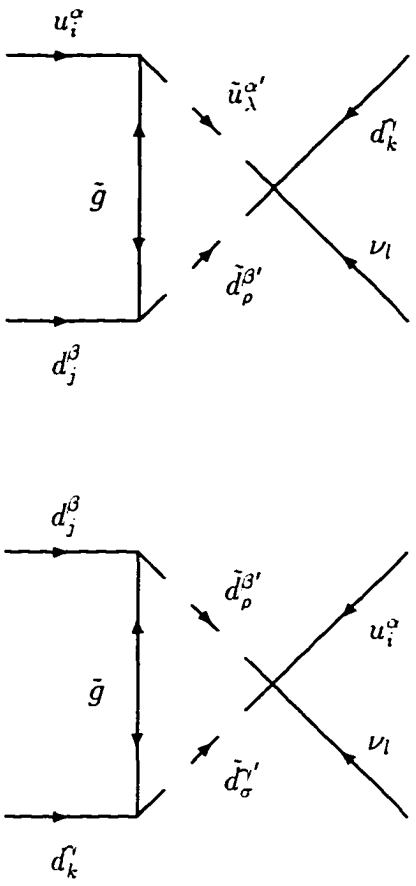

Figure 4.1: The one-loop gluino diagrams contributing to $C_{ijkl}^{(ud)(d\nu)[G]}$

operator type		
LLLL	LLRR	RRRR
$C_{ijkl}^{(ud)(d\nu)[G]}(u_i^\alpha d_j^\beta)(d_k^\gamma \nu_l)\epsilon_{\alpha\beta\gamma}$	$C_{ijkl}^{(\overline{dd})(u\nu)[G]}(\overline{d_j^{*\beta}}\,\overline{d_k^{*\gamma}})(u_i^\alpha \nu_l)\epsilon_{\alpha\beta\gamma}$ $C_{ijkl}^{(\overline{ud})(d\nu)[G]}(\overline{u_i^{*\alpha}}\,\overline{d_j^{*\beta}})(d_k^\gamma \nu_l)\epsilon_{\alpha\beta\gamma}$	
$C_{ijkl}^{(ud)(ue)[G]}(u_i^\alpha d_j^\beta)(u_k^\gamma e_l)\epsilon_{\alpha\beta\gamma}$	$C_{ijkl}^{(\overline{ud})(ue)[G]}(\overline{u_i^{*\alpha}}\,\overline{d_j^{*\beta}})(u_k^\gamma e_l)\epsilon_{\alpha\beta\gamma}$ $C_{ijkl}^{(ud)(\overline{ue})[G]}(u_i^\alpha d_j^\beta)(\overline{u_k^{*\gamma}}\,\overline{e_l^*})\epsilon_{\alpha\beta\gamma}$	$C_{ijkl}^{(\overline{ud})(\overline{ue})[G]}(\overline{u_i^{*\alpha}}\,\overline{d_j^{*\beta}})(\overline{u_k^{*\gamma}}\,\overline{e_l^*})\epsilon_{\alpha\beta\gamma}$

Table 4.3: Table of all gluino-dressed four fermion operators relevant to nucleon decay

As observed in ref. [34], the contribution of gluino dressed operators is zero in the limit that all squarks are degenerate at the electroweak scale. In this analysis, however, squarks and sleptons are assumed degenerate at M_{GUT} and as a consequence of renormalization group running they are explicitly non-degenerate at the weak scale. Thus we retain the gluino contribution in our analysis.

In principle, we could also have four-fermion operators like $C_{ijkl}^{(\overline{uu})(de)[G]}(\overline{u_i^{c\alpha}}\overline{u_k^{c\gamma}}) \times (d_j^{\beta}e_l)\epsilon_{\alpha\beta\gamma}$ pairing two up type quarks in a Weyl index contracted pair. However, since we are only interested in the first generation of up quarks, the portions of these operators that would be relevant to nucleon decay are identically zero.

4.2.2 Chargino diagrams

Using the vertices in Appendix B, the chargino diagrams can be readily computed. According to analyses by many other authors on proton decay in SUSY GUTs, the dominant operators would be expected to be the LLLL operators, i.e. $C_{ijkl}^{(ud)(d\nu)[W]} \times (u_i^{\alpha}d_j^{\beta})(d_k^{\gamma}\nu_l)\epsilon_{\alpha\beta\gamma}$ and $C_{ijkl}^{(ud)(ue)[W]}(u_i^{\alpha}d_j^{\beta})(u_k^{\gamma}e_l)\epsilon_{\alpha\beta\gamma}$. The C_{ijkl}s for these operators are equal to

$$
\begin{aligned}
C_{ijkl}^{(ud)(d\nu)[W]} = \frac{1}{16\pi^2 M_t}\Big\{ & [(g_2\Gamma_{D,L}U_{-\,1n} - \Gamma_{D,R}\hat{Y}_d\ U_{-\,2n})V_{KM}^{\dagger}]_{\rho i} \\
& \times [(g_2\Gamma_{U,L}U_{+\,1n} - \Gamma_{U,R}\hat{Y}_u\ U_{+\,2n})V_{KM}]_{\lambda j} \\
& \times \Gamma^{*}_{U,L\,\lambda i'}\Gamma^{*}_{D,L\,\rho j'}\hat{c}_{qq}{}^{i'[j'}\hat{c}_{ql}{}^{k]l}m_{\tilde{\chi}_n}I(\tilde{\chi}_n, \tilde{u}_{\lambda}, \tilde{d}_{\rho}) \\
& + [(g_2\Gamma_{U,L}U_{+\,1n} - \Gamma_{U,R}\hat{Y}_u\ U_{+\,2n})V_{KM}]_{\lambda k} \\
& \times [(g_2\Gamma_{E,L}U_{-\,1n} - \Gamma_{E,R}\hat{Y}_e\ U_{-\,2n})]_{\rho l} \\
& \times \Gamma^{*}_{U,L\,\lambda k'}\Gamma^{*}_{E,L\,\rho l'}\hat{c}_{qq}{}^{[ij}\hat{c}_{ql}{}^{k']l'}m_{\tilde{\chi}_n}I(\tilde{\chi}_n, \tilde{u}_{\lambda}, \tilde{e}_{\rho})\Big\}
\end{aligned}
$$

$$C_{ijkl}^{(ud)(ue)[W]} = -\frac{1}{16\pi^2 M_t}\Big\{[(g_2\Gamma_{D,L}U_{-\,1n} - \Gamma_{D,R}\hat{Y}_d\ U_{-\,2n})V_{KM}^\dagger]_{\rho i}$$
$$\times[(g_2\Gamma_{U,L}U_{+\,1n} - \Gamma_{U,R}\hat{Y}_u\ U_{+\,2n})V_{KM}]_{\lambda j}$$
$$\times\Gamma^*_{U,L\,\lambda i'}\Gamma^*_{D,L\,\rho j'}\hat{c}_{qq}{}^{[i'j'}\hat{c}_{ql}{}^{k]l}m_{\tilde{\chi}_n}I(\tilde{\chi}_n,\tilde{u}_\lambda,\tilde{d}_\rho)$$
$$+[(g_2\Gamma_{D,L}U_{-\,1n} - \Gamma_{D,R}\hat{Y}_d\ U_{-\,2n})V_{KM}^\dagger]_{\rho k}$$
$$\times g_2\Gamma_{\nu\,\lambda l}U_{+\,1n}\Gamma^*_{D,L\,\rho k'}\Gamma^*_{\nu\,\lambda l'}\hat{c}_{qq}{}^{i[j}\hat{c}_{ql}{}^{k']l'}m_{\tilde{\chi}_n}I(\tilde{\chi}_n,\tilde{d}_\rho,\tilde{\nu}_\lambda)\Big\} \tag{4.3}$$

The C_{ijkl}s for the LLRR and RRRR operators are

$$C_{ijkl}^{(\overline{ud})(d\nu)[W]} = \frac{1}{16\pi^2 M_t}\Big\{U^*_{+\,2n}(\Gamma_{D,L}V_{KM}^\dagger\hat{Y}_u)_{\rho i}U^*_{-\,2n}(\Gamma_{U,L}V_{KM}\hat{Y}_d)_{\lambda j}$$
$$\times\Gamma^*_{U,L\,\lambda i'}\Gamma^*_{D,L\,\rho j'}\hat{c}_{qq}{}^{i'[j'}\hat{c}_{ql}{}^{k]l}m_{\tilde{\chi}_n}I(\tilde{\chi}_n,\tilde{u}_\lambda,\tilde{d}_\rho)$$
$$+[(g_2\Gamma_{U,L}U_{+\,1n} - \Gamma_{U,R}\hat{Y}_u\ U_{+\,2n})V_{KM}]_{\lambda k}$$
$$\times[(g_2\Gamma_{E,L}U_{-\,1n} - \Gamma_{E,R}\hat{Y}_e\ U_{-\,2n})]_{\rho l}$$
$$\times\Gamma^*_{U,R\,\lambda k'}\Gamma^*_{E,R\,\rho l'}\hat{c}^*_{ud}{}^{[ij}\hat{c}^*_{ue}{}^{k']l'}m_{\tilde{\chi}_n}I(\tilde{\chi}_n,\tilde{u}_\lambda,\tilde{e}_\rho)\Big\} \tag{4.4}$$

$$C_{ijkl}^{(ud)(\overline{ue})[W]} = -\frac{1}{16\pi^2 M_t}\Big\{[(g_2\Gamma_{D,L}U_{-\,1n} - \Gamma_{D,R}\hat{Y}_d\ U_{-\,2n})V_{KM}^\dagger]_{\rho i}$$
$$\times[(g_2\Gamma_{U,L}U_{+\,1n} - \Gamma_{U,R}\hat{Y}_u\ U_{+\,2n})V_{KM}]_{\lambda j}$$
$$\times\Gamma^*_{U,R\,\lambda i'}\Gamma^*_{D,R\,\rho j'}\hat{c}^*_{ud}{}^{[i'j'}\hat{c}^*_{ue}{}^{k]l}m_{\tilde{\chi}_n}I(\tilde{\chi}_n,\tilde{u}_\lambda,\tilde{d}_\rho)$$
$$+U^*_{+\,2n}(\Gamma_{D,L}V_{KM}^\dagger\hat{Y}_u)_{\rho k}U^*_{-\,2n}(\Gamma_\nu\hat{Y}_e)_{\lambda l}$$
$$\times\Gamma^*_{D,L\,\rho k'}\Gamma^*_{\nu\,\lambda l'}\hat{c}_{qq}{}^{i[j}\hat{c}_{ql}{}^{k']l'}m_{\tilde{\chi}_n}I(\tilde{\chi}_n,\tilde{d}_\rho,\tilde{\nu}_\lambda)\Big\} \tag{4.5}$$

$$C_{ijkl}^{(\overline{ud})(ue)[W]} = -\frac{1}{16\pi^2 M_t}\Big\{U^*_{+\,2n}(\Gamma_{D,L}V_{KM}^\dagger\hat{Y}_u)_{\rho i}U^*_{-\,2n}(\Gamma_{U,L}V_{KM}\hat{Y}_d)_{\lambda j}$$
$$\times\Gamma^*_{U,L\,\lambda i'}\Gamma^*_{D,L\,\rho j'}\hat{c}_{qq}{}^{[i'j'}\hat{c}_{ql}{}^{k]l}m_{\tilde{\chi}_n}I(\tilde{\chi}_n,\tilde{u}_\lambda,\tilde{d}_\rho)\Big\} \tag{4.6}$$

$$C_{ijkl}^{(\overline{ud})(\overline{ue})[W]} = -\frac{1}{16\pi^2 M_t}\Big\{U^*_{+\,2n}(\Gamma_{D,L}V^\dagger_{KM}\hat{Y}_u)_{\rho i}U^*_{-\,2n}(\Gamma_{U,L}V_{KM}\hat{Y}_d)_{\lambda j}$$
$$\times\Gamma^*_{U,R\,\lambda i'}\Gamma^*_{D,R\,\rho j'}\hat{c}^{*\,[i'j']}_{ud}\hat{c}^{*\,k]l}_{ue}m_{\tilde{\chi}_n}I(\tilde{\chi}_n,\tilde{u}_\lambda,\tilde{d}_\rho)\Big\} \qquad (4.7)$$

4.2.3 Neutralino contribution

The neutralino contribution has the same flavor structure as that of gluinos. However it is suppressed by a factor of $\frac{3\alpha_2}{8\alpha_3} \sim \frac{1}{10}$ compared to gluinos. We have neglected this contribution in our calculations.

4.3 Numerical procedure and results

In calculating the following nucleon decay rates, we make the standard universality assumptions about the soft SUSY parameters at M_{GUT},[35] except that we allow non-universal values for M_{H_u} and M_{H_d}.[12] We have also taken all the SUSY breaking parameters at M_G to be real.[13] We define M_{GUT} such that $\alpha_1 = \alpha_2 \equiv \tilde{\alpha}_{GUT}$ at M_{GUT} and define ϵ_3, representing the contribution of GUT scale threshold corrections to the gauge couplings, to be $(\alpha_3(M_{GUT}) - \tilde{\alpha}_{GUT})/\tilde{\alpha}_{GUT}$. The dimensionless (dimensionful) parameters are renormalized at two (one) loops to M_Z using the renormalization

[12]Note that if the messenger scale of SUSY breaking is M_{Planck} then our analysis is not completely self-consistent. In any complete SUSY GUT defined up to an effective cut-off scale $M > M_G$, the interactions above M_G will renormalize the soft breaking parameters. This will, in general, split the degeneracy of squark and slepton masses at M_G even if they are degenerate at M. On the other hand, bounds on flavor changing neutral current processes, severely constrain the magnitude of possible splitting. Thus these corrections must be small. In addition, in theories where SUSY breaking is mediated by gauge exchanges with a messenger scale below (but near) M_G, the present analysis is expected to apply unchanged. Since in this case squarks and sleptons will be nearly degenerate at the messenger scale. The Higgs masses, on the other hand, are probably dominated by new interactions which also generate a μ term. It is thus plausible to expect the Higgs masses to be split and independent of squark and slepton masses. The parameter A_0 could also be universal at the messenger scale.

[13]Complex phases would introduce new CP violating effects. Limits on the electron or neutron electric dipole moments, however, constrain these phases to be small.

group equations of Martin and Vaughn [36], except that c_{qq}, c_{ql}, c_{ud}, and c_{ue} are renormalized at one loop using the equations of this chapter.

Renormalization of the C_{ijkl}s from M_Z to 1 GeV is taken into account by multiplying them by the A_L calculated in [37], and then chiral Lagrangian techniques [38] are used to obtain nucleon decay amplitudes. Formulas for nucleon decay rates in terms of the chiral Lagrangian parameters are contained in Appendix D.

The decay rates depend heavily on the chiral Lagrangian factors α and β where

$$\beta U(\mathbf{k}) = \epsilon_{\alpha\beta\gamma}\langle 0|(u^\alpha d^\beta)u^\gamma|\text{proton}(\mathbf{k})\rangle,$$

$$\alpha U(\mathbf{k}) = \epsilon_{\alpha\beta\gamma}\langle 0|(\overline{u}^\alpha \overline{d}^\beta)u^\gamma|\text{proton}(\mathbf{k})\rangle$$

and $U(\mathbf{k})$ is the left handed component of the proton's wavefunction. See, e.g., ref. [39]. It is known that $|\beta| = |\alpha|$ [39, 40] and that $|\beta|$ ranges from .003 to .03 GeV^3 [41]. Lattice calculations have not reduced the uncertainty in $|\beta|$; lattice calculations have reported $|\beta|$ as low as .006 GeV^3 [40] and as high as .03 GeV^3 [42]. Additionally, the phase between α and β is not widely reported, although a relatively recent lattice calculation suggests that $\beta = -\alpha$ [40]. Therefore, we have left the phase between α and β a free variable, and report three values for many of the quantities predicted in our tables. Namely, the max (min) referred to in the tables is the value for the quantity predicted when the phase between α and β is such that the quantity is maximized (minimized). Hence, each entry in the max and min columns uses a different value of $\arg(\beta/\alpha)$.

In the following tables, we have calculated decay rates using $\tilde{M}_t = 10^{19}$ GeV and $|\beta| = .003$ GeV^3. In the previous chapter, we argued that it seems unnatural to have $\tilde{M}_t$ much bigger than $\approx 10^{19}$ GeV. Therefore, the values presented in the tables are

roughly upper bounds on the nucleons' lifetimes, based on naturalness[14]. Since all decay rates scale as $(\frac{|\beta|}{.003\ \mathrm{GeV}^3}\frac{10^{19}\ \mathrm{GeV}}{\tilde{M}_t})^2$, the lifetimes for different values of $\tilde{M}_t$ and $|\beta|$ can easily be extracted from the tables.

In Tables 4.4 through 4.13, we calculate nucleon decay using model 4(c) (including the $\mathcal{O}_{13}$ operator), since it appears to be the model which best fits the low energy data [25]. Initial values for the dimensionless Yukawa parameters; soft SUSY parameters; and M_{GUT}, $\tilde{\alpha}_{GUT}$, and $\tan\beta$ are taken from the global χ^2 analysis of Blažek et al. [25]. This global χ^2 analysis shows that these values of the GUT parameters are consistent with electroweak symmetry breaking and the experimental bounds on the sparticle masses; and that, for the particular values of the soft SUSY breaking parameters used, these parameters give the best global fit to 20 low energy observables, including experimental measurements for the gauge couplings; fermion masses and mixing angles; and $b \to s\gamma$. The main results of [25] for model 4(c) — the plot of χ^2 contours in the $m_0 - m_{1/2}$ plane for various values of μ — have been reprinted in 4.2. We present nucleon decay results at five representative points, labeled I,II, and III(1,2,3), chosen near the χ^2/d.o.f. = 1 border, with χ^2/d.o.f. $< 1\frac{1}{3}$ for all points. Points I and II give nucleon decay results typical of a low m_0 scenario, while points III(1,2,3) give results typical of a high m_0, low $m_{1/2}$ scenario. In addition, the series of points III(1,2,3) were chosen in order to demonstrate the effect of varying the ratio $\mu/m_{1/2}$.

[14]A note of caution - it was also shown in ref. [40] that chiral Lagrangian techniques overestimate the amplitude $\epsilon_{\alpha\beta\gamma}<\pi^0|(u^\alpha d^\beta)u^\gamma|p>$ by at least a factor of 2.4 (for $\beta = 0.006$). Thus the proton decay rate is overestimated by almost a factor of 6 or more in this case. As a result, for any given $|\beta|$, the actual nucleon lifetimes for that β, could be a factor of 6 or more larger than the results reported here, as extrapolated from our tables for that value of $|\beta|$. These remarks are indicative of the theoretical uncertainty in the calculation due to strong interaction effects.

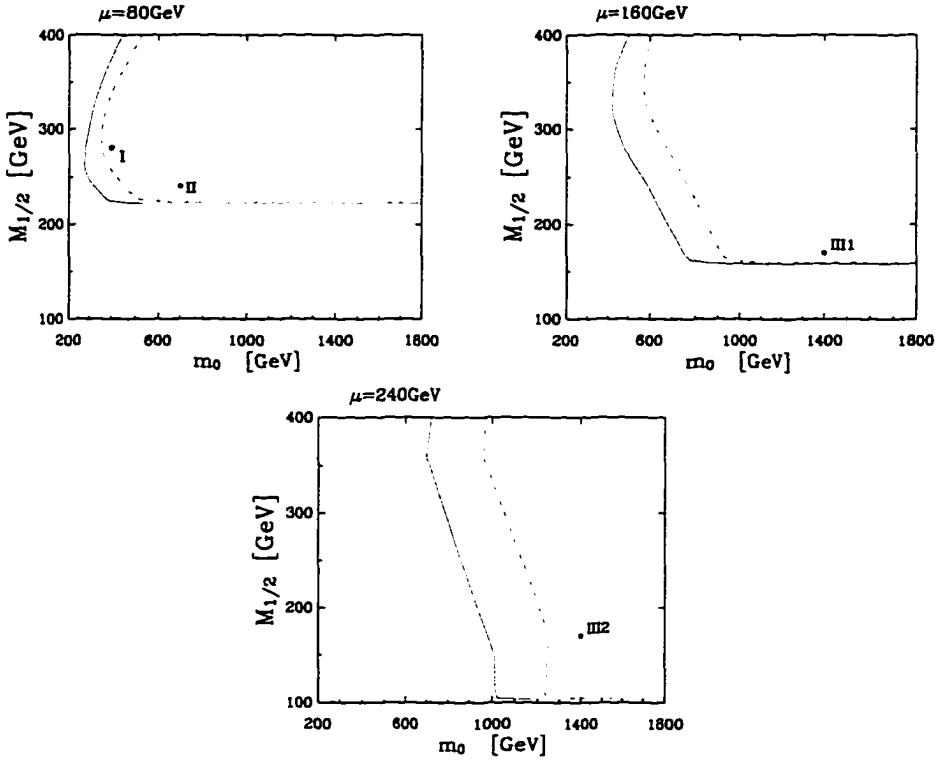

Figure 4.2: Results of the global χ^2 analysis of Blazek, et al. for model 4(c), plotted in the $m_0 - m_{1/2}$ plane for $\mu = 80$ GeV, 160 GeV, and 240 GeV. The solid, double-dashed-dotted, and dotted lines represent contour lines of constant χ^2, with χ^2/d.o.f. = 2.1, and $\frac{1}{2}$, respectively. Points I,II, and III(1,2), at which we present nucleon decay results for model 4(c), are also shown in the figure.

Tables 4.4 and 4.5 contain the lifetimes for $p \to K^+\overline{\nu}$ and $n \to K^0\overline{\nu}$ and compares these rates with the rates of decay into the other significant decay modes involving spin zero mesons, for various values of the GUT scale parameters. These are the main results of this chapter. Note however that only the three or four most significant decay modes are included in these tables.

In the subsequent tables we evaluate the relative contributions to these rates from different sources - (LLRR vs. LLLL operators) or (gluinos vs. charginos). Tables 4.6, 4.7, 4.8, and 4.9 compare the contributions of chargino and gluino diagrams to the total decay rate. Table 4.10 compares the contribution of LLLL versus LLRR operators for decays into anti-neutrinos, for each of the three anti-neutrino species. Tables 4.11 and 4.12 compare the relative importance of each generation of anti-neutrino to the total proton decay rate, for decay modes involving anti-neutrinos. Finally, Table 4.13 contains the values of the GUT scale parameters for points I,II, and III(1,2,3) of Tables 4.4 through 4.12.

Tables 4.14 through 4.21 contain information similar to that in the Tables 4.4 through 4.13 except that they compare models 4(a) through (f), without the $\mathcal{O}_{13}$ operator. We used values for the initial (GUT scale) parameters, taken from unreported data from the collaboration of ref. [25], which are consistent with electroweak symmetry breaking and the experimental bounds on sparticle masses, and which give predictions agreeing to within 2.1σ with experimental measurements for gauge couplings, fermion masses and mixing angles, and $b \to s\gamma$. This comparison gives us information on the model dependence of nucleon decay branching ratios. Note that models 4(a) through (f) (without the $\mathcal{O}_{13}$ operator) give identical results for fermion

masses and mixing angles. This is because the contribution of the different $\mathcal{O}_{22}$ operators to the 22 entry of the Yukawa matrices all give the same Clebsch relation 0:1:3 for u:d:e matrices [9]. They however have different Clebsch relations for the 22 entry of the matrices c_{qq}, c_{ql}, c_{ud}, and c_{ue} relevant for nucleon decay.

In addition, the comparison of model 4(c), with the $\mathcal{O}_{13}$ operator, to models 4(a) through (f), without the $\mathcal{O}_{13}$ operator, gives us information on the sensitivity of predictions for nucleon decay with respect to the quality of the fit for fermion masses and mixing angles. In order to compare the runs in the Tables 4.4 through 4.13 directly with the runs in the Tables 4.14 through 4.21, we chose the GUT scale parameters such that for each run in Tables 4.14 through 4.21, the values for $\tilde{\alpha}_{GUT}^{-1}$, M_{GUT}, ϵ_3; the soft SUSY breaking parameters $\tan\beta$, μ, $m_{1/2}$, m_0, m_{H_u}, m_{H_d}, and A_0; and the Yukawa parameter A are nearly the same as they are for the run of the same name in the Tables 4.4 through 4.13.

4.4 Discussion of the results

4.4.1 Overall Rates

Many significant results appear from the tables of the previous section. First, comparing the rates of proton decay predicted in the tables above with the results of experimental searches for proton and baryon-number violating neutron decay summarized in Table 4.22, it can be seen that the predicted upper bounds on the lifetimes for nucleon decay are above, and, in most cases, well above, the experimental lower bounds. The loop integral $I(M_{gaugino}, M_{\substack{squark\\(slepton)}}, M_{\substack{squark\\(slepton)}})$ goes roughly like $1/M^2_{\substack{squark\\(slepton)}}$ in the limit where squarks and sleptons are much heavier than gauginos. Hence, the decay rates go naively like $(m_{1/2}^2 + \mu_R^2)/m_0^4$, where $\mu_R \equiv \mu(M_Z)$. This

run no.	$\tau(p \to K^+\overline{\nu})/(10^{32}\text{yrs})$			$\frac{\Gamma(p\to\pi^+\overline{\nu})}{\Gamma(p\to K^+\overline{\nu})}$			$\frac{\Gamma(p\to K^0\mu^+)}{\Gamma(p\to K^+\overline{\nu})} \times 10^2$			$\frac{\Gamma(p\to\pi^0\mu^+)}{\Gamma(p\to K^+\overline{\nu})} \times 10^2$			$\frac{\Gamma(p\to\eta\mu^+)}{\Gamma(p\to K^+\overline{\nu})} \times 10^2$		
	max	$\beta = -\alpha$	min	max	$\beta = -\alpha$	min	max	$\beta = -\alpha$	min	max	$\beta = -\alpha$	min	max	$\beta = -\alpha$	min
I	27.	15.	15.	0.44	0.38	0.38	0.53	0.29	0.29	0.29	0.16	0.16	0.10	0.056	0.056
II	61.	38.	37.	0.36	0.32	0.31	0.53	0.33	0.33	0.29	0.18	0.18	0.10	0.063	0.061
III(1)	220.	130.	99.	1.1	0.74	0.68	0.31	0.19	0.14	0.12	0.073	0.055	0.028	0.017	0.013
III(2)	150.	98.	75.	1.5	1.0	0.93	0.37	0.23	0.18	0.11	0.071	0.054	0.017	0.011	0.0084
III(3)	110.	76.	59.	1.5	1.1	1.0	0.34	0.23	0.18	0.092	0.063	0.049	0.011	0.0078	0.0061

Table 4.4: Partial mean lifetime for proton decaying into kaon plus anti-neutrino and ratios of the rates of proton decay into various decay products versus rate of decay into kaon plus anti-neutrino for various values of the GUT scale parameters, when the $\mathcal{O}_{13}$ operator is included.

run no.	$\tau(n \to K^0\overline{\nu})/(10^{32}\text{yrs})$			$\frac{\Gamma(n\to\pi^0\overline{\nu})}{\Gamma(n\to K^0\overline{\nu})} \times 10^2$			$\frac{\Gamma(n\to\eta\overline{\nu})}{\Gamma(n\to K^0\overline{\nu})} \times 10^2$			$\frac{\Gamma(n\to\pi^-\mu^+)}{\Gamma(n\to K^0\overline{\nu})} \times 10^2$		
	max	$\beta = -\alpha$	min	max	$\beta = -\alpha$	min	max	$\beta = -\alpha$	min	max	$\beta = -\alpha$	min
I	4.1	2.4	2.4	3.3	3.2	3.2	0.40	0.18	0.18	0.089	0.053	0.053
II	12.	7.5	7.1	3.3	3.2	3.2	0.51	0.26	0.24	0.12	0.072	0.069
III(1)	14.	12.	10.	3.5	3.5	3.4	0.13	0.089	0.036	0.016	0.014	0.011
III(2)	6.6	5.9	5.1	3.2	3.1	3.1	0.080	0.055	0.022	0.0095	0.0085	0.0073
III(3)	4.6	4.2	3.7	3.2	3.1	3.1	0.064	0.045	0.019	0.0076	0.0070	0.0062

Table 4.5: Partial mean lifetime for neutron decaying into kaon plus anti-neutrino and ratios of the rates of proton decay into various decay products versus rate of decay into kaon plus anti-neutrino for various values of the GUT scale parameters, when the $\mathcal{O}_{13}$ operator is included.

run no.	$\frac{\Gamma^{chargino}_{p\to K^+\bar{\nu}}}{\Gamma^{total}_{p\to K^+\bar{\nu}}}$			$\frac{\Gamma^{chargino}_{p\to \pi^+\bar{\nu}}}{\Gamma^{total}_{p\to \pi^+\bar{\nu}}}$			$\frac{\Gamma^{chargino}_{p\to K^0\mu^+}}{\Gamma^{total}_{p\to K^0\mu^+}}$		
	max	$\beta=-\alpha$	min	max	$\beta=-\alpha$	min	max	$\beta=-\alpha$	min
I	1.1	1.1	0.90	1.1	1.1	0.87	0.99	0.99	0.99
II	1.3	1.2	0.83	1.3	1.2	0.72	1.0	1.0	1.0
III(1)	1.9	1.4	0.45	1.4	1.3	0.71	1.2	1.2	1.2
III(2)	1.7	1.3	0.51	1.3	1.2	0.79	1.1	1.1	1.1
III(3)	1.6	1.3	0.57	1.2	1.2	0.83	1.1	1.1	1.1

Table 4.6: Ratios of the rate of proton decay that would occur if chargino diagrams contributed only versus total proton decay rate for the three most dominant decay modes, for various values of the GUT scale parameters, when the $\mathcal{O}_{13}$ operator is included.

run no.	$\frac{\Gamma^{chargino}_{n\to K^0\bar{\nu}}}{\Gamma^{total}_{n\to K^0\bar{\nu}}}$			$\frac{\Gamma^{chargino}_{n\to \pi^0\bar{\nu}}}{\Gamma^{total}_{n\to \pi^0\bar{\nu}}}$			$\frac{\Gamma^{chargino}_{n\to \eta\bar{\nu}}}{\Gamma^{total}_{n\to \eta\bar{\nu}}}$			$\frac{\Gamma^{chargino}_{n\to \pi^-\mu^+}}{\Gamma^{total}_{n\to \pi^-\mu^+}}$		
	max	$\beta=-\alpha$	min	max	$\beta=-\alpha$	min	max	$\beta=-\alpha$	min	max	$\beta=-\alpha$	min
I	1.1	1.1	0.87	1.1	1.1	0.87	1.1	1.0	0.98	0.81	0.81	0.81
II	1.3	1.2	0.73	1.3	1.2	0.72	1.2	0.99	0.96	0.64	0.64	0.64
III(1)	1.4	1.3	0.71	1.4	1.3	0.71	2.2	0.44	0.40	0.42	0.42	0.42
III(2)	1.2	1.2	0.80	1.3	1.2	0.79	2.2	0.42	0.39	0.54	0.54	0.54
III(3)	1.2	1.1	0.84	1.2	1.2	0.83	2.2	0.43	0.41	0.62	0.62	0.62

Table 4.7: Ratios of the rate of neutron decay that would occur if chargino diagrams contributed only versus total neutron decay rate, for various values of the GUT scale parameters, when the $\mathcal{O}_{13}$ operator is included.

run no.	$\frac{\Gamma^{gluino}_{p\to K^+\bar{\nu}}}{\Gamma^{total}_{p\to K^+\bar{\nu}}}$			$\frac{\Gamma^{gluino}_{p\to \pi^+\bar{\nu}}}{\Gamma^{total}_{p\to \pi^+\bar{\nu}}}$			$\frac{\Gamma^{gluino}_{p\to K^0\mu^+}}{\Gamma^{total}_{p\to K^0\mu^+}}$		
	max	$\beta=-\alpha$	min	max	$\beta=-\alpha$	min	max	$\beta=-\alpha$	min
I	0.019	0.011	0.011	0.0064	0.0040	0.0040	0.00038	0.00038	0.00038
II	0.085	0.053	0.052	0.038	0.025	0.023	0.00067	0.00067	0.00067
III(1)	0.25	0.15	0.11	0.035	0.030	0.024	0.020	0.020	0.020
III(2)	0.16	0.10	0.077	0.016	0.014	0.012	0.014	0.014	0.014
III(3)	0.10	0.072	0.056	0.010	0.0092	0.0080	0.011	0.011	0.011

Table 4.8: Ratios of the rate of proton decay that would occur if gluino diagrams contributed only versus total proton decay rate for the three most dominant decay modes, for various values of the GUT scale parameters, when the $\mathcal{O}_{13}$ operator is included.

run no.	$\frac{\Gamma^{gluino}_{n\to K^0\bar{\nu}}}{\Gamma^{total}_{n\to K^0\bar{\nu}}}$			$\frac{\Gamma^{gluino}_{n\to \pi^0\bar{\nu}}}{\Gamma^{total}_{n\to \pi^0\bar{\nu}}}$			$\frac{\Gamma^{gluino}_{n\to \eta\bar{\nu}}}{\Gamma^{total}_{n\to \eta\bar{\nu}}}$			$\frac{\Gamma^{gluino}_{n\to \pi^-\mu^+}}{\Gamma^{total}_{n\to \pi^-\mu^+}}$		
	max	$\beta=-\alpha$	min	max	$\beta=-\alpha$	min	max	$\beta=-\alpha$	min	max	$\beta=-\alpha$	min
I	0.0059	0.0036	0.0035	0.0064	0.0040	0.0040	0.025	0.025	0.019	0.0099	0.0099	0.0099
II	0.035	0.022	0.021	0.038	0.025	0.023	0.11	0.11	0.088	0.043	0.043	0.043
III(1)	0.033	0.029	0.023	0.035	0.030	0.024	0.83	0.42	0.32	0.20	0.20	0.20
III(2)	0.014	0.012	0.011	0.016	0.014	0.012	0.61	0.29	0.22	0.19	0.19	0.19
III(3)	0.0089	0.0081	0.0072	0.010	0.0092	0.0080	0.47	0.23	0.17	0.16	0.16	0.16

Table 4.9: Ratios of the rate of neutron decay that would occur if gluino diagrams contributed only versus total neutron decay rate for various values of the GUT scale parameters, when the $\mathcal{O}_{13}$ operator is included.

run no.	$\sqrt{\frac{\Gamma^{LLRR}_{p\to K^+\overline{\nu}_l}}{\Gamma^{LLLL}_{p\to K^+\overline{\nu}_l}}}$			$\sqrt{\frac{\Gamma^{LLRR}_{p\to \pi^+\overline{\nu}_l}}{\Gamma^{LLLL}_{p\to \pi^+\overline{\nu}_l}}}$		
	$\overline{\nu}_e$	$\overline{\nu}_\mu$	$\overline{\nu}_\tau$	$\overline{\nu}_e$	$\overline{\nu}_\mu$	$\overline{\nu}_\tau$
I	0.000081	0.011	1.9	0.00018	0.024	6.8
II	0.000084	0.011	1.7	0.00020	0.024	6.2
III(1)	0.00021	0.028	3.8	0.00055	0.068	10.
III(2)	0.00025	0.039	4.6	0.00066	0.096	14.
III(3)	0.00030	0.047	5.7	0.00079	0.12	17.

Table 4.10: Ratios of the rate of proton decay that would occur if LLLL operators contributed only versus the rate of proton decay that would occur if LLRR operators contributed only, for each of the three anti-neutrino generations, for various values of the GUT scale parameters, when the $\mathcal{O}_{13}$ operator is included.

run no.	$\sqrt{\frac{\Gamma^{LLLL}_{p\to K^+\overline{\nu}_e}}{\Gamma^{LLRR}_{p\to K^+\overline{\nu}_\tau}}}$	$\sqrt{\frac{\Gamma^{LLRR}_{p\to K^+\overline{\nu}_e}}{\Gamma^{LLRR}_{p\to K^+\overline{\nu}_\tau}}}$	$\sqrt{\frac{\Gamma^{LLLL}_{p\to K^+\overline{\nu}_\mu}}{\Gamma^{LLRR}_{p\to K^+\overline{\nu}_\tau}}}$	$\sqrt{\frac{\Gamma^{LLRR}_{p\to K^+\overline{\nu}_\mu}}{\Gamma^{LLRR}_{p\to K^+\overline{\nu}_\tau}}}$	$\sqrt{\frac{\Gamma^{LLLL}_{p\to K^+\overline{\nu}_\tau}}{\Gamma^{LLRR}_{p\to K^+\overline{\nu}_\tau}}}$
I	0.085	6.9×10^{-6}	1.6	0.017	0.52
II	0.10	8.7×10^{-6}	1.9	0.021	0.58
III(1)	0.035	7.3×10^{-6}	0.61	0.017	0.26
III(2)	0.033	8.3×10^{-6}	0.50	0.020	0.22
III(3)	0.027	8.2×10^{-6}	0.41	0.020	0.18

Table 4.11: Ratios of partial decay rates for $p \to K^+\overline{\nu}$, which compare the importance of the LLLL and LLRR operators for each generation of anti-neutrino versus contribution of the LLRR operator of the third generation anti-neutrino for various values of the GUT scale parameters, when the $\mathcal{O}_{13}$ operator is included.

run no.	$\sqrt{\frac{\Gamma^{LLLL}_{p\to\pi^+\bar{\nu}_e}}{\Gamma^{LLRR}_{p\to\pi^+\bar{\nu}_\tau}}}$	$\sqrt{\frac{\Gamma^{LLRR}_{p\to\pi^+\bar{\nu}_e}}{\Gamma^{LLRR}_{p\to\pi^+\bar{\nu}_\tau}}}$	$\sqrt{\frac{\Gamma^{LLLL}_{p\to\pi^+\bar{\nu}_\mu}}{\Gamma^{LLRR}_{p\to\pi^+\bar{\nu}_\tau}}}$	$\sqrt{\frac{\Gamma^{LLRR}_{p\to\pi^+\bar{\nu}_\mu}}{\Gamma^{LLRR}_{p\to\pi^+\bar{\nu}_\tau}}}$	$\sqrt{\frac{\Gamma^{LLLL}_{p\to\pi^+\bar{\nu}_\tau}}{\Gamma^{LLRR}_{p\to\pi^+\bar{\nu}_\tau}}}$
I	0.027	4.9×10^{-6}	0.50	0.012	0.15
II	0.031	6.1×10^{-6}	0.61	0.015	0.16
III(1)	0.0096	5.3×10^{-6}	0.19	0.013	0.099
III(2)	0.0082	5.4×10^{-6}	0.14	0.013	0.071
III(3)	0.0068	5.4×10^{-6}	0.11	0.013	0.058

Table 4.12: Ratios of partial decay rates for $p \to \pi^+\overline{\nu}$, which compare the importance of the LLLL and LLRR operators for each generation of anti-neutrino versus contribution of the LLRR operator of the third generation anti-neutrino for various values of the GUT scale parameters, when the $\mathcal{O}_{13}$ operator is included.

run no.	I	II	III(1)	III(2)	III(3)
$\tilde{\alpha}_{GUT}^{-1}$	24.43	24.36	24.51	24.65	24.75
M_{GUT}	2.498×10^{16}	3.172×10^{16}	3.327×10^{16}	2.857×10^{16}	2.513×10^{16}
ϵ_3	−0.04760	−0.04886	−0.04342	−0.04420	−0.04550
A	0.7640	0.8067	0.8523	0.8867	0.8872
B	0.05259	0.05439	0.05630	0.05882	0.05956
C	0.0001096	0.0001155	0.0001213	0.0001231	0.0001226
E	0.01251	0.01308	0.01360	0.01397	0.01397
ϕ	1.066	1.041	1.020	1.023	1.038
D	0.0004633	0.0004944	0.0005064	0.0005691	0.0005665
δ	5.698	5.706	5.698	5.742	5.744
$\tan\beta$	52.77	54.38	55.39	55.86	55.92
$\mu(M_Z)$	80.0	80.0	160.	240.	300.
$m_{1/2}$	280.	240.	170.	170.	170.
m_0	400.	700.	1400.	1400.	1400.
m_{H_d}	706.4	994.6	1858.	1859.	1855.
m_{H_u}	635.6	865.3	1599.	1591.	1585.
A_0	322.2	458.4	−982.4	−1079.	−1274.

Table 4.13: Values of the GUT scale parameters used in Tables 4.4 through 4.12. All dimensions in GeV units.

run no.	model	$\frac{\tau(p\to K^+\bar{\nu})}{10^{32}\text{yrs}}$	$\frac{\Gamma(p\to\pi^+\bar{\nu})}{\Gamma(p\to K^+\bar{\nu})}$	$\frac{\Gamma(p\to K^0\mu^+)}{\Gamma(p\to K^+\bar{\nu})}$	$\frac{\Gamma(p\to\pi^0\mu^+)}{\Gamma(p\to K^+\bar{\nu})}$	$\frac{\Gamma(p\to\eta\mu^+)}{\Gamma(p\to K^+\bar{\nu})}$
I	*a*	7.6	0.22	0.0021	0.0011	0.00040
	b	3.5	0.17	0.0032	0.0017	0.00060
	c	11.	0.25	0.0013	0.00070	0.00025
	d	4.2	0.15	0.0048	0.0024	0.00083
	e	15.	0.25	0.0030	0.0014	0.00048
	f	2.0	0.13	0.0049	0.0024	0.00086
II	*a*	24.	0.20	0.0029	0.0016	0.00056
	b	10.	0.16	0.0040	0.0022	0.00076
	c	37.	0.24	0.0018	0.0010	0.00035
	d	10.	0.14	0.0051	0.0025	0.00088
	e	40.	0.23	0.0037	0.0016	0.00057
	f	4.9	0.13	0.0052	0.0026	0.00091
III(1)	*a*	60.	0.30	0.00079	0.00035	0.00011
	b	68.	0.28	0.0023	0.0012	0.00039
	c	70.	0.31	0.00052	0.00017	0.000045
	d	33.	0.24	0.0017	0.00073	0.00025
	e	58.	0.30	0.00082	0.00026	0.000078
	f	22.	0.21	0.0021	0.00099	0.00034
III(2)	*a*	26.	0.31	0.00049	0.00017	0.000048
	b	33.	0.32	0.0013	0.00059	0.00019
	c	30.	0.32	0.00039	0.000094	0.000019
	d	19.	0.27	0.0011	0.00043	0.00014
	e	27.	0.32	0.00054	0.00014	0.000037
	f	14.	0.24	0.0014	0.00063	0.00022
III(3)	*a*	18.	0.31	0.00040	0.00012	0.000031
	b	23.	0.33	0.0010	0.00040	0.00012
	c	21.	0.32	0.00034	0.000073	0.000012
	d	14.	0.28	0.00083	0.00032	0.00010
	e	20.	0.32	0.00045	0.00011	0.000025
	f	11.	0.26	0.0011	0.00048	0.00016

Table 4.14: Partial mean lifetime for proton decaying into kaon plus anti-neutrino and ratios of the rates of proton decay into various decay products versus rate of decay into kaon plus anti-neutrino for various values of the GUT scale parameters, when the $\mathcal{O}_{13}$ operator is not included. For all entries, $\beta = -\alpha$.

run no.	model	$\frac{\tau(n\to\bar{K}^0\bar{\nu})}{10^{32}\text{yrs}}$	$\frac{\Gamma(n\to\pi^0\bar{\nu})}{\Gamma(n\to\bar{K}^0\bar{\nu})}$	$\frac{\Gamma(n\to\eta\bar{\nu})}{\Gamma(n\to\bar{K}^0\bar{\nu})}$	$\frac{\Gamma(n\to\pi^-\mu^+)}{\Gamma(n\to\bar{K}^0\bar{\nu})}$
I	*a*	2.5	0.036	0.0021	0.00075
	b	1.4	0.033	0.0048	0.0013
	c	3.2	0.036	0.00099	0.00041
	d	2.0	0.035	0.011	0.0023
	e	4.3	0.036	0.0043	0.00079
	f	1.1	0.035	0.012	0.0026
II	*a*	8.3	0.035	0.0029	0.0011
	b	4.3	0.033	0.0064	0.0018
	c	11.	0.035	0.0016	0.00061
	d	4.9	0.035	0.010	0.0024
	e	13.	0.036	0.0046	0.0011
	f	2.5	0.034	0.011	0.0027
III(1)	*a*	16.	0.039	0.0011	0.00018
	b	18.	0.036	0.0038	0.00061
	c	17.	0.038	0.00075	0.000083
	d	10.	0.037	0.0016	0.00045
	e	14.	0.036	0.00038	0.00012
	f	7.6	0.036	0.0027	0.00069
III(2)	*a*	6.7	0.039	0.00065	0.000087
	b	7.5	0.037	0.0020	0.00027
	c	7.1	0.038	0.00051	0.000045
	d	5.2	0.037	0.00087	0.00024
	e	6.2	0.036	0.00029	0.000065
	f	4.2	0.037	0.0016	0.00039
III(3)	*a*	4.6	0.039	0.00054	0.000061
	b	5.1	0.037	0.0014	0.00018
	c	4.9	0.038	0.00044	0.000034
	d	3.8	0.037	0.00066	0.00017
	e	4.4	0.037	0.00027	0.000049
	f	3.3	0.038	0.0012	0.00028

Table 4.15: Partial mean lifetime for neutron decaying into kaon plus anti-neutrino and ratios of the rates of neutron decay into various decay products versus rate of decay into kaon plus anti-neutrino for various values of the GUT scale parameters, when the $\mathcal{O}_{13}$ operator is not included. For all entries, $\beta = -\alpha$.

run no.	model	$\frac{\Gamma^{\text{chargino}}_{p\to K^+\bar{\nu}}}{\Gamma^{\text{total}}_{p\to K^+\bar{\nu}}}$			$\frac{\Gamma^{\text{chargino}}_{p\to \pi^+\bar{\nu}}}{\Gamma^{\text{total}}_{p\to \pi^+\bar{\nu}}}$			$\frac{\Gamma^{\text{chargino}}_{p\to K^0\mu^+}}{\Gamma^{\text{total}}_{p\to K^0\mu^+}}$		
		max	$\mathcal{Z}=-\alpha$	min	max	$\mathcal{Z}=-\alpha$	min	max	$\mathcal{Z}=-\alpha$	min
I	*a*	1.2	1.1	0.85	1.1	1.1	0.86	1.0	1.0	1.0
	b	1.2	1.2	0.94	1.2	1.2	0.86	1.0	1.0	1.0
	c	1.2	1.1	0.82	1.1	1.1	0.89	0.99	0.99	0.99
	d	1.2	1.0	0.99	1.2	0.92	0.91	1.0	1.0	1.0
	e	1.2	0.91	0.91	1.1	0.91	0.91	1.0	1.0	1.0
	f	1.2	1.0	1.0	1.2	0.97	0.95	1.0	1.0	1.0
II	*a*	1.5	1.3	0.72	1.4	1.3	0.72	1.0	1.0	1.0
	b	1.4	1.4	0.91	1.4	1.4	0.76	1.0	1.0	1.0
	c	1.4	1.3	0.64	1.3	1.2	0.74	1.0	1.0	1.0
	d	1.4	1.0	1.0	1.4	0.88	0.87	1.0	1.0	1.0
	e	1.4	0.85	0.85	1.3	0.81	0.81	1.0	1.0	1.0
	f	1.4	1.1	1.1	1.4	0.98	0.94	1.0	1.0	1.0
III(1)	*a*	1.9	1.5	0.53	1.5	1.3	0.68	1.1	1.1	1.1
	b	2.6	2.4	0.34	2.0	2.0	0.47	1.2	1.2	1.2
	c	1.6	1.4	0.61	1.3	1.2	0.76	1.2	1.2	1.2
	d	2.7	0.48	0.42	2.0	0.52	0.49	1.1	1.1	1.1
	e	1.7	0.65	0.64	1.3	0.76	0.76	0.98	0.98	0.98
	f	2.8	0.54	0.42	2.3	0.50	0.42	1.1	1.1	1.1
III(2)	*a*	1.5	1.3	0.64	1.3	1.2	0.77	1.1	1.1	1.1
	b	2.2	2.0	0.41	1.7	1.6	0.58	1.2	1.2	1.2
	c	1.4	1.2	0.72	1.2	1.2	0.83	1.1	1.1	1.1
	d	2.2	0.52	0.46	1.7	0.62	0.59	1.0	1.0	1.0
	e	1.4	0.73	0.73	1.2	0.83	0.83	0.98	0.98	0.98
	f	2.5	0.51	0.41	1.9	0.56	0.50	1.1	1.1	1.1
III(3)	*a*	1.4	1.3	0.70	1.2	1.2	0.81	1.1	1.1	1.1
	b	1.9	1.8	0.47	1.5	1.5	0.64	1.1	1.1	1.1
	c	1.3	1.2	0.77	1.2	1.1	0.86	1.1	1.1	1.1
	d	1.9	0.56	0.51	1.5	0.67	0.65	1.0	1.0	1.0
	e	1.3	0.78	0.78	1.2	0.86	0.86	0.98	0.98	0.98
	f	2.3	0.53	0.43	1.7	0.61	0.55	1.1	1.1	1.1

Table 4.16: Ratios of the rate of proton decay that would occur if chargino diagrams contributed only versus total proton decay rate for the three most dominant decay modes, for various values of the GUT scale parameters, when the $\mathcal{O}_{13}$ operator is not included.

run no.	model	$\frac{\Gamma^{\text{chargino}}_{n\to K^0\bar{\nu}}}{\Gamma^{\text{total}}_{n\to K^0\bar{\nu}}}$			$\frac{\Gamma^{\text{chargino}}_{n\to \pi^0\bar{\nu}}}{\Gamma^{\text{total}}_{n\to \pi^0\bar{\nu}}}$			$\frac{\Gamma^{\text{chargino}}_{n\to \eta\bar{\nu}}}{\Gamma^{\text{total}}_{n\to \eta\bar{\nu}}}$		
		max	$\beta=-\alpha$	min	max	$\beta=-\alpha$	min	max	$\beta=-\alpha$	min
I	*a*	1.2	1.1	0.85	1.1	1.1	0.86	1.2	1.1	1.0
	b	1.2	1.2	0.86	1.2	1.2	0.86	1.1	1.1	1.1
	c	1.1	1.1	0.87	1.1	1.1	0.89	1.2	0.96	0.93
	d	1.2	0.93	0.93	1.2	0.92	0.91	1.1	1.1	1.1
	e	1.1	0.91	0.91	1.1	0.91	0.91	1.2	1.2	1.1
	f	1.2	0.98	0.97	1.2	0.97	0.95	1.1	1.1	1.1
II	*a*	1.4	1.3	0.69	1.4	1.3	0.72	1.4	1.1	1.1
	b	1.4	1.4	0.77	1.4	1.4	0.76	1.3	1.1	1.1
	c	1.3	1.3	0.70	1.3	1.2	0.74	1.4	0.93	0.88
	d	1.4	0.90	0.89	1.4	0.88	0.87	1.3	1.3	1.2
	e	1.3	0.81	0.81	1.3	0.81	0.81	1.4	1.4	1.2
	f	1.4	1.0	0.98	1.4	0.98	0.94	1.3	1.3	1.2
III(1)	*a*	1.6	1.4	0.64	1.5	1.3	0.68	3.0	0.54	0.43
	b	2.1	2.1	0.43	2.0	2.0	0.47	1.9	0.65	0.64
	c	1.4	1.3	0.72	1.3	1.2	0.76	3.1	0.35	0.31
	d	2.2	0.49	0.47	2.0	0.52	0.49	2.1	2.1	0.88
	e	1.4	0.75	0.75	1.3	0.76	0.76	3.1	2.9	0.66
	f	2.6	0.46	0.40	2.3	0.50	0.42	1.8	1.8	0.95
III(2)	*a*	1.3	1.3	0.74	1.3	1.2	0.77	3.1	0.49	0.38
	b	1.7	1.7	0.55	1.7	1.6	0.58	2.2	0.53	0.52
	c	1.2	1.2	0.80	1.2	1.2	0.83	2.8	0.40	0.36
	d	1.7	0.58	0.57	1.7	0.62	0.59	2.4	2.4	0.73
	e	1.2	0.82	0.82	1.2	0.83	0.83	2.7	2.6	0.55
	f	2.1	0.52	0.47	1.9	0.56	0.50	2.1	2.0	0.83
III(3)	*a*	1.3	1.2	0.78	1.2	1.2	0.81	2.9	0.49	0.39
	b	1.6	1.6	0.61	1.5	1.5	0.64	2.4	0.48	0.47
	c	1.2	1.2	0.84	1.2	1.1	0.86	2.4	0.45	0.40
	d	1.6	0.63	0.63	1.5	0.67	0.65	2.5	2.5	0.66
	e	1.2	0.86	0.85	1.2	0.86	0.86	2.4	2.3	0.54
	f	1.9	0.56	0.52	1.7	0.61	0.55	2.2	2.1	0.77

Table 4.17: Ratios of the rate of neutron decay that would occur if chargino diagrams contributed only versus total neutron decay rate for various values of the GUT scale parameters, when the $\mathcal{O}_{13}$ operator is not included.

run no.	model	$\sqrt{\frac{\Gamma^{LLRR}_{p\to K^+\bar{\nu}_l}}{\Gamma^{LLLL}_{p\to K^+\bar{\nu}_l}}}$			$\sqrt{\frac{\Gamma^{LLRR}_{p\to \pi^+\bar{\nu}_l}}{\Gamma^{LLLL}_{p\to \pi^+\bar{\nu}_l}}}$		
		$\bar{\nu}_e$	$\bar{\nu}_\mu$	$\bar{\nu}_\tau$	$\bar{\nu}_e$	$\bar{\nu}_\mu$	$\bar{\nu}_\tau$
I	*a*	0.000043	0.010	3.9	0.000071	0.017	7.7
	b	0.000021	0.0048	1.7	0.000036	0.0081	3.3
	c	0.000063	0.017	5.3	0.00010	0.028	11.
	d	0.000022	0.0042	1.6	0.000036	0.0069	2.6
	e	0.000060	0.010	3.9	0.00010	0.017	6.0
	f	0.000015	0.0030	1.2	0.000025	0.0049	1.9
II	*a*	0.000047	0.011	4.9	0.000077	0.018	10.
	b	0.000022	0.0048	2.5	0.000037	0.0082	5.1
	c	0.000070	0.017	5.5	0.00011	0.028	11.
	d	0.000022	0.0043	2.1	0.000036	0.0071	3.3
	e	0.000060	0.011	4.0	0.00010	0.018	6.1
	f	0.000015	0.0031	1.6	0.000025	0.0050	2.5
III(1)	*a*	0.00019	0.032	6.4	0.00031	0.054	10.
	b	0.000071	0.013	3.4	0.00012	0.023	5.8
	c	0.00030	0.044	7.6	0.00048	0.079	12.
	d	0.000059	0.013	3.8	0.000097	0.022	6.8
	e	0.00015	0.041	8.5	0.00025	0.064	15.
	f	0.000042	0.0093	2.8	0.000068	0.015	4.8
III(2)	*a*	0.00029	0.047	10.	0.00046	0.080	16.
	b	0.00010	0.020	5.4	0.00018	0.034	9.3
	c	0.00044	0.065	12.	0.00072	0.12	19.
	d	0.000087	0.020	6.2	0.00014	0.032	11.
	e	0.00022	0.061	13.	0.00037	0.095	24.
	f	0.000062	0.014	4.5	0.00010	0.022	7.7
III(3)	*a*	0.00035	0.058	13.	0.00056	0.098	21.
	b	0.00013	0.024	7.0	0.00022	0.042	12.
	c	0.00054	0.080	15.	0.00089	0.14	24.
	d	0.00011	0.024	8.1	0.00018	0.039	14.
	e	0.00028	0.075	17.	0.00045	0.12	30.
	f	0.000075	0.017	5.8	0.00012	0.027	10.

Table 4.18: Ratios of the rate of proton decay that would occur if LLLL operators contributed only versus the rate of proton decay that would occur if LLRR operators contributed only, for each of the three anti-neutrino generations, for various values of the GUT scale parameters, when the $\mathcal{O}_{13}$ operator is not included.

run no.	model	$\sqrt{\frac{\Gamma^{LLLL}_{p\to K^+\bar{\nu}_e}}{\Gamma^{LLRR}_{p\to K^+\bar{\nu}_\tau}}}$	$\sqrt{\frac{\Gamma^{LLRR}_{p\to K^+\bar{\nu}_e}}{\Gamma^{LLRR}_{p\to K^+\bar{\nu}_\tau}}}$	$\sqrt{\frac{\Gamma^{LLLL}_{p\to K^+\bar{\nu}_\mu}}{\Gamma^{LLRR}_{p\to K^+\bar{\nu}_\tau}}}$	$\sqrt{\frac{\Gamma^{LLRR}_{p\to K^+\bar{\nu}_\mu}}{\Gamma^{LLRR}_{p\to K^+\bar{\nu}_\tau}}}$	$\sqrt{\frac{\Gamma^{LLLL}_{p\to K^+\bar{\nu}_\tau}}{\Gamma^{LLRR}_{p\to K^+\bar{\nu}_\tau}}}$
I	*a*	0.065	2.8×10^{-6}	0.81	0.0085	0.26
	b	0.13	2.8×10^{-6}	1.8	0.0086	0.58
	c	0.045	2.8×10^{-6}	0.51	0.0085	0.19
	d	0.13	2.8×10^{-6}	2.0	0.0084	0.62
	e	0.047	2.8×10^{-6}	0.83	0.0086	0.26
	f	0.18	2.7×10^{-6}	2.8	0.0083	0.86
II	*a*	0.073	3.5×10^{-6}	0.98	0.011	0.21
	b	0.16	3.5×10^{-6}	2.2	0.011	0.40
	c	0.050	3.5×10^{-6}	0.63	0.011	0.18
	d	0.16	3.4×10^{-6}	2.4	0.010	0.47
	e	0.059	3.5×10^{-6}	0.96	0.011	0.25
	f	0.22	3.4×10^{-6}	3.3	0.010	0.62
III(1)	*a*	0.016	3.0×10^{-6}	0.29	0.0092	0.16
	b	0.043	3.1×10^{-6}	0.70	0.0093	0.30
	c	0.010	3.0×10^{-6}	0.21	0.0092	0.13
	d	0.051	3.0×10^{-6}	0.68	0.0091	0.26
	e	0.020	3.1×10^{-6}	0.22	0.0093	0.12
	f	0.070	2.9×10^{-6}	0.96	0.0089	0.36
III(2)	*a*	0.010	3.0×10^{-6}	0.19	0.0091	0.099
	b	0.029	3.0×10^{-6}	0.47	0.0092	0.18
	c	0.0068	3.0×10^{-6}	0.14	0.0091	0.085
	d	0.034	3.0×10^{-6}	0.45	0.0090	0.16
	e	0.013	3.0×10^{-6}	0.15	0.0092	0.076
	f	0.047	2.9×10^{-6}	0.65	0.0088	0.22
III(3)	*a*	0.0086	3.0×10^{-6}	0.16	0.0091	0.078
	b	0.024	3.0×10^{-6}	0.38	0.0092	0.14
	c	0.0056	3.0×10^{-6}	0.12	0.0092	0.067
	d	0.028	3.0×10^{-6}	0.37	0.0091	0.12
	e	0.011	3.0×10^{-6}	0.12	0.0092	0.060
	f	0.039	2.9×10^{-6}	0.53	0.0089	0.17

Table 4.19: Ratios of partial decay rates for $p \to K^+\overline{\nu}$, which compare the importance of the LLLL and LLRR operators for each generation of anti-neutrino versus contribution of the LLRR operator of the third generation anti-neutrino for various values of the GUT scale parameters, when the $\mathcal{O}_{13}$ operator is not included.

run no.	model	$\sqrt{\frac{\Gamma^{LLLL}_{p\to\pi^+\bar{\nu}_e}}{\Gamma^{LLRR}_{p\to\pi^+\bar{\nu}_\tau}}}$	$\sqrt{\frac{\Gamma^{LLRR}_{p\to\pi^+\bar{\nu}_e}}{\Gamma^{LLRR}_{p\to\pi^+\bar{\nu}_\tau}}}$	$\sqrt{\frac{\Gamma^{LLLL}_{p\to\pi^+\bar{\nu}_\mu}}{\Gamma^{LLRR}_{p\to\pi^+\bar{\nu}_\tau}}}$	$\sqrt{\frac{\Gamma^{LLRR}_{p\to\pi^+\bar{\nu}_\mu}}{\Gamma^{LLRR}_{p\to\pi^+\bar{\nu}_\tau}}}$	$\sqrt{\frac{\Gamma^{LLLL}_{p\to\pi^+\bar{\nu}_\tau}}{\Gamma^{LLRR}_{p\to\pi^+\bar{\nu}_\tau}}}$
I	*a*	0.040	2.8×10^{-6}	0.50	0.0086	0.13
	b	0.079	2.8×10^{-6}	1.1	0.0086	0.30
	c	0.027	2.8×10^{-6}	0.31	0.0086	0.091
	d	0.079	2.8×10^{-6}	1.2	0.0085	0.38
	e	0.028	2.8×10^{-6}	0.50	0.0086	0.17
	f	0.11	2.8×10^{-6}	1.7	0.0084	0.52
II	*a*	0.046	3.5×10^{-6}	0.60	0.011	0.099
	b	0.094	3.5×10^{-6}	1.3	0.011	0.20
	c	0.031	3.5×10^{-6}	0.38	0.011	0.091
	d	0.097	3.5×10^{-6}	1.5	0.011	0.30
	e	0.035	3.5×10^{-6}	0.58	0.011	0.16
	f	0.14	3.4×10^{-6}	2.1	0.010	0.39
III(1)	*a*	0.0098	3.0×10^{-6}	0.17	0.0092	0.096
	b	0.026	3.1×10^{-6}	0.41	0.0093	0.17
	c	0.0063	3.1×10^{-6}	0.12	0.0093	0.080
	d	0.031	3.0×10^{-6}	0.43	0.0092	0.15
	e	0.012	3.1×10^{-6}	0.15	0.0093	0.065
	f	0.044	3.0×10^{-6}	0.61	0.0090	0.21
III(2)	*a*	0.0066	3.0×10^{-6}	0.11	0.0091	0.061
	b	0.017	3.0×10^{-6}	0.27	0.0092	0.11
	c	0.0042	3.0×10^{-6}	0.079	0.0092	0.052
	d	0.021	3.0×10^{-6}	0.29	0.0091	0.091
	e	0.0083	3.0×10^{-6}	0.097	0.0092	0.042
	f	0.029	3.0×10^{-6}	0.41	0.0090	0.13
III(3)	*a*	0.0054	3.0×10^{-6}	0.093	0.0092	0.048
	b	0.014	3.0×10^{-6}	0.22	0.0092	0.083
	c	0.0034	3.0×10^{-6}	0.065	0.0092	0.041
	d	0.017	3.0×10^{-6}	0.23	0.0092	0.070
	e	0.0068	3.1×10^{-6}	0.079	0.0093	0.033
	f	0.024	3.0×10^{-6}	0.33	0.0090	0.099

Table 4.20: Ratios of partial decay rates for $p \to \pi^+\overline{\nu}$, which compare the importance of the LLLL and LLRR operators for each generation of anti-neutrino versus contribution of the LLRR operator of the third generation anti-neutrino for various values of the GUT scale parameters, when the $\mathcal{O}_{13}$ operator is not included.

run no.	I	II	III(1)	III(2)	III(3)
$\tilde{\alpha}_{GUT}^{-1}$	24.43	24.36	24.51	24.65	24.75
M_{GUT}	2.498×10^{16}	3.172×10^{16}	3.327×10^{16}	2.857×10^{16}	2.513×10^{16}
ϵ_3	−0.04760	−0.04886	−0.04342	−0.04420	−0.04550
A	0.7640	0.8067	0.8523	0.8867	0.8872
B	0.05798	0.06019	0.06254	0.06533	0.06607
C	0.00008824	0.00009204	0.00009550	0.00009801	0.00009809
E	0.01063	0.01111	0.01154	0.01182	0.01180
ϕ	1.762	1.765	1.767	1.765	1.763
$\tan\beta$	52.71	54.31	55.32	55.79	55.87
$\mu(M_Z)$	80.0	80.0	160.	240.	300.
$m_{1/2}$	280.	240.	170.	170.	170.
m_0	400.	700.	1400.	1400.	1400.
m_{H_d}	706.3	994.4	1858.	1859.	1855.
m_{H_u}	635.9	865.6	1599.	1592.	1585.
A_0	322.2	458.4	−982.4	−1079.	−1274.

Table 4.21: Values of the GUT scale parameters used in Tables 4.14 through 4.20. All dimensions in GeV units.

$\tau(p \to K^+\overline{\nu})$	$>$	1.0×10^{32} yrs
$\tau(p \to \pi^+\overline{\nu})$	$>$	$.25 \times 10^{32}$ yrs
$\tau(p \to \pi^0\mu^+)$	$>$	2.7×10^{32} yrs
$\tau(p \to \eta\mu^+)$	$>$	$.69 \times 10^{32}$ yrs
$\tau(p \to \pi^0 e^+)$	$>$	5.5×10^{32} yrs
$\tau(p \to \eta e^+)$	$>$	1.4×10^{32} yrs
$\tau(n \to K^0\overline{\nu})$	$>$	$.86 \times 10^{32}$ yrs
$\tau(n \to \pi^0\overline{\nu})$	$>$	1.0×10^{32} yrs
$\tau(n \to \eta\overline{\nu})$	$>$	$.54 \times 10^{32}$ yrs
$\tau(n \to \pi^-\mu^+)$	$>$	1.0×10^{32} yrs
$\tau(n \to \pi^- e^+)$	$>$	1.3×10^{32} yrs

Table 4.22: Current experimental lower bounds on the various partial lifetimes of the nucleons [2]

approximation roughly explains the dependence of the nucleon decay rates on m_0, $\mu(M_Z)$, and $m_{1/2}$ seen in Tables 4.4, 4.5, 4.14, and 4.15.

4.4.2 LLRR vs. LLLL Operators

Secondly, LLRR operators dominate over LLLL operators for the third generation anti-neutrino, for the decays into $K\overline{\nu}$ and $\pi\overline{\nu}$. (See Tables 4.10 and 4.18.) We can gain an intuitive understanding of why this is if we neglect the gluino contribution to the decay rates and look at approximate formulas for the rate of decay due to charginos. The loop integral $I(a,b,c)$ is a relatively smooth function of the masses and as a result, to a very good approximation, when calculating chargino diagrams for the third generation anti-neutrino, sums over gamma matrices of the form $\Gamma_{L\,\lambda i}\Gamma^*_{R\,\lambda j} I(\tilde{\Omega}_\lambda, b, c)$ are approximately zero while sums of the form $\Gamma_{L\,\lambda i}\Gamma^*_{L\,\lambda j} I(\tilde{\Omega}_\lambda, b, c)$ and $\Gamma_{R\,\lambda i}\Gamma^*_{R\,\lambda j} I(\tilde{\Omega}_\lambda, b, c)$ are approximately equal to $\delta_{ij} I(\tilde{\Omega}_{i_L}, b, c)$

and $\delta_{ij} I(\tilde{\Omega}_{i_R}, b, c)$, respectively, due to the orthogonality of the gamma matrices. Hence,

$$
\begin{aligned}
C_{1jk3}^{(\overline{ud})(d\nu)} \approx & \\
& \frac{1}{16\pi^2 \tilde{M}_t} (\Gamma_{U,R} \hat{Y}_U V_{KM})_{\lambda k} \Gamma^*_{U,R\,\lambda k'} (\Gamma_{E,R} \hat{Y}_e)_{\rho 3} \Gamma^*_{E,R\rho l'} \\
& \quad \times \hat{c}^*_{ud}{}^{[1j} \hat{c}^*_{ue}{}^{k']l'} U_{+\,2n} U_{-\,2n} m_{\tilde{\chi}_n} I(\tilde{\chi}_n, \tilde{u}_\lambda, \tilde{e}_\rho) \\
\approx & \frac{1}{16\pi^2 \tilde{M}_t} \lambda_\tau \lambda_{u_{k'}} (V_{KM})_{k'k} \hat{c}^*_{ud}{}^{[1j} \hat{c}^*_{ue}{}^{k']3} U_{+\,2n} U_{-\,2n} m_{\tilde{\chi}_n} I(\tilde{\chi}_n, \tilde{u}_{k'_R}, \tilde{e}_{3_R}) \\
\approx & \frac{1}{16\pi^2 \tilde{M}_t} \lambda_\tau \lambda_t (V_{KM})_{3k} \hat{c}^*_{ud}{}^{[1j} \hat{c}^*_{ue}{}^{3]3} U_{+\,2n} U_{-\,2n} m_{\tilde{\chi}_n} I(\tilde{\chi}_n, \tilde{u}_{3_R}, \tilde{e}_{3_R})
\end{aligned}
\tag{4.8}
$$

See fig. 4.3 for the Feynman diagram giving the dominant contribution to eqn. (4.8). Similarly,

$$
\begin{aligned}
C_{1jk3}^{(ud)(d\nu)} \approx & \\
& \frac{1}{16\pi^2 \tilde{M}_t} U_{+\,1n} U_{-\,1n} m_{\tilde{\chi}_n} \{ g_2^2 (V_{KM})_{i'j} (V^\dagger_{KM})_{j'1} \hat{c}_{qq}{}^{i'[j'} \hat{c}_{ql}{}^{k]3} I(\tilde{\chi}_n, \tilde{u}_{i'_L}, \tilde{d}_{j'_L}) \\
& \quad + g_2^2 (V_{KM})_{k'k} \hat{c}_{qq}{}^{[1j} \hat{c}_{ql}{}^{k']3} I(\tilde{\chi}_n, \tilde{u}_{k'_L}, \tilde{e}_{3_L}) \}
\end{aligned}
\tag{4.9}
$$

The loop integral factors $\sum_n U_{+\,an} U_{-\,a'n} m_{\tilde{\chi}_n} I(\tilde{\chi}_n, b, c)$ can further be approximated

$$
\sum_n U_{+\,an} U_{-\,a'n} m_{\tilde{\chi}_n} I(\tilde{\chi}_n, b, c) \approx \begin{cases} M_{wino} I(\tilde{W}_\pm, b, c) & \text{if } a = a' = 1 \\ \mu_R I(\tilde{H}_\pm, b, c) & \text{if } a = a' = 2 \end{cases}.
$$

Hence,

$$
\frac{C_{1jk3}^{(\overline{ud})(d\nu)}}{C_{1jk3}^{(ud)(d\nu)}} \approx
$$

$$
\frac{\mu_R}{M_{wino}} \frac{\lambda_\tau \lambda_t (V_{KM})_{3k} \hat{c}^*_{ud}{}^{[1j} \hat{c}^*_{ue}{}^{3]3} I(\tilde{H}_\pm, \tilde{u}_{3_R}, \tilde{e}_{3_R})}{g_2^2 (V_{KM})_{i'j} (V^\dagger_{KM})_{j'1} \hat{c}_{qq}{}^{i'[j'} \hat{c}_{ql}{}^{k]3} I(\tilde{W}_\pm, \tilde{u}_{i'_L}, \tilde{d}_{j'_L}) + g_2^2 (V_{KM})_{k'k} \hat{c}_{qq}{}^{[1j} \hat{c}_{ql}{}^{k']3} I(\tilde{W}_\pm, \tilde{u}_{k'_L}, \tilde{e}_{3_L})}
\tag{4.10}
$$

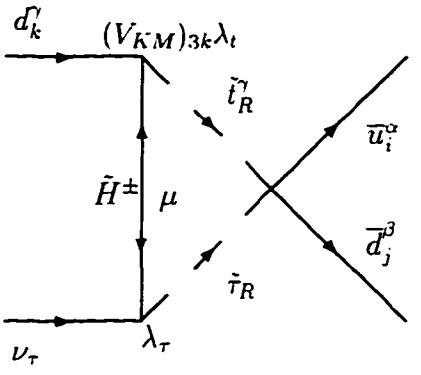

Figure 4.3: Feynman diagram that gives the dominant contribution to $C_{1jk3}^{(\overline{ud})(d\nu)}$.

The integral $I(a,b,c)$ is approximately $\log(b^2/c^2)/(b^2-c^2)$ in the limit where $a \ll b,c$. i.e. when squarks and sleptons are much more massive than gauginos, which generally is the limit we are interested in. Using the fact that the first and second generation squarks are approximately degenerate, and that the first and second generation squarks are usually more massive than the third generation squarks and sleptons, the ratio can be further approximated

$$\frac{C_{1jk3}^{(\overline{ud})(d\nu)}}{C_{1jk3}^{(ud)(d\nu)}} \approx \frac{\mu_R}{M_{wino}} \frac{(m_{\rm squark}^{1,2})^2 \log(m^2_{\tilde{u}_{3R}}/m^2_{\tilde{e}_{3R}})}{m^2_{\tilde{u}_{3R}} - m^2_{\tilde{e}_{3R}}} \times \frac{\lambda_\tau \lambda_t (V_{KM})_{3k} \hat{c}_{ud}^{*\,[1j} \hat{c}_{ue}^{*\,3]3}}{g_2^2 (V_{KM})_{i'j} (V_{KM}^\dagger)_{j'1} \hat{c}_{qq}{}^{i'[j'} \hat{c}_{ql}{}^{k]3} + g_2^2 (V_{KM})_{k'k} \hat{c}_{qq}{}^{[1j} \hat{c}_{ql}{}^{k']3}} \tag{4.11}$$

where $m_{squark}^{1,2}$ is the mass of the first and second generation squarks.

Several factors contribute to the fact that this ratio is often greater than one. Since the third generation squarks and sleptons are lighter than the first and second

generation squarks, the ratio is significantly enhanced by the factor

$$\frac{(m^{1,2}_{\rm squark})^2 \log(m^2_{\tilde{u}_{3_R}}/m^2_{\tilde{e}_{3_R}})}{m^2_{\tilde{u}_{3_R}} - m^2_{\tilde{e}_{3_R}}} \approx \left(\frac{m^{1,2}_{\rm squark}}{\max(m_{\tilde{u}_{3_R}}, m_{\tilde{e}_{3_R}})}\right)^2 .$$

Second, the ratio

$$\frac{\lambda_\tau \lambda_t (V_{KM})_{3k} \hat{c}^*_{ud}{}^{[1j} \hat{c}^*_{ue}{}^{3]3}}{g_2^2 (V_{KM})_{i'j} (V^\dagger_{KM})_{j'1} \hat{c}_{qq}{}^{i'[j'} \hat{c}_{ql}{}^{k]3} + g_2^2 (V_{KM})_{k'k} \hat{c}_{qq}{}^{[1j} \hat{c}_{ql}{}^{k']3}} \tag{4.12}$$

is itself typically of order unity for many values of the GUT scale initial parameters. Note, this ratio is greatly enhanced in the regime of large $\tan\beta$ considered in this thesis.

Finally, the ratio μ_R/M_{wino} plays a critical role in whether the LLRR operators dominate over LLLL operators in the third generation and whether the third generation anti-neutrino dominates over the second-generation. Comparing Tables 4.10, 4.11, 4.12, 4.18, 4.19, and 4.20 with Tables 4.13 and 4.21, we see that there is a direct correlation between $\mu_R/m_{1/2}$ and the dominance of the third generation LLRR operators. When $\mu_R/m_{1/2}$ is small, the third generation LLRR operators can be suppressed. Moreover, because the third generation LLRR operators are suppressed when $\mu_R/m_{1/2}$ is small, the second generation anti-neutrino contributes more significantly than the third when $\mu_R/m_{1/2}$ is small.[15] In particular, in runs I and II, $\mu_R/m_{1/2}$ is small ($\sim .3$) while in runs III(1), III(2), and III(3), $\mu_R/m_{1/2}$ is near 1 or greater, and $\mu_R/m_{1/2}$ increases as one goes from run III(1) to run III(2) to run III(3). As a result, looking at the tau anti-neutrino columns of Tables 4.10 and 4.18, we see that, for any particular model, the entries of those columns for runs I and II are smaller than they are for runs III(1), III(2), and III(3), and that the entries in those columns increase

[15]Arnowitt, et al. observed that LLRR operators can be significant to nucleon decay rates under certain circumstances in ref. [43].

steadily in going from run III(1) to III(2) to III(3). Similarly, looking at the 3rd columns of Tables 4.11, 4.12, 4.19, and 4.20, we see that the LLLL operators of the second generation anti-neutrino are fairly significant to the overall decay rate in runs I and II, while they are not quite as significant in runs III(1), III(2), and III(3), and that the significance of the LLLL operators of the second generation anti-neutrino continually decreases in going from run III(1) to III(2) to III(3).

For the first and second generation anti-neutrinos, on the other hand, the LLRR operators are negligible because they are suppressed in comparison to the LLLL operators by the up and charm Yukawa couplings, respectively. Thus, the entries in the electron and muon anti-neutrino columns of Tables 4.10 and 4.18 are fairly small, and the entries in columns 2 and 4 of Tables 4.11, 4.12, 4.19, and 4.20 are fairly small. In comparison, the second generation anti-neutrino LLLL operator is the most significant of the LLLL operators, but the third generation LLLL operator is not negligible in comparison to the second generation LLLL operator. (See columns 1, 3, and 5 of Tables 4.11, 4.12, 4.19, and 4.20.).

4.4.3 $p \to \pi^+\overline{\nu}$ vs. $p \to K^+\overline{\nu}$

Secondly, we see that under certain circumstances, the decay $p \to \pi^+\overline{\nu}$ dominates over $K^+\overline{\nu}$ when the $\mathcal{O}_{13}$ operator is included in model 4(c). When the third generation anti-neutrino dominates over the the other generations, we have the approximate result

$$\frac{\Gamma(p \to \pi^+\overline{\nu})}{\Gamma(p \to K^+\overline{\nu})} \approx 3.9 \frac{\left|(V_{KM})_{31}\hat{c}''_{ud}{}^{[11}\hat{c}''_{ue}{}^{3]3}\right|^2}{\left|.28(V_{KM})_{31}\hat{c}''_{ud}{}^{[12}\hat{c}''_{ue}{}^{3]3} + (V_{KM})_{32}\hat{c}''_{ud}{}^{[11}\hat{c}''_{ue}{}^{3]3}\right|^2}$$

$$= 3.9 \left|\frac{(V_{KM})_{31}}{(V_{KM})_{32}}\right|^2 \frac{\left|\hat{c}''_{ud}{}^{[11}\hat{c}''_{ue}{}^{3]3}\right|^2}{\left|.28\frac{(V_{KM})_{31}}{(V_{KM})_{32}}\hat{c}''_{ud}{}^{[12}\hat{c}''_{ue}{}^{3]3} + \hat{c}''_{ud}{}^{[11}\hat{c}''_{ue}{}^{3]3}\right|^2} \qquad (4.13)$$

In section 4.6, we show that $|(V_{KM})_{31}| \equiv |V_{td}|$ increases when the $\mathcal{O}_{13}$ operator is included. The increase in the ratio of the rate of $p \to \pi^+\overline{\nu}$ versus $p \to K^+\overline{\nu}$ when the $\mathcal{O}_{13}$ operator is included can be attributed in large part to this increase in $|V_{td}|$, since eqn. 4.13 contains a multiplicative factor of $|V_{td}/V_{ts}|^2$. This increase is further enhanced by the fact that $(V_{KM})_{31}\hat{c}^*_{ud}{}^{[12}\hat{c}^*_{ue}{}^{3]3}$ has roughly the opposite sign of $(V_{KM})_{32}\hat{c}^*_{ud}{}^{[11}\hat{c}^*_{ue}{}^{3]3}$, and hence increasing $|V_{td}|$ decreases the denominator in eqn. 4.13. Thus, the addition of the $\mathcal{O}_{13}$ operator in model 4(c) increases the ratio of the $p \to \pi^+\overline{\nu}$ decay rate to $p \to K^+\overline{\nu}$, *provided* that the third generation anti-neutrino dominates.

Whether the third generation dominates over the second depends on the ratio of $\mu_R/m_{1/2}$. Thus, $p \to \pi^+\overline{\nu}$ will be larger than $p \to K^+\overline{\nu}$ if the $\mathcal{O}_{13}$ operator is included and $\mu_R/m_{1/2}$ is not much smaller than one. Thus, in runs III(1), III(2), and III(3) of Table 4.4, $\mu_R/m_{1/2}$ is approximately one or bigger, and as a result the third generation anti-neutrino dominates the rate of decay, and the ratio of the rate of decay into $\pi^+\overline{\nu}$ versus the rate of decay into $K^+\overline{\nu}$ is significantly enhanced in comparison to the runs without the $\mathcal{O}_{13}$ operator in Table 4.14. On the other hand, in runs I and II, $\mu_R/m_{1/2}$ is small, and as a result, the second generation dominates and the ratio of the rate of decay into $\pi^+\overline{\nu}$ versus $K^+\overline{\nu}$ remains near what it was without the $\mathcal{O}_{13}$ operator.

4.4.4 "Generic" SU(5) vs Large $\tan\beta$ SO(10) models

$n \to \pi^0\overline{\nu}$ vs. $n \to \eta\overline{\nu}$

Furthermore, the tables of the previous section show some important differences between the nucleon decay predictions for our SO(10) model versus the predictions of a generic SUSY minimal SU(5) model. Because the effective color triplet Higgs mass is constrained to be lower than around 10^{17} GeV in SUSY minimal SU(5) [24], and

because the lifetimes of the nucleons are proportional to $\sin^2 2\beta$ [44, 43, 24], minimal SU(5) models use small $\tan\beta$ to be consistent with the experimental limits on proton decay. When $\tan\beta$ is small, LLRR operators can often be neglected. When LLRR operators are negligible, the ratio $\Gamma(n \to \pi^0\overline{\nu})/\Gamma(n \to \eta\overline{\nu})$ just depends on chiral Lagrangian factors.

$$\begin{aligned}\frac{\Gamma(n \to \pi^0\overline{\nu})}{\Gamma(n \to \eta\overline{\nu})} &\approx 2.8\frac{\sum_i \left|\beta C^{(ud)(d\nu_i)} + \alpha C^{(\overline{ud})(d\nu_i)}\right|^2}{\sum_i \left|\beta C^{(ud)(d\nu_i)} - .140\alpha C^{(\overline{ud})(d\nu_i)}\right|^2} \\ &\approx 2.8 \end{aligned} \tag{4.14}$$

In contrast, when $\tan\beta$ is large, LLRR operators are not negligible. The contribution of LLRR operators to $n \to \eta\overline{\nu}$ is significantly suppressed in comparison to its contribution to $n \to \pi^0\overline{\nu}$ by chiral Lagrangian factors. Hence, looking at Tables 4.5 and 4.15, the rate of $n \to \pi^0\overline{\nu}$ can be anywhere from 2.9 to over 100 times larger than the rate of $n \to \eta\overline{\nu}$, depending on whether the third generation LLRR operators or the second generation LLLL operators dominate.

$n \to K^{\cdot 0}\overline{\nu}$ vs. $p \to K^{\cdot +}\overline{\nu}$

Secondly, the ratio $\Gamma(n \to K^{\cdot 0}\overline{\nu})/\Gamma(p \to K^{\cdot +}\overline{\nu})$ differs significantly from the generic SU(5) models. Numerically,

$$\frac{\Gamma(n \to K^{\cdot 0}\overline{\nu})}{\Gamma(p \to K^{\cdot +}\overline{\nu})} \approx \left|\frac{\beta(1.14C^{(us)(d\nu_i)} + 1.58C^{(ud)(s\nu_i)}) + \alpha(-.86C^{(\overline{us})(d\nu_i)} + 1.58C^{(\overline{ud})(s\nu_i)})}{\beta(.44C^{(us)(d\nu_i)} + 1.58C^{(ud)(s\nu_i)}) + \alpha(.44C^{(\overline{us})(d\nu_i)} + 1.58C^{(\overline{ud})(s\nu_i)})}\right|^2 \tag{4.15}$$

In the minimal SU(5) model, the $C^{(us)(d\nu_i)}$ operator is approximately equal to the $C^{(ud)(s\nu_i)}$ [44, 43, 24], and, since LLRR operators are often negligible, $\Gamma(n \to K^{\cdot 0}\overline{\nu})/\Gamma(p \to K^{\cdot +}\overline{\nu}) \approx 1.8$. [24]. However, in our SO(10) model, LLRR operators tend to dominate. Not only are the chiral Lagrangian factors different when the LLRR operators

dominate, but $C^{(\overline{us})(d\nu_i)}$ tends to point in the *opposite* direction as $C^{(\overline{ud})(s\nu_i)}$. Hence, $\Gamma(n \to K^0\overline{\nu})/\Gamma(p \to K^+\overline{\nu})$ is much larger than its value in the minimal SU(5) models. Indeed, $n \to K^0\overline{\nu}$ can be over 18 times bigger than $p \to K^+\overline{\nu}$.

Also noteworthy is the fact that when LLRR operators dominate, $\Gamma(n \to K^0\overline{\nu})/\Gamma(p \to K^+\overline{\nu})$ is significantly higher when the $\mathcal{O}_{13}$ operator is included in comparison to when it is not. (For example, in run III(3) $\Gamma(n \to K^0\overline{\nu})/\Gamma(p \to K^+\overline{\nu})$ is 18.1 with the $\mathcal{O}_{13}$ operator included while it is no greater than 4.5 for run III(3) without the $\mathcal{O}_{13}$ operator.) Much of the enhancement can be explained by the fact that $|V_{td}|$ is larger when the $\mathcal{O}_{13}$ operator is included. When LLRR operators dominate,

$$\frac{\Gamma(n \to K^0\overline{\nu})}{\Gamma(p \to K^+\overline{\nu})} \approx \left| \frac{-.86C^{(\overline{us})(d\nu_i)} + 1.58C^{(\overline{ud})(s\nu_i)}}{.44C^{(\overline{us})(d\nu_i)} + 1.58C^{(\overline{ud})(s\nu_i)}} \right|^2 \tag{4.16}$$

Plugging eqn. 4.8 into this formula, this becomes

$$\frac{\Gamma(n \to K^0\overline{\nu})}{\Gamma(p \to K^+\overline{\nu})} \approx \left| \frac{-.86(V_{KM})_{31}\hat{c}^*_{ud}{}^{[12}\hat{c}^*_{ue}{}^{3]3} + 1.58(V_{KM})_{32}\hat{c}^*_{ud}{}^{[11}\hat{c}^*_{ue}{}^{3]3}}{.44(V_{KM})_{31}\hat{c}^*_{ud}{}^{[12}\hat{c}^*_{ue}{}^{3]3} + 1.58(V_{KM})_{32}\hat{c}^*_{ud}{}^{[11}\hat{c}^*_{ue}{}^{3]3}} \right|^2 \tag{4.17}$$

Since $(V_{KM})_{31}\hat{c}^*_{ud}{}^{[12}\hat{c}^*_{ue}{}^{3]3}$ tends to have the opposite sign as $(V_{KM})_{32}\hat{c}^*_{ud}{}^{[11}\hat{c}^*_{ue}{}^{3]3}$, $\Gamma(n \to K^0\overline{\nu})/\Gamma(p \to K^+\overline{\nu})$ is enhanced when $|V_{td}|$ is increased.

4.4.5 Sensitivity to "22" Clebsch

Furthermore, by looking at Tables 4.14 through 4.21, we can determine how sensitive nucleon decay rate predictions are on the Clebsches that enter into the c_{qq}, c_{ql}, c_{ud}, and c_{ue} matrices. For each of the five runs of Tables 4.14 through 4.21, the *only* difference between the versions a through f in each run are the y_{qq}, y_{ql}, y_{ud} and y_{ue} Clebsches of Table 4.1 that enter into the c_{qq}, c_{ql}, c_{ud}, and c_{ue} matrices. We see that the overall rate of decay is quite sensitive to the different choices for Clebsches. For example, with $\beta = -\alpha$, $\tau(p \to K^+\overline{\nu})$ for run I(e) is

7.5 times larger than $\tau(p \to K^{+}\overline{\nu})$ for run I(f). The branching ratios generally exhibit less sensitivity: $\Gamma(n \to \pi^{0}\overline{\nu})/\Gamma(n \to K^{0}\overline{\nu})$ exhibits virtually no sensitivity and $\Gamma(p \to \pi^{+}\overline{\nu})/\Gamma(p \to K^{+}\overline{\nu})$ exhibits relatively mild sensitivity. However, branching ratios into less dominant decay modes can at certain times exhibit high sensitivity. For example, with $\beta = -\alpha$, $\Gamma(n \to \eta\overline{\nu})/\Gamma(n \to K^{0}\overline{\nu})$ is over 12 times larger for run I(f) than it is for run I(c).

4.4.6 Gluino vs. Chargino contributions

It can also be seen that the contributions of gluinos to the rate of nucleon decay is often not negligible. Indeed, in several examples, excluding the gluinos' contribution can lead to a decrease in the predicted rate of decay of greater than 60%, in cases where gluinos constructively interfere, or an increase in the rate of decay by over 150%, where gluinos destructively interfere.[16] Note also that whether gluinos constructively or destructively interfere depends heavily on the phase of the chiral Lagrangian parameter $\arg(\beta/\alpha)$.

4.4.7 Proton decay from gauge boson exchange

Finally we note that our analysis only includes the contribution to nucleon decay from the effective dimension 5 operators resulting from colored triplet Higgs exchanges. We have neglected the contribution to nucleon decay via heavy gauge boson exchange (effective dimension 6 operators). This approximation is justified in our models for the dominant decay modes. For example, in order to obtain the ϵ_3 of run III(1), we can choose the vevs a_1, a_2, $\tilde{a}$, and a singlet field $\mathcal{S}_4$, defined in Chapter

[16]Goto, et al. observed that gluino loops can be important in the minimal SU(5) model in ref. [45]. For an earlier discussion, see [43]

3, which enter into the SO(10) breaking sector of the theory, to be 2.0×10^{16} GeV, 1.0×10^{16} GeV, 6.0×10^{16} GeV, and $.66 \times 10^{16}$ GeV, respectively, i.e. all of order M_{GUT}. Then the masses of the gauge bosons contained in $SO(10)/(SU(3) \times SU(2) \times U(1))$ - $X^{\pm}$, $Q^{\pm}$, $U^{\pm}$, and $E^{\pm}$ are 3.2×10^{16} GeV, 1.2×10^{17} GeV, 1.3×10^{17} GeV, and 1.3×10^{17} GeV, respectively[17]. The decay mode which would be the most dominant if all other contributions to proton decay except the contribution due to gauge boson exchanges were neglected is $p \to \pi^0 e^+$. With the above gauge boson masses, the partial proton lifetime due to heavy gauge boson exchanges for $p \to \pi^0 e^+$ is 1.2×10^{38} yrs, corresponding to a branching ratio of order $< 10^{-4}$. Of the decay modes listed in Tables 4.4 and 4.14, gauge exchange is competitive only with $p \to \eta \mu^+$.

4.5 Conclusions for Chapter 4

We have shown that model 4(c) predicts nucleon decay rates consistent with all current experimental bounds, while using values of GUT parameters that give fermion masses, mixing angles, and gauge couplings in good agreement with experimental observations. Our main results can be found in Tables 4.4, 4.5, and 4.13. We conclude that our model predicts that nucleon decay is likely to be observed by SuperKAMIOKANDE or ICARUS, which are expected to probe nucleon lifetimes up to around 10^{34} yrs [46, 47], for various decay modes predicted by GUTs.

In order to avoid this conclusion one would need to make squarks and sleptons "unnaturally" heavy and beyond the reach of LHC or increase the effective color

[17]Note, the $X^{\pm}$ gauge boson is the massive gauge boson from the 24 representation of SU(5); $Q^{\pm}$ is the gauge boson from the 10, 15, $\overline{10}$, and $\overline{15}$ representations of SU(5) which is in the $(3, 2, \frac{1}{3})$ and $(\overline{3}, 2, -\frac{1}{3})$ representations of SU(3)×SU(2)×U(1); and $U^{\pm}$ and $E^{\pm}$ are gauge bosons from the 10 and $\overline{10}$ representations of SU(5) which are in $\{(3, 1, \frac{4}{3}), (\overline{3}, 1, -\frac{4}{3})\}$ and $\{(1, 1, -2), (1, 1, 2)\}$ representations of SU(3)×SU(2)×U(1), respectively.

triplet Higgs mass $\tilde{M}_t$, which would require a supermassive Higgs doublet in the GUT desert with mass many orders of magnitude lower than the GUT scale and at least an order of magnitude lighter than any other particle getting mass around the GUT scale. Moreover, we have chosen the poorly known chiral Lagrangian parameter $|\beta|$ to be at the lowest value suggested by the data. If it could be shown that $|\beta|$ lies in the higher range of its current bounds, non-observation of nucleon decay by SuperKAMIOKANDE and ICARUS could make our model unnatural for any reasonable values of the squark and slepton masses.[18] For these reasons, we believe that these models, if correct, necessarily lead to observable nucleon decay rates.

We have shown that LLRR operators are not only significant, but often dominate, nucleon decay in the large tan β regime - as long as $\mu_R/m_{1/2}$ is not very small. As a result, if nucleon decay is observed, there are two key experimental observables that may distinguish between large or small tan β SUSY GUTs: the ratios $\Gamma(n \to K^0\overline{\nu})/\Gamma(p \to K^+\overline{\nu})$ and $\Gamma(n \to \eta\overline{\nu})/\Gamma(n \to \pi^0\overline{\nu})$. In particular, evidence for a neutron lifetime $(\frac{1}{5} - \frac{1}{20})\times$ the proton lifetime would be a strong indication for large tan β SUSY GUTs. Observation of $\Gamma(n \to \eta\overline{\nu})/\Gamma(n \to \pi^0\overline{\nu})$ significantly lower than than the predicted value when LLRR operators are negligible could also indicate large tan β SUSY GUTs.

We have also shown that gaugino loops cannot be neglected when calculating proton decay rates in models such as ours. In fact, neglecting gaugino loops could lead to an underestimation of the decay rates of over 60% or overestimation of over 150%.

[18]Recall, however, that the chiral Lagrangian approach tends to overestimate nucleon decay rates [40] and thus underestimates the lifetimes.

Finally, we have studied the sensitivity of nucleon lifetime and branching ratio predictions on the "quality" of the predictions that these models make for fermion masses and mixing angles. In the models we have analyzed, the entries in the c_{qq}, c_{ql}, c_{ud}, and c_{ue} matrices are related to entries in the Y_u, Y_d, and Y_e matrices by Clebsches which depend on the version of the model being considered. As we have seen, the lifetimes and branching ratios can be quite sensitive to the choice of Clebsches — some predictions vary by nearly an order of magnitude depending on the choice of Clebsches. In models 4(a) through (f), without the $\mathcal{O}_{13}$ operator, the different Clebsches have no effect on the predictions for fermion masses and mixing angles. Comparing models 4(a) through (f), without the $\mathcal{O}_{13}$ operator, which is consistent with fermion masses and mixing angles at 2σ, with model 4(c), with the $\mathcal{O}_{13}$ operator, which is consistent within 1σ, one is lead to conclude that fitting the data within 1 or 2 σ can have a significant effect on the nucleon decay predictions. Thus "predictions" for nucleon decay lifetimes and branching ratios cannot be expected to be any better than the complementary predictions for fermion masses and mixing angles.

4.6 Why $|V_{td}|$ increases when the $\mathcal{O}_{13}$ is included in model 4(c)

It can be seen that our Y_d and Y_e matrices, which have the general form,

$$\begin{pmatrix} 0 & zC & uDe^{i\delta} \\ zC & yEe^{i\phi} & xB \\ u'De^{i\delta} & x'B & A \end{pmatrix}$$

with $C, D \ll B, E \ll A$, can be diagonalized by multiplying the matrices on the left and right by matrices S and T, respectively, where

$$S \approx \begin{pmatrix} 1 & -(zC - \frac{x'uBD}{A}e^{i\delta})\frac{e^{-i\phi}}{yE} & -\frac{uDe^{i\delta}}{A} + \frac{xBe^{-i\phi}}{yEA}(zC - \frac{x'uBD}{A}e^{i\delta}) \\ (zC - \frac{x'uBD}{A}e^{-i\delta})\frac{e^{i\phi}}{yE} & 1 & -\frac{xB}{A} \\ \frac{uDe^{-i\delta}}{A} & \frac{xB}{A} & 1 \end{pmatrix}$$

$$T \approx \begin{pmatrix} 1 & (zC - \frac{xu'BD}{A}e^{-i\delta})\frac{e^{i\phi}}{yE} & \frac{u'De^{-i\delta}}{A} \\ -(zC - \frac{xu'BD}{A}e^{i\delta})\frac{e^{-i\phi}}{yE} & 1 & \frac{x'B}{A} \\ -\frac{u'De^{i\delta}}{A} + \frac{x'Be^{-i\phi}}{yEA}(zC - \frac{xu'BD}{A}e^{i\delta}) & -\frac{x'B}{A} & 1 \end{pmatrix}$$

Our Y_u matrix, which has the general form

$$\begin{pmatrix} 0 & zC & uDe^{i\delta} \\ zC & 0 & xB \\ u'De^{i\delta} & x'B & A \end{pmatrix}$$

with $C, D \ll B, E \ll A$ and $C \ll xx'B^2/A$, is diagonalized by the S and T matrices

$$S \approx \begin{pmatrix} 1 & \frac{A}{xx'B^2}(zC - \frac{x'uBD}{A}e^{i\delta}) & -\frac{zC}{x'B} \\ -\frac{A}{xx'B^2}(zC - \frac{x'uBD}{A}e^{-i\delta}) & 1 & -\frac{xB}{A} \\ \frac{uD}{A}e^{-i\delta} & \frac{xB}{A} & 1 \end{pmatrix}$$

$$T \approx \begin{pmatrix} 1 & -\frac{A}{xx'B^2}(zC - \frac{xu'BD}{A}e^{-i\delta}) & \frac{u'D}{A}e^{-i\delta} \\ \frac{A}{xx'B^2}(zC - \frac{xu'BD}{A}e^{i\delta}) & 1 & \frac{x'B}{A} \\ -\frac{zC}{xB} & -\frac{x'B}{A} & 1 \end{pmatrix}$$

Therefore, at M_{GUT}

$$V_{td} \approx$$

$$\frac{D}{A}e^{i\delta}(u_u - u_d) + \frac{BC}{AE}e^{-i\phi}\frac{z_d}{y_d}(x_d - x_u) + (\frac{B}{A})^2\frac{D}{E}\frac{(x_u - x_d)x'_d u_d}{y_d}e^{i(\delta-\phi)}$$

$$\begin{aligned} &= -2\frac{D}{A}e^{i\delta} - 12\frac{BC}{AE}e^{-i\phi} + \frac{16}{243}(\frac{B}{A})^2\frac{D}{E}e^{i(\delta-\phi)} \\ &\approx -12e^{-i\phi}(\frac{BC}{AE} + \frac{1}{6}\frac{D}{A}e^{i(\delta+\phi)}) \end{aligned} \tag{4.18}$$

Since $\delta + \phi \approx 30°$, the $De^{i(\delta+\phi)}/(6A)$ term will increase $|V_{td}|$ provided that the $BC/(AE)$ term does not decrease too much when the $\mathcal{O}_{13}$ operator is included.

What effect does the $\mathcal{O}_{13}$ operator have on the A, B, C, and E parameters? The A parameter will not be affected at all because A is fixed purely by the third generation masses m_b and m_τ [9]. Moreover, the first generation Yukawa coupling λ_e of the Y_e matrix is approximately equal to

$$\frac{243}{E}\left|C^2 - \frac{109}{27}CD\frac{B}{A}e^{i\delta}\right| \tag{4.19}$$

at M_{GUT}. Since δ is typically close to 2π, the term of the absolute value linear in D decreases the eigenvalue. Therefore, C must be increased to compensate for the $\mathcal{O}_{13}$ operator.

On the other hand, when B is evaluated by using the global χ^2 analysis of ref. [25], B actually decreases when the $\mathcal{O}_{13}$ operator is included. It was shown in ref. [25] that when a global χ^2 analysis is done, B_K, the bag constant which comes into the theoretical formula for the experimental observable ϵ_K measuring CP violation, and $|V_{cb}|$ come out too high; and $|V_{ub}/V_{cb}|$ comes out too low, in comparison with their experimental measurements, for model 4 without an $\mathcal{O}_{13}$ operator. Since $V_{cb} \approx \zeta|x_d - x_u|B/A$ where ζ is a renormalization group factor, this means that B is too high. It was also shown in ref. [25] that unless an $\mathcal{O}_{13}$ operator is included, V_{cb} and V_{ub}/V_{cb} cannot be corrected by changing the parameters without further increasing B_K, which is already too high. Furthermore, B and E are related by the equation

$$\left|3AEe^{i\phi} - B^2\right| \approx \lambda_\mu \lambda_\tau.$$

Since $\mathrm{Re}\,\phi < 0$, E is lower when the $\mathcal{O}_{13}$ operator is not included because B is higher than it should be.

However, when the $\mathcal{O}_{13}$ operator is added to model 4(c), it is possible to lower B to bring it in line with the experimental value for $|V_{cb}|$ while simultaneously having reasonable values for B_K as well as for the other observables [25]. The net effect of including the $\mathcal{O}_{13}$ operator to model 4(c) is that B is typically decreased by $\sim 10\%$, E is increased by $\sim 18\%$, and C is increased by $\sim 25\%$. Therefore, $BC/(AE)$ actually decreases slightly ($\sim 3\%$). However, the decrease in that term is more than compensated for by the increase in $|V_{td}|$ due to the $\frac{D}{6A}e^{i(\delta+\phi)}$ term. The net result of the inclusion of the $\mathcal{O}_{13}$ operator is an increase in $|V_{td}|$ typically of $\sim 11\%$.

CHAPTER 5

INDIVIDUAL LEPTON NUMBER VIOLATION

5.1 Introduction

In SUSY GUTs, the non-conservation of individual lepton number is particularly interesting and potentially problematic. In the Standard Model, individual lepton number is conserved. However, extensions of the Standard Model as simple as giving neutrinos non-degenerate masses will break this symmetry.[19] [51] In supersymmetric models, individual lepton number is generally violated by processes such as those shown in Fig. 5.1. [7, 8, 6] Because of supersymmetry breaking, sleptons and leptons in the same supermultiplet will not in be in the same mass eigenstate. Accordingly, there are the matrices $\Gamma_{E,L}$ $\Gamma_{E,R}$, and Γ_{ν} which transform the basis in which the sleptons' corresponding lepton superpartners are in mass eigenstates into the slepton mass eigenstate basis. These Γ matrices appear at the slepton-lepton-gaugino and slepton-lepton-higgsino interaction vertices. The Γ matrices' off-diagonal elements correspond to interactions in which a lepton of one generation can be converted to a slepton of a different generation, which, through another interaction, can in turn be

[19]It should be noted however that the branching ratio for $\mu \to e\gamma$ resulting when the Standard Model is extended to give neutrinos mass is around 30 orders of magnitude lower than the experimental bound. [51] The branching ratio for $\mu \to e\gamma$ is the most significant experimental constraint on individual lepton number violation.

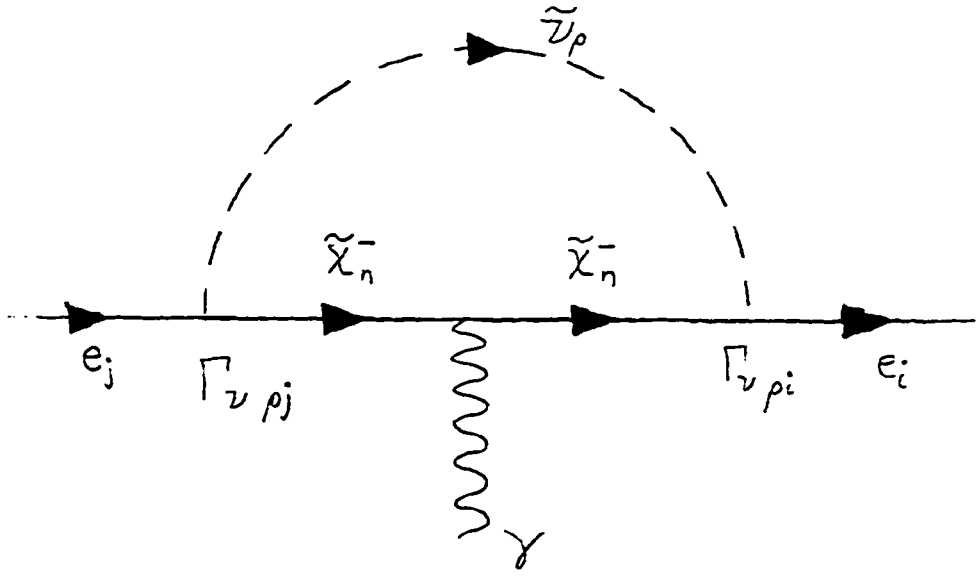

Figure 5.1: One loop chargino Feynman diagram contributing to $e_j \to e_i\gamma$. (Fermions in diagram are Dirac fermions.)

converted to a lepton of a different generation than the original lepton. Moreover, if the sleptons were all degenerate, there would be no individual lepton number violating processes. Since any basis would be a mass eigenstate basis for the sleptons, one could always choose the Γ matrices to be diagonal.

Thus, in supersymmetric extensions of the Standard Model, the rates of individual lepton number violating processes depend critically on the form of the slepton mass matrices. In the MSSM, sleptons obtain their masses primarily through explicit soft supersymmetry-breaking terms, namely, through the terms

$$\tilde{l}^* m_L^2 \tilde{l} + \tilde{e} m_E^2 \tilde{e}^* + (\tilde{l} A_e \tilde{e} h - \mu \tilde{l} Y_e \tilde{e} \bar{h}^* + \text{h.c.})$$

in the potential. (See Appendix A.) Constraints from experimental measurements of individual lepton number violating processes put strong constraints on the form of

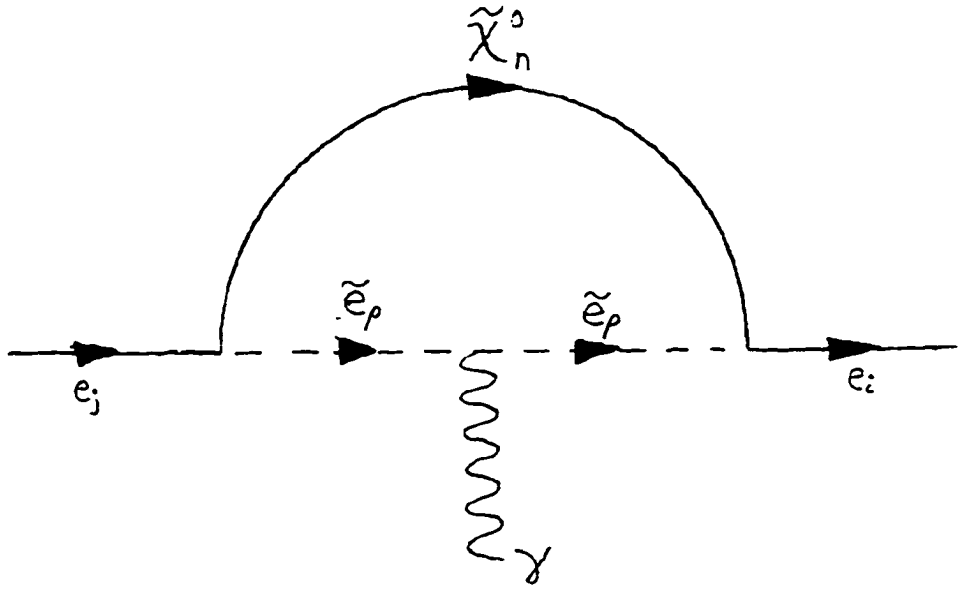

Figure 5.2: One loop neutralino Feynman diagram contributing to $e_j \rightarrow e_i\gamma$. (Fermions in diagram are Dirac fermions.)

the m_L^2, m_E^2, and A_e matrices. The most severe constraint of these is from $\mu \rightarrow e\gamma$. The branching ratio for $\mu \rightarrow e\gamma$ is known to be lower than 4.9×10^{-11}. [52] If sparticle masses are constrained to be lower than around a few TeV, a high degree of degeneracy in the first and second generations is usually necessary in order to satisfy the experimental bounds on $\mu \rightarrow e\gamma$.

One can justify a large degree of degeneracy by hypothesizing that whatever model is being built is a low energy effective theory corresponding to a minimal supergravity theory. Minimal supergravity theories predict "universal" values for the running values of soft supersymmetry breaking parameters at a scale around the Planck scale. [35] For a general supersymmetric theory, universal values of the supersymmetry-breaking terms at some mass scale M means that if the superspace potential for the

theory is of the form

$$Y_i^1\Phi_i + Y_{ij}^2\Phi_i\Phi_j + Y_{ijk}^3\Phi_i\Phi_j\Phi_k + ...$$

where the Φ's are chiral superfields and the Y's are coupling constants, the SUSY-breaking terms will be

$$-m_0^2\tilde{\Phi}_i^*\tilde{\Phi}_i - A_1Y_i^1\tilde{\Phi}_i - A_2Y_{ij}^2\tilde{\Phi}_i\tilde{\Phi}_j - A_3Y_{ijk}^3\tilde{\Phi}_i\tilde{\Phi}_j\tilde{\Phi}_k + ...$$

at M, where $\tilde{\Phi}$ is the (non-auxiliary) scalar field in the Φ supermultiplet; and m_0 and the A's are parameters of the theory. Namely, if the MSSM were a valid effective theory up to around the Planck scale and if the MSSM were a low energy manifestation of a minimal supergravity model, minimal supergravity theories would predict

$$m_{H_u}^2 = m_{H_d}^2 = m_0^2$$

$$m_Q^2 = m_U^2 = m_D^2 = m_E^2 = m_L^2 = m_0^2 I$$

$$A_u = A_0 Y_u$$

$$A_d = A_0 Y_d$$

$$A_e = A_0 Y_e$$

at around M_{Planck}.

Universality can be justified also in terms of a superstring theory [49], in which case the SUSY-breaking parameters will be universal at the string scale M_{string}.

An additional advantage of assuming universal values of the soft supersymmetry-breaking terms which is especially attractive from the point of view of model building, is that it reduces the nearly one hundred parameters [53] that appear in the soft supersymmetry-breaking terms to just seven, thus making the theory substantially

more predictive. Accordingly, we will assume universal SUSY-breaking terms at some scale M_s, which is near the Planck or string scales.

In fact, if the soft SUSY breaking parameters were universal at the scale M_s and if the MSSM were a valid effective theory up to the M_s scale, there would be no individual lepton number violation at all. In the MSSM, if the supersymmetry-breaking terms are universal at some scale, then the full Lagrangian will have individual lepton number-conserving symmetry, as can easily be seen by choosing a basis for the lepton supermultiplets in which the Yukawa matrices are diagonal.

However, supersymmetric grand unification theories predict that the MSSM is not a valid theory above the Grand Unification Scale $M_{GUT} \approx 10^{16}$ GeV. Individual lepton number conservation is not generally a symmetry of such theories, even if the running masses of the grand unified theory are universal at M_s. As a result, the supersymmetry-breaking scalar mass terms will start off universal at M_s and will develop a certain amount of non-universality as a result of the renormalization group running from M_s to the Grand Unification scale. [6] We will show, in addition, that non-universality can occur in higher dimension effective supersymmetry-breaking multilinear[20] terms when the multilinear terms are formed from lower dimensioned multilinear terms by integrating out superheavy scalar fields from the full theory. This source of non-universality does not appear as the result of the renormalization group running of the theory above the GUT scale, but instead appears in the boundary conditions at the GUT scale matching the quantities of the full theory to the quantities appearing in the effective theory valid below the GUT scale. Since there

[20] "SUSY-breaking multilinear terms" are simply generalizations of SUSY-breaking bilinear and trilinear terms such as those found in eqn. (A.5). Namely, they are terms in the Lagrangian of the form $a(\phi_1\phi_2\ldots\phi_n)$, where ϕ_1 to ϕ_n are scalar fields and a is some coupling constant.

would be no individual lepton number violation if the symmetry breaking terms of the *effective* theory below the GUT scale were universal at the Grand Unification scale. any individual lepton number violation that does occur is the result of the renormalization group running between the M_s and Grand Unification scales and/or the form of the boundary conditions at the GUT scale. Hence, individual lepton number violating processes are interesting because they potentially can give clues about physics at energies many orders of magnitude above energies accessible by current particle colliders.

Note also that, unlike baryon number-violating processes, individual lepton number-violating processes are *not* suppressed by the mass of the GUT scale to some power. In SUSY GUTs having R parity, baryon number-violating processes are mediated by particles with mass of order the GUT scale and, hence, are suppressed by the mass of these superheavy particles. By contrast, individual lepton number-violating processes are not mediated by supermassive particles and thus are not suppressed because of the massiveness of such particles, but instead are suppressed because of the smallness of the slepton-lepton mixing angles and the mass splittings between the sleptons. Because the GUT scale is so close to the M_s scale, only a small amount of non-universality can develop as a result of the renormalization group running between the M_s scale and GUT scale, and therefore, as long as the non-universality introduced as a result of the GUT scale boundary conditions is not too large, the sizes of the inter-generational slepton mixing angles and of the slepton mass splittings are suppressed. Thus, individual lepton number-violating processes are interesting because the mechanism by which they are suppressed is qualitatively different from the mechanism through which baryon number-violating processes are suppressed. Moreover, because

the rates of baryon number-violating processes depend critically on the effective color triplet mass, the predictions for the overall rates of baryon number-violating processes are only as good as the prediction for the effective color triplet mass. By contrast, because the mechanism for suppression of individual lepton number-violating processes does not depend on placing a bound on the mass of some superheavy particle(s) mediating the process, predictions for individual lepton number violation do not have the degree of flexibility that baryon number-violating processes have. Thus, much more stringent constraints on models can potentially be achieved by studying individual lepton-number violation.

5.2 Model 4(c), RG running above the GUT scale, and boundary conditions at the GUT scale

5.2.1 Model 4(c)

Recall that in model 4(c), the superspace potential for the full theory W_{FULL} is given by

$$W_{FULL} = W_{sym.breaking} + W_{fermion} + W_{neutrino} + W_{extraneous}$$

where

$$\begin{aligned} W_{sym\,breaking} = \quad & \tfrac{1}{M} A_1'(A_1^3 + \mathcal{S}_3 S A_1 + \mathcal{S}_4 A_1 A_2) \\ & + A_2(\psi\overline{\psi} + \mathcal{S}_1 \tilde{A}) + S\tilde{A}^2 \\ & + S'(S\mathcal{S}_2 + A_1\tilde{A}) + \mathcal{S}_3 S'^2, \end{aligned} \tag{5.1}$$

$$\begin{aligned} W_{fermion} = \quad & \\ & 16_3 10_1 16_3 + \bar{\psi}_1 A_1 16_3 + \bar{\psi}_1 \tilde{A}\psi_1 + \psi_1 10_1 \psi_2 \\ & + \bar{\psi}_2 \tilde{A}\psi_2 + \bar{\psi}_2 A_2 16_2 + \bar{\psi}_3 A_1 16_2 \end{aligned}$$

$$+\psi_3 10_1 \psi_4 + \mathcal{S}_M \textstyle\sum_{a=3}^{9} (\bar{\psi}_a \psi_a)$$

$$+\bar{\psi}_4 \tilde{A} 16_2 + \bar{\psi}_5 \tilde{A} \psi_4 + \bar{\psi}_6 \tilde{A} \psi_5$$

$$+\psi_6 10_1 \psi_7 + \bar{\psi}_7 \tilde{A} \psi_8 + \bar{\psi}_8 \tilde{A} \psi_9 + \bar{\psi}_9 \tilde{A} 16_1 + \bar{\psi}_6 A_2 16_3,$$

$$W_{neutrino} = \quad \bar{\psi} \textstyle\sum_{i=1}^{3} 16_i \, N_i, \qquad \text{and}$$

$$W_{extraneous} = \quad \bar{\psi}_2 A_1' \psi_1 \mathcal{S}_2 + \bar{\psi}_2 A_1' 16_3 \mathcal{S}_3 + \bar{\psi}_5 A_1' \psi_3 \mathcal{S}_3.$$

where it is implied that each term is multiplied by some coupling constant. The field $\mathcal{S}_M$ gets a vev of order M_{Planck}. Moreover, the field S typically gets a vev of order 10^{14} GeV. This, in turn, through the vacuum minimization conditions for the superpotential (eqn. 3.17) means that $\mathcal{S}_2$ and $\mathcal{S}_3$ get vacuum expectation values of order 10^{18} GeV. In turn, the $SS'\mathcal{S}_2$ and $S'^2\mathcal{S}_3$ terms give S and S' SO(10) invariant masses around the Planck scale. Accordingly, one can integrate out the fields ψ_3, ψ_4, ..., ψ_9, $\overline{\psi}_3$, $\overline{\psi}_4$, ..., $\overline{\psi}_9$, S, and S' since they get masses greater than the Planck scale, and instead consider below the Planck scale an effective theory whose superspace potential is the following:

$$\begin{aligned}
W \;=\; & \lambda_A 16_3 10_1 16_3 + \gamma_1 \overline{\psi}_1 A_1 16_3 + \gamma_2 \overline{\psi}_2 A_2 16_2 + \gamma_{\tilde{A}1} \overline{\psi}_1 A_1 \psi_1 + \gamma_{\tilde{A}2} \overline{\psi}_2 A_2 \psi_2 \\
& + \lambda_B \psi_1 10_1 \psi_2 + \frac{1}{M^2} \lambda_E e^{i\phi} 16_2 A_1 10_1 \tilde{A} 16_2 + \frac{1}{M^4} \lambda_D e^{i\delta} 16_1 \tilde{A}^3 10_1 A_2 16_3 \\
& + \frac{1}{M^6} \lambda_C 16_2 \tilde{A}^3 10_1 \tilde{A}^3 16_1 + \gamma_{10_1 A_1 10_2} 10_1 A_1 10_2 + \gamma_{\mathcal{S}_-} 10_2^2 \\
& + \frac{1}{M} \gamma_{A_1' A_1^3} A_1' A_1^3 + \frac{1}{M} \gamma_{\mathcal{S}_4} \mathcal{S}_4 A_1' A_1 A_2 \\
& + \gamma_{\psi A_2 \overline{\psi}} \overline{\psi} A_2 \psi + \gamma_{\mathcal{S}_1} \mathcal{S}_1 A_2 \tilde{A} + W_{eff} \\
& + \frac{1}{M} \gamma_{16_3 A_1' \overline{\psi}_2 \mathcal{S}_3} 16_3 A_1' \overline{\psi}_2 \mathcal{S}_3 + \frac{1}{M} \gamma_{\psi_1 A_1' \overline{\psi}_2 \mathcal{S}_2} \psi_1 A_1' \overline{\psi}_2 \mathcal{S}_2 \\
& + \lambda_{N_1} \overline{\psi} N_1 16_1 + \lambda_{N_2} \overline{\psi} N_2 16_2 + \lambda_{N_3} \overline{\psi} N_3 16_3
\end{aligned} \tag{5.2}$$

where we have now explicitly included the coupling constants in the superspace potential and where W_{eff} is the effective superspace potential obtained after integrating S and S' out of $W_{S,S'}$ at the Planck scale, and where

$$W_{S,S'} = \frac{1}{M} A_1' S_3 S A_1 + S\tilde{A}^2 + S'(SS_2 + A_1\tilde{A}) + S_3 S'^2.$$

Note that λ_A, λ_B, λ_C, λ_D, and λ_E are real while all other coupling constants are complex, because we have already performed phase rotations on the fields to remove physically irrelevant phases from the terms in the superpotential which those constants multiply. As a part of this phase rotation, we have rotated the phases so that $\gamma_1\gamma_2/(\gamma_{\tilde{A}1}\gamma_{\tilde{A}2})$ is real.

What values are these coefficients allowed to have? λ_A is, of course, simply the Yukawa parameter A entering into the Yukawa matrices of the effective theory below M_{GUT}, and is therefore fixed by fitting experimental fermion mass data to be around .8 or .9. In terms of the "naturalness" of the theory, the natural requirement to make for the rest of the Yukawa coupling coefficients would be to require their magnitudes to be within around an order of magnitude of each other and of λ_A.

Observe, however, that if we assume that all couplings constants in the superpotential are around the same order of magnitude, we run into problems due to the splitting of the first and second generations through one-loop diagrams such as the ones shown in Fig. 5.3. We will therefore make an additional assumption that, for reasons having to do with physics above the Planck scale, the coupling constants for terms that involve adjoints fields (i.e. A_1', A_1, A_2, $\tilde{A}$) are one or two orders of magnitude below the coupling constants for terms that do not involve the adjoints fields, so that the terms involving adjoint fields can effectively be neglected in the renormalization group running below the Planck scale. For example, one way this

could occur is if the Kahler potential of the full supergravity theory is of the form

$$-\frac{1}{2M}\sum c_i z_i^* z_i$$

where the z_is are the superfields of the theory and the c_i's are some group theoretic number that grows with the size of the representation of the fields which it multiplies. In other words, in the effective SO(10) theory valid below the Planck scale, each kinetic term in the Lagrangian will be multiplied by a coefficient which grows with the size of the representation of the fields contained in the term. When the kinetic terms are normalized to their standard normalization, the couplings in the superpotential involving the adjoint fields will be smaller than those that do not. In section 5.5.3, we will explore just how much the adjoint couplings need to be suppressed in order to have acceptable rates for lepton flavor violating processes.

We will use a convention that all Yukawa couplings, presumed to be small are denoted using γ's, whereas Yukawa couplings not presumed to be small are denoted using λ's.

Universality at the M_s scale mandates that all of the following terms appear as supersymmetry-breaking terms in the Lagrangian.

$$\begin{aligned}
&-\mathcal{L}^0_{SUSY\ breaking} = \\
&m^2_{16_3}\widetilde{16}^*_3\widetilde{16}_3 + m^2_{16_2}\widetilde{16}^*_2\widetilde{16}_2 + m^2_{16_1}\widetilde{16}^*_1\widetilde{16}_1 + m^2_{\psi_1}\tilde{\psi}^*_1\tilde{\psi}_1 + m^2_{\psi_2}\tilde{\psi}^*_2\tilde{\psi}_2 + \ldots \\
&+(a_A\widetilde{16}_3\widetilde{10}_1\widetilde{16}_3 + \alpha_1\bar{\tilde{\psi}}_1\tilde{A}_1\widetilde{16}_3 + \alpha_2\bar{\tilde{\psi}}_2\tilde{A}_2\widetilde{16}_2 + \alpha_{\tilde{A}1}\bar{\tilde{\psi}}_1\tilde{A}_1\tilde{\psi}_1 + \alpha_{\tilde{A}2}\bar{\tilde{\psi}}_2\tilde{A}_2\tilde{\psi}_2 \\
&+a_B\tilde{\psi}_1\widetilde{10}_1\tilde{\psi}_2 + \frac{1}{M^2}a_E e^{i\phi}\widetilde{16}_2\tilde{A}_1\widetilde{10}_1\tilde{\tilde{A}}\widetilde{16}_2 + \frac{1}{M^4}\tilde{a}_D e^{i\delta}\widetilde{16}_1\tilde{\tilde{A}}^3\widetilde{10}_1\tilde{A}_2\widetilde{16}_3 \\
&+\frac{1}{M^6}a_C\widetilde{16}_2\tilde{\tilde{A}}^3\widetilde{10}_1\tilde{\tilde{A}}^3\widetilde{16}_1 + \alpha_{10_1A_110_2}\widetilde{10}_1\tilde{A}_1\widetilde{10}_2 + \alpha_{\tilde{S}}\tilde{S}\widetilde{10}^2_2 \\
&+\frac{1}{M}\alpha_{A'_1A^3_1}\tilde{A}'_1\tilde{A}^3_1 + \frac{1}{M}\alpha_{S_4}\widetilde{S}_4\tilde{A}'_1\tilde{A}_1\tilde{A}_2 \\
&+\alpha_{\psi A_2\bar{\psi}}\bar{\tilde{\psi}}\tilde{A}_2\tilde{\psi} + \alpha_{S_1}\widetilde{S}_1\tilde{A}_2\tilde{\tilde{A}} + \int W_{eff}\delta(\theta)\delta(\bar{\theta})\,d^4\theta
\end{aligned}$$

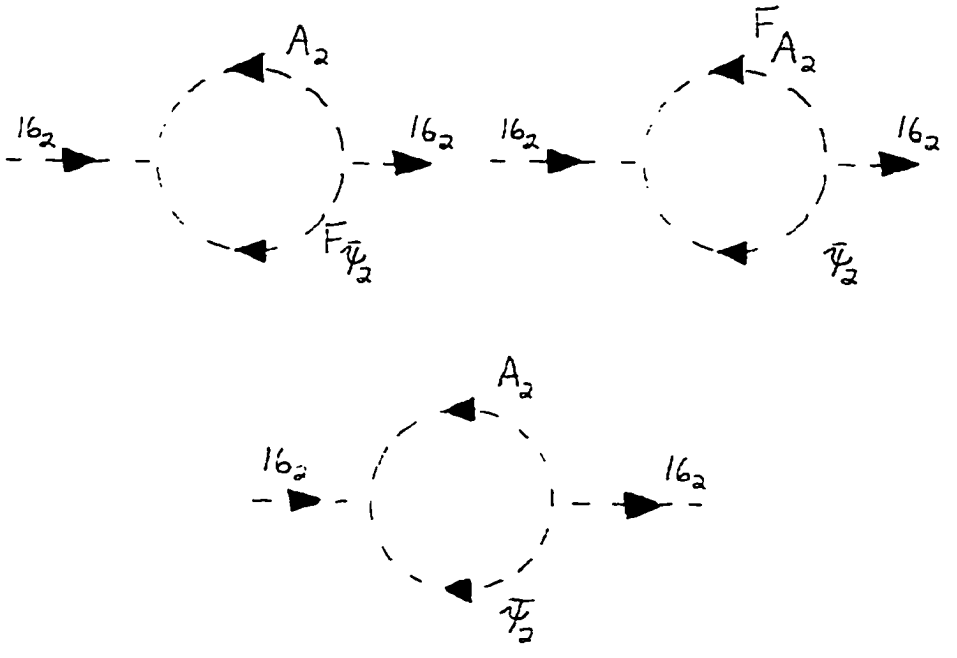

Figure 5.3: Feynman diagrams which will give rise to large mass splittings between the first and second generations of sleptons if the Yukawa couplings at the vertices are $\mathcal{O}(1)$.

$$+\frac{1}{M}\alpha_{16_3 A_1' \bar{\psi}_2 S_3}\widetilde{16}_3\tilde{A}_1'\tilde{\bar{\psi}}_2\widetilde{S}_3+\frac{1}{M}\alpha_{\psi_1 A_1' \bar{\psi}_2 S_2}\tilde{\psi}_1\tilde{A}_1'\tilde{\bar{\psi}}_2\widetilde{S}_2$$
$$+a_{N_1}\tilde{\bar{\psi}}\widetilde{N}_1\widetilde{16}_1+a_{N_2}\tilde{\bar{\psi}}\widetilde{N}_2\widetilde{16}_2+a_{N_3}\tilde{\bar{\psi}}\widetilde{N}_3\widetilde{16}_3$$

Furthermore, by the requirement of universality at the M_s scale, only these terms and terms which are generated radiatively from them can appear in the supersymmetry-breaking sector of the Lagrangian.

At one-loop order, there are six supersymmetry-breaking multilinear terms that are generated radiatively. They are depicted in Fig. 5.4. However, terms (iv), (v), and (vi) can be neglected because they do not contribute to the SUSY-breaking trilinear term parameters of the effective theory below the GUT scale. Term (iv) does not contribute because it contains $\mathrm{tr}(A_2\tilde{A})$. When A_2 and $\tilde{A}$ get vevs, $\mathrm{tr}\langle A_2\tilde{A}\rangle = 0$ and therefore term (iv) does not contribute to the effective low energy Lagrangian. Likewise, term (v) does not contribute to the A_u, A_d, or A_e matrices because the Higgs doublets of 10_1 are projected away by the vev of A_1 in the B-L direction. Term (vi) involves the 10_2 Higgs, which gets a mass of order M_{GUT}, and which therefore does not appear in the effective low energy Lagrangian.

The remaining three terms, (i), (ii), and (iii), do contribute to the low energy quantities A_u, A_d, and A_e of the effective theory below the GUT scale and therefore have been included in our calculations. Accordingly, the SUSY breaking portion of the Lagrangian $\mathcal{L}_{SUSY\ breaking}$ is given by

$$\mathcal{L}_{SUSY\ breaking}=\mathcal{L}^0_{SUSY\ breaking}+\mathcal{L}_{radiative}$$

where

$$-\mathcal{L}_{radiative}=\frac{1}{M^4}a_C' e^{i\delta}\tilde{16}_1\tilde{\bar{A}}^3\tilde{A}_2\tilde{A}_1\tilde{\bar{\psi}}_1+\frac{1}{M^4}a_D' e^{i\delta}\tilde{16}_1\tilde{\bar{A}}^3\tilde{A}_2\tilde{10}_1\tilde{16}_3+ \qquad (5.3)$$

Figure 5.4

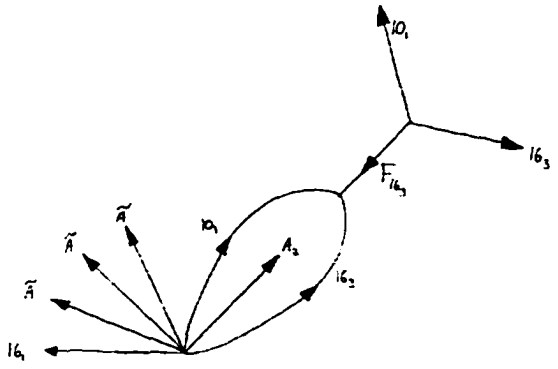

(i) $\frac{1}{M^4} 16_1 \tilde{A}^3 A_2 10_1 16_3$

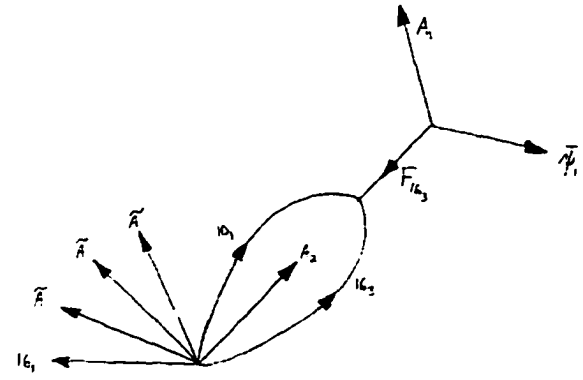

(ii) $\frac{1}{M^4} 16_1 \tilde{A}^3 A_2 A_1 \bar{\psi}_1$

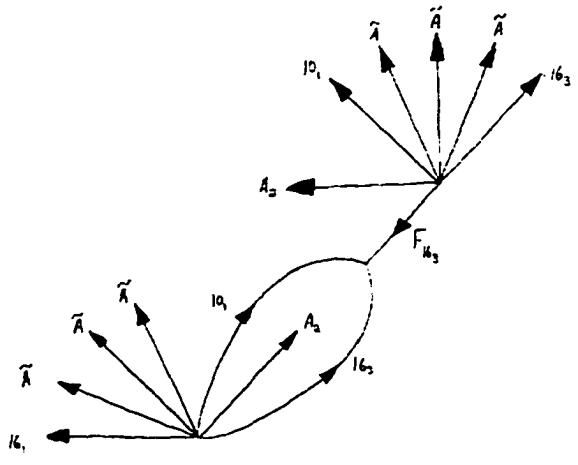

(iii) $\frac{1}{M^8} 16_1 \tilde{A}^3 A_2^2 10_1 \tilde{A}^3 16_1$

(figure continued on next page)

Figure 5.4 (continued)

(iv)

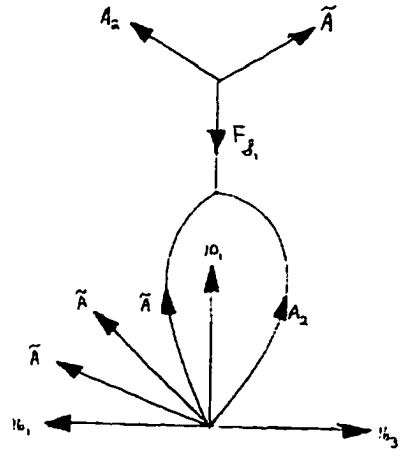

$\frac{1}{M^4}(16_1\tilde{A}^2 10_1 16_3)\mathrm{tr}(\tilde{A}A_2)$

(v)

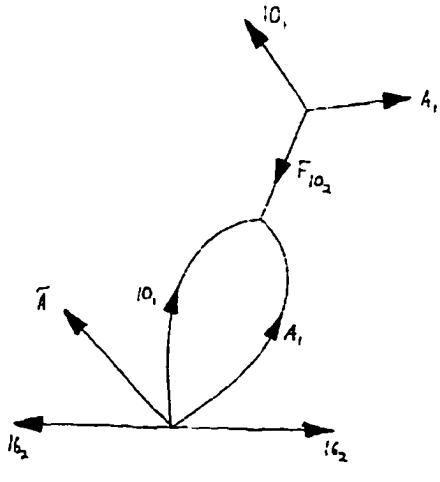

$\frac{1}{M^2}(16_2)^\alpha(\tilde{A})^\beta_\alpha\Gamma^m_{\beta\gamma}(16_2)^\gamma(10_1)^n(A_1)^{nm}$

(figure continued on next page)

Figure 5.4 (continued)

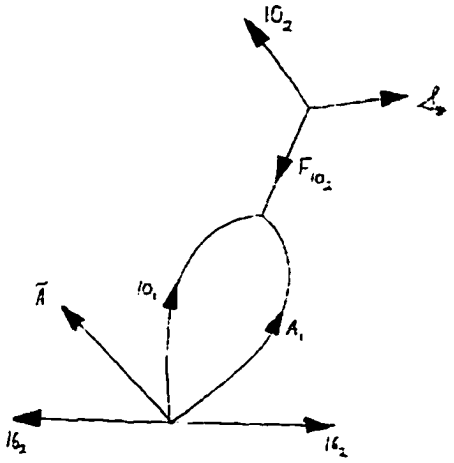

(vi) $\frac{1}{M^2}16_2\bar{A}10_2 16_2 S$

Figure 5.4: Radiatively generated SUSY breaking multilinear terms. All fields in the diagrams are scalars.

$$\frac{1}{M^8}a_F e^{2i\delta}\tilde{1}6_1\tilde{A}^3\tilde{A}_2^2\tilde{1}0_1\tilde{A}^3\tilde{1}6_1 + \ldots$$

and where the ellipsis represents the phenomenologically irrelevant terms (iv), (v), and (vi) and terms which are generated by two-loop or higher effects.[21]

5.2.2 Renormalization group equation running above the GUT scale

We will assume the standard supergravity-inspired universal boundary conditions at M_{Planck} for the RGEs above the GUT scale, except that we will include an E(6) type splitting of the scalar masses. D term splittings occur whenever a D auxiliary field obtains a non-zero vacuum expectation value. [54] The D term will then contribute

[21]Terms which are radiatively generated as the result of terms which are themselves radiatively generated are considered two-loop or higher effects. The error in the calculations resulting from neglecting such terms is of the same order of magnitude as the error introduced by truncating the renormalization group equations to one loop.

a mass term

$$\mathcal{L}_{D\,term} = g\langle D^A\rangle \varphi^\dagger T^A \varphi \tag{5.4}$$

which splits the scalar masses. In general, for each U(1) gauge symmetry of the gauge group that is broken, there may exist a corresponding D term splitting of the scalar masses. These D term splittings modify the RGE boundary conditions at the scale at which the corresponding U(1) gauge symmetry is broken, by an amount proportional to the vevs of the D fields. In sec. 5.2.4. we argue that D term splittings at the Planck scale are essential for model 4(c) in order to fit low energy data.

Thus, the RGE boundary conditions are

$$\begin{aligned}
m^2_{16_3} &= m_0^2 + \text{D-term contribution} \\
m^2_{16_2} &= m_0^2 + \text{D-term contribution} \\
m^2_{16_1} &= m_0^2 + \text{D-term contribution} \\
m^2_{\psi_1} &= m_0^2 + \text{D-term contribution} \\
&\text{etc.} \\
a_\Omega &= A_\Omega \lambda_\Omega, \qquad \text{for all } \Omega \notin \{C', D', F\} \\
\alpha_\Omega &= A_\Omega \gamma_\Omega \\
a'_C &= a'_D = a_F = 0
\end{aligned} \tag{5.5}$$

at M_{Planck}, where Ω runs over all coupling constant indices, and, for all Ω, $A_\Omega = A_i$ if A_Ω multiplies a multilinear term with i fields in it. The D term splittings will be specified in sec. 5.2.4. Note that the α's are all negligible in comparison to the a's since the γ's are negligible in comparison to the λ's. In order to make the problem of analyzing the lepton flavor violation more tractable, the number of parameters in the theory will be reduced by assuming by fiat that at the M_s scale all the A_i's are

equal. The value which they are equal to, denoted A_0, will be called the universal multilinear parameter.

Renormalization group effects are taken into account using one-loop renormalization group equations from M_{Planck} to M_{GUT}. The sort of diagrams that enter into the calculation of the one-loop RGEs for this theory are shown schematically in Fig. 5.5. The full one-loop RGEs for model 4(c) are given in the Appendix.

5.2.3 GUT scale RGE boundary conditions

An effective field theory valid below the GUT scale is obtained by integrating superheavy fields out of the full theory. The quantities in the full theory are related to the quantities in the effective theory by calculating the boundary conditions at M_{GUT} for the RGEs for quantities of the effective theory in terms of the quantities in the full theory.

The model 4(c) superpotential generates effective fermion mass operators $\mathcal{O}_{33}$, $\mathcal{O}_{23}$, $\mathcal{O}_{22}$, $\mathcal{O}_{13}$, and $\mathcal{O}_{12}$, which, in turn, produces the Yukawa matrices Y_u, Y_d, and Y_e, expressions for which are given at M_{GUT} by eqn. (4.1). The Yukawa parameters A, B, C, D, and E appearing in that equation are related to the quantities in the full theory by the boundary condition

$$\begin{aligned} A &= \lambda_A \\ B &= \frac{3}{2}\lambda_B \zeta_1 \zeta_2 \\ C &= (\frac{\tilde{a}}{2M})^6 \frac{1}{2}\lambda_C \\ D &= \frac{3}{32}\frac{\tilde{a}^3 a_2}{M^4}\lambda_D \\ E &= \frac{a_1 \tilde{a}}{2M^2}\lambda_E \end{aligned} \tag{5.6}$$

Figure 5.5

Wavefunction renormalization

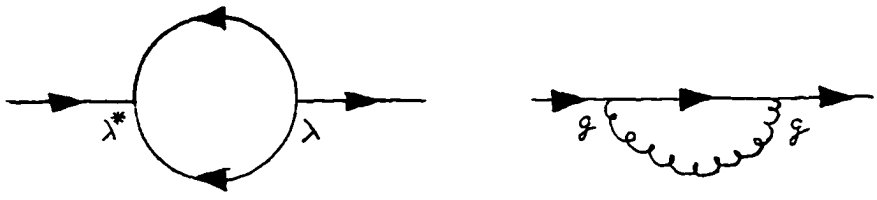

SUSY breaking multilinear term renormalization

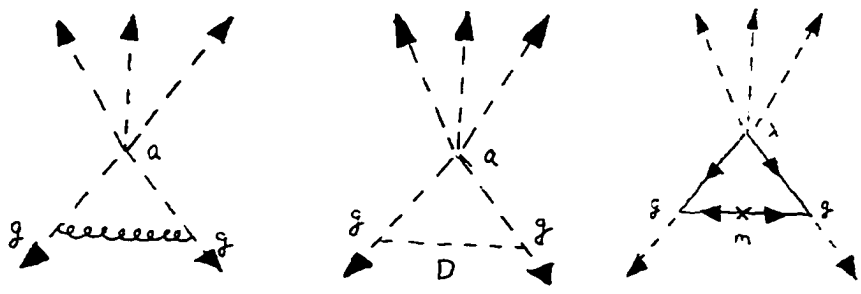

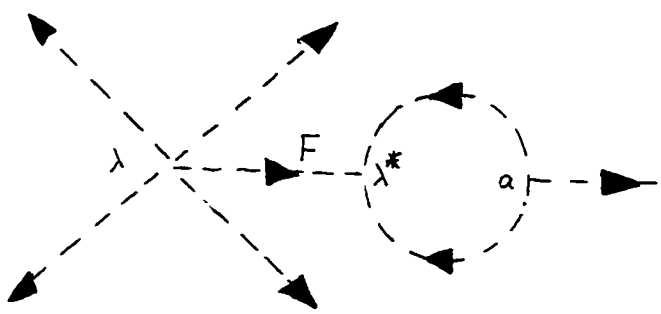

(figure continued on next page)

Figure 5.5 (continued)

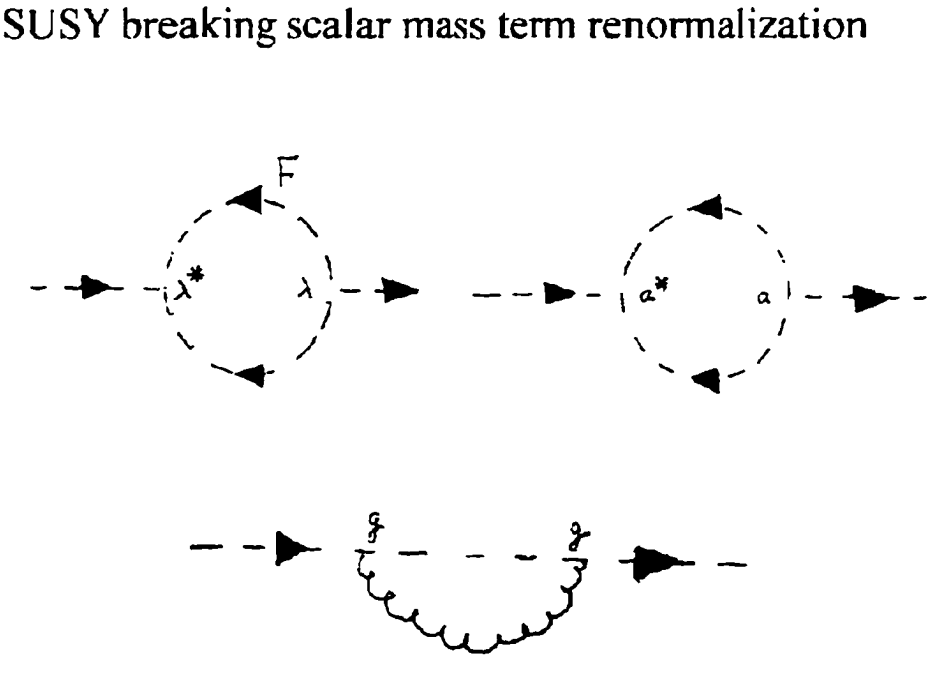

Figure 5.5: Feynman diagrams entering the calculation of the one loop RGEs above the GUT scale. The lines in the wavefunction renormalization diagrams represent superfields. In all other diagrams, solid and dashed lines represent scalar and fermionic fields, respectively.

where

$$\zeta_1 = \frac{\gamma_1 a_1}{\gamma_{\tilde{A}1}\tilde{a}}$$
$$\zeta_2 = \frac{\gamma_2 a_2}{\gamma_{\tilde{A}2}\tilde{a}} \tag{5.7}$$

Similarly, integrating the superheavy fields out leads to effective SUSY breaking trilinear operators $\widetilde{\mathcal{O}_{33}}$, $\widetilde{\mathcal{O}_{23}}$, $\widetilde{\mathcal{O}_{22}}$, $\widetilde{\mathcal{O}_{13}}$, and $\widetilde{\mathcal{O}_{12}}$ given by

$$\widetilde{\mathcal{O}_{33}} = A_A \widetilde{16}_3 \widetilde{10}_1 \widetilde{16}_3$$
$$\widetilde{\mathcal{O}_{23}} = 2A_B \widetilde{16}_3 (\tfrac{Y}{X}) \widetilde{10}_1 (\tfrac{B-L}{X}) \widetilde{16}_2$$
$$\widetilde{\mathcal{O}_{22}} = A_E e^{i\phi} \widetilde{16}_2 (B-L) \widetilde{10}_1 X \widetilde{16}_2$$
$$\widetilde{\mathcal{O}_{12}} = 2A_C \widetilde{16}_2 X^3 \widetilde{10}_1 X^3 \widetilde{16}_1$$
$$\widetilde{\mathcal{O}_{13}} = 2A_D e^{i\delta} \widetilde{16}_1 X^3 \widetilde{10}_1 Y \widetilde{16}_3 \tag{5.8}$$

However, there are additional effective SUSY-breaking trilinear operators, $\widetilde{\mathcal{O}_{13}}'$, $\widetilde{\mathcal{O}_{12}}'$, and $\widetilde{\mathcal{O}_{11}}'$, generated as a result of the radiatively induced multilinear operators of the full theory. These operators are given by

$$\begin{aligned}
\widetilde{\mathcal{O}_{13}}' &= 2A'_D e^{i\delta} \widetilde{16}_1 X^3 Y \widetilde{10}_1 \widetilde{16}_3 \\
\widetilde{\mathcal{O}_{12}}' &= 2A'_C e^{i\delta} \widetilde{16}_1 X^2 Y (B-L) \widetilde{10}_1 \frac{Y}{X} \widetilde{16}_2 \\
\widetilde{\mathcal{O}_{11}}' &= A_F e^{2i\delta} \widetilde{16}_1 X^3 Y^2 \widetilde{10}_1 X^3 \widetilde{16}_1
\end{aligned} \tag{5.9}$$

Using these operators, the matrices A_u, A_d, and A_e entering into the low energy supersymmetry-breaking trilinear terms can be calculated at M_{GUT}.

$$A_u = \begin{pmatrix} \frac{17}{9}A_F e^{2i\delta} & A_C - \frac{4}{9}A'_C e^{i\delta} & (-\frac{4}{3}A_D + \frac{1}{3}A'_D)e^{i\delta} \\ A_C + \frac{4}{9}A'_C e^{i\delta} & 0 & -\frac{1}{3}A_B \\ (\frac{1}{3}A_D - \frac{4}{3}A'_D)e^{i\delta} & -\frac{4}{3}A_B & A_A \end{pmatrix}$$

$$A_d = \begin{pmatrix} -15A_F e^{2i\delta} & -27A_C - \frac{2}{27}A'_C e^{i\delta} & (\frac{2}{3}A_D + \frac{1}{3}A'_D)e^{i\delta} \\ -27A_C - 2A'_C e^{i\delta} & A_E e^{i\phi} & \frac{1}{9}A_B \\ (-9A_D - 18A'_D)e^{i\delta} & -\frac{2}{9}A_B & A_A \end{pmatrix}$$

$$A_e = \begin{pmatrix} -135A_F e^{2i\delta} & -27A_C + 54A'_C e^{i\delta} & (-54A_D + 27A'_D)e^{i\delta} \\ -27A_C + 2A'_C e^{i\delta} & 3A_E e^{i\phi} & A_B \\ (-A_D + 2A'_D)e^{i\delta} & 2A_B & A_A \end{pmatrix}.$$

The quantities in the matrices for the trilinear terms of the effective theory are related to those in the full theory by the RGE boundary conditions

$$A_A = a_A \tag{5.10}$$

$$A_B = \frac{3}{2}(a_B \frac{\gamma_1\gamma_2}{\gamma_{\tilde{A}1}\gamma_{\tilde{A}2}} + \alpha_1 \frac{\lambda_B\gamma_2}{\gamma_{\tilde{A}1}\gamma_{\tilde{A}2}} + \alpha_2 \frac{\lambda_B\gamma_1}{\gamma_{\tilde{A}1}\gamma_{\tilde{A}2}})\frac{a_1 a_2}{\tilde{a}^2} \tag{5.11}$$

$$A_C = (\frac{\tilde{a}}{2M})^6 \frac{1}{2} a_C \tag{5.12}$$

$$A_D = \frac{3}{32}\frac{\tilde{a}^3 a_2}{M_4} a_D \tag{5.13}$$

$$A_E = \frac{a_1\tilde{a}}{2M^2} a_E \tag{5.14}$$

$$A'_C = -\frac{9}{32}\lambda_b \frac{\gamma_2}{\gamma_{\tilde{A}1}\gamma_{\tilde{A}2}} \frac{\tilde{a}a_1 a_2^2}{M^4} a'_C \tag{5.15}$$

$$A'_D = -\frac{3}{32}\frac{\tilde{a}^3 a_2}{M^4} a'_D \tag{5.16}$$

$$A_F = -\frac{1}{2}(\frac{\tilde{a}}{2M})^6 (\frac{3a_2}{2M})^2 a_F. \tag{5.17}$$

at M_{GUT}. Note in particular the boundary condition for A_B. There are three terms in the boundary condition for A_B, corresponding to the three ways depicted in Fig. 5.6 of integrating superheavy fields out of the full theory to generate $\widetilde{\mathcal{O}_{23}}$. The three ways of generating the $\widetilde{\mathcal{O}_{23}}$ operator mean that, contrary to the current literature, universality of the quantities in the full theory at M_{GUT} does *not* imply universality of the quantities in the effective theory at M_{GUT}. In fact, A_B will be equal to $3A_0$ plus corrections resulting from RG running of the full theory from the Planck scale to the GUT scale, instead of A_0 plus corrections resulting from RG running from the Planck scale to GUT scale. This non-universality due to the boundary conditions at the GUT scale for the SUSY breaking trilinear quantities is a general feature of any effective theory whose effective trilinear terms are formed from higher dimensional

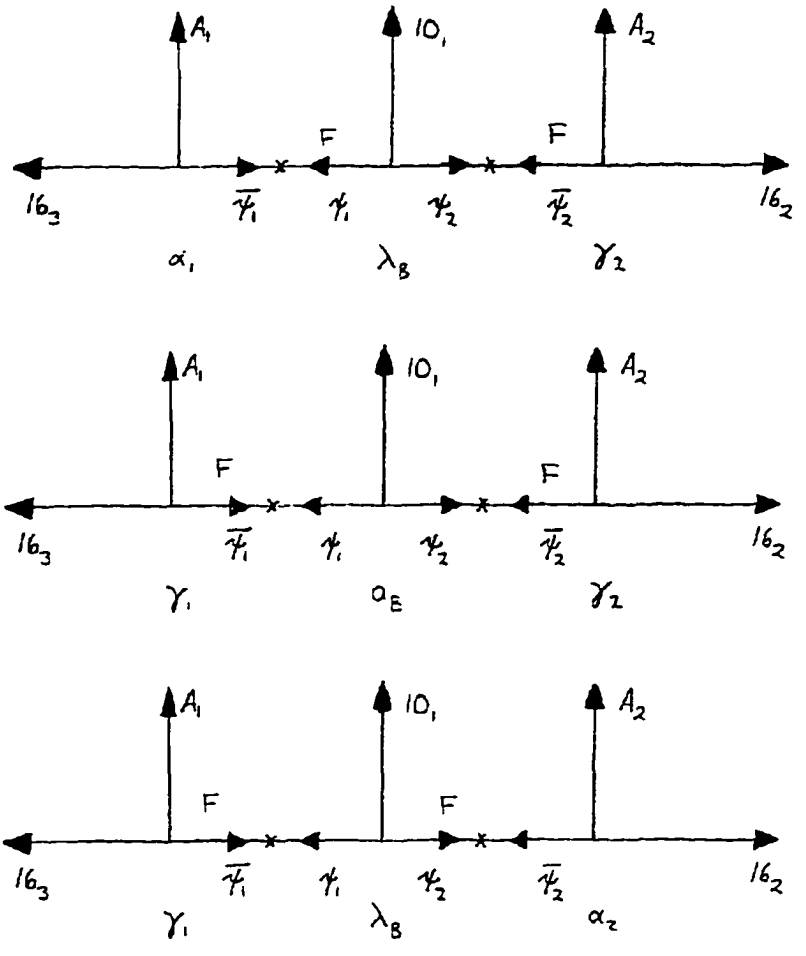

Figure 5.6: Feynman diagrams contributing to $\tilde{\mathcal{O}}_{23}$. All fields in the diagrams are scalar fields.

operators by integrating out superheavy scalars from lower dimensioned multilinear terms of some full theory. This source of non-universality was avoided for the $\mathcal{O}_{22}$, $\mathcal{O}_{12}$, and $\mathcal{O}_{13}$ operators only because the superheavy fields forming them were already integrated out at the Planck scale.

Finally, we give the boundary conditions for the scalar masses. In calculating the boundary conditions, two complications arise. First, the second and third generations

of fermions in the effective theory below the GUT scale are not the fermions in the 16_2 and 16_3 superfields of the full theory but instead are the massless mixture of fermions from the 16_2 and ψ_2, and 16_3 and ψ_1 fields, respectively. [50] The 16_3 state mixes with the ψ_1 state, and the 16_2 state mixes with the ψ_2 state through the terms $\gamma_1 16_1 A_1 \overline{\psi}_1$ and $\gamma_2 16_2 A_2 \overline{\psi}_2$. Namely, the mass terms for the 16_2 and 16_3 states are

$$W_{mass} = (\ 16_3 \quad \psi_1\ ) \begin{pmatrix} \gamma_1 \langle A_1 \rangle \\ \gamma_{\tilde{A}1} \langle \tilde{A} \rangle \end{pmatrix} \overline{\psi}_1 + (\ 16_2 \quad \psi_2\ ) \begin{pmatrix} \gamma_2 \langle A_2 \rangle \\ \gamma_{\tilde{A}2} \langle \tilde{A} \rangle \end{pmatrix} \overline{\psi}_2. \tag{5.18}$$

16_2 and 16_3 are mixtures of massless states 16_2^{massless} and 16_3^{massless}, corresponding to the second and third generations of MSSM fermions; and supermassive mass eigenstates 16_2^{massive} and 16_3^{massive}. This mixture is given by

$$\begin{pmatrix} 16_2^{\text{massive}} \\ 16_2^{\text{massless}} \end{pmatrix} = \frac{1}{\sqrt{(\gamma_2 \langle A_2 \rangle)^2 + (\gamma_{\tilde{A}2} \langle \tilde{A} \rangle)^2}} \begin{pmatrix} \gamma_2 \langle A_2 \rangle & \gamma_{\tilde{A}2} \langle \tilde{A} \rangle \\ -\gamma_{\tilde{A}2} \langle \tilde{A} \rangle & \gamma_2 \langle A_2 \rangle \end{pmatrix} \begin{pmatrix} 16_2 \\ \psi_2 \end{pmatrix} \tag{5.19}$$

$$\begin{pmatrix} 16_3^{\text{massive}} \\ 16_3^{\text{massless}} \end{pmatrix} = \frac{1}{\sqrt{(\gamma_1 \langle A_1 \rangle)^2 + (\gamma_{\tilde{A}1} \langle \tilde{A} \rangle)^2}} \begin{pmatrix} \gamma_1 \langle A_1 \rangle & \gamma_{\tilde{A}1} \langle \tilde{A} \rangle \\ -\gamma_{\tilde{A}1} \langle \tilde{A} \rangle & \gamma_1 \langle A_1 \rangle \end{pmatrix} \begin{pmatrix} 16_3 \\ \psi_1 \end{pmatrix} \tag{5.20}$$

Hence, the relevant SUSY breaking mass terms can be reexpressed

$$\begin{aligned} & m_{16_2}^2 \tilde{16}_2^* \tilde{16}_2 + m_{16_3}^2 \tilde{16}_3^* \tilde{16}_3 + m_{\psi_1}^2 \tilde{\psi}_1^* \tilde{\psi}_1 + m_{\psi_2}^2 \tilde{\psi}_2^* \tilde{\psi}_2 = \\ & \widetilde{16}_2^{\text{massless}} \frac{(\gamma_{\tilde{A}2} \langle \tilde{A} \rangle)^2 m_{16_2}^2 + (\gamma_2 \langle A_2 \rangle)^2 m_{\psi_2}^2}{(\gamma_2 \langle A_2 \rangle)^2 + (\gamma_{\tilde{A}2} \langle \tilde{A} \rangle)^2} \widetilde{16}_2^{\text{massless}} \\ & + \widetilde{16}_3^{\text{massless}} \frac{(\gamma_{\tilde{A}1} \langle \tilde{A} \rangle)^2 m_{16_3}^2 + (\gamma_1 \langle A_1 \rangle)^2 m_{\psi_1}^2}{(\gamma_1 \langle A_1 \rangle)^2 + (\gamma_{\tilde{A}1} \langle \tilde{A} \rangle)^2} \widetilde{16}_3^{\text{massless}} \\ & \quad + \text{terms involving supermassive fields} \end{aligned} \tag{5.21}$$

Second, there are D term splittings of the scalar fields resulting because the $U(1)_X$ subgroup of SO(10) is broken to reduce the rank of SO(10) down to SU(5). When the ψ and $\overline{\psi}$ fields develop vevs in the right-handed neutrino-like direction, the $U(1)_X$ D field acquires a vev proportional to $(m_\psi^2 - m_{\overline{\psi}}^2)|_{M_{GUT}}$. [54, 55] The D term splittings may be parameterized by a value M_X defined

$$M_X^2 = m_\psi^2 - m_{\overline{\psi}}^2|_{M_{GUT}} \tag{5.22}$$

Using eqn. (5.21) and treatment of D term splittings for the $U(1)_X$ symmetry given in [55], the boundary conditions for the SUSY breaking scalar masses can be calculated. They are

$$m_Q^2 = \begin{pmatrix} m_{16_1}^2 & 0 & 0 \\ 0 & \frac{m_{16_2}^2+\zeta_2^2 m_{\psi_2}^2}{1+\zeta_2^2} & 0 \\ 0 & 0 & \frac{m_{16_3}^2+\zeta_1^2 m_{\psi_1}^2}{1+\zeta_1^2} \end{pmatrix} + \frac{1}{10} M_X^2 I$$

$$m_U^2 = \begin{pmatrix} m_{16_1}^2 & 0 & 0 \\ 0 & \frac{m_{16_2}^2+16\zeta_2^2 m_{\psi_2}^2}{1+16\zeta_2^2} & 0 \\ 0 & 0 & \frac{m_{16_3}^2+\zeta_1^2 m_{\psi_1}^2}{1+\zeta_1^2} \end{pmatrix} + \frac{1}{10} M_X^2 I$$

$$m_D^2 = \begin{pmatrix} m_{16_1}^2 & 0 & 0 \\ 0 & \frac{m_{16_2}^2+\frac{4}{9}\zeta_2^2 m_{\psi_2}^2}{1+\frac{4}{9}\zeta_2^2} & 0 \\ 0 & 0 & \frac{m_{16_3}^2+\frac{1}{9}\zeta_1^2 m_{\psi_1}^2}{1+\frac{1}{9}\zeta_1^2} \end{pmatrix} - \frac{3}{10} M_X^2 I$$

$$m_L^2 = \begin{pmatrix} m_{16_1}^2 & 0 & 0 \\ 0 & \frac{m_{16_2}^2+\zeta_2^2 m_{\psi_2}^2}{1+\zeta_2^2} & 0 \\ 0 & 0 & \frac{m_{16_3}^2+\zeta_1^2 m_{\psi_1}^2}{1+\zeta_1^2} \end{pmatrix} - \frac{3}{10} M_X^2 I$$

$$m_E^2 = \begin{pmatrix} m_{16_1}^2 & 0 & 0 \\ 0 & \frac{m_{16_2}^2+36\zeta_2^2 m_{\psi_2}^2}{1+36\zeta_2^2} & 0 \\ 0 & 0 & \frac{m_{16_3}^2+9\zeta_1^2 m_{\psi_1}^2}{1+9\zeta_1^2} \end{pmatrix} + \frac{1}{10} M_X^2 I$$

$$m_{H_d}^2 = m_{10_1}^2 + \frac{2}{10} M_X^2$$

$$m_{H_u}^2 = m_{10_1}^2 - \frac{2}{10} M_X^2 \qquad (5.23)$$

Note that, the non-universality from the $U(1)_X$ D term splitting is the same for each generation. As a result, D term splittings by themselves do *not* cause lepton flavor violation.

5.2.4 Non-universality assumptions for m_{H_u} and m_{H_d} coming from D-term splittings and radiative electroweak symmetry breaking requirements

We now argue that D term splittings at the GUT and Planck scales are essential to the viability of the model 4(c) of this thesis and ADHRS models because D term splittings can be used to relax constraints on the supersymmetry-breaking parameters coming from electroweak symmetry breaking that have phenomenologically bad consequences for these models. At tree level, radiative electroweak symmetry breaking for large $\tan\beta$ models requires

$$\mu^2 = -\frac{1}{2}M_Z^2 - m_{H_u}^2 > 0 \qquad \text{at } M_Z \tag{5.24}$$

$$m_A^2 = m_{H_d}^2 - m_{H_u}^2 - M_Z^2 > 0 \qquad \text{at } M_Z \tag{5.25}$$

To understand how radiative electroweak symmetry breaking constrains the SUSY-breaking parameters, consider what happens if the SUSY-breaking parameters are universal at M_{GUT}. If the SUSY-breaking parameters were universal at M_{GUT}, eqn. (5.24) would mean that μ would be entirely determined in terms of the third generation Yukawa couplings and the other SUSY-breaking parameters m_0, $m_{1/2}$, and A_0. A detailed analysis of the constraints electroweak symmetry breaking places on the supersymmetry-breaking parameters in the case where $\tan\beta$ is large, there is top-bottom-tau Yukawa unification, and the supersymmetry-breaking parameters are universal at M_{GUT} was done in [20]. That analysis showed that $\mu(M_Z)$ and $m_A(M_Z)$ can be expressed in terms of the GUT scale values of the supersymmetry-breaking parameters

$$\mu^2 \approx 3.0\ m_{1/2}^2 + 0.3\ m_0^2 - \frac{1}{2}M_Z^2 \tag{5.26}$$

$$m_A^2 \approx a m_{1/2}^2 + b m_0^2 - M_Z^2 \tag{5.27}$$

where a and b are coefficients with $a > 0$, $b < 0$, and $|a|$ and $|b|$ are both around 20%. Combining these with constraints (5.24) and (5.25), the following relationships can be obtained for the supersymmetry-breaking parameters.

$$\mu^2 \approx 3m_{1/2}^2 \tag{5.28}$$

$$m_{1/2} > m_0 \tag{5.29}$$

However, this hierarchy for the SUSY-breaking parameters is disastrous for model 4(c) due to the size of one-loop threshold corrections to the mass of the bottom quark m_b under such a scenario. In constructing the models of ADHRS and subsequently model 4(c) of Chapter 3, one-loop threshold corrections to the fermion masses and mixing angles were neglected. As a consequence, model 4(c) fits fermion masses and mixing angles best when one-loop threshold corrections to fermion masses and mixing angles are small. However, it is known that one-loop threshold corrections to down-type quark masses and KM elements can be quite large when $\tan\beta$ is large. [20, 22] In fact, under the hierarchy for the SUSY-breaking parameters in eqns. (5.28) and (5.29), the corrections to the bottom quark mass are around 20 to 45 percent. [20] A recent χ^2 analysis of model 4(c) explicitly shows that model 4(c) gives poor χ^2 fits when the SUSY-breaking parameter hierarchy of eqns. (5.28) and (5.29) hold true. [25]

However, in the presence of $U(1)_X$ D term splittings, eqns. (5.26) and (5.27) are modified as follows. [55]

$$\mu^2 \approx 3.0m_{1/2}^2 + .3m_0^2 + .2M_X^2 - \frac{1}{2}M_Z^2 \tag{5.30}$$

$$m_A^2 \approx am_{1/2}^2 + bm_0^2 + .4M_X^2 - M_Z^2 \tag{5.31}$$

Inspecting the RGEs for m_ψ and $m_{\overline{\psi}}$, it can be seen that $m^2_\psi(M_{GUT}) > m^2_{\overline{\psi}}(M_{GUT})$ and hence that $M^2_X > 0$. From (5.31), it can be seen that as long as $M^2_X > .5m^2_0$, m^2_A will always be greater than $-m^2_Z$. Hence, having $M^2_X > .5m^2_0$ entirely eliminates relation (5.29) between $m_{1/2}$ and m_0. Nevertheless, even with constraint (5.29) eliminated, there is still a problem because μ is still too big if we want good fits to the experimental data with m_0 below a few TeV because of the correlation between m_0 and μ via (5.30).

However, we can use the idea of D term splittings to eliminate this problem if we postulate that the full superstring or other theory above the Planck scale from which model 4(c) is ultimately derived contains an additional U(1) gauge subgroup which is broken above the Planck scale and which results in D term splittings of the scalar masses at the Planck scale. In particular, we will postulate that the theory above the Planck scale from which model 4(c) is derived contains an E(6) gauge symmetry. We will assume that the 10_1 representation and the three generations of 16 representations come from a 27 representation of E(6). When this is done, D term splittings modify the RGE equations at M_{Planck} as follows.[22]

$$m^2_{10_1} = m^2_0 + 2M^2_H$$
$$m^2_{16_1} = m^2_{16_2} = m^2_{16_3} = m^2_0 - M^2_H \qquad (5.32)$$

where M_H parameterizes the size of the D term splitting. From eqns. (5.24) and (5.25), it can be seen that if m^2_H is positive, M^2_H will have the effect of raising $m^2_{H_u}$ and therefore lowering $|\mu|$ while at the same time keeping $m^2_{H_d} - m^2_{H_u}$, and hence m^2_A, approximately the same. Hence, by introducing a generation-independent E(6)-type D term splitting, constraints (5.28) and (5.29) can both be eliminated and thus values

[22]A complete description of the assignment of SO(10) representations in model 4(c) to E(6) representations and the resulting RGE boundary conditions at M_s is contained in Appendix G.

for the SUSY-breaking parameters can be chosen in the same region of parameter space where model 4(c) best fits the experimental data.

5.3 Formulas for $e_j \to e_i\gamma$ and the electron and muon dipole moments in terms of low energy parameters

The one-loop Feynman diagrams for $e_j \to e_i\gamma$ are given in Figs. 5.1 and 5.2. The ratio of decay rates $\Gamma(e_j \to e_i\gamma)/\Gamma(e_j \to e_i\nu_j\overline{\nu}_i)$ is given by

$$\frac{\Gamma(e_j \to e_i\gamma)}{\Gamma(e_j \to e_i\nu_j\overline{\nu}_i)} = \frac{6\alpha}{\pi} M_W^4(|X_L|^2 + |X_R|^2) \tag{5.33}$$

where M_W is the W-boson mass. X_L is the sum of the contributions of diagrams where a left-handed lepton is the decay product and X_R is the sum of the contributions from all diagrams where a right-handed lepton is the decay product. Expressions for the Feynman vertices relevant to these diagrams are given in Appendix B. Evaluation of the Feynman diagrams in Figs. 5.1 and 5.2 shows that

$$X_L = X_{L_f} + X_{L_g} + X_{L_h} + X_{L_j} + \frac{\lambda_{e_i}}{\lambda_{e_j}}(X_{R_f} + X_{R_g}) \tag{5.34}$$

$$X_R = X_{R_f} + X_{R_g} + X_{R_h} + X_{R_j} + \frac{\lambda_{e_i}}{\lambda_{e_j}}(X_{L_f} + X_{L_g}) \tag{5.35}$$

where

$$X_{L_f} = [\frac{1}{\sqrt{2}}\Gamma_{E,L\ \rho i}(\frac{g'}{g}U^0_{1n} + U^0_{2n}) + \Gamma_{E,R\ \rho i}\frac{\lambda_{e_i}}{g}U^0_{3n}]^*$$
$$\times[\frac{1}{\sqrt{2}}\Gamma_{E,L\ \rho j}(\frac{g'}{g}U^0_{1n} + U^0_{2n}) + \Gamma_{E,R\ \rho j}\frac{\lambda_{e_j}}{g}U^0_{3n}]\frac{1}{m^2_{\tilde{e}_\rho}} f(\frac{m^2_{\tilde{\chi}^0_n}}{m^2_{\tilde{e}_\rho}}) \tag{5.36}$$

$$X_{L_h} = [\frac{1}{\sqrt{2}}\Gamma_{E,L\ \rho i}(\frac{g'}{g}U^0_{1n} + U^0_{2n}) + \Gamma_{E,R\ \rho i}\frac{\lambda_{e_i}}{g}U^0_{3n}]^*$$
$$\times[-\sqrt{2}\frac{g'}{g}U^{0\,*}_{1n}\Gamma_{E,R\ \rho j} + \frac{\lambda_{e_j}}{g}\Gamma_{E,L\ \rho j}U^{0\,*}_{3n}]\frac{m_{\tilde{\chi}^0_n}}{m_{e_j}}\frac{1}{m^2_{\tilde{e}_\rho}} h(\frac{m^2_{\tilde{\chi}^0_n}}{m^2_{\tilde{e}_\rho}}) \tag{5.37}$$

$$X_{L_g} = -|U_{+\ 1n}|^2 \Gamma^*_{\nu\ \rho i} \Gamma_{\nu\ \rho j} \frac{1}{m^2_{\tilde{\nu}_\rho}} g(\frac{m^2_{\tilde{\chi}^\pm_n}}{m^2_{\tilde{\nu}_\rho}}) \tag{5.38}$$

$$X_{L_j} = -\Gamma^*_{\nu\ \rho i} \Gamma_{\nu\ \rho j} U_{-\ 2n} U_{+\ 1n} \frac{m_{\tilde{\chi}^\pm_n}}{g v_1} \frac{1}{m^2_{\tilde{\nu}_\rho}} j(\frac{m^2_{\tilde{\chi}^\pm_n}}{m^2_{\tilde{\nu}_\rho}}) \tag{5.39}$$

$$X_{R_f} = [-\sqrt{2}\frac{g'}{g} U^{0\ *}_{1n} \Gamma_{E.R\ \rho i} + \frac{\lambda_{e_i}}{g} \Gamma_{E.L\ \rho i} U^{0\ *}_{3n}]^*$$
$$\times [-\sqrt{2}\frac{g'}{g} U^{0\ *}_{1n} \Gamma_{E.R\ \rho j} + \frac{\lambda_{e_j}}{g} \Gamma_{E.L\ \rho j} U^{0\ *}_{3n}] \frac{1}{m^2_{\tilde{e}_\rho}} f(\frac{m^2_{\tilde{\chi}^0_n}}{m^2_{\tilde{e}_\rho}}) \tag{5.40}$$

$$X_{R_h} = [-\sqrt{2}\frac{g'}{g} U^{0\ *}_{1n} \Gamma_{E.R\ \rho i} + \frac{\lambda_{e_i}}{g} \Gamma_{E.L\ \rho i} U^{0\ *}_{3n}]^*$$
$$\times [\frac{1}{\sqrt{2}} \Gamma_{E.L\ \rho j} (\frac{g'}{g} U^0_{1n} + U^0_{2n}) + \Gamma_{E.R\ \rho j} \frac{\lambda_{e_j}}{g} U^0_{3n}] \frac{m_{\tilde{\chi}^0_n}}{m_{e_j}} \frac{1}{m^2_{\tilde{e}_\rho}} h(\frac{m^2_{\tilde{\chi}^0_n}}{m^2_{\tilde{e}_\rho}}) \tag{5.41}$$

$$X_{R_g} = -\frac{\lambda_{e_i} \lambda_{e_j}}{g^2} |U_{-\ 2n}|^2 \Gamma^*_{\nu\ \rho i} \Gamma_{\nu\ \rho j} \frac{1}{m^2_{\tilde{\nu}_\rho}} g(\frac{m^2_{\tilde{\chi}^\pm_n}}{m^2_{\tilde{\nu}_\rho}}) \tag{5.42}$$

$$X_{R_j} = -\frac{\lambda_{e_i}}{\lambda_{e_j}} \Gamma^*_{\nu\ \rho i} \Gamma_{\nu\ \rho j} U_{-\ 2n} U_{+\ 1n} \frac{m_{\tilde{\chi}^\pm_n}}{g v_1} \frac{1}{m^2_{\tilde{\nu}_\rho}} j(\frac{m^2_{\tilde{\chi}^\pm_n}}{m^2_{\tilde{\nu}_\rho}}) \tag{5.43}$$

and where

$$f(x) = \frac{1}{12(1-x)^4}(1 - 6x + 3x^2 + 2x^3 - 6x^2 \ln x)$$
$$g(x) = \frac{1}{x} f(\frac{1}{x})$$
$$h(x) = \frac{1}{2(1-x)^3}(1 - x^2 + 2x \ln x)$$
$$j(x) = \frac{1}{2(1-x)^3}(3 - 4x + x^2 + 2\ln x) \tag{5.44}$$

See [56, 53]. Note that X_{L_j}, X_{R_j}, X_{L_h}, and X_{R_h} have contributions proportional to $\tan\beta$, as can be seen in Fig. 5.7, which uses the mass insertion approximation.

It has also been suggested that the electron electric dipole moment may be competitive with the branching ratio for $\mu \to e\gamma$ as a constraint on supersymmetric

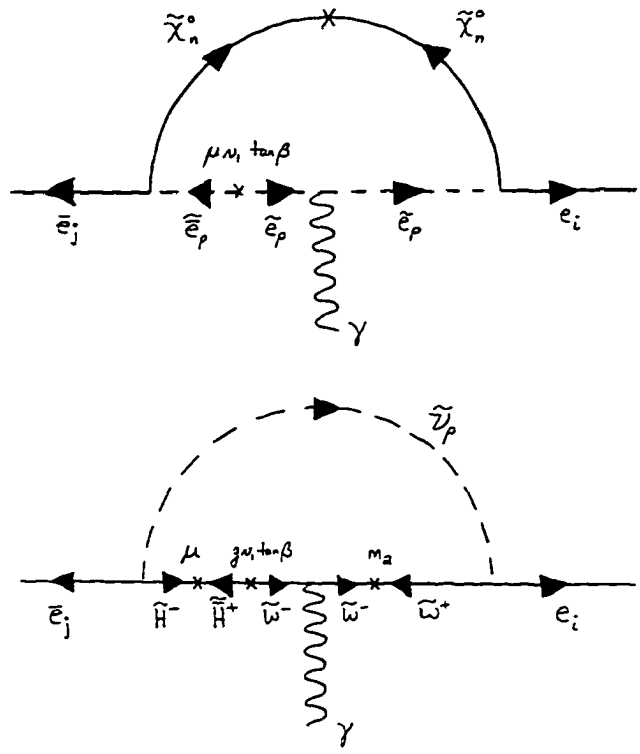

Figure 5.7: Several Feynman diagrams which are enhanced by large $\tan\beta$. Not all diagrams enhanced by large $\tan\beta$ are shown.

SO(10) theories [8]. Accordingly, we also compute the electric dipole moments of the electron and muon, d_e and d_μ, since they can readily be calculated using the Feynman diagrams for $e_i \to e_j\gamma$ decays. The electric dipole moment d_{e_i} can be calculated by computing the coefficient of the low-energy effective CP violating operator $\overline{e_i}\gamma_5\gamma_\mu e_i A_\mu$. Doing so, we find

$$d_{e_i} = \frac{1}{16\pi^2} g^2 m_{e_i}(X_L - X_R) \tag{5.45}$$

Note, however, that only X_{L_h} and X_{R_h} contribute to the electric dipole moment because the other terms cancel out when X_L is subtracted from X_R.

5.4 Numerical procedure

The low energy Yukawa parameters A, B, C, D, E, ϕ, and δ are fixed by fitting fermion masses and mixing angles and therefore are treated as essentially fixed in the numerical calculations. Values for these parameters are taken from the χ^2 analysis of [25]. Namely, in all the calculations, $A = .888$, $B = 5.89 \times 10^{-2}$, $C = 1.23 \times 10^{-4}$, $D = 5.69 \times 10^{-4}$, $E = 1.40 \times 10^{-2}$, $\phi = 1.02$, and $\delta = 5.74$. From A, B, C, D, and E: the GUT scale vevs; and the GUT scale values of γ_1, γ_2, γ_{A1}, and γ_{A2}; the values of λ_A, λ_B, λ_C, λ_D, and λ_E can be determined. The values for $\tilde{\alpha}_G$, M_G, $v_{e.w.}$, and $\tan\beta$ are also taken from [25]. In all the calculations, $\tilde{\alpha}_G^{-1} = 24.65$, $M_{GUT} = 2.86 \times 10^{16}$, $v_{e.w.} = 250$ GeV, and $\tan\beta = 55.9$. M_s is chosen to be 5.0×10^{17} GeV.

As a simplifying assumption we parameterize the effects of the γ Yukawa coupling constants by setting all of the γ's equal to a common value γ at M_{GUT}. The Yukawa couplings are set to a common values at M_{GUT}, as opposed to M_s, largely as a matter of convenience. λ_A is fixed at .888 at M_{GUT} by fermion mass data. However, the value for λ_A at M_s necessary to get $\lambda_A = .888$ at M_{GUT} depends on the values of all

the other Yukawa parameters through the RGEs. If some of the Yukawa parameters were fixed at M_s and λ_A is fixed at M_{GUT}, one would have to iteratively guess at what λ_A needs to be at the M_s in order to get $\lambda_A = .888$ at M_{GUT}. Instead, it is much more convenient to fix all of the Yukawa couplings at the same scale, M_{GUT}.

The remaining Yukawa parameters and the ratios ζ_1 and ζ_2, defined in eqn. (5.7), were chosen to satisfy three conditions:

1. ζ_1 and ζ_2 must be less than 2/3. Recall that the effective operators $\mathcal{O}_{23}$, $\mathcal{O}_{22}$, and so forth, are merely the dominant operators in an expansion in powers of M_{GUT}/M_{Planck} and M_{GUT}/M_{10}, where M_{10} is the scale at which SO(10) breaks to SU(5). In particular, there are corrections to $\mathcal{O}_{23}$ from subdominant operators, suppressed by powers to ζ_1^2 and ζ_2^2. If these corrections are too large, they will likely destroy the good agreement of model 4(c) with the experimental data. Hence, the constraint $\zeta_1, \zeta_2 < 2/3$ is placed in order to suppress these corrections.

2. It is required that all Yukawa couplings and gauge couplings remain perturbative up to M_s.

3. The parameters should be roughly in the neighborhood of where $Br(\mu \to e\gamma)$ is minimized.

Unless otherwise stated, the values for the parameters used in the numerical calculations are given in Table 5.1. These values were chosen by a mixture of theoretical analysis of what values of the parameters would be expected to minimize $\mu \to e\gamma$ and by trial and error.

A	.888	B	.0589
C	1.23×10^{-4}	D	5.6×10^{-4}
E	.014	o	1.02
δ	5.74	$\tilde{\alpha}_G^{-1}$	24.65
$\tan\beta$	55.9	$v_{e.w.}$	250
ϵ_3	$-.03$	Δ_2	-9.0
M_{GUT}	2.86×10^{16}	M_{Planck}	5.0×10^{17}
ζ_1	.67	ζ_2	.083
$\lambda_{N_1}(M_{GUT})$	1.0	$\lambda_{N_2}(M_{GUT})$	1.0
$\lambda_{N_3}(M_{GUT})$	0.1		

Table 5.1: Default values used for the parameters. All quantities in GeV units.

In order to obtain these values of ζ_1 and ζ_2 while keeping ϵ_3 and $\tilde{M}_t$ as given in Chapter 3, we set $a_1 = 4 \times 10^{16}$ GeV/γ, $a_2 = .5 \times 10^{16}$ GeV/γ, $\tilde{a} = 6 \times 10^{16}$ GeV/γ, $S_4 = 8 \times 10^{16}$ GeV/γ, $S_* = 10^{13}$ GeV/γ, and $M = 5 \times 10^{17}$ GeV/γ. With these values, ζ of eqn. (3.19) is 16 and $\epsilon_3 \approx -3\%$ while $\tilde{M}_t^{-1} = 4 \times 10^{19}$ GeV. The vevs are divided by γ in order to keep the spectrum of states getting GUT scale masses centered around 10^{16} GeV. The effect of multiplying the SO(10) symmetry-breaking portion of the superspace potential by γ while dividing the vevs by γ is to keep most of the masses fixed near what they would be if the superpotential and vevs were not multiplied and divided, resp., by γ, while splitting the gauge supermultiplet mass from the rest of the masses.

In addition, the threshold correction $\Delta_2 \equiv \alpha_G^{-1}(M_{GUT}) - \tilde{\alpha}_G^{-1}$ to the running unified gauge coupling is taken into account by setting $\Delta_2 = -9.0$ in the calculations. This value for Δ_2 represents a typical value for Δ_2 that could be obtained by appropriate choice of the GUT scale vevs and the ratios of the γ Yukawa coupling constants.

The basic procedure is as follows. The GUT scale values of the Yukawa and gauge couplings are fixed as described above. The Yukawa and gauge couplings are then run up to M_s using the equations of Appendix F. The M_s scale values for the SUSY breaking scalar masses and multilinear term couplings are determined using the boundary conditions of eqns. (5.5) and Appendix G.

The correct value of m_H^2 to use in the equations of Appendix G is determined by μ. In order to determine the value of m_H^2 necessary to give the desired value of μ, advantage is taken of the linearity of the RGEs for the scalar masses. Namely, if $\mathbf{m}_1^2$ and $\mathbf{m}_2^2$ are solutions to the RGEs for the scalar masses, then for any x, $x\mathbf{m}_1^2 + (1 - x)\mathbf{m}_2^2$ is also a solution. Except in plots where the electron sneutrino mass is held fixed, the running quantities are run twice from M_s to the electroweak scale: once with $m_H^2 = 0$ and the second time with $m_H^2 = (1000\ \text{GeV})^2$. At the electroweak scale, eqn. (5.24) and the linearity of the RGEs are used in order to determine what m_H^2 should be in order to obtain the value of μ desired. Then, the values of the scalar mass matrices m_Q^2, m_U^2, m_D^2, m_L^2, and m_E^2 are determined for that value of m_H^2 using the results of the two runs plus the linearity of the RGEs.

In plots where the electron sneutrino mass is held fixed, a similar procedure is followed except that the running quantities are run three times from M_s to the electroweak scale, using different values of m_H^2 and m_0, and then the values for m_H^2 and m_0 necessary to obtain the desired values of μ and the electron sneutrino mass are determined using the linearity of the scalar mass RGEs.

Each time the quantities are run from M_s to the electroweak scale, the equations in Appendix F are used in running from the Planck scale to the GUT scale. The GUT scale boundary conditions of sec. 5.2.3 are then used. Then, the dimensionless

(dimensionful) quantities are run from the GUT scale to M_Z using the one loop (two loop) equations of [36]. At M_Z, equations (5.33), *et seq.* are used to determine the branching ratios and electric dipole moments. In order to obtain the branching ratios for $e_j \to e_i\gamma$ the ratio of rates $\Gamma(e_j \to e_i\gamma)/\Gamma(e_j \to e_i\nu_j\bar{\nu}_i)$ is multiplied by the experimentally obtained branching ratios for $e_j \to e_i\nu_j\bar{\nu}_i$. Namely, $Br(\mu \to e\nu_\mu\bar{\nu}_e) \approx 100\%$, $Br(\tau \to \mu\nu_\tau\bar{\nu}_\mu) = 17.6\%$, and $Br(\tau \to e\nu_\tau\bar{\nu}_e) = 18.0\%$. [2].

5.5 Results

5.5.1 $Br(\mu \to e\gamma)$ vs. $m_{\tilde{\nu}_e}$, $m_{1/2}(M_{GUT})$, μ, and A_τ

We first show the branching ratio for $\mu \to e\gamma$ as a function of $m_{\tilde{\nu}_e}$, $m_{1/2}$, μ, and A_τ. We have traded the parameters m_0 and A_0 for the physically more interesting quantities $m_{\tilde{\nu}_e}$ and A_τ, where A_τ is the 33 element of A_e/λ_τ at M_Z, expressed in a basis where the lepton Yukawa matrix is diagonal.[23] The quantity $m_{\tilde{\nu}_e}$ gives information about the slepton mass spectrum, while A_τ gives information about the amount of left-right mixing for the sleptons. Figs. 5.8 - 5.10 are contour plots for the branching ratio for $\mu \to e\gamma$ in the $m_{\tilde{\nu}_e}$- $m_{1/2}$, $m_{\tilde{\nu}_e}$- μ, and $m_{\tilde{\nu}_e}$- A_τ planes, respectively. The numerical calculations were cut off at $m_0 < 700$ GeV. This was done as a matter of convenience; there is no physical significance to this cutoff. In all figures, unless stated otherwise, $\mu = 80$ GeV and $m_{1/2}(M_{GUT}) = 240$ GeV. In the plots where A_τ is not being varied, $\overline{A}_0 = 500$ GeV, where $\overline{A}_0 \equiv a_A/\lambda_A|_{M_{GUT}}$. The values $\mu = 80$ and $m_{1/2} = 240$ were chosen because they are the values of μ and $m_{1/2}$ for point II of [25]. $\overline{A}_0 = 500$ GeV was chosen because it is very near the value of $\overline{A}_0$ at which the

[23]This is in analogy to the treatment of [8]. However, we trade m_0 for $m_{\tilde{\nu}_e}$ instead of $m_{\tilde{e}_R}$ because graphs involving chargino diagrams dominate over those where neutralinos dominate in our model.

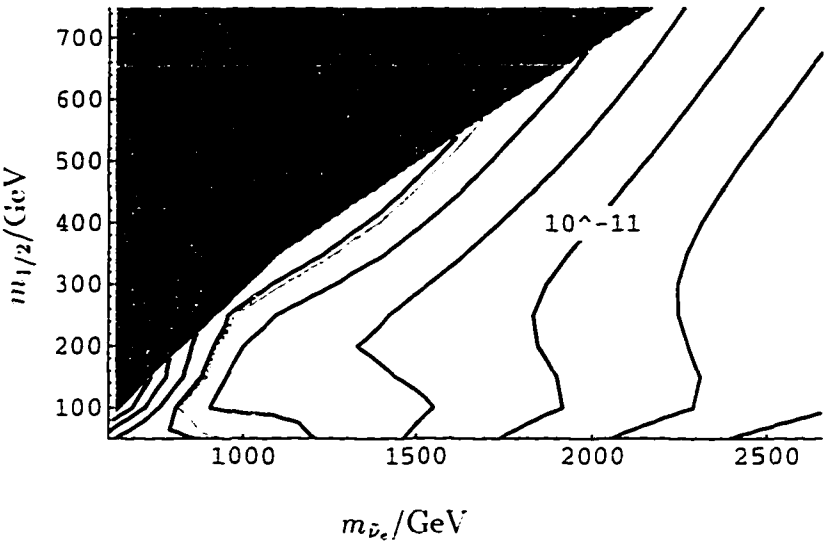

Figure 5.8: Contour plot of $Br(\mu \to e\gamma)$ in the $m_{\tilde{\nu}_e}$ - $m_{1/2}(M_{GUT})$ plane, with 4 contours per order of magnitude. The gray line shows the experimental upper bound. The gray region denotes a region of parameter space where $m_0 < 700$ GeV.

branching ratio is minimized. We find that values of $Br(\mu \to e\gamma)$ consistent with the experimental data can be found with $m_{\tilde{\nu}_e}$ as low as ~ 800 GeV.

Analysis

The dependence of the branching ratio on $m_{\tilde{\nu}_e}$ is easiest to understand. As the slepton masses get larger, they increasingly get more decoupled from low energy physics, and hence the branching ratio decreases as $m_{\tilde{\nu}_e}$ increases. Asymptotically, the branching ratio scales as $1/m_{\tilde{\nu}_e}^4$.

The dependence on μ is somewhat more complicated. For the most part, the branching ratio decreases as μ increases. This is because smaller values of μ require larger values of m_H^2 and hence larger values of $m_{10_1}^2(M_{Planck})$ in comparison to m_0^2. However, increasing $m_{10_1}^2(M_{Planck})$ in comparison to m_0^2 has the effect of increasing

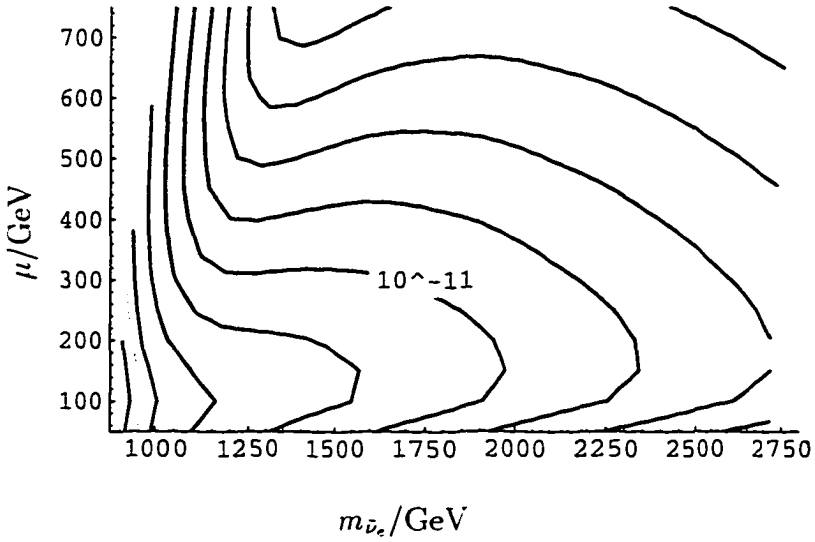

Figure 5.9: Contour plot of $Br(\mu \to e\gamma)$ in the $m_{\tilde{\nu}_e}$ - μ plane. with 4 contours per order of magnitude. The gray line shows the experimental upper bound.

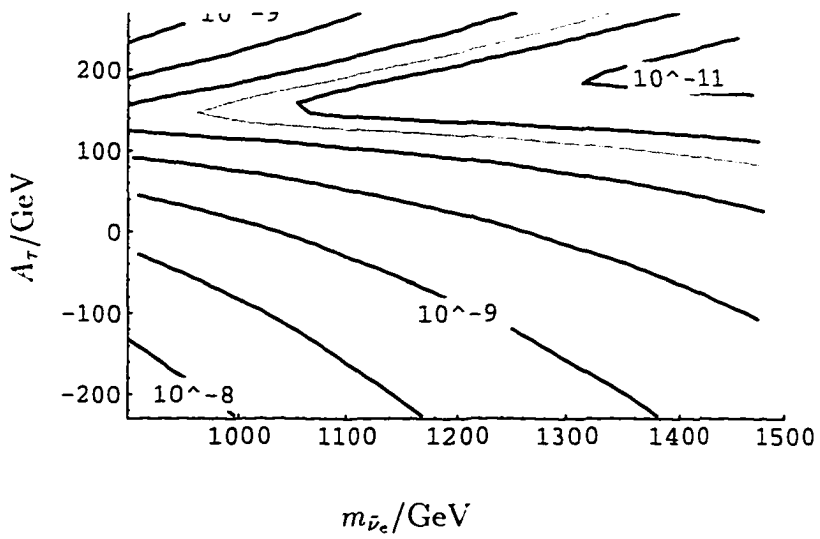

Figure 5.10: Contour plot of $Br(\mu \to e\gamma)$ in the $m_{\tilde{\nu}_e}$ - A_τ plane, with 2 contours per order of magnitude. The gray line shows the experimental upper bound.

the splitting of $m^2_{16_3}$, $m^2_{\psi_1}$, and $m^2_{\psi_2}$ from $m^2_{16_1}$ and $m^2_{16_2}$ via terms in the RGEs for $m^2_{16_3}$, $m^2_{\psi_1}$, and $m^2_{\psi_2}$ involving $m^2_{10_1}$. Hence, the branching ratio generally increases as m^2_H is increased. Note however, μ also affects $\mu \to e\gamma$ through its effects on the chargino and neutralino masses, hence complicating the dependence of $\mu \to e\gamma$ on μ.

In order to understand the dependence of the branching ratio on A_τ, we first observe that the X_{L_j} term dominates all other terms contributing to $\mu \to e\gamma$ by at least an order of magnitude. We therefore neglect the other terms and consider only X_{L_j}. The Γ_ν matrix can be approximated

$$\Gamma_\nu \approx \begin{pmatrix} 1 & \frac{(\overline{m}^2_L)^*_{12}}{(\overline{m}^2_L)_{11}-(\overline{m}^2_L)_{22}} & \frac{(\overline{m}^2_L)^*_{13}}{(\overline{m}^2_L)_{11}-(\overline{m}^2_L)_{33}} \\ -\frac{(\overline{m}^2_L)_{12}}{(\overline{m}^2_L)_{11}-(\overline{m}^2_L)_{22}} & 1 & \frac{(\overline{m}^2_L)^*_{23}}{(\overline{m}^2_L)_{22}-(\overline{m}^2_L)_{33}} \\ -\frac{(\overline{m}^2_L)_{13}}{(\overline{m}^2_L)_{11}-(\overline{m}^2_L)_{33}} & -\frac{(\overline{m}^2_L)_{23}}{(\overline{m}^2_L)_{22}-(\overline{m}^2_L)_{33}} & 1 \end{pmatrix} \tag{5.46}$$

where $\overline{m}^2_L$ is the m^2_L matrix expressed in a basis in which the lepton Yukawa matrix Y_e is diagonal, and we have used the fact that $(\overline{m}^2_L)_{ij}/[(\overline{m}^2_L)_{ii} - (\overline{m}^2_L)_{jj}] \ll 1$, for all i, j such that $i \neq j$. From this expression, X_{L_j} can be approximated

$$X_{L_j} = [X_{L_j}]_1 + [X_{L_j}]_3$$

where

$$[X_{L_j}]_1 \approx \frac{(\overline{m}^2_L)^*_{12}}{m^2_{\tilde{\nu}_e}} \Big[m^2 \frac{\partial}{\partial m^2} \mathcal{J}(m^2) \Big|_{m^2=m^2_{\tilde{\nu}_e}} \tag{5.47}$$

$$[X_{L_j}]_3 \approx \frac{(\overline{m}^2_L)^*_{13}(\overline{m}^2_L)_{23}}{(m^2_{\tilde{\nu}_e} - m^2_{\tilde{\nu}_\tau})(m^2_{\tilde{\nu}_\mu} - m^2_{\tilde{\nu}_\tau})} \mathcal{J}(m^2_{\tilde{\nu}_\tau}) \tag{5.48}$$

where

$$\mathcal{J}(m^2) = -U^*_{-\,2n} U^*_{+\,1n} \frac{m_{\tilde{\chi}^\pm_n}}{g v_1} \frac{1}{m^2} j\Big(\frac{m^2_{\tilde{\chi}^\pm_n}}{m^2}\Big)$$

and we have used the fact that $(\overline{m}^2_L)_{ii} \approx m^2_{\tilde{\nu}_i}$ and that the electron and muon sneutrinos are approximately degenerate. Hence, two terms contribute to X_{L_j}, one proportional to $(\overline{m}^2_L)^*_{12}$ and one proportional to $(\overline{m}^2_L)^*_{13}(\overline{m}^2_L)_{23}$.

In order to understand the dependence of X_{L_j} on A_τ, we therefore need to understand the dependence of the off-diagonal elements of $(\overline{m}_L^2)$ on A_τ. At the GUT scale, the magnitudes of the off-diagonal elements of $(\overline{m}_L^2)$ have a minimum around $A_\tau = 0$ and are approximately symmetric, parabolic functions of A_τ. This is because the renormalization group equations above the GUT scale for the scalar masses have terms proportional to the squares of SUSY breaking trilinear term couplings. (E.g. the RGE for $m_{\tilde{\psi}_2}^2$ has terms proportional to a_B^2 and $\alpha_{\tilde{A}2}^2$.) These terms therefore contribute an amount to the GUT scale splittings of the scalar masses approximately proportional to A_τ^2.

However, this is not the whole story because the off diagonal elements of $(\overline{m}_L^2)$ receive sizable corrections in the RGE running from the Planck scale to the electroweak scale due to the $A_e A_e^\dagger$ term in the RGE for $(\overline{m}_L^2)$. The correction from the $A_e A_e^\dagger$ term is not simply proportional to $\overline{A}_0^2$ as one might naively expect. This is due to the largeness of the contribution of the gaugino term to the RG running above the GUT for the quantities a_C, a_D, and a_E entering GUT scale boundary conditions for A_e. Each RGE for the SUSY breaking multilinear term couplings is linear in the SUSY breaking multilinear term couplings except for one inhomogeneous term – the gaugino term – which does not depend on the multilinear term couplings. As a result, the solution to the RGEs above the GUT scale for the SUSY breaking multilinear term couplings has the generic form $\mathbf{a} = m_{1/2}\mathbf{c}_1 + \overline{A}_0\mathbf{c}_2$, where $\mathbf{c}_1$ and $\mathbf{c}_2$ are vectors that depend on the initial values for the gauge and Yukawa couplings. Thus, the effect of the gaugino term in the RGE equations is to vertically offset the graph of any multilinear coupling plotted as a function of $\overline{A}_0$.

By the definition of $\overline{A}_0$, a_A goes through the origin as a function of $\overline{A}_0$. Similarly, the graphs of a_B, α_1, and α_2 as a function of $\overline{A}_0$ approximately go through the origin since the numerical constant multiplying the gaugino terms in the RGE for a_B, α_1, and α_2 are either the same or nearly the same as for a_A. However, the relative size of the gaugino contributions to a_C, a_D, and a_E are substantially larger than they are for a_A and a_B because of the size of the numerical constant multiplying the gaugino term in the RGEs for a_C, a_D, and a_E. Hence, the graphs of a_C, a_D, and a_E are substantially offset from the origin.[24]

As a result, $A_e A_e^\dagger$ at M_{GUT} is the sum of terms of the form $(\alpha + \beta\overline{A}_0)(\alpha' + \beta'\overline{A}_0)$ where α, α', β, β' are complex constants. Due to the large offsets to a_C, a_D, and a_E, the off-diagonal elements of $A_e A_e^\dagger$ appear more linear than parabolic for the range of A_τ plotted in Figs. 5.8 - 5.10.

The result of this is shown in Figs. 5.11–5.13, plots of $(\overline{m}_L^2)_{12}$, $(\overline{m}_L^2)_{13}$, and $(\overline{m}_L^2)_{23}$ at M_Z in the complex plane as $\overline{A}_0$ varies from -1 TeV to 1 TeV. As can be seen, $(\overline{m}_L^2)_{12}$ and $(\overline{m}_L^2)_{13}$ behave as linear functions of $\overline{A}_0$ instead of as the parabolic functions of $\overline{A}_0$ they started off as at the GUT scale. Even more importantly, $(\overline{m}_L^2)_{12}$ changes sign as it varies as a function of $\overline{A}_0$, starting off in the lower right-hand quadrant of the complex plane at $\overline{A}_0 = -1$ TeV and switching to the upper left-hand quadrant by time $\overline{A}_0 = 1$ TeV. As a result, as is demonstrated in Fig. 5.14, $[X_{L_j}]_1$ enters the lower left hand quadrant of the complex plane at sufficiently large $\overline{A}_0$, causing a partial cancellation between $[X_{L_j}]_1$ and $[X_{L_j}]_3$, which remains in the upper right

[24]For example, with $m_{1/2} = 280$ GeV and all other initial conditions as in Table 5.1, A_C varies linearly from $-.59$ GeV at $\overline{A}_0$=-1000 GeV (corresponding approximately to A_τ=-215 GeV) to $-.3$ GeV at $\overline{A}_0$=1000 GeV (corresponding approximately to A_τ=270 GeV); A_D varies from -1.9 GeV at $\overline{A}_0$=1000 GeV to $-.78$ GeV at $\overline{A}_0$=1000, and A_e varies from -34 GeV to nearly zero.

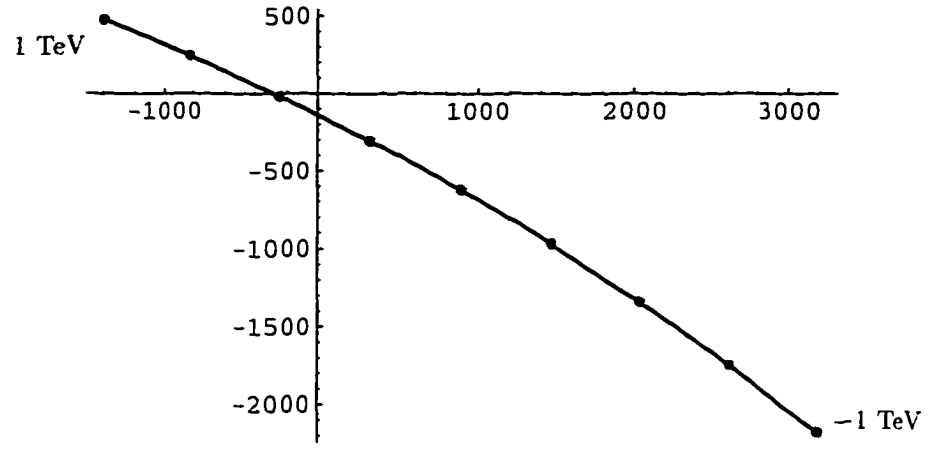

Figure 5.11: Plot of $(\overline{m}_L^2)_{12}(M_Z)/GeV^2$ in the complex plane as $\overline{A}_0$ is varied from -1 TeV to 1 TeV, when $m_{\tilde{\nu}_e} = 1$ TeV. The gray points represent points at which $\overline{A}_0$ is a multiple of 250 GeV. The lower-rightmost point is $\overline{A}_0 = -1$ TeV and the upper-leftmost point is $\overline{A}_0 = 1$ TeV.

hand quadrant of the complex plane when $\overline{A}_0$ is positive.[25] This partial cancellation between $[X_{L_j}]_1$ and $[X_{L_j}]_3$ explains why there is a sharp minimum in $Br(\mu \to e\gamma)$ at around $A_\tau = 150$ GeV.

5.5.2 Dependence on ζ_1, ζ_2, λ_{N_1}, and λ_{N_2}

We next consider how the branching ratio for $\mu \to e\gamma$ depends on ζ_1, ζ_2, λ_{N_1}, and λ_{N_2}. Contour plots of $Br(\mu \to e\gamma)$ versus A_τ and these variables are shown in the figures that follow. To aid the analysis of these plots, we also plot the GUT scale mass splittings of the eigenvalues of m_L^2 as a function A_τ and these parameters. Namely, contour plots are shown of the relative splitting between the first and second

[25]Note, $\mathcal{J}$ is positive while $\partial\mathcal{J}/\partial m^2$ is negative. Using these facts, one can see that the signs for $[X_{L_j}]_1$ and $[X_{L_j}]_3$ shown in fig. 5.14 agrees with the signs for $(\overline{m}_L^2)_{12}$, $(\overline{m}_L^2)_{13}$, and $(\overline{m}_L^2)_{23}$ shown in figs. 5.11 - 5.13

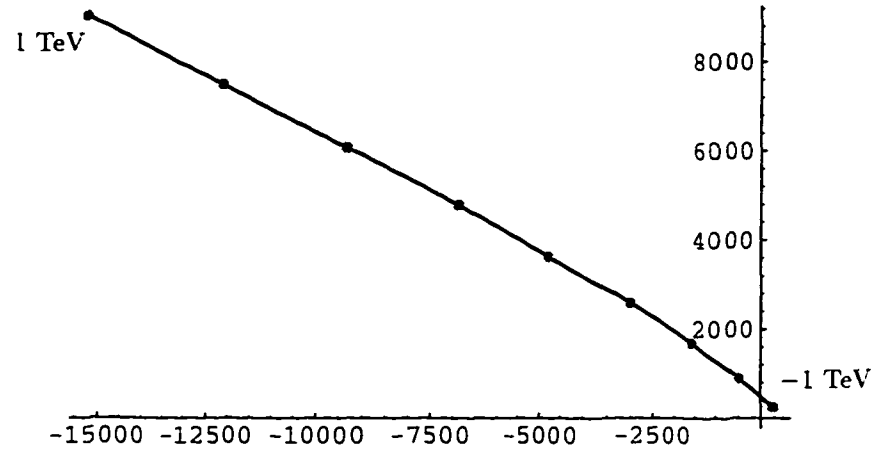

Figure 5.12: Plot of $(\overline{m}_L^2)_{13}(M_Z)/GeV^2$ in the complex plane as $\overline{A}_0$ is varied from -1 TeV to 1 TeV, when $m_{\tilde{\nu}_e} = 1$ TeV. The gray points represent points at which $\overline{A}_0$ is a multiple of 250 GeV. The lower-rightmost point is $\overline{A}_0 = -1$ TeV and the upper-leftmost point is $\overline{A}_0 = 1$ TeV.

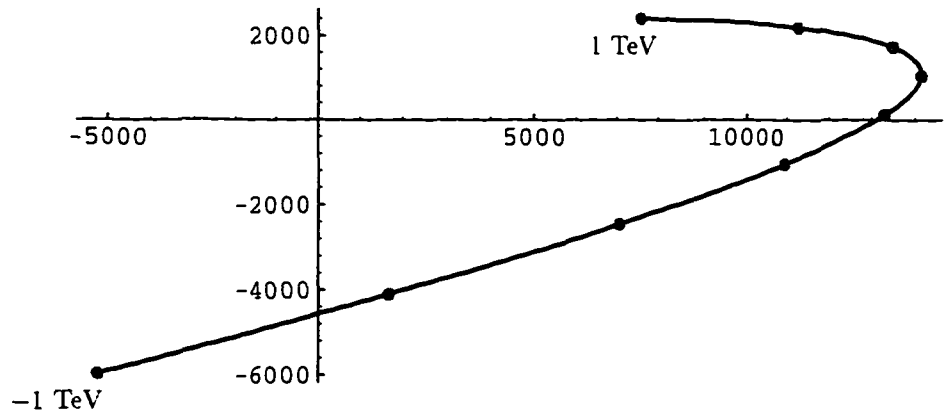

Figure 5.13: Plot of $(\overline{m}_L^2)_{23}(M_Z)/GeV^2$ in the complex plane as $\overline{A}_0$ is varied from -1 TeV to 1 TeV, when $m_{\tilde{\nu}_e} = 1$ TeV. The gray points represent points at which $\overline{A}_0$ is a multiple of 250 GeV. The lower-leftmost point is $\overline{A}_0 = -1$ TeV.

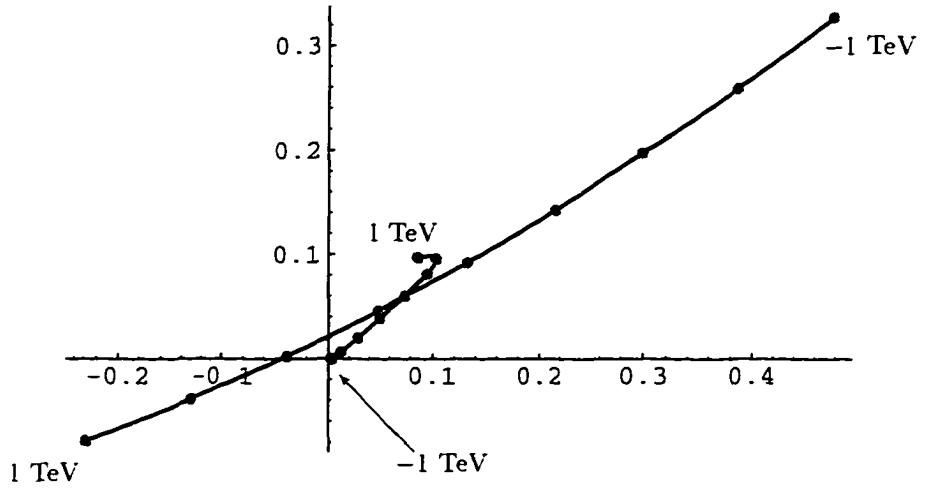

Figure 5.14: Plot of $1000M_W^2[X_{L_J}]_1$ and $1000M_W^2[X_{L_J}]_3$ in the complex plane, where M_W is the W boson mass, as $\overline{A}_0$ is varied from -1 TeV to 1 TeV, when $m_{\tilde{\nu}_e}$=1 TeV. The gray points represent points at which $\overline{A}_0$ is a multiple of 250 GeV. The longer line is $[X_{L_J}]_1$ and the shorter is $[X_{L_J}]_3$. The upper-rightmost point of $[X_{L_J}]_1$ is $\overline{A}_0 = -1$ TeV and the lower-leftmost point is $\overline{A}_0 = 1$ TeV. The lower-leftmost point of $[X_{L_J}]_3$ is $\overline{A}_0 = -1$ TeV.

generation eigenvalues x_2 defined

$$\begin{aligned} x_2 &\equiv [(\tilde{m}_L^2)_{22} - (\tilde{m}_L^2)_{11}]/(\tilde{m}_L^2)_{11} \\ &= \frac{(m_{16_2}^2 - m_{16_1}^2) + \zeta_2(m_{\psi_2}^2 - m_{16_1}^2)}{m_{16_1}^2(1+\zeta_2^2)} \end{aligned}$$

and the relative splitting between the first and third generations x_3 defined

$$\begin{aligned} x_3 &\equiv [(\tilde{m}_L^2)_{33} - (\tilde{m}_L^2)_{11}]/(\tilde{m}_L^2)_{11} \\ &= \frac{(m_{16_3}^2 - m_{16_1}^2) + \zeta_1(m_{\psi_1}^2 - m_{16_1}^2)]}{m_{16_1}^2(1+\zeta_1^2)} \end{aligned}$$

where $\tilde{m}_L^2$ is m_L^2 expressed in a basis in which it is diagonal. For the values of the low energy Yukawa parameters used in the calculations, the off-diagonal elements of $\overline{m}_L^2$ are related to the mass splittings of $\tilde{m}_L^2$ as follows.

$$\begin{aligned} (\overline{m}_L^2)_{12}(M_{GUT}) &\approx (\tilde{m}_L^2)_{11}[(.049 + .024i)x_2 + (-.0018 + .0014i)x_3] \\ (\overline{m}_L^2)_{13}(M_{GUT}) &\approx (\tilde{m}_L^2)_{11}[(.0032 + .0019i)x_2 + (.026 - .019i)x_3] \\ (\overline{m}_L^2)_{23}(M_{GUT}) &\approx (\tilde{m}_L^2)_{11}[(.068 + .0052i)x_2 + (-.069 - .0037i)x_3] \end{aligned} \quad (5.49)$$

ζ_1 and ζ_2

In order to understand the dependence of $Br(\mu \to e\gamma)$ on ζ_1 and ζ_2, we first need to understand the general features of the mass splittings. First, substantial splitting occurs between $m_{16_3}^2$ in comparison to $m_{16_1}^2$ and $m_{16_2}^2$. This is because $m_{16_3}^2$ receives large negative radiative corrections proportional to λ_A^2 and a_A^2 from graphs having 10_1 and 16_3 in a loop arising due to the $\lambda_A 16_3 10_1 16_3$ term in the superpotential and its corresponding SUSY breaking trilinear term. This radiative correction is especially large because of the large SO(10) group theoretic factor multiplying the term in the RGE for $m_{16_3}^2$ proportional to λ_A^2. By contrast, as long as γ is small and

λ_{N_1} is approximately equal to λ_{N_2}, $m^2_{16_1}$ will approximately be equal to $m^2_{16_2}$. This is because the only dimension four terms in the superpotential that involve 16_1 or 16_2 are either couplings to adjoint fields or couplings to the singlet fields N_1 or N_2. Because the coupling constants for any coupling involving adjoint fields have been presumed to be negligible, the only radiative corrections to $m^2_{16_1}$ and $m^2_{16_2}$ come from the gauge coupling and the coupling to the singlets N_1 and N_2. Since 16_1 and 16_2 are in the same representation of SO(10), the radiative correction due to gauge couplings will be the same. Moreover, if λ_{N_1} equals λ_{N_2}, then the correction due to the N_1 and N_2 couplings are the same for $m^2_{16_1}$ and $m^2_{16_2}$, and hence the splitting between $m^2_{16_1}$ and $m^2_{16_2}$ will be negligible.

Nevertheless, splitting between the first and second generation scalar mass eigenstates does occur because the second generation supermultiplet is a linear combination of the 16_2 and ψ_2 supermultiplets, due to the mixing coming from the $\gamma_1 \overline{\psi}_2 A_2 16_2$ term in the superpotential. Hence, the splitting of the first and second generation scalar mass eigenstates also depends on $m^2_{\psi_2}$. $m^2_{\psi_2}$ receives radiative corrections proportional to λ_B^2 and a_B^2 due to the term $\lambda_B \psi_1 10_1 \psi_2$ in the superpotential and its corresponding SUSY breaking trilinear term, whereas $m^2_{16_1}$ does not receive corrections proportional to λ_B^2 and a_B^2. On the other hand, $m^2_{\psi_2}$ does not receive corrections proportional to λ_{N_1}, whereas $m^2_{16_1}$ does. As a consequence, $m^2_{\psi_2}$ may be greater or less than $m^2_{16_1}$, depending on the values of λ_{N_1} and λ_B.

Additionally, there is mixing between the 16_3 and ψ_1 states coming from the $\gamma_1 \overline{\psi}_1 A_1 16_3$ term in the superpotential. $m^2_{\psi_1}$ also receives radiative corrections proportional to λ_B^2 and a_B^2 due to the $\lambda_B \psi_1 10_1 \psi_2$ term in the superpotential and its corresponding SUSY breaking trilinear term. However, the splitting of $m^2_{\psi_1}$ from

$m^2_{16_1}$ is smaller than the splitting of $m^2_{16_3}$ from $m^2_{16_1}$ in almost all parameter space. The reason why is because λ_B needs to be very large in order for the splitting of $m^2_{\psi_1}$ from $m^2_{16_1}$ to be larger than the splitting of $m^2_{16_3}$ from $m^2_{16_1}$. However, if λ_B is too large, λ_A will become non-perturbative. It happens to be the case that unless m^2_H is very large, λ_A will become non-perturbative before the splitting of $m^2_{\psi_1}$ from $m^2_{16_1}$ catches up with the splitting of $m^2_{16_3}$ from $m^2_{16_1}$. Since $m^2_{\psi_1}$ is split from $m^2_{16_1}$ less than $m^2_{16_3}$ is split from $m^2_{16_1}$ in almost all parameter space, the mixing of the 16_3 with ψ_1 decreases the splitting of the third generation scalar mass eigenstate from the first generation eigenstate.

With these observations in mind, the qualitative behavior of the branching ratio for $\mu \to e\gamma$ as a function of ζ_1 can be understood as follows. The dominant effect ζ_1 has on the branching ratio comes from the effect it has on the splitting of the third generation scalar mass eigenstate from the first two. Increasing ζ_1 decreases the splitting of the third generation scalar mass eigenstate from the first (hence increasing x_3) for two reasons. First, increasing ζ_1 decreases λ_B through eqn. (5.6), and therefore decreases the splitting of $m^2_{\psi_1}$ from $m^2_{16_1}$. Second, ζ_1 controls the size of the mixing of 16_3 and ψ_1. Increasing ζ_1 increases the size of this mixing which therefore decreases the splitting of the third generation from the second generation. This decrease in the splitting of the third generation from the first can clearly be seen in Fig. 5.17.

The effect this decrease in the splitting of the third generation from the first two has is to shift $(\overline{m}^2_L)_{13}$ downward and to the right in the complex plane and to shift $(\overline{m}^2_L)_{23}$ to the left in the complex plane, while keeping $(\overline{m}^2_L)_{12}$ approximately the same. See eqn. (5.49). This has the general effect of shrinking the distance from the origin of $[X_{L_j}]_3$ in the complex plane while keeping $[X_{L_j}]_1$ roughly the same, as is illustrated

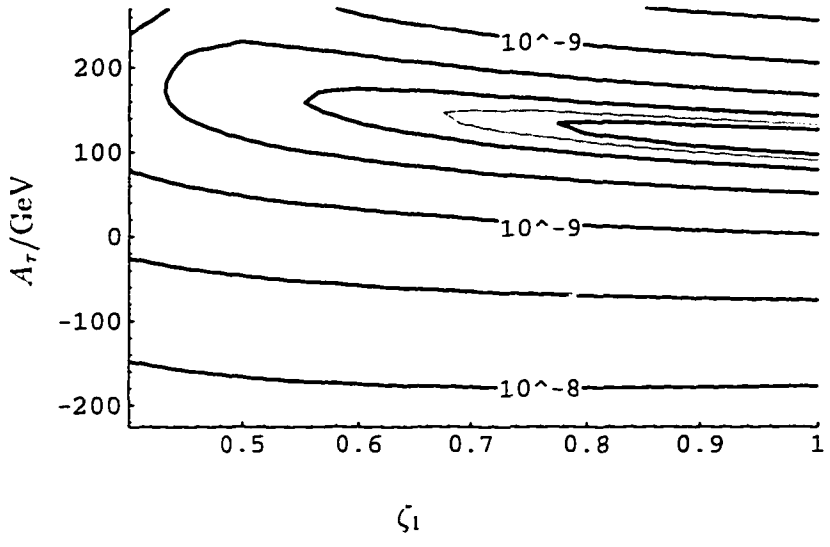

Figure 5.15: Contour plot of $Br(\mu \rightarrow e\gamma)$ in the A_τ - ζ_1 plane, with 2 contours per order of magnitude. The gray line shows the experimental upper bound.

in Fig. 5.18. As that figure illustrates, when x_3 is decreased, as it is when ζ_1 is increased, the value of A_τ at which the branching ratio is at a minimum decreases. In addition, because $[X_{L_j}]_1$ and $[X_{L_j}]_3$ converge near the origin, decreasing the point at which A_τ is at a minimum also has the effect of decreasing the minimum itself. Both of these effects are seen in Fig. 5.15, the contour plot of $Br(\mu \rightarrow e\gamma)$ is the A_τ-ζ_1 plane.

As ζ_2 is increased, the mixing between 16_2 and ψ_2 increases, and thus the splitting between the first and second generation scalar mass eigenstates increases when ζ_2 is increased, as is seen in Fig. 5.20. Hence, increasing ζ_2 increases x_2.

The primary effect increasing x_2 has is to shift $(\overline{m}_L^2)_{12}$ upward and to the right, hence shifting $[X_{L_j}]_1$ downward and to the right in the complex plane. If one were to draw a line perpendicular to the plot of $[X_{L_j}]_1$ versus $\overline{A}_0$ in the complex plane, the

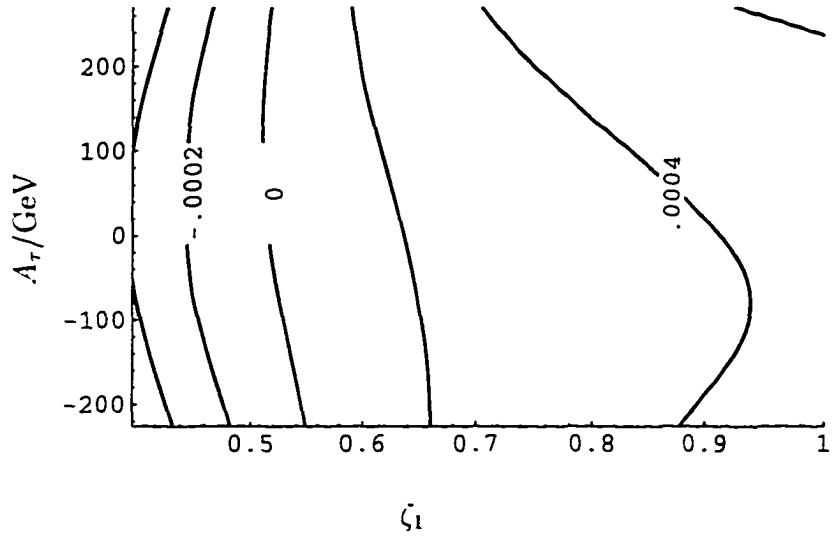

Figure 5.16: Contour plot of x_2 in the A_τ - ζ_1 plane.

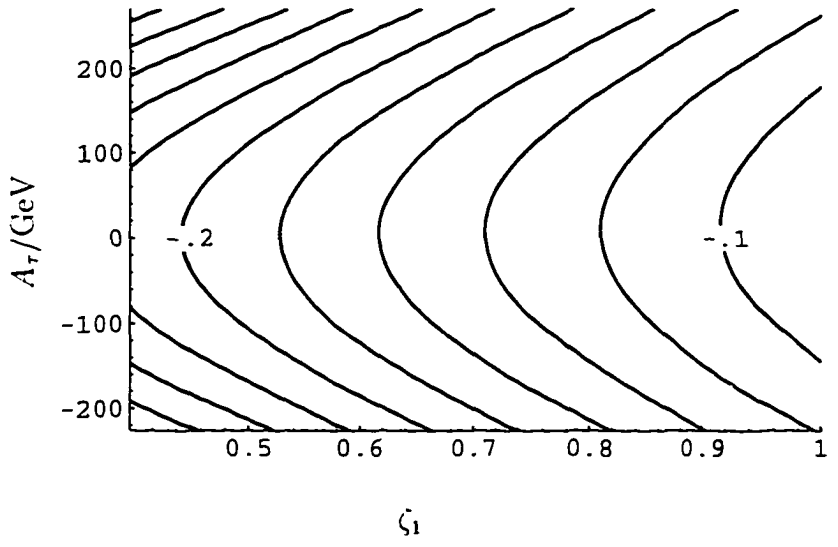

Figure 5.17: Contour plot of x_3 in the A_τ - ζ_1 plane.

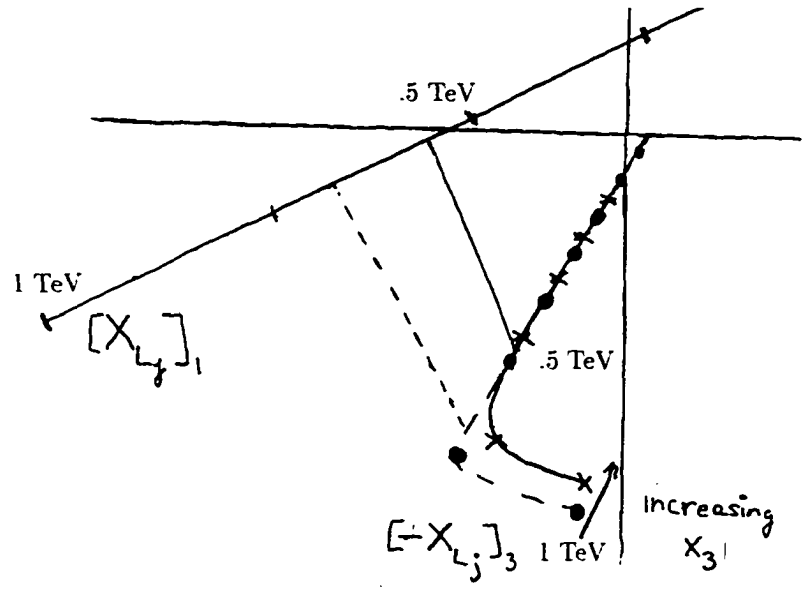

Figure 5.18: Sketch illustrating the effect changing x_3 has on the X_{L_j}. $[X_{L_j}]_1$ and $[-X_{L_j}]_3$ are sketched in the complex plane. This sketch corresponds to fig. 5.14. except that $[-X_{L_j}]_3$ is sketched instead of $[X_{L_j}]_3$. The distance between two points of equal $\overline{A}_0$ on these two lines represents $|X_{L_j}|$. The dashed line represents the old $[-X_{L_j}]_3$ and the solid line represents the $[-X_{L_j}]_3$ when x_3 is increased. The hash marks and the circles on the $[X_{L_j}]_1$ and the old $[-X_{L_j}]_3$ lines represent points where $\overline{A}_0$ is a multiple of 250 GeV. The crosses represent how those points on $[-X_{L_j}]_3$ change as x_3 is increased. The length of the dashed line extending from $[X_{L_j}]_1$ to the old $[-X_{L_j}]_3$ line represents the old minimum of $|X_{L_j}|$ with respect to $\overline{A}_0$ and the length of the solid line extending from $[X_{L_j}]_1$ to the new $[-X_{L_j}]_3$ represents how that minimum changes as x_3 increases.

shift would be in a direction to the right of the perpendicular. This shift is illustrated in Fig. 5.22. Because of the direction of this shift, the shift has the effect of increasing the value of A_τ at which X_{L_j} is at a minimum with respect to $\overline{A}_0$.

However, increasing ζ_2 also decreases λ_B. Decreasing λ_B has the effect of decreasing λ_A through the term in the RGE for λ_A proportional to λ_B^2. λ_A becomes non-perturbative near $\lambda_B = 1.1$, corresponding to $\zeta_2 \approx .05$. As a result, λ_A rapidly increases as a function of λ_B in the region near where λ_A becomes non-perturbative. A rapid increase in λ_A causes a rapid decrease in $m_{16_3}^2 - m_{16_1}^2$ through the term in the RGE for $m_{16_3}^2$ proportional to λ_A^2. The result is that the splitting of the third generation from the first is close to constant as function of ζ_2 when ζ_2 is greater than $\approx .09$. Below $\zeta_2 \approx .09$, the splitting rapidly decreases as ζ_2 increases.

When ζ_2 is greater than approximately 0.09, the effect of ζ_2 on x_2 dominates. Increasing ζ_2 increases x_2, hence increasing the value of A_τ for which $Br(\mu \to e\gamma)$ is at a minimum with respect to A_τ. See Fig. 5.19. When ζ_2 is less than approximately 0.09, the effect ζ_2 has on x_3 dominates. As a result, when ζ_2 is less than around 0.09, increasing ζ_2 has the effect of decreasing the value of A_τ for which $Br(\mu \to e\gamma)$ is minimized with respect to A_τ.

The fact that $Br(\mu \to e\gamma)$ has a minimum with respect to ζ_2 around $\zeta_2 = 0.24$ can also be understood qualitatively in terms of the behavior of $[X_{L_j}]_1$ and $[X_{L_j}]_3$ in the complex plane as ζ_2 is varied. In the region around $\zeta_2 = 0.24$, the effect ζ_2 has on x_2 dominates. Below $\zeta_2 \approx 0.24$, the plot of $[X_{L_j}]_1$ in the complex plane is to the left of the plot of $[-X_{L_j}]_3$. Hence, when $[X_{L_j}]_1$ is shifted to the right by increasing x_2, $[X_{L_j}]_1$ moves closer to $-[X_{L_j}]_3$, causing the minimum of $Br(\mu \to e\gamma)$ with respect to $\overline{A}_0$ to decrease. Near $\zeta_2 = 0.24$, $[X_{L_j}]_1$ passes through $[-X_{L_j}]_3$. After $[X_{L_j}]_1$ passes through

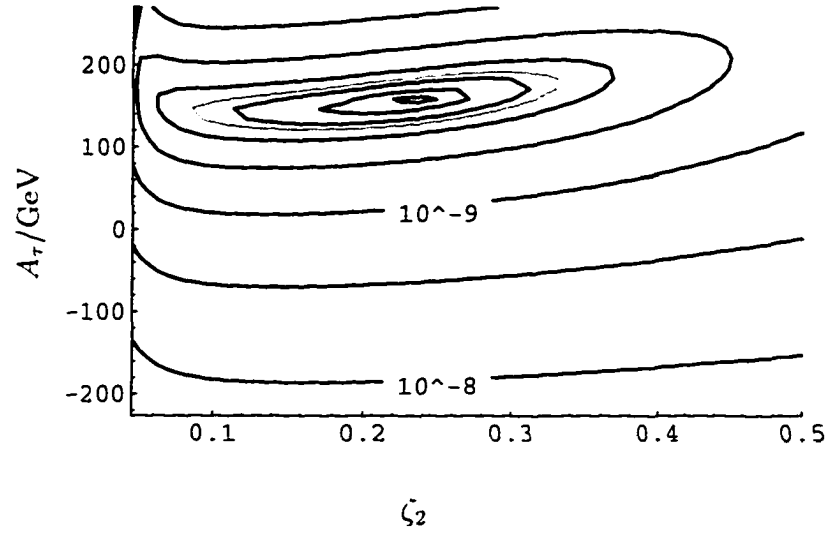

Figure 5.19: Contour plot of $Br(\mu \to e\gamma)$ in the $A_\tau - \zeta_2$ plane, with 2 contours per order of magnitude. The gray line shows the experimental upper bound.

$[X_{L_j}]_3$, shifting $[X_{L_j}]_1$ to the right has the effect of increasing the distance between $[X_{L_j}]_1$ and $[-X_{L_j}]_3$, thus increasing the minimum of $Br(\mu \to e\gamma)$ with respect to $\overline{A}_0$.

Dependence on λ_{N_1} and λ_{N_2}

The couplings λ_{N_1}, λ_{N_2}, and λ_{N_3} can be used as a mechanism to decrease the GUT scale scalar mass splittings. Namely, if λ_{N_3} is small and λ_{N_1} and λ_{N_2} are large, the radiative corrections to $m^2_{16_1}$ and $m^2_{16_2}$ due to λ_{N_1} and λ_{N_2} will decrease $m^2_{16_1}$ and $m^2_{16_2}$, thereby partially canceling the splitting of the third generation from the first two due to λ_A. However, the requirement of perturbativity puts constraints on how large λ_{N_1} and λ_{N_2} can be made. Moreover, if λ_{N_1} and λ_{N_2} are to be used as a mechanism to suppress $\mu \to e\gamma$, they must be nearly equal, since splitting between the first two generations of scalars occurs if there is any difference between λ_{N_1} and λ_{N_2}.

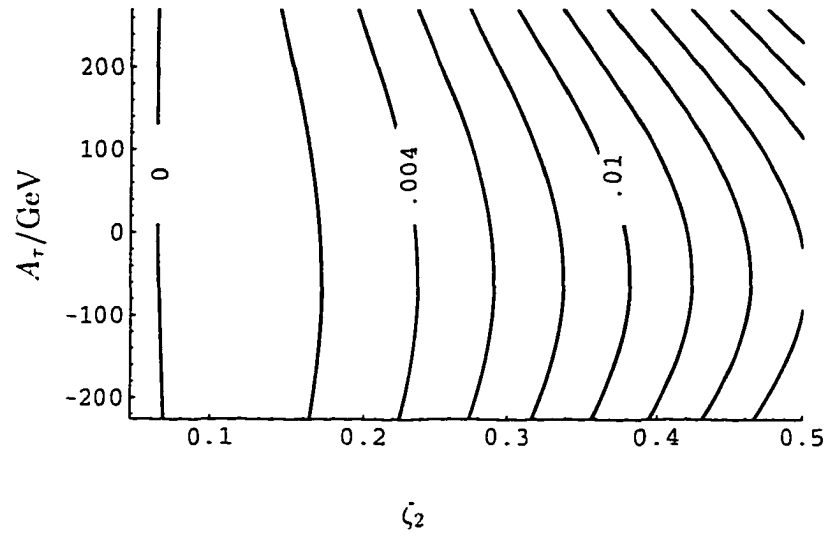

Figure 5.20: Contour plot of x_2 in the A_τ – ζ_2 plane.

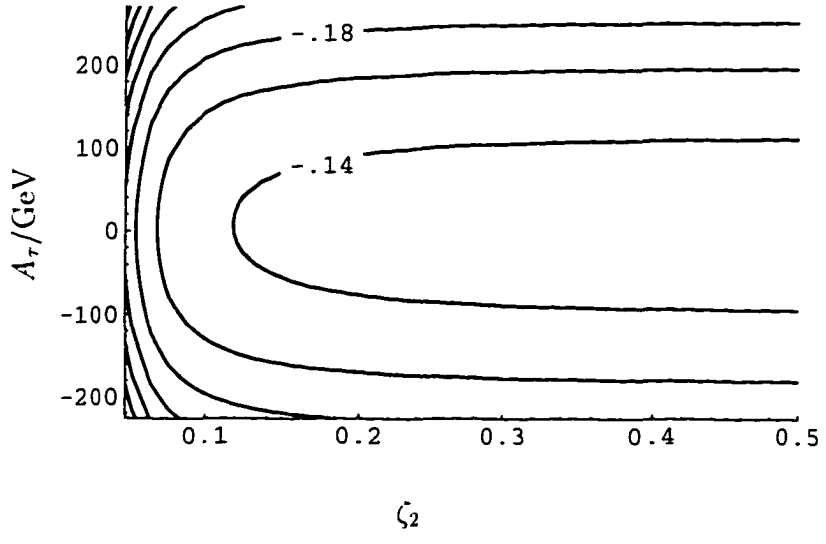

Figure 5.21: Contour plot of x_3 in the A_τ – ζ_2 plane.

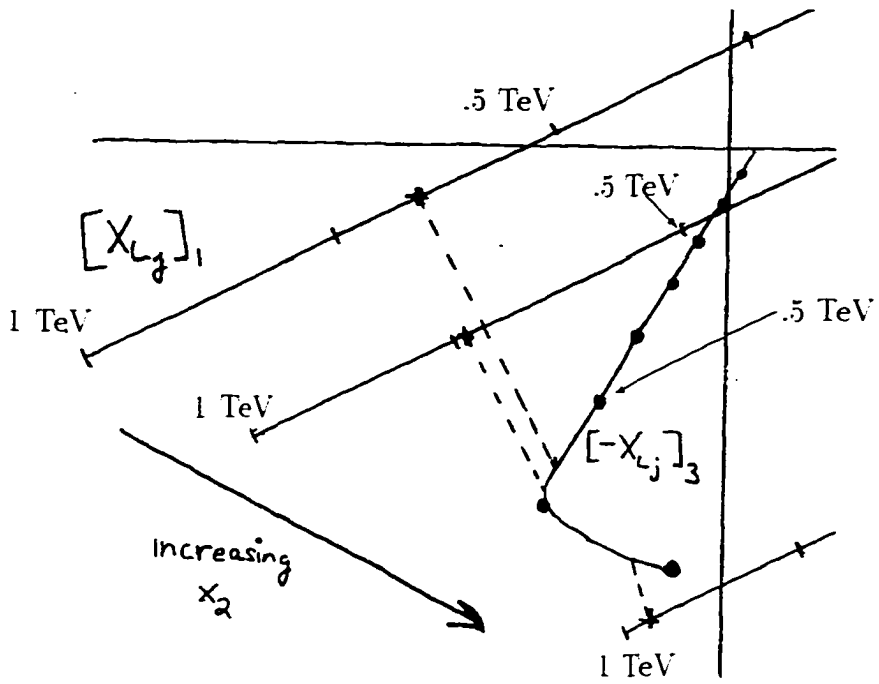

Figure 5.22: Sketch illustrating the effect changing x_2 has on the X_{L_j}. $[X_{L_j}]_1$ and $[-X_{L_j}]_3$ are sketched in the complex plane for various values of x_2. The distance between two points of equal $\overline{A}_0$ on these two lines represents $|X_{L_j}|$. The hash marks and the circles on the $[X_{L_j}]_1$ and the $[-X_{L_j}]_3$ lines represent points where $\overline{A}_0$ is a multiple of 250 GeV. The length of the dashed lines extending from $[X_{L_j}]_1$ to the $[-X_{L_j}]_3$ line represents the minimum of $|X_{L_j}|$ with respect to $\overline{A}_0$ for various values of x_2.

In Fig. 5.23, the viability of λ_{N_1}, λ_{N_2}, and λ_{N_3} as a mechanism for suppressing scalar mass splittings is tested. The branching ratio for $\mu \to e\gamma$ is plotted against A_τ and λ_{N_1} with $\lambda_{N_1} = \lambda_{N_2}$, and with $\lambda_{N_3} = 0.1$. As can be seen, the dominant effect of increasing $\lambda \equiv \lambda_{N_1} = \lambda_{N_2}$ is to decrease the splitting of the third generation scalar mass eigenvalue from the first two. Increasing λ also has the effect of increasing x_2, because $m^2_{16_1}$ receives negative radiative corrections proportional to λ^2 whereas $m^2_{\psi_2}$ does not. Indeed, λ can be adjusted so that there is no splitting between the first and second generation scalar masses. However, in terms of $\mu \to e\gamma$, the effect λ has on the splitting of the first two generations is numerically not nearly as significant as its effect in decreasing the splitting of the third generation from the first two, simply because the splitting of the first two generations is suppressed by ζ_2^2.

Because the dominant effect of increasing λ is to decrease the splitting of the third generation from the first two, the plot of $Br(\mu \to e\gamma)$ against λ exhibits much of the same behavior as the plot of $Br(\mu \to e\gamma)$ against ζ_1: As λ is increased, the value of A_τ at which $Br(\mu \to e\gamma)$ is at a minimum with respect to A_τ is decreased. Furthermore, as λ is increased, the minimum of $Br(\mu \to e\gamma)$ with respect to A_τ is decreased.

5.5.3 Dependence on γ

In Figs. 5.26 and 5.27, the branching ratio for $\mu \to e\gamma$ is plotted against γ and A_τ, and Fig. 5.28 shows the relative splitting of $m^2_{16_3}$, $m^2_{16_2}$, $m^2_{\psi_1}$, and $m^2_{\psi_2}$ from $m^2_{16_1}$, for $m_{\tilde{\nu}_e} = 3$ TeV. As can be seen, the scalar mass splittings are very sensitive to γ. A mass splitting as large as 30% is obtained between $m^2_{16_1}$ and $m^2_{16_2}$. The branching ratio for $\mu \to e\gamma$ is particularly sensitive to any splitting between the first and second generations. With such a large mass splitting between the first and second

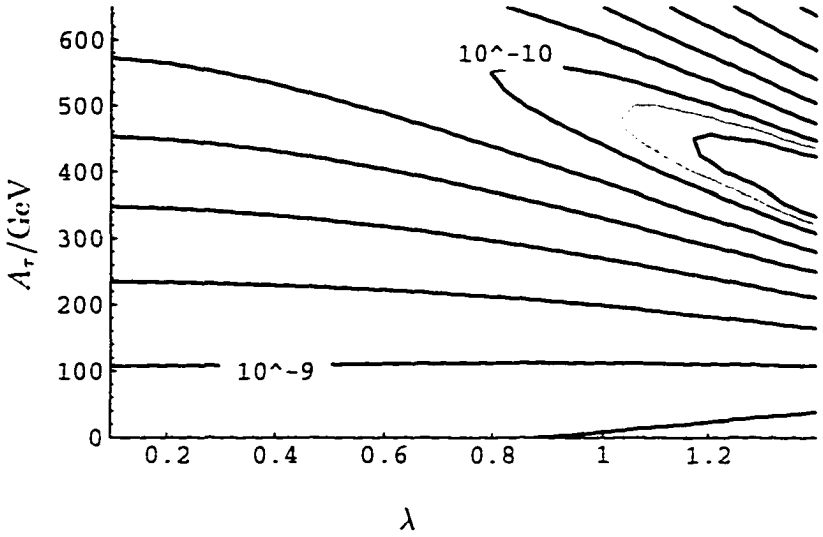

Figure 5.23: Contour plot of $Br(\mu \to e\gamma)$ in the A_τ - λ plane, with 5 contours per order of magnitude, where $\lambda = \lambda_{N_1} = \lambda_{N_2}$. The gray line shows the experimental upper bound.

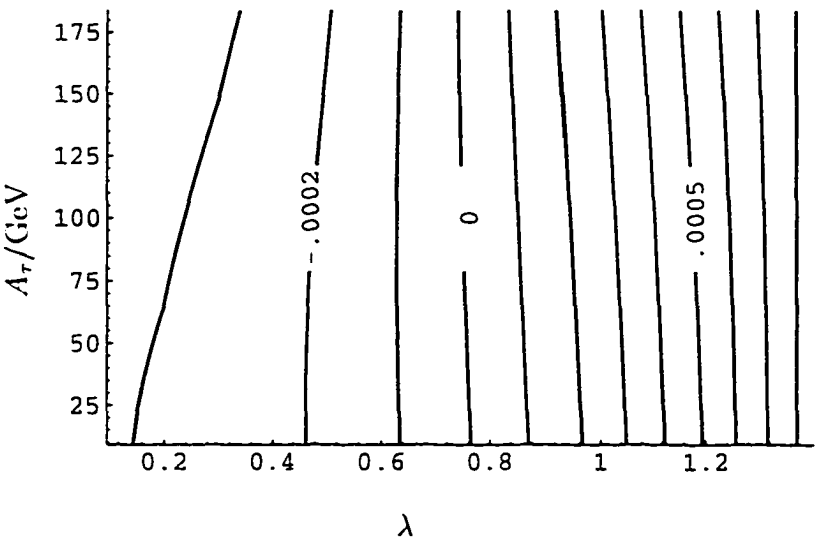

Figure 5.24: Contour plot of x_2 in the A_τ - λ plane, where $\lambda = \lambda_{N_1} = \lambda_{N_2}$.

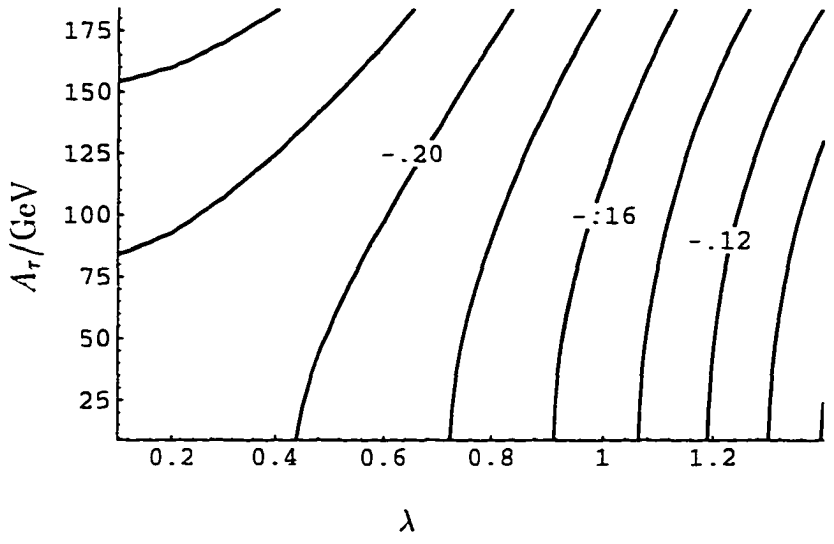

Figure 5.25: Contour plot of x_3 in the A_τ - λ plane, where $\lambda = \lambda_{N_1} = \lambda_{N_2}$

generations, the branching ratio for $\mu \to e\gamma$ is many orders of magnitude above the experimental upper bound.

However, if, for example, $\gamma = 0.1$, the mass splitting between the first and second generations is less than one percent. A mass splitting between the first two generations of around one percent is not unreasonably large for $\mu \to e\gamma$. With $\gamma = 0.1$, the branching ratio for $\mu \to e\gamma$ is increased by at most an order of magnitude. This increase can be compensated for by adjusting the other parameters. For example, $m_{\tilde{\nu}_e}$ can be increased to compensate for the increase in γ without violating the requirement that squark and slepton masses be lower than a few TeV. By contrast, a mass splitting between the first and second generations in the tens of percent clearly cannot be compensated for unless squark and slepton masses are greater than several TeV and therefore unnaturally heavy.

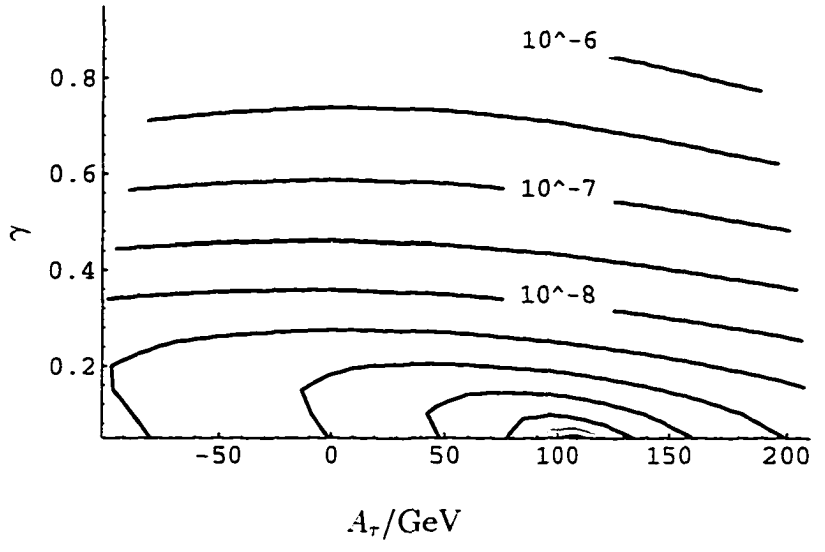

Figure 5.26: Contour plot of $Br(\mu \to e\gamma)$ in the A_τ - γ plane, with 2 contours per order of magnitude. The gray line shows the experimental upper bound. ($m_{\tilde{\nu}_e}$=1 TeV.)

The fact that rates for $\mu \to e\gamma$ consistent with experiment can be obtained with $\gamma = 0.1$ also tells us that it was unnecessary to require that physics in the ultimate superstring or other theory above the Planck scale of which our model is an effective field theory manifestation, include some sort of mechanism to suppress the Yukawa couplings involving the adjoints of our theory, as we speculated may be required in sec. 5.2.1. The value of $\gamma = 0.1$ is within an order of magnitude of the rest of the coupling constants and therefore not unnaturally small in comparison to them.

5.5.4 Branching ratios for $\tau \to e\gamma$, $\tau \to \mu\gamma$, and the electron and muon dipole moments

In Figs. 5.29 - 5.32, we present contour plots for $\tau \to e\gamma$, $\tau \to \mu\gamma$, and the electron and muon dipole moments in the $m_{\tilde{\nu}_e}$- $m_{1/2}(M_{GUT})$ plane using the same values for the other parameters as in Fig. 5.8. The current experimental bounds

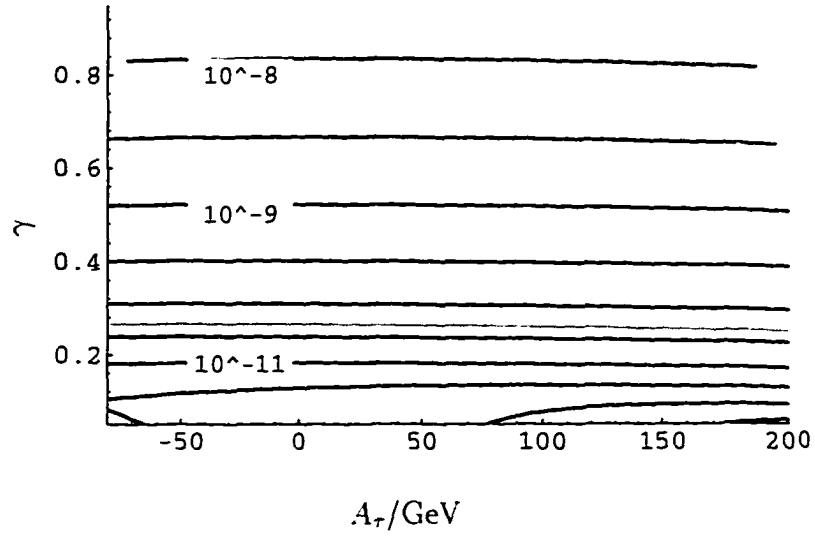

Figure 5.27: Contour plot of $Br(\mu \to e\gamma)$ in the A_τ - γ plane, with 2 contours per order of magnitude and $m_{\tilde{\nu}_e} = 3$ TeV. The gray line shows the experimental upper bound.

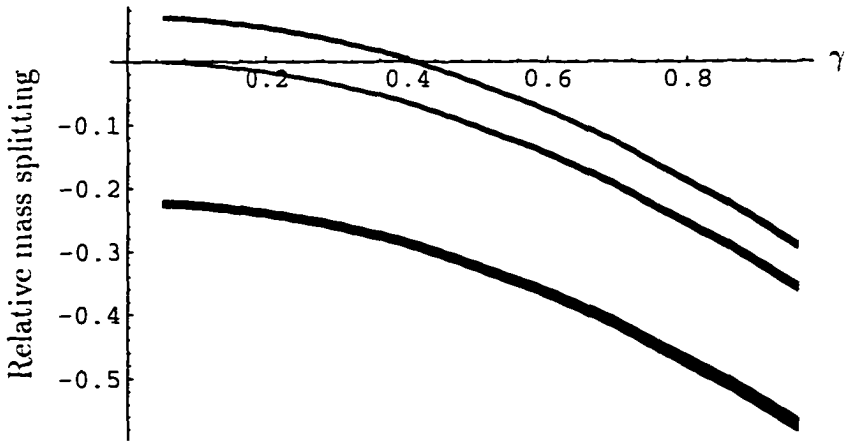

Figure 5.28: Plot of γ versus the relative mass splittings of $m^2_{16_2}$, $m^2_{16_1}$, and $m^2_{\psi_1}$ with respect to $m^2_{16_1}$ at M_{GUT}, with $m_{\tilde{\nu}_e}$=3 TeV. The upper, middle, and bottom lines represent $[m^2_{\psi_1} - m^2_{16_1}]/m^2_{16_1}$, $[m^2_{16_2} - m^2_{16_1}]/m^2_{16_1}$, and $[m^2_{16_3} - m^2_{16_1}]/m^2_{16_1}$, respectively. The thickness in the lines represents how much the relative mass splitting varies as A_τ is varied from -200 GeV to 200 GeV. The mass splitting for $m^2_{\psi_2}$ is not shown because $m^2_{\psi_2} \approx m^2_{\psi_1}$.

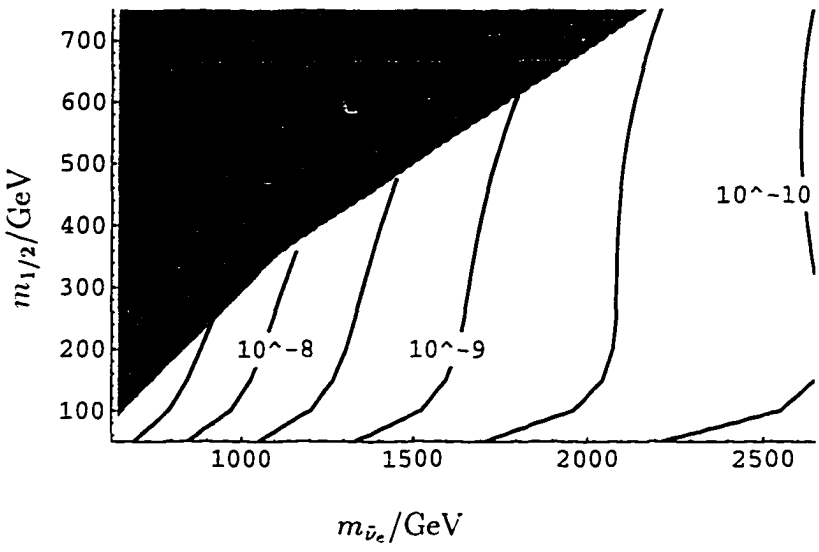

Figure 5.29: Contour plot of $Br(\tau \to e\gamma)$ in the $m_{\tilde{\nu}_e}$ - $m_{1/2}(M_{GUT})$ plane, with 2 contours per order of magnitude. The gray region denotes a region of parameter space where $m_0 < 700$ GeV.

for these processes are that $Br(\tau \to e\gamma) < 1.1 \times 10^{-4}$, $Br(\tau \to \mu\gamma) < 4.2 \times 10^{-6}$, $|d_e| < 4.3 \times 10^{-27} e$ cm, and $d_\mu < (3.7 \pm 3.4) \times 10^{-19} e$ cm. [2, 57] As can be seen, the rates for these processes are not competitive with $\mu \to e\gamma$ as a constraint on our model.

5.5.5 Affect of non-universality of GUT scale boundary conditions for A_B

In Figs. 5.33 and 5.34, we show the branching ratio for $\mu \to e\gamma$ in the $m_{\tilde{\nu}_e}$- $m_{1/2}$ and $m_{\tilde{\nu}_e}$- A_τ planes if we used as a GUT scale boundary condition

$$A_B = \frac{3}{2} a_B \frac{\gamma_1 \gamma_2}{\gamma_{\tilde{A}1} \gamma_{\tilde{A}2}} \frac{a_1 a_2}{\tilde{a}^2} \tag{5.50}$$

instead of the correct boundary condition of eqn. (5.11). In previous analyses of lepton flavor violation in SUSY GUTs [8, 58], non-universality in the SUSY-breaking

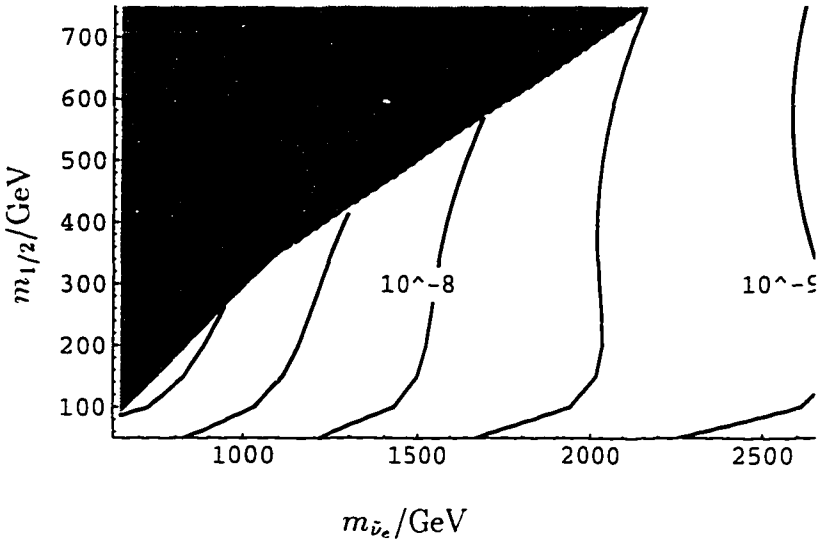

Figure 5.30: Contour plot of $Br(\tau \to \mu\gamma)$ in the $m_{\tilde{\nu}_e}$ - $m_{1/2}(M_{GUT})$ plane, with 2 contours per order of magnitude. The gray region denotes a region of parameter space where $m_0 < 700$ GeV.

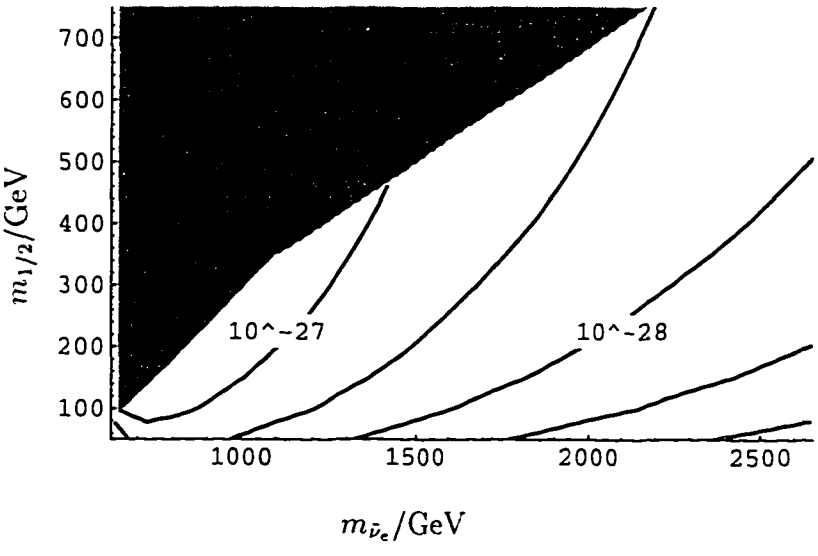

Figure 5.31: Contour plot of $d_e/(e$ cm) in the $m_{\tilde{\nu}_e}$ - $m_{1/2}(M_{GUT})$ plane, with 2 contours per order of magnitude. The gray region denotes a region of parameter space where $m_0 < 700$ GeV.

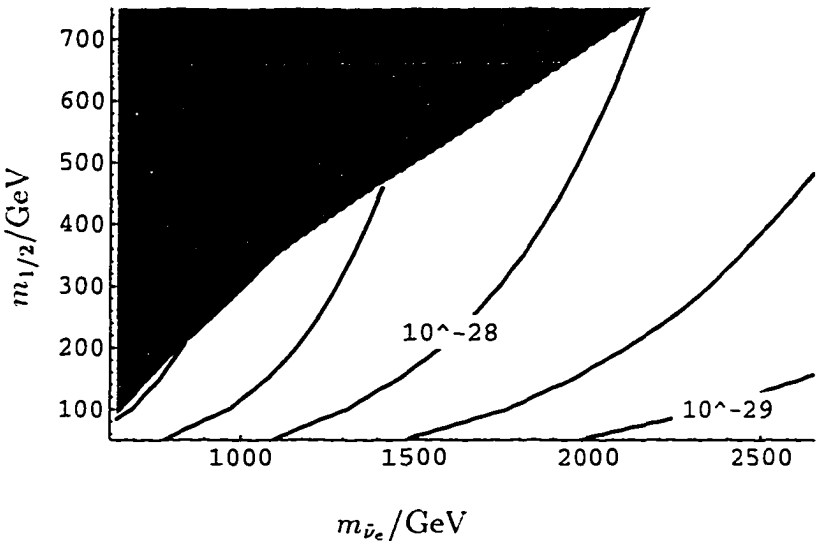

Figure 5.32: Contour plot of $d_\mu/(e$ cm) in the $m_{\tilde{\nu}_e}$ - $m_{1/2}(M_{GUT})$ plane, with 2 contours per order of magnitude. The gray region denotes a region of parameter space where $m_0 < 700$ GeV.

parameters was solely the result of RG running between the Planck and GUT scales. However, in sec. 5.2.3, we argued that non-universality in the SUSY-breaking trilinear parameters could also be the result of the RG boundary conditions at M_{GUT}. Eqn. (5.50) is what one might naively expect the correct boundary condition for A_B would be. No GUT scale non-universality would be introduced as a result of the GUT scale RGE boundary conditions if eqn. (5.50) were the correct boundary condition. Hence, comparing lepton flavor violation when eqn. (5.50) is used with lepton flavor violation when (5.11) is used gives us an idea of how important this new source of non-universality is. All other parameters are the same as they were in Figs. 5.8 and 5.10.

As can be seen, the dependence of the branching ratio on $m_{1/2}$ and $m_{\tilde{\nu}_e}$ remains qualitatively the same, while the dependence on A_τ changes drastically. In particular,

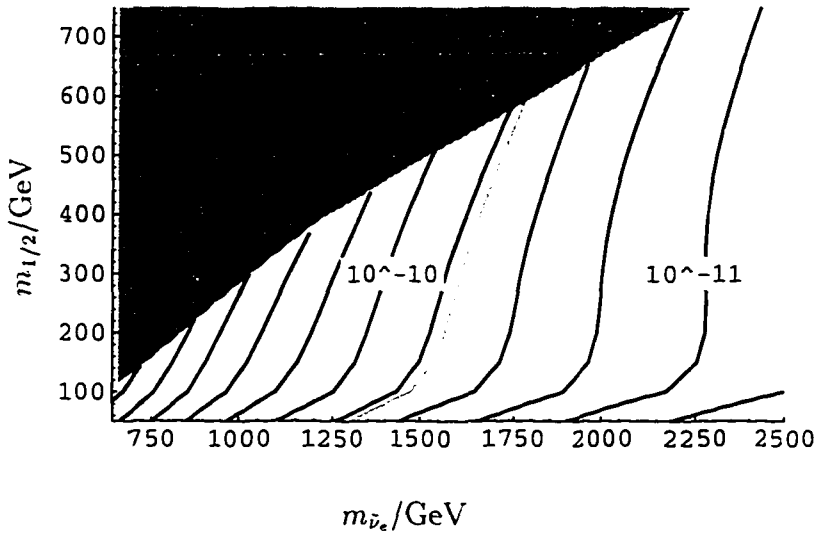

Figure 5.33: Contour plot of $Br(\mu \to e\gamma)$ in the $m_{\tilde{\nu}_e}$ - $m_{1/2}(M_{GUT})$ plane, using the (incorrect) universal GUT scale boundary condition eqn. (5.50), with 4 contours per order of magnitude. The gray line shows the experimental upper bound. The gray region denotes a region of parameter space where $m_0 < 700$ GeV.

when the correct boundary conditions for A_B are used, there is a valley centered around $A_\tau = 150$ GeV in which the branching ratio for $\mu \to e\gamma$ is much smaller than it is when the universal boundary condition (5.50) is used. On the other hand, when A_τ is large and negative, the branching ratio for $\mu \to e\gamma$ is larger when the non-universal boundary condition for A_B is used instead of the universal one.

The change in behavior when universal boundary condition eqn. (5.50) is used instead of the correct one can be understood as follows. Using eqn. (5.50) has the effect of decreasing the slope of the plot of A_B with respect to $\overline{A}_0$. This has the effect of decreasing the effect the $A_e A_e^\dagger$ term in RGE running for $\overline{m}_L^2$ has on $\overline{m}_L^2(M_Z)$. In particular, the length of the plot of $(\overline{m}_L^2)_{12}|_{M_Z}$, and hence $[X_{L_j}]_1$ in the complex plane is shrunk so that $[X_{L_j}]_1$ remains in the upper-right quadrant throughout the range

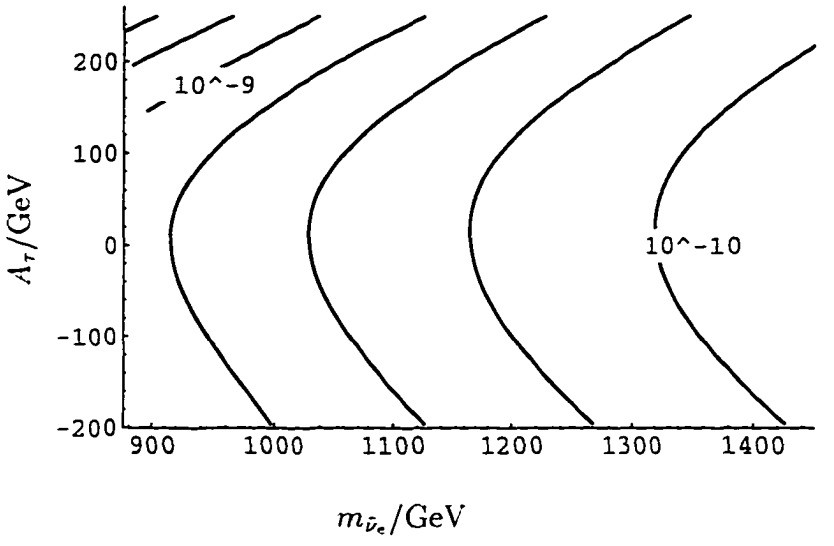

Figure 5.34: Contour plot of $Br(\mu \to e\gamma)$ in the $m_{\tilde{\nu}_e} - A_\tau$ plane, using the (incorrect) universal GUT scale boundary condition eqn. (5.50), with 2 contours per order of magnitude.

of $\overline{A}_0$ for which it has been plotted. Since $[X_{L_j}]_1$ and $[X_{L_j}]_3$ are both in the first quadrant of the complex plane throughout the range of $\overline{A}_0$ for which they have been graphed, the partial cancellation that occurred between $[X_{L_j}]_1$ and $[X_{L_j}]_3$ does not occur when the universal boundary condition is used. Hence, the sharp minimum in the plot of $Br(\mu \to e\gamma)$ as a function of A_τ that appeared when the correct boundary condition is used does not appear when the (incorrect) universal boundary condition is used.

5.6 Conclusions for Chapter 5

We have studied individual lepton number violation in the context of a supersymmetric SO(10) GUT valid up to the Planck scale that explains fermion masses and mixing angles in terms of several low energy effective fermion mass-generating

operators. We found that the model predicts rates of lepton flavor violation not inconsistent with the current experimental bounds, without using unreasonably heavy squarks and sleptons or fine tuning.

We have further found that when we extend an effective operator theory such as ADHRS model 4(c) to a full theory valid up to the Planck scale and consider lepton flavor violation in such a model, several interesting new features entered into the analysis which have either not been considered or not fully considered in the current literature. For example, we find that, as in the case of the low $\tan\beta$ minimal SO(10) theory studied in [8], there is substantial splitting of the third generation sleptons from the first two at the GUT scale, due to the largeness of the top quark Yukawa coupling λ_A, which can lead to rates of lepton flavor violation close to the current experimental bounds. We find, however, that our theory built based on an effective fermion mass operator theory has two mechanisms which can decrease the splitting of the third generation from the first two, and hence decrease the rate of lepton flavor violation: (1) In our theory, there are couplings associated with terms we needed to introduce to give the right-handed neutrinos a sufficiently large mass so as to explain why they have not been experimentally observed yet. These couplings can be just as large as the top quark Yukawa coupling, and give rise to interactions which push down the masses of the sleptons. By adjusting these couplings so that the couplings for the first two generations are large but the coupling for the third generation is small, the masses of the first two generations of sleptons can be decreased to reduce the splitting of the third generation from the first two. (2) The third generation scalars of the low energy theory are a mixture of two states[26], one which couples through

[26] Dimopoulos and Pomarol were the first to recognize the significance of this type of mixing. [50]

the top quark Yukawa coupling and one that does not. Thus, increasing the amount of the state which does not couple through the top quark Yukawa coupling in the mixing can decrease the size of the splitting of the third generation of sleptons from the first two.

However, the mixing of states in our theory is a double-edged sword. The second generation scalars of the low energy theory are also a mixture of states, one, $m^2_{16_2}$, which couples only through adjoints and the couplings introduced to give the right-handed neutrinos mass and one, $m^2_{\psi_2}$, which couples through a coupling λ_B, which cannot be set arbitrarily small because of its relation to the Yukawa coupling of one of the fermion mass-generating operators of our low energy effective theory. Because of the sensitivity of $\mu \to e\gamma$ to any splitting between the first two generation scalars, the amount of the mixing of the ψ_2 state in the mixing of the second generations scalars needs to be small or λ_B needs to be made small.

We also found that in a theory such as ours which uses adjoints or other large representations of SO(10) to explain fermion masses and mixing angles, the non-universality introduced into the lepton SUSY breaking trilinear coupling matrix due to couplings to the gaugino field has a substantial effect. This is in accord with [58] which analyzed lepton flavor violation in the context of a low $\tan\beta$ SO(10) effective operator theory and which found that even if one ignored the effect of the top Yukawa coupling on GUT scale mass splittings, rates of $\mu \to e\gamma$ would occur which could be experimentally accessible in the near future. This source of non-universality did not appear in [8] because that paper used a 'generic' SO(10) model which does not agree with experimental fermion mass and mixing angle data. However, any SO(10) theory which gives realistic predictions for fermion masses and mixing angles will either

need to use very large representations, such as 120s or 126s, or effective fermion mass operators such as model 4(c) uses. In either case, the gaugino interactions will have a substantial effect on the renormalization group running of the SUSY-breaking trilinear terms. Therefore, we would typically expect large gaugino-induced effects on lepton flavor violating processes in any realistic SO(10) theory using the traditional approach to supersymmetry-breaking with a messenger scale around M_{Planck}.

In addition, we found that GUT scale non-universality in the low energy SUSY breaking trilinear terms can be introduced purely as a result of the GUT scale boundary conditions matching the quantities in the full theory valid up to the Planck scale to quantities in the low energy effective theory below the GUT scale. This non-universality in the GUT scale boundary conditions has to do with the way that superheavy scalar fields are integrated out of the low energy theory to form higher dimensioned effective SUSY breaking trilinear operators from the multilinear operators of the full theory. This is a source of GUT scale non-universality that, to our knowledge, has not been explored before in the literature on lepton flavor violation. This source of non-universality has a big effect on rates of lepton flavor-violating processes. For our model, this source of non-universality allows for a partial cancellation of contributions to the rate for $\mu \to e\gamma$ in certain regions of the parameter space that would not have occurred otherwise.

Additionally, in our theory, there are a number of Yukawa couplings of the second generation of scalars to adjoints which are potentially dangerous because they could split the first generation from the second. We find, however, that the effects of these Yukawa couplings can be brought under control without requiring these couplings to be "unnaturally" small in comparison to the other Yukawa couplings in the theory.

For example, $\mu \rightarrow e\gamma$ consistent with experimental bounds can be obtained when these couplings are around 1/10 or lower.

Lastly, we note that experiments are under way by the MEGA collaboration which, unless $\mu \rightarrow e\gamma$ is observed by the collaboration, are expected to tighten the experimental upper bound on $\mu \rightarrow e\gamma$ to $Br(\mu \rightarrow e\gamma) < 6 \times 10^{-13}$. [59] Such a small value for the branching ratio for $\mu \rightarrow e\gamma$ is clearly inconsistent with the values for $\mu \rightarrow e\gamma$ in this analysis. The only way our analysis could possibly be consistent with $Br(\mu \rightarrow e\gamma) < 6 \times 10^{-13}$ is if there was an excessively large amount of fine tuning to achieve nearly perfect cancellation of the terms contributing to $\mu \rightarrow e\gamma$ or if sleptons were made excessively heavy, which also implies a high degree of fine tuning.

However, our analysis has been contingent on the assumption of traditional supersymmetry breaking, in which the supersymmetry-breaking terms are hard terms at the Planck scale and below. Recently, it has been discovered that supersymmetry breaking can be achieved by another means — low-energy dynamical supersymmetry breaking. [60]. It has been argued that models with dynamical supersymmetry breaking do not suffer from rates of lepton flavor violating processes as high as those in models with traditional supersymmetry breaking. [60, 53, 61]. Hence, if MEGA concludes that the branching ratio for $\mu \rightarrow e\gamma$ is lower than 6×10^{-13}, neither the model 4(c) superpotential nor the effective operator theory derived from it will be ruled out; it will only show that the messenger scale for SUSY breaking must be lower than M_{Planck} in order for model 4(c) to be viable.

APPENDIX A

REVIEW OF THE MSSM

A.1 Particle content

The full particle content of the MSSM is given in Table A.1. Capital letters without tildes refer to superfields. Lower case letters without tildes refer to the non-superpartner component of the supermultiplet (i.e. a particle in the minimal, two Higgs doublet extension of the Standard Model). Letters with tildes over them refer to the superpartner component of the supermultiplet.

A.2 Lagrangian

The MSSM superpotential is

$$W = QY_u\overline{U}H_u + QY_dDH_d + LY_e\overline{E}H_d + \mu(-H_{u,0}H_{d,0} + H_+H_-) \qquad \text{(A.1)}$$

where Y_u, Y_d, and Y_e are 3×3 flavor matrices.

At low energies, the matrices Y_u, Y_d, and Y_e are diagonalized by unitary matrices called S and T defined so that

$$S_uY_uT_u = \begin{pmatrix} \lambda_u & & \\ & \lambda_c & \\ & & \lambda_t \end{pmatrix} \equiv \hat{Y}_u,$$

superfield	gauge group representation	contains
$Q_f = \begin{pmatrix} U_f \\ D_f \end{pmatrix}$, $(f = 1,2,3)$	$(3,2,1/3)$	q_f quark doublet $\tilde{q}_f$ squark doublet
$\overline{U}_f$	$(\overline{3},1,-4/3)$	$\overline{u}_f$ up-type quark singlet $\tilde{\overline{u}}_f$ up-type squark singlet
$\overline{D}_f$	$(\overline{3},1,2/3)$	$\overline{d}_f$ down-type quark singlet $\tilde{\overline{d}}_f$ down-type squark singlet
$L_f = \begin{pmatrix} \nu_f \\ E_f \end{pmatrix}$	$(1,2,-1)$	l_f lepton doublet $\tilde{l}_f$ slepton doublet
$\overline{E}_f$	$(1,1,2)$	$\overline{e}_f$ electron-type singlet $\tilde{\overline{e}}_f$ selectron-type singlet
$H_d = \begin{pmatrix} H_{d,0} \\ H_- \end{pmatrix}$	$(1,2,-1)$	higgs, higgsino
$H_u = \begin{pmatrix} H_+ \\ H_{u,0} \end{pmatrix}$	$(1,2,1)$	higgs, higgsino
G	$(8,1,0)$	g gluon $\tilde{g}$ gluino
W	$(1,3,0)$	$w^{\pm}$ W-boson z Z-boson $\tilde{W}^{\pm}$ wino $\tilde{Z}$ zino
B	$(1,1,0)$	γ photon $\tilde{\gamma}$ photino

Table A.1: Particle content of the MSSM

and so forth, with all diagonal entries in $\hat{Y}_u$, $\hat{Y}_d$, and $\hat{Y}_e$ being real and positive. Note that in this notation, the KM matrix V_{KM} is given by

$$V_{KM} = S_u^* S_d^T \tag{A.2}$$

The supersymmetry breaking terms of the Lagrangian $\mathcal{L}_{SUSY\ breaking}$ are

1. scalar mass terms for the chiral scalars

$$\mathcal{L}_{scalar} = -\tilde{q}^* m_Q^2 \tilde{q} - \tilde{\bar{u}} m_U^2 \tilde{\bar{u}}^* - \tilde{\bar{d}} m_D^2 \tilde{\bar{d}}^* - \tilde{l}^* m_L^2 \tilde{l} \tag{A.3}$$

$$-\tilde{\bar{e}} m_E^2 \tilde{\bar{e}}^* - m_{H_d}^2 h_d^* h_d - m_{H_u}^2 h_u^* h_u$$

where m_Q^2, m_U^2, m_D^2, m_E^2, and m_L^2 are 3×3 flavor matrices.

2. gaugino mass terms

$$\mathcal{L}_{gaugino} = \frac{1}{2}(M' \tilde{b}\tilde{b} + M_2\, \tilde{w}\tilde{w} + M_3\, \tilde{g}\tilde{g}) + \text{h.c.} \tag{A.4}$$

Note that if the MSSM is the low energy remnant of a SUSY GUT, the gaugino masses will be unified at the GUT scale, just as the gauge couplings are. I.e.

$$\sqrt{\frac{5}{3}} M' = M_2 = M_3 \equiv m_{1/2}$$

at M_{GUT}.

3. soft SUSY breaking bilinear and trilinear terms

$$\mathcal{L}_{multilinear} = -[\tilde{q} A_u \tilde{\bar{u}} h_u + \tilde{q} A_d \tilde{\bar{d}} h_d + \tilde{l} A_e \tilde{\bar{e}} h_e + B\mu(-h_{u,0} h_{d,0} + h_+ h_-)] - \text{h.c.} \tag{A.5}$$

where A_u, A_d, and A_e are 3×3 flavor matrices.

The full Lagrangian is hence

$$\mathcal{L} = \mathcal{L}_{kinetic} + \int [W\delta(\bar{\theta}) + \text{h.c}]\ d^4\theta + \mathcal{L}_{SUSY\ breaking} \tag{A.6}$$

where $\mathcal{L}_{SUSYbreaking} = \mathcal{L}_{scalar} + \mathcal{L}_{gaugino} + \mathcal{L}_{multilinear}$ and

$$\mathcal{L}_{kinetic} = \int \frac{1}{4}\{\mathrm{tr}(\mathcal{W}[G]^2 + \mathcal{W}[W]^2 + \mathcal{W}[B]^2)\delta(\bar{\theta}) + \mathrm{h.c.}\}\, d^4\theta \qquad (A.7)$$

$$+ \int \sum_{\Phi \in \{Q,\bar{U},\bar{D},\bar{E},L,H_u,H_d\}} \Phi^\dagger e^{2g_3 G\cdot T_{SU(3)} + 2g_2 W\cdot T_{SU(2)} + g'BY}\Phi\, d^4\theta$$

where $\mathcal{W}$ is the gauge field strength, given by

$$\mathcal{W}[V] = -\frac{1}{4g_V^2}\overline{D}^2 e^{-g_V V} D e^{g_V V}, \qquad V \in \{G, W, B\}, \qquad (A.8)$$

where g_V is the coupling constant for field V; D and $\overline{D}$ are supersymmetry covariant derivatives, see [62]; and $T_{SU(3)}$, $T_{SU(2)}$, and Y are generators of $\mathrm{SU}(3)_{color}$, $\mathrm{SU}(2)_{weak}$, and $\mathrm{U}(1)_Y$, respectively.

In addition, notice that

- The coupling g' refers to the hypercharge coupling with ordinary Standard Model normalization. By contrast, g_1 refers to the hypercharge coupling with GUT inspired normalization, so that $g_3 = g_2 = g_1$ at M_{GUT}. These two are related by

$$g' = \sqrt{3/5}g_1. \qquad (A.9)$$

- The couplings g_2 and g_3 are also referred to as g and g_s, respectively, in the thesis.

A.3 Electroweak symmetry breaking

In addition to splitting the masses of the SUSY particles from their corresponding partners, the SUSY breaking terms also provide a mechanism for electroweak symmetry breaking. We define

$$\langle h_{d,0}\rangle \equiv v_1, \qquad \langle h_{u,0}\rangle \equiv v_2, \qquad (A.10)$$

and

$$\tan\beta \equiv \frac{v_2}{v_1}. \tag{A.11}$$

The tree level potential for the electrically neutral Higgs scalars is

$$V = \mu_d^2|h_{d,0}|^2+\mu_u^2|h_{u,0}|^2-B\mu(h_{d,0}h_{u,0}+h_{d,0}^*h_{u,0}^*)+\frac{1}{8}(g_2^2+g'^2)(|h_{d,0}|^2-|h_{u,0}|^2)^2 \tag{A.12}$$

where

$$\mu_d^2 = m_{H_d}^2 + \mu^2, \qquad \mu_u^2 = m_{H_u}^2 + \mu^2.$$

From this potential, it can be seen that, at tree level, electroweak symmetry breaking will occur if the following conditions hold true at the scale of electroweak symmetry breaking.

$$\sin 2\beta = \frac{2B\mu}{\mu_d^2+\mu_u^2} \tag{A.13}$$

$$\mu^2 = -\frac{1}{2}M_Z^2 - \frac{m_{H_d}^2 - m_{H_u}^2\tan^2\beta}{\tan^2\beta - 1} \tag{A.14}$$

$$\mu_d^2+\mu_u^2-2|B\mu| > 0 \tag{A.15}$$

$$\mu_d^2\mu_u^2-(B\mu)^4 < 0 \tag{A.16}$$

where M_Z is the Z boson mass. Note that we have used the fact that $M_Z^2 = (1/2)(g_2^2+g'^2)(v_1^2+v_2^2)$.

A.4 Mass terms

A.4.1 Chargino, neutralino masses

From the MSSM Lagrangian, the following mass matrices for the higgsino and electroweak gaugino fields can be computed.

$$\mathcal{L}_{chargino}^{mass} = (\tilde{W}_+ \quad \tilde{H}_+)\begin{pmatrix} M_2 & gv_1 \\ gv_2 & \mu \end{pmatrix}\begin{pmatrix} \tilde{W}_- \\ \tilde{H}_- \end{pmatrix} + \text{h.c.} \tag{A.17}$$

$$\mathcal{L}^{mass}_{neutralino} =$$

$$\frac{1}{2}\left(\tilde{B} \quad \tilde{W}_3 \quad \tilde{H}_{d,0} \quad \tilde{H}_{u,0}\right)\begin{pmatrix} M' & 0 & \frac{1}{\sqrt{2}}g'v_1 & -\frac{1}{\sqrt{2}}g'v_2 \\ 0 & M_2 & -\frac{1}{\sqrt{2}}g_2v_1 & \frac{1}{\sqrt{2}}g_2v_2 \\ \frac{1}{\sqrt{2}}g'v_1 & -\frac{1}{\sqrt{2}}g_2v_1 & 0 & -\mu \\ -\frac{1}{\sqrt{2}}g'v_2 & \frac{1}{\sqrt{2}}g_2v_2 & -\mu & 0 \end{pmatrix}\begin{pmatrix} \tilde{B} \\ \tilde{W}_3 \\ \tilde{H}_{d,0} \\ \tilde{H}_{u,0} \end{pmatrix} + \text{h.c.} \tag{A.18}$$

These mass matrices are diagonalized by unitary matrices defined

$$\begin{pmatrix} \tilde{W}_+ \\ \tilde{H}_+ \end{pmatrix} = U_+ \begin{pmatrix} \tilde{\chi}^+_1 \\ \tilde{\chi}^+_2 \end{pmatrix},$$

$$\begin{pmatrix} \tilde{W}_- \\ \tilde{H}_- \end{pmatrix} = U_- \begin{pmatrix} \tilde{\chi}^-_1 \\ \tilde{\chi}^-_2 \end{pmatrix},$$

$$\begin{pmatrix} \tilde{B} \\ \tilde{W}_3 \\ \tilde{H}_{d,0} \\ \tilde{H}_{u,0} \end{pmatrix} = U_0 \begin{pmatrix} \tilde{\chi}^0_1 \\ \tilde{\chi}^0_2 \\ \tilde{\chi}^0_3 \\ \tilde{\chi}^0_4 \end{pmatrix}. \tag{A.19}$$

Moreover, U_- and U_+ are chosen so that they are real.

The mass eigenstates thus obtained from the charged gauginos and charged Higgsinos are referred to as charginos and the mass eigenstates from the electroweak, uncharged gauginos and higgsinos are referred to as neutralinos.

A.4.2 Squark and slepton masses

Similarly, the following mass matrices for squarks and sleptons can be derived from the MSSM Lagrangian.

$$\begin{aligned} \mathcal{L}^{mass}_{SUSY\ scalars} = \quad & (\tilde{u}^* \quad \tilde{\bar{u}})\left(\begin{array}{c|c} m_Q^2 + v_2^2 Y_u Y_u^\dagger + D_{U,L} & v_2 A_u - \mu v_1 Y_u \\ \hline v_2 A_u^\dagger - \mu v_1 Y_u^\dagger & m_U^2 + v_2^2 Y_u^\dagger Y_u + D_{U,R} \end{array}\right)\begin{pmatrix} \tilde{u} \\ \tilde{\bar{u}}^* \end{pmatrix} \\ & + \left(\tilde{d}^* \quad \tilde{\bar{d}}\right)\left(\begin{array}{c|c} m_Q^2 + v_1^2 Y_d Y_d^\dagger + D_{D,L} & v_1 A_d - \mu v_2 Y_d \\ \hline v_1 A_d^\dagger - \mu v_2 Y_d^\dagger & m_D^2 + v_1^2 Y_d^\dagger Y_d + D_{D,R} \end{array}\right)\begin{pmatrix} \tilde{d} \\ \tilde{\bar{d}}^* \end{pmatrix} \\ & + (\tilde{e}^* \quad \tilde{\bar{e}})\left(\begin{array}{c|c} m_L^2 + v_1^2 Y_e Y_e^\dagger + D_{E,L} & v_1 A_e - \mu v_2 Y_e \\ \hline v_1 A_e^\dagger - \mu v_2 Y_e^\dagger & m_E^2 + v_1^2 Y_e^\dagger Y_e + D_{E,R} \end{array}\right)\begin{pmatrix} \tilde{e} \\ \tilde{\bar{e}}^* \end{pmatrix} \\ & + \tilde{\nu}^*(m_L^2 + D_\nu)\tilde{\nu} \end{aligned} \tag{A.20}$$

where

$$\begin{aligned}
D_{U,L} &= (\frac{1}{2} - \frac{2}{3}\sin^2\theta_W)M_Z^2\cos 2\beta \\
D_{U,R} &= (\frac{2}{3}\sin^2\theta_W)M_Z^2\cos 2\beta \\
D_{D,L} &= (-\frac{1}{2} + \frac{1}{3}\sin^2\theta_W)M_Z^2\cos 2\beta \\
D_{D,R} &= (-\frac{1}{3}\sin^2\theta_W)M_Z^2\cos 2\beta \\
D_{E,L} &= (-\frac{1}{2} + \sin^2\theta_W)M_Z^2\cos 2\beta \\
D_{E,R} &= -(\sin^2\theta_W)M_Z^2\cos 2\beta \\
D_{\nu} &= \frac{1}{2}M_Z^2\cos 2\beta.
\end{aligned}$$

and θ_W is the Weinberg angle. Note that the left-handed and right-handed fields mix via the μ and A terms.

Squark and slepton mass matrices are diagonalized using 6×6 matrices Γ defined

$$\Gamma_\Omega \left(\begin{array}{c|c} S_\Omega^* & \\ \hline & T_\Omega^\dagger \end{array}\right) \begin{pmatrix} \tilde{\Omega}' \\ \tilde{\bar{\Omega}}'^* \end{pmatrix} = \tilde{\Omega}, \qquad \Omega \in \{u, d, e\}$$

where $\tilde{\Omega}$ is a six dimensional vector of mass eigenstates and $\tilde{\Omega}'$ and $\tilde{\bar{\Omega}}'$ are weak eigenstates. Cf. notation of [63]. Additionally, we define $\Gamma_{\Omega,L}$ and $\Gamma_{\Omega,R}$ to be 6×3 matrices so that $\Gamma_{\Omega,L}$ consists of the first three columns of Γ_Ω and $\Gamma_{\Omega,R}$ consists of the last three columns. In block matrix notation,

$$\Gamma_\Omega = \left(\Gamma_{\Omega,L} \mid \Gamma_{\Omega,R} \right)$$

Finally, we will define Γ_ν so that

$$\Gamma_\nu S_e^* \tilde{\nu}' = \tilde{\nu}$$

where $\tilde{\nu}'$ is the weak eigenstate basis for the sneutrinos and $\tilde{\nu}$ is a mass eigenstate basis for the sneutrinos.

APPENDIX B

FEYNMAN VERTICES

Figure B.1: Feynman vertices relevant to calculations of baryon number and individual lepton number violating processes.

Figure B.1 (continued)

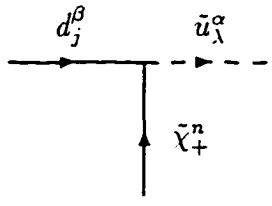

$$i[(g_2\Gamma_{U,L}U_{+\,1n} - \Gamma_{U,R}\hat{Y}_u\ U_{+\,2n})V_{KM}]_{\lambda j}\delta^\alpha_\beta$$

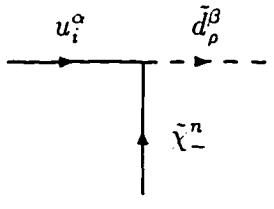

$$i[(g_2\Gamma_{D,L}U_{-\,1n} - \Gamma_{D,R}\hat{Y}_d\ U_{-\,2n})V_{KM}^\dagger]_{\rho i}\delta^\alpha_\beta$$

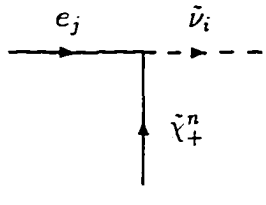

$$ig_2\Gamma_{\nu\ ij}U_{+\,1n}$$

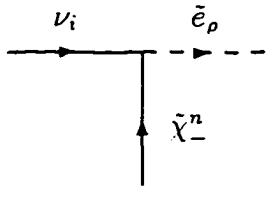

$$i[(g_2\Gamma_{E,L}U_{-\,1n} - \Gamma_{E,R}\hat{Y}_e\ U_{-\,2n})]_{\rho i}$$

(figure continued on next page)

Figure B.1 (continued)

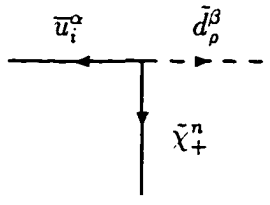

$$-iU^*_{+\,2n}(\Gamma_{D,L}V^\dagger_{KM}\hat{Y}_u)_{\rho i}\delta^\beta_\alpha$$

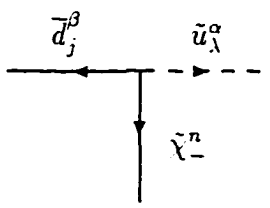

$$-iU^*_{-\,2n}(\Gamma_{U,L}V_{KM}\hat{Y}_d)_{\lambda j}\delta^\beta_\alpha$$

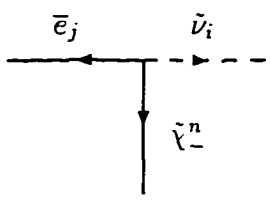

$$-iU^*_{-\,2n}(\Gamma_\nu\hat{Y}_e)_{ij}$$

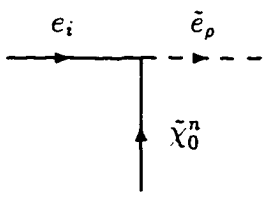

$$-ig_2[\frac{1}{\sqrt{2}}\Gamma_{E,L\ \rho i}(\frac{g'}{g_2}U^0_{1n}+U^0_{2n})+\Gamma_{E,R\ \rho i}\frac{\lambda_{e_i}}{g_2}U^0_{3n}]$$

(figure continued on next page)

Figure B.1 (continued)

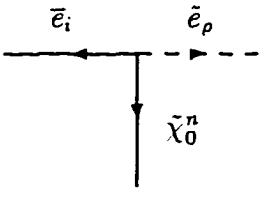

$$-ig_2[-\sqrt{2}\frac{g'}{g_2}U_{1n}^{0\,*}\Gamma_{E,R\ \rho i}+\frac{\lambda_{e_i}}{g_2}\Gamma_{E,L\ \rho i}U_{3n}^{0\,*}]$$

APPENDIX C

REVIEW OF SO(10)

The primary goals of this appendix are to (1) introduce various conventions and notations for the SO(10) invariant combinations of fields appearing in the superpotentials for the models in this thesis; (2) give formulas for the SU(5) decomposition of those SO(10) invariant combinations of fields, which then can be used to compute such things as the mass matrices found in Appendix E or the the group theoretic coefficients appearing in the renormalization group equations found in Appendix F; and (3) introduce a formalism in which those coefficients can be computed directly in SO(10), without resort to SU(5) decomposition. It is assumed that the reader is familiar with the basic theory of the classical Lie groups, including such things as Lie algebras and subalgebras; Cartan subalgebras; raising and lowering operators; roots and weights; and so forth. For those not familiar with these concepts, a good treatment can be found in [64]. This appendix follows much of the treatment of SO(10) given in that reference.

C.1 The fundamental representation

In the fundamental representation, the generators of SO(10), denoted M_{ab}, are defined

$$(M_{ab})_{jk} = -i(\delta_{aj}\delta_{bk} - \delta_{ak}\delta_{bj}), \tag{C.1}$$

where $(M_{ab})_{jk}$ denotes the j,kth entry of matrix M_{ab} and a, b, j, and k run from 1 to 10. Technically, eqn. (C.1) states how the generators of SO(10) appear in a particular basis for the fundamental representation of SO(10), which will be referred to as the "standard basis" for the fundamental representation.

We will choose the Cartan subalgebra for SO(10) to be

$$H_i = M_{i,i+5}, \qquad i = 1 \text{ to } 5. \tag{C.2}$$

The roots of SO(10) are then

$$\{\eta \mathbf{e}_i + \eta' \mathbf{e}_j \mid \eta, \eta' \in \{-1, 1\}; i, j \in \{1, \ldots, 5\}; i \neq j\} \tag{C.3}$$

The raising and lowering operators, denoted $E_{\boldsymbol{\alpha}}$, are defined to satisfy

$$[H_i, E_{\boldsymbol{\alpha}}] = \alpha_i E_{\boldsymbol{\alpha}}, \qquad i \in \{1, \ldots, 5\}, \boldsymbol{\alpha} \in \text{set of roots of SO(10)} \tag{C.4}$$

The raising and lowering operators are determined by eqn. (C.4) up to some arbitrary choices of complex phases. These phases can be chosen so that

$$E_{\mathbf{e}_i - \mathbf{e}_j} = \frac{1}{2}(M_{ij} + iM_{i+5,j} - iM_{i,j+5} + M_{i+5,j+5}), \quad \text{and} \tag{C.5}$$

$$E_{\eta(\mathbf{e}_i + \mathbf{e}_j)} = \frac{1}{2}(M_{ij} + i\eta M_{i+5,j} + i\eta M_{i,j+5} - M_{i+5,j+5}), \qquad \text{if } \eta = \pm 1, i < j$$

The eigenvector basis for the fundamental representation is

$$\{|\eta \mathbf{e}_i\rangle \,|\eta \in \{-1, 1\}, i \in \{1, \ldots, 5\}\} \tag{C.6}$$

where $|\boldsymbol{\mu}\rangle$ denotes a vector with weight $\boldsymbol{\mu}$. That is to say, a vector where $H_i\,|\boldsymbol{\mu}\rangle = \mu_i\,|\boldsymbol{\mu}\rangle$ for all i. An explicit phase convention will be used, in which the eigenvectors are

$$|\pm \mathbf{e}_1\rangle = \frac{1}{\sqrt{2}} \begin{pmatrix} \mp i \\ 0 \\ 0 \\ 0 \\ 0 \\ 1 \\ 0 \\ 0 \\ 0 \\ 0 \end{pmatrix}, \quad |\pm \mathbf{e}_2\rangle = \frac{1}{\sqrt{2}} \begin{pmatrix} 0 \\ \mp i \\ 0 \\ 0 \\ 0 \\ 0 \\ 1 \\ 0 \\ 0 \\ 0 \end{pmatrix}, \qquad \text{etc.} \tag{C.7}$$

where the above are expressions in terms of the standard basis for the fundamental representation of SO(10). It can be verified that, with the phase conventions of eqns. (C.5) and (C.7),

$$E_{\mathbf{e}_i - \mathbf{e}_j}\,|\mathbf{e}_k\rangle = -i\,|\mathbf{e}_i\rangle\,\delta_{jk}, \tag{C.8}$$

$$E_{\mathbf{e}_i - \mathbf{e}_j}\,|-\mathbf{e}_k\rangle = i\,|-\mathbf{e}_j\rangle\,\delta_{ik}$$

$$E_{\pm(\mathbf{e}_i + \mathbf{e}_j)}\,|\mp \mathbf{e}_k\rangle = i\,|\pm \mathbf{e}_i\rangle\,\delta_{jk} - i\,|\pm \mathbf{e}_j\rangle\,\delta_{ik}, \quad \text{if } i < j.$$

C.2 SU(5)×U(1) subgroup of SO(10)

Let $(T^A)^\alpha{}_\beta$ represent a generator of SU(5), where $A \in \{1, \ldots, 24\}$, and α, β, running from 1 to 5, are SU(5) indices. In addition, we also define $(T^{25})^\alpha{}_\beta \equiv \frac{1}{\sqrt{10}}\delta^\alpha{}_\beta$, as a U(1) generator which commutes with the SU(5) generators. Consider the SO(10) Lie algebra elements $\hat{T}^A$ defined

$$\hat{T}^A = (T^A)^\alpha{}_\alpha H_\alpha + i(T^A)^\alpha{}_\beta E_{\mathbf{e}_\alpha - \mathbf{e}_\beta}. \tag{C.9}$$

We shall express $\hat{T}^A$ in an eigenvector basis for SO(10). That is, a basis where

$$|e_1\rangle = \begin{pmatrix} 1 \\ 0 \\ 0 \\ 0 \\ 0 \\ 0 \\ 0 \\ 0 \\ 0 \\ 0 \end{pmatrix}, |e_2\rangle = \begin{pmatrix} 0 \\ 1 \\ 0 \\ 0 \\ 0 \\ 0 \\ 0 \\ 0 \\ 0 \\ 0 \end{pmatrix}, \text{etc.}, \quad |-e_1\rangle = \begin{pmatrix} 0 \\ 0 \\ 0 \\ 0 \\ 0 \\ 1 \\ 0 \\ 0 \\ 0 \\ 0 \end{pmatrix}, \text{etc.}$$

This basis is related to the standard basis in which the eigenvectors are expressed as in eqn. (C.7) by a unitary transformation. Using eqn. (C.8), it can be seen that in this basis

$$\begin{aligned} \hat{T}^A &= \left(\begin{array}{ccc|ccc} (T^A)^1_{\ 1} & (T^A)^1_{\ 2} & \cdots & & & \\ (T^A)^2_{\ 1} & (T^A)^2_{\ 2} & \cdots & & & \\ \vdots & \vdots & \ddots & & & \\ \hline & & & -(T^A)^1_{\ 1} & -(T^A)^2_{\ 1} & \cdots \\ & & & -(T^A)^1_{\ 2} & -(T^A)^2_{\ 2} & \cdots \\ & & & \vdots & \vdots & \ddots \end{array}\right) \\ &= \left(\begin{array}{c|c} T^A & 0 \\ \hline 0 & -(T^A)^* \end{array}\right) \end{aligned} \tag{C.10}$$

Then,

$$\begin{aligned} [\hat{T}^A, \hat{T}^B] &= \left(\begin{array}{c|c} [T^A, T^B] & 0 \\ \hline 0 & -([T^A, T^B])^* \end{array}\right) \\ &= if^{ABC} \left(\begin{array}{c|c} T^C & 0 \\ \hline 0 & (T^C)^* \end{array}\right) \\ &= if^{ABC}\hat{T}^C \end{aligned} \tag{C.11}$$

where the f^{ABC}s are the structure constants for the SU(5)×U(1) Lie algebra, defined $[T^A, T^B] \equiv if^{ABC}T^C$. Hence, we have shown that the $\hat{T}^A$s satisfy the same Lie algebra as the SU(5)×U(1) generators. In fact, the $\hat{T}^A$s are explicit generators of an

SU(5)×U(1) subgroup of SO(10). Furthermore, eqn. (C.11) shows that

$$\begin{aligned} V &\equiv V^{\alpha}\,|\mathbf{e}_{\alpha}\rangle \\ \overline{V} &\equiv \overline{V}_{\alpha}\,|-\mathbf{e}_{\alpha}\rangle \end{aligned} \tag{C.12}$$

transform as 5 and $\overline{5}$ representations of SU(5), respectively, under the SU(5) subgroup. Using eqn. (C.7) to reexpress this in terms of the standard basis, we find

$$\mathbf{10} = \begin{pmatrix} \frac{V-\overline{V}}{\sqrt{2}i} \\ \frac{V+\overline{V}}{\sqrt{2}} \end{pmatrix} \tag{C.13}$$

C.3 45 and 54 representations

We next consider the decomposition of $10 \otimes 10 = 45 + 54 + 1$ into SU(5). As we shall show, the 45 and 54 representations decompose in the following manner under SU(5):

$$\begin{aligned} 45 &\rightarrow 24 + 10 + \overline{10} + 1 \\ 54 &\rightarrow 24 + 15 + \overline{15} \end{aligned}$$

We will use H_A, χ, $\overline{\chi}$, and h to represent irreducible representations of SU(5) coming from a 45 of SO(10). Namely, H_A is a traceless, Hermitian 5×5 matrix, transforming as a 24 under SU(5); χ and $\overline{\chi}$ are 5×5 antisymmetric matrices transforming as 10 and $\overline{10}$ representations, respectively, of SU(5); and h is an SU(5) singlet. Similarly, H_S, ρ, and $\overline{\rho}$ will represent irreducible representations of SU(5) coming from a 54 of SO(10). H_S is a traceless, Hermitian 5×5 matrix, transforming as a 24 under under SU(5); and ρ and $\overline{\rho}$ are 5×5 symmetric matrices transforming as 15 and $\overline{15}$ representations, respectively, of SU(5). Additionally, we will use a normalization convention for the

SU(5) matrices such that

$$\begin{aligned}
\mathbf{10}^\dagger\mathbf{10} &= V^\dagger V + \overline{V}^\dagger \overline{V} \\
\mathrm{tr}(\mathbf{45}^\dagger\mathbf{45}) &= \mathrm{tr}(H_A^\dagger H_A + \chi^\dagger \chi + \overline{\chi}^\dagger \overline{\chi}) + h^* h \\
\mathrm{tr}(\mathbf{54}^\dagger\mathbf{54}) &= \mathrm{tr}(H_S^\dagger H_S + \rho^\dagger \rho + \overline{\rho}^\dagger \overline{\rho})
\end{aligned} \tag{C.14}$$

where **45** and **54** are 10×10 matrices forming 45 and 54 representations, respectively, of SO(10).

The 45 and 54 representations will be expressed using a tensor product of 10 representations. The tensor product of two vectors $|\mathbf{A}\rangle$ and $|\mathbf{B}\rangle$ will be denoted $|\mathbf{A} \otimes \mathbf{B}\rangle$ or equivalently $|\mathbf{A}\rangle \otimes |\mathbf{B}\rangle$. The generators of SO(10) operate on the tensor product as

$$T\,|\mathbf{A} \otimes \mathbf{B}\rangle = (T\,|\mathbf{A}\rangle) \otimes |\mathbf{B}\rangle + |\mathbf{A}\rangle \otimes (T\,|\mathbf{B}\rangle) \tag{C.15}$$

where T is a generator of SO(10). We define

$$\begin{aligned}
|[\mathbf{A},\mathbf{B}]\rangle &\equiv \frac{1}{\sqrt{2}}(|\mathbf{A} \otimes \mathbf{B}\rangle - |\mathbf{B} \otimes \mathbf{A}\rangle) \\
|\{\mathbf{A},\mathbf{B}\}\rangle &\equiv \frac{1}{\sqrt{2}}(|\mathbf{A} \otimes \mathbf{B}\rangle + |\mathbf{B} \otimes \mathbf{A}\rangle)
\end{aligned} \tag{C.16}$$

Using eqns. (C.8), (C.9), and (C.15), it can be seen that

$$\begin{aligned}
(\hat{T}^A)H^\alpha{}_\beta\,|\mathbf{e}_\alpha \otimes -\mathbf{e}_\beta\rangle &= \left((T^A)^\alpha{}_\gamma H^\gamma{}_\beta - (T^A)^\gamma{}_\beta H^\alpha{}_\gamma\right)|\mathbf{e}_\alpha \otimes -\mathbf{e}_\beta\rangle \\
(\hat{T}^A)H^\alpha{}_\beta\,|-\mathbf{e}_\beta \otimes \mathbf{e}_\alpha\rangle &= \left((T^A)^\alpha{}_\gamma H^\gamma{}_\beta - (T^A)^\gamma{}_\beta H^\alpha{}_\gamma\right)|-\mathbf{e}_\beta \otimes \mathbf{e}_\alpha\rangle \\
(\hat{T}^A)P^{\alpha\beta}\,|\mathbf{e}_\alpha \otimes \mathbf{e}_\beta\rangle &= \left((T^A)^\alpha{}_\gamma P^{\gamma\beta} + (T^A)^\beta{}_\gamma P^{\alpha\gamma}\right)|\mathbf{e}_\alpha \otimes \mathbf{e}_\beta\rangle \\
(\hat{T}^A)\overline{P}_{\alpha\beta}\,|-\mathbf{e}_\alpha \otimes -\mathbf{e}_\beta\rangle &= \left(-(T^A)^\gamma{}_\alpha \overline{P}_{\gamma\beta} - (T^A)^\gamma{}_\beta \overline{P}_{\alpha\gamma}\right)|-\mathbf{e}_\alpha \otimes -\mathbf{e}_\beta\rangle
\end{aligned} \tag{C.17}$$

Hence, $H^\alpha{}_\beta\,|[\mathbf{e}_\alpha, -\mathbf{e}_\beta]\rangle$ and $H^\alpha{}_\beta\,|\{\mathbf{e}_\alpha, -\mathbf{e}_\beta\}\rangle$ transform as 24 representations under SU(5); $\chi^{\alpha\beta}\,|[\mathbf{e}_\alpha, \mathbf{e}_\beta]\rangle$ and $\overline{\chi}_{\alpha\beta}\,|[-\mathbf{e}_\alpha, -\mathbf{e}_\beta]\rangle$ transform as 10 and $\overline{10}$ representations of

SU(5), respectively; and $\rho^{\alpha\beta}\,|\{\mathbf{e}_\alpha, \mathbf{e}_\beta\}\rangle$ and $\overline{\rho}_{\alpha\beta}\,|\{-\mathbf{e}_\alpha, -\mathbf{e}_\beta\}\rangle$ transform as 15 and $\overline{15}$ representations of SU(5), respectively. Accordingly, the 45 and 54 representations can be decomposed

$$\begin{aligned}\mathbf{45} &= \frac{1}{i}\left((H_A)^\alpha{}_\beta + \frac{h}{\sqrt{5}}\delta^\alpha{}_\beta\right)|[\mathbf{e}_\alpha, -\mathbf{e}_\beta]\rangle - \frac{1}{\sqrt{2}}\chi^{\alpha\beta}\,|[\mathbf{e}_\alpha, \mathbf{e}_\beta]\rangle \\ &\quad -\frac{1}{\sqrt{2}}\overline{\chi}_{\alpha\beta}\,|[-\mathbf{e}_\alpha, -\mathbf{e}_\beta]\rangle \qquad \text{(C.18)} \\ \mathbf{54} &= (H_S)^\alpha{}_\beta\,|\{\mathbf{e}_\alpha, -\mathbf{e}_\beta\}\rangle - \frac{1}{\sqrt{2}}\rho^{\alpha\beta}\,|\{\mathbf{e}_\alpha, \mathbf{e}_\beta\}\rangle \\ &\quad -\frac{1}{\sqrt{2}}\overline{\rho}_{\alpha\beta}\,|\{-\mathbf{e}_\alpha, -\mathbf{e}_\beta\}\rangle \qquad \text{(C.19)}\end{aligned}$$

The $1/\sqrt{2}$ factors come from the normalization conventions given by eqn. (C.14), and the complex phases that appear were chosen as a convention. Using eqn. (C.7) to express this in the standard basis for SO(10), we find

$$\mathbf{45} = \begin{pmatrix} A + C_A & -S - B_A \\ S - B_A & A - C_A \end{pmatrix} \qquad \text{(C.20)}$$

where

$$S = \frac{1}{2\sqrt{2}}(H + H^T), \qquad A = \frac{1}{2i\sqrt{2}}(H - H^T)$$
$$B_A = \frac{1}{2i}(\chi - \overline{\chi}), \qquad C_A = \frac{1}{2}(\chi + \overline{\chi}), \quad \text{and}$$
$$H = H_A + \frac{h}{\sqrt{5}}I$$

where I is the 5×5 identity matrix.

$$\mathbf{54} = \begin{pmatrix} S + C_S & A - B_S \\ -A - B_S & S - C_S \end{pmatrix} \qquad \text{(C.21)}$$

where

$$S = \frac{1}{2\sqrt{2}}(H_S + H_S^T), \qquad A = \frac{1}{2i\sqrt{2}}(H_S - H_S^T)$$
$$B_S = \frac{1}{2i}(\rho - \overline{\rho}), \qquad C_S = \frac{1}{2}(\rho + \overline{\rho}).$$

Using eqns. (C.12), (C.20), and (C.21), the following SU(5) decompositions of various SO(10) invariant combinations of 10, 45, and 54 representations can be derived.[27]

$$
\begin{aligned}
\mathbf{10'\ 10} &= \overline{V}'V + V'\overline{V} \qquad (C.22)\\
\mathbf{45'\ 45} &= -HH' + \chi\overline{\chi}' + \chi'\overline{\chi}\\
\mathbf{54'\ 54} &= H_S H'_S + \rho\overline{\rho}' + \rho'\overline{\rho}\\
\mathbf{10\ 45\ 10'} &= \frac{i}{\sqrt{2}}(\overline{V}'HV - \overline{V}HV') - \overline{V}\chi\overline{V}' - V\overline{\chi}V'\\
\mathbf{54\ 45\ 45'} &= -\frac{1}{2\sqrt{2}}H_S\{H, H'\} + \frac{1}{\sqrt{2}}(H_S\chi\overline{\chi}' + H_S\chi'\overline{\chi})\\
&\quad + \frac{1}{i\sqrt{2}}(\overline{\chi}'H\rho + \overline{\chi}H'\rho + \overline{\rho}H\chi' + \overline{\rho}H'\chi)\\
\mathbf{45\ 45'\ 45''} &= \frac{i}{2\sqrt{2}}H_A[H'_A, H''_A] + \frac{i}{2}[(\overline{\chi}'H\chi'' - \overline{\chi}''H\chi') + (\overline{\chi}''H'\chi - \overline{\chi}H'\chi'')\\
&\quad + (\overline{\chi}H''\chi' - \overline{\chi}'H''\chi)]\\
\mathbf{54\ 54'\ 45} &= -\frac{i}{2\sqrt{2}}[H_S, H'_S]H + \frac{1}{\sqrt{2}}[(\overline{\rho}H'_S\chi - \overline{\chi}H'_S\rho) + (\overline{\chi}H_S\rho' - \overline{\rho}'H_S\chi)\\
&\quad + i(\overline{\rho}H\rho' - \overline{\rho}'H\rho)]\\
\mathbf{54\ 54'\ 54''} &= \frac{1}{2\sqrt{2}}H_S\{H'_S, H''_S\} + \frac{1}{\sqrt{2}}[\overline{\rho}H'_S\rho'' + \overline{\rho}H''_S\rho' + \overline{\rho}'H_S\rho'' +\\
&\quad \overline{\rho}'H''_S\rho + \overline{\rho}''H_S\rho' + \overline{\rho}''H'_S\rho]
\end{aligned}
$$

Here, SO(10) and SU(5) traces are implied. For example, $\mathbf{45\ 45'\ 45''} \equiv \mathrm{tr}(\mathbf{45\ 45'\ 45''})$; $\overline{\chi}H\chi \equiv \mathrm{tr}(\overline{\chi}H\chi)$. The same convention of implied traces is used in the expressions for the superpotentials found in this thesis.

C.4 The spinor representation

It is convenient to construct the spinor representation of SO(10) by first constructing a spinor representation in SO(11), and then converting to SO(10) by considering

[27]These decompositions, independently derived, are consistent with those found in [65], which we later used to verify the correctness of our results.

an SO(10) subgroup of SO(11). The Cartan subalgebra of SO(11) can be chosen the same as before. That is, $H_i = M_{i,i+5}$ for $i \in \{1,\ldots,5\}$. However, in addition to the raising and lowering operators of SO(10) given by eqn. (C.5), there are the operators

$$E_{\pm \mathbf{e}_j} = \frac{1}{\sqrt{2}}(M_{j,11} \pm i M_{j+5,11}), \qquad j \in \{1,\ldots,5\}. \tag{C.23}$$

The raising and lowering operators of eqn. (C.5) satisfy the relationship

$$\begin{aligned} iE_{\mathbf{e}_i - \mathbf{e}_j} &= [E_{\mathbf{e}_i}, E_{-\mathbf{e}_j}] \\ iE_{\pm(\mathbf{e}_i + \mathbf{e}_j)} &= [E_{\pm\mathbf{e}_i}, E_{\pm\mathbf{e}_j}], \quad i < j. \end{aligned} \tag{C.24}$$

Note also that

$$H_i = [E_{\mathbf{e}_i}, E_{-\mathbf{e}_i}] \quad \text{and} \quad E_{-\mathbf{e}_i} = E^{\dagger}_{\mathbf{e}_i}. \tag{C.25}$$

Using eqns. (C.24) and (C.25) allows a simple expression for the $\hat{T}^A$s.

$$\hat{T}^A = (T^A)^{\alpha}{}_{\beta}[E_{\mathbf{e}_\alpha}, E_{-\mathbf{e}_\beta}]. \tag{C.26}$$

The SO(11) spinor representation is the set

$$\left\{ \left| \frac{1}{2}(\eta_1 \mathbf{e}_1 + \eta_2 \mathbf{e}_2 + \eta_3 \mathbf{e}_3 + \eta_4 \mathbf{e}_4 + \eta_5 \mathbf{e}_5) \right\rangle \mid \forall i, \eta_i \in \{-1, 1\} \right\}.$$

Let σ_k^j represent a Pauli matrix σ_k which operates on the jth spin eigenvalue. For example,

$$\begin{aligned} \sigma_2^3 |+++++\rangle &\equiv |+\rangle \otimes |+\rangle \otimes (\sigma_2 |+\rangle) \otimes |+\rangle \otimes |+\rangle \\ &= |+\rangle \otimes |+\rangle \otimes (i|-\rangle) \otimes |+\rangle \otimes |+\rangle \\ &= i|++-++\rangle. \end{aligned} \tag{C.27}$$

The Cartan subalgebra in this notation is then

$$H_i = \frac{1}{2}\sigma_3^i. \tag{C.28}$$

Expressions for the raising and lowering operators, derived in [64], are as follows.

$$E_{\pm \mathbf{e}_j} = \frac{1}{2}\left(\prod_{i=1}^{j-1} \sigma_3^i\right)\sigma_\pm^j \tag{C.29}$$

where $\sigma_\pm \equiv (\sigma_1 \pm i\sigma_2)/\sqrt{2}$. The remaining raising and lowering operators are constructed using eqn. (C.24).

In addition, the following are useful relationships in practical calculations involving the spinor representation.

$$\{E_{\mathbf{e}_j}, E_{\mathbf{e}_k}\} = 0; \quad \{E_{-\mathbf{e}_j}, E_{-\mathbf{e}_k}\} = 0 \tag{C.30}$$

$$\{E_{\mathbf{e}_j}, E_{-\mathbf{e}_k}\} = \frac{1}{2}\delta_k^j.$$

Note, these relations are not necessarily true in other representations besides the spinor representation.

Under an SO(10) subgroup of SO(11), the 32 dimensional spinor representation decomposes into two irreducible representations, 16 and $\overline{16}$, where

$$16 = \left\{ \left| \frac{1}{2}(\eta_1\mathbf{e}_1 + \eta_2\mathbf{e}_2 + \eta_3\mathbf{e}_3 + \eta_4\mathbf{e}_4 + \eta_5\mathbf{e}_5) \right\rangle \mid \forall i, \eta_i \in \{-1, 1\}; \prod_i \eta_i = -1 \right\}.$$

$$\overline{16} = \left\{ \left| \frac{1}{2}(\eta_1\mathbf{e}_1 + \eta_2\mathbf{e}_2 + \eta_3\mathbf{e}_3 + \eta_4\mathbf{e}_4 + \eta_5\mathbf{e}_5) \right\rangle \mid \forall i, \eta_i \in \{-1, 1\}; \prod_i \eta_i = 1 \right\}.$$

Under the SU(5) subgroup of SO(10), the 16 decomposes into $1 + \bar{5} + 10$. We will use χ, $\overline{\psi}$, and ν to represent irreducible representations of SU(5) coming from a 16 of SO(10). As before, χ is an antisymmetric matrix transforming as an SU(5) 10 representation; $\overline{\psi}$ is an $\bar{5}$ vector, and ν is an SU(5) singlet. Analogous notation is used for the $\overline{16}$.

A straightforward calculation using eqn. (C.30) shows that

$$\nu|-----\rangle,$$

$$\overline{V}_\gamma E_{-e_\gamma} |+++++\rangle, \text{ and}$$

$$\chi^{\gamma\delta} E_{e_\gamma} E_{e_\delta} |-----\rangle \tag{C.31}$$

transform as 1, $\overline{5}$, and 10 representations of SU(5), respectively. For example,

$$\begin{aligned}
(\hat{T}^A)\overline{\psi}_\gamma E_{-e_\gamma} |+++++\rangle \;\equiv\; & \\
& (T^A)^\alpha{}_\beta [E_{e_\alpha}, E_{-e_\beta}] \overline{\psi}_\gamma E_{-e_\gamma} |+++++\rangle \\
= \; & (T^A)^\alpha{}_\beta (\frac{1}{2}\delta^\beta_\alpha - 2E_{-e_\beta} E_{e_\alpha}) \overline{\psi}_\gamma E_{-e_\gamma} |+++++\rangle \\
= \; & (T^A)^\alpha{}_\beta (\frac{1}{2}\delta^\beta_\alpha E_{-e_\gamma} - E_{-e_\beta}\delta^\gamma_\alpha + 2E_{-e_\beta} E_{-e_\gamma} E_{e_\alpha}) \\
& \times \overline{\psi}_\gamma |+++++\rangle \\
= \; & -\left((T^A)^{\gamma'}_\gamma \overline{\psi}_{\gamma'}\right) E_{-e_\gamma} |+++++\rangle .
\end{aligned}$$

As before, a normalization convention is chosen so that

$$\mathbf{16}^\dagger \mathbf{16} = \nu^* \nu + \overline{\psi}^\dagger \overline{\psi} + \chi^\dagger \chi. \tag{C.32}$$

Using eqn. (C.31) and appropriate normalization factors, the 16 can therefore be decomposed

$$\mathbf{16} = \nu |-----\rangle + \sqrt{2}\, \overline{\psi}_\gamma E_{-e_\gamma} |+++++\rangle - \sqrt{2}\, \chi^{\gamma\delta} E_{e_\gamma} E_{e_\delta} |-----\rangle . \tag{C.33}$$

The coupling $\overline{\mathbf{16}}\ \mathbf{45}\ \mathbf{16}$ is defined

$$\overline{\mathbf{16}}\ \mathbf{45}\ \mathbf{16} \equiv (\overline{\mathbf{16}})_\alpha\ (\hat{M}_{ab})^\alpha{}_\beta\ (\mathbf{16})^\beta\ 45^{ab} \tag{C.34}$$

where the $\hat{M}_{ab}$s are the generators of SO(10), M_{ab}, expressed in the spinor representation; α and β are spinor indices running from 1 to 16; and $\mathbf{45} \equiv 45^{ab}\ M^{\mathbf{10}}_{ab}$ where $M^{\mathbf{10}}_{ab}$ is the SO(10) generator M_{ab}, in the 10 representation. Eqn. (C.34) means that

in order to find the the SU(5) decomposition of $\overline{\mathbf{16}}$ **45** **16**, one should reexpress eqn. (C.18) in terms of the generators of SO(10) in the 10 representation, and then convert those generators to the corresponding generators in the spinor representation. Using eqns. (C.5), (C.7), (C.24), and (C.25), the expression for the 45 representation given by eqn. (C.18) can be reexpressed

$$\mathbf{45} = -\frac{i}{\sqrt{2}} H^{\alpha}{}_{\beta}[E_{\mathbf{e}_\alpha}, E_{-\mathbf{e}_\beta}] + \frac{1}{2}\left(\chi^{\alpha\beta}[E_{\mathbf{e}_\alpha}, E_{\mathbf{e}_\beta}] + \overline{\chi}_{\alpha\beta}[E_{-\mathbf{e}_\alpha}, E_{-\mathbf{e}_\beta}]\right) \tag{C.35}$$

Using eqns. (C.33) and (C.35) and the anticommutation relations of (C.30), an expression for the SU(5) decomposition of $\overline{\mathbf{16}}$ **45** **16** can be derived. A tedious but straightforward calculation shows

$$\begin{aligned}
\overline{\mathbf{16}}\ \mathbf{45}\ \mathbf{16}\ = \\
& -i\left\{\frac{h}{\sqrt{10}}\left(\frac{3}{2}\overline{\psi}\psi - \frac{1}{2}\chi\overline{\chi} - \frac{5}{2}\overline{\nu}\nu\right) - \frac{i}{\sqrt{2}}(\nu\chi_{45}\overline{\chi} + \overline{\nu}\overline{\chi}_{45}\chi)\right. \\
& -\frac{i}{2\sqrt{2}}\left(\epsilon_{ijklm}\chi_{45}^{ij}\chi^{kl}\psi^{m} + \epsilon^{ijklm}(\overline{\chi}_{45})_{ij}\overline{\chi}_{kl}\overline{\psi}_{m}\right) \\
& \left.-\frac{1}{\sqrt{2}}\overline{\psi}H_A\psi + \sqrt{2}\overline{\chi}H_A\chi\right\}.
\end{aligned} \tag{C.36}$$

where χ_{45} and $\overline{\chi}_{45}$ come from the 45; and χ and $\overline{\chi}$ come from the spinor representations, and all other notation follows the conventions previously given.

C.5 Clifford algebras

A Clifford algebra is a set of matrices satisfying the relationship

$$\{\Gamma_i, \Gamma_j\} = 2\delta_{ij}, \quad i, j = 1, \ldots, N \tag{C.37}$$

for some N. Using the anti-commutation relations of eqn. (C.30), a Clifford algebra can be constructed in terms of the SO(11) spinor representation.

$$\Gamma_j = \sqrt{2}(E_{\mathbf{e}_j} + E_{-\mathbf{e}_j})(i\Gamma_{11})$$

$$\begin{aligned}\Gamma_{j+5} &= \sqrt{2}(E_{e_j} - E_{-e_j})(\Gamma_{11}) \\ \Gamma_{11} &= 2^5 H_1 H_2 H_3 H_4 H_5. \end{aligned} \tag{C.38}$$

for $j = 1, \ldots, 5$. It can further be seen that this Clifford algebra satisfies the property

$$\hat{M}_{ab} = \frac{1}{4i}[\Gamma_a, \Gamma_b] \tag{C.39}$$

where the $\hat{M}_{ab}$s are the generators of SO(11) in the spinor representation. Furthermore, it can be shown

$$[\hat{M}_{ab}, \Gamma_c] = i(\delta_{ac}\Gamma_b - \delta_{ab}\Gamma_c). \tag{C.40}$$

However, the quantity $-i(\delta_{ac}\Gamma_b - \delta_{ab}\Gamma_c)$ is precisely how an 11 dimensional vector Γ_c transforms when acted upon by the generators of SO(11). That is to say,

$$(M_{ab}^{11})_{cc'}\Gamma_{c'} = -i(\delta_{ac}\Gamma_b - \delta_{ab}\Gamma_c).$$

where M_{ab}^{11} is the generator M_{ab}, in the 11 representation. Hence,

$$[\hat{M}_{ab}, \Gamma_c] + (M_{ab}^{11})_{cc'}\Gamma_{c'} = 0. \tag{C.41}$$

An immediate application of this is to use the Clifford algebra to construct an SO(11) invariant combination **32 11 32**.

$$\mathbf{32'\ 11\ 32} \equiv (\mathbf{32'})_\alpha (B\Gamma_n)_{\alpha\beta}(\mathbf{32})_\beta(\mathbf{11})_n \tag{C.42}$$

where α and β are spinor indices running from 1 to 32. The matrix B is a matrix satisfying the property

$$M_{ab}^T B = -BM_{ab} \tag{C.43}$$

for all M_{ab}s. Note that this is the same matrix necessary to form an SO(11) invariant combination of two **32**s.

Equation (C.43) will be satisfied if

$$\Gamma_n^T B = -B\Gamma_n \tag{C.44}$$

for all Γ_n. It can be shown that this is satisfied by the matrix

$$B = \Gamma_1\Gamma_2\Gamma_3\Gamma_4\Gamma_5. \tag{C.45}$$

Under an infinitesable SO(11) transformation

$$\begin{aligned}
&\mathbf{32}'(B\Gamma_n)\mathbf{32}(\mathbf{11})_n \rightarrow \\
&\qquad \mathbf{32}'(1 + i\epsilon_{ab}\hat{M}_{ab}^T)(B\Gamma_n)(1 + i\epsilon_{ab}\hat{M}_{ab})\mathbf{32}\ (\mathbf{11})_n \\
&\qquad\quad +\mathbf{32}'(B\Gamma_n)\mathbf{32}\left(\delta_{nn'} + i\epsilon_{ab}(M_{ab}^{\mathbf{11}})_{nn'}\right)(\mathbf{11})_{n'} \\
&\qquad = \mathbf{32}'(B\Gamma_n)\mathbf{32}\ (\mathbf{11})_n + i\epsilon_{ab}\Big\{\mathbf{32}'(B[\Gamma_n, M_{ab}])\,\mathbf{32}\ (\mathbf{11})_n + \\
&\qquad\quad \mathbf{32}'(B\Gamma_n)\mathbf{32}\ (M_{ab}^{\mathbf{11}})_{nn'}(\mathbf{11})_{n'}\Big\} \\
&\qquad = \mathbf{32}'(B\Gamma_n)\mathbf{32}(\mathbf{11})_n
\end{aligned}$$

By projecting 16 or $\overline{16}$ spinors out of the 32 representation of SO(11), the **32 11 32** can be used to construct an SO(10) invariant combination of spinors and 10s. Let P_{10} denote a projection operator that projects the 10 representation of the SO(10) subgroup out of the 11; and let P_{16} and $P_{\overline{16}}$ denote projection operators that project 16 and $\overline{16}$ representations out of the 32. Then,

$$\begin{aligned}
\mathbf{32}'\ (B\Gamma_n)\ (P_{16}\mathbf{32})\ (P_{10}\mathbf{11})_n \ &= \\
&\mathbf{32}'\ (B\Gamma_n P_{16}^3)\ \mathbf{32}\ (P_{10}\mathbf{11}) \\
&= (P_{16}\mathbf{32}')\ (B\Gamma_n P_{16})\ (P_{16}\mathbf{32})\ (P_{10}\mathbf{11}) \\
&= \sum_n^{10} \mathbf{16}'\ (B\Gamma_n P_{16})\ \mathbf{16}\ (\mathbf{10})_n
\end{aligned} \tag{C.46}$$

Hence, $\mathbf{16'}\ (B\Gamma_n P_{16})\ \mathbf{16}\ (\mathbf{10})_n$, where n runs from 1 to 10, is SO(10) invariant.[28]

We will use a normalization convention for the **16 10 16** coupling in which

$$\begin{aligned} \mathbf{16\ 10\ 16} &= \sqrt{2}\overline{\psi}\chi\overline{V} + \frac{1}{4}\epsilon_{ijklm}\chi^{ij}\chi^{kl}V^m + \overline{\psi}V\nu \\ &= q\bar{u}h_u + q\bar{d}h_d + l\bar{e}h_d + \ldots \end{aligned} \tag{C.47}$$

where the last line of the above equation show the decomposition into SU(3)×SU(2)× U(1). Hence, using the above normalization convention

$$\mathbf{16'\ 10\ 16} \equiv (\mathbf{16})^\alpha\ (\digamma_n)_{\alpha\beta}\ (\mathbf{16})^\beta\ (\mathbf{10})_n \tag{C.48}$$

where

$$\digamma_n \equiv \frac{1}{2\sqrt{2}} B\Gamma_n P_{16}.$$

The Clifford algebra is useful for calculating a variety of coefficients entering the renormalization group equations for the models in this thesis. For example, the $1/\epsilon$ term for the graph shown in fig. C.1, resulting from the $\lambda_B\ \psi_1\ 10_1\ \psi_2$ term of eqn. (5.2) is equal to

$$\begin{aligned} & \frac{i}{16\pi^2\epsilon}\lambda_B^2 \digamma_n^* \digamma_n \\ = & \frac{i}{16\pi^2\epsilon}\lambda_B^2 \left(\frac{1}{2\sqrt{2}}\right)^2 B^* \Gamma_n^* B\Gamma_n P_{16} \\ = & \frac{i}{16\pi^2\epsilon}\lambda_B^2 \frac{1}{8}\Gamma_n^\dagger B^2 \Gamma_n P_{16} \\ = & \frac{i}{16\pi^2\epsilon}\lambda_B^2 \frac{1}{8}\Gamma_n \Gamma_n P_{16} \\ & \qquad (\text{since } B = B^{-1} \text{ and } \Gamma = \Gamma^\dagger) \\ = & \frac{i}{16\pi^2\epsilon}\lambda_B^2 (\frac{10}{8}) P_{16} \end{aligned}$$

[28]This derivation of the **16 10 16** SO(10) invariant follows in large part the derivation in [66].

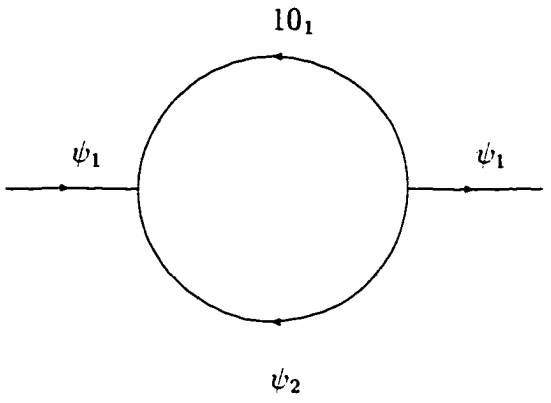

Figure C.1: Feynman diagram contributing to the wavefunction renormalization for ψ_1.

Similarly, the $1/\epsilon$ term for the graph shown in figure C.2 is

$$\begin{aligned}
& \frac{i}{16\pi^2\epsilon}\lambda_B^2 \mathrm{tr}(\Gamma_n^* \Gamma_m) \\
= & \frac{i}{16\pi^2\epsilon}\lambda_B^2 \frac{1}{8}\mathrm{tr}(B^* \Gamma_n^* B \Gamma_m P_{16}) \\
= & \frac{i}{16\pi^2\epsilon}\lambda_B^2 \frac{1}{8}\mathrm{tr}(\Gamma_n \Gamma_m P_{16}) \\
= & \frac{i}{16\pi^2\epsilon}\lambda_B^2 \frac{16}{8}\delta_{nm}
\end{aligned}$$

As a final example, the $1/\epsilon$ term for the diagram in fig. 5.4, generating the effective operator $\widetilde{\mathcal{O}_{13}}$ is equal to

$$\begin{aligned}
& a_D(2\lambda_A)^2 \frac{i}{16\pi^2\epsilon}(\widetilde{16}_1\ \tilde{A}^3)^\alpha\ (\Gamma_n)_{\alpha\beta}\ (A_2)^\beta_{\ \gamma}\ (\Gamma_n^*)^{\gamma\delta}\ (\Gamma_m)_{\delta\epsilon}\ (\widetilde{16}_3)^\epsilon\ (\widetilde{10}_1)_m \\
= & \ 4a_D\lambda_A^2 \frac{i}{16\pi^2\epsilon}(\widetilde{16}_1\ \tilde{A}^3)^\alpha\ (\Gamma_m)_{\delta\epsilon}\ (\widetilde{16}_3)^\epsilon\ (\widetilde{10}_1)_m \Big(\frac{1}{8} B\Gamma_n A_2 \Gamma_n B P_{16}\Big)^\delta_\alpha \\
= & \ 4a_D\lambda_A^2 \frac{i}{16\pi^2\epsilon}(\widetilde{16}_1\ \tilde{A}^3)^\alpha\ (\Gamma_m)_{\delta\epsilon}\ (\widetilde{16}_3)^\epsilon\ (\widetilde{10}_1)_m \Big(\frac{1}{8} B\Gamma_n (A_2)^{ab} \frac{1}{4i}[\Gamma_a, \Gamma_b]\Gamma_n B P_{16}\Big)^\delta_\alpha \\
= & \ 4a_D\lambda_A^2 \frac{i}{16\pi^2\epsilon}(\widetilde{16}_1\ \tilde{A}^3)^\alpha\ (\Gamma_m)_{\delta\epsilon}\ (\widetilde{16}_3)^\epsilon\ (\widetilde{10}_1)_m
\end{aligned}$$

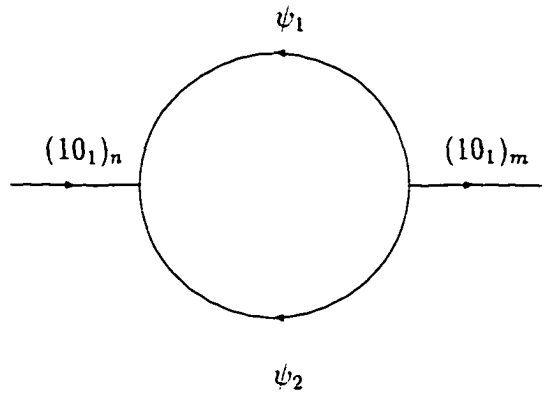

Figure C.2: Feynman diagram contributing to the wavefunction renormalization for 10_1.

$$
\begin{aligned}
&\times\Big(\frac{1}{8}B\Gamma_n(A_2)^{ab}\frac{1}{4i}\{[2(\Gamma_b\Gamma_a-\Gamma_a\Gamma_b)+\Gamma_n\Gamma_n\Gamma_a\Gamma_b]\\
&-[2(\Gamma_a\Gamma_b-\Gamma_b\Gamma_a)+\Gamma_n\Gamma_n\Gamma_b\Gamma_a]\}BP_{16}\Big)_\alpha^\delta\\
=\;& 4a_D\lambda_A^2\frac{i}{16\pi^2\epsilon}(\widetilde{16}_1\,\tilde{A}^3)^\alpha\,(F_m)_{\delta\epsilon}\,(\widetilde{16}_3)^\epsilon\,(\widetilde{10}_1)_m\Big(\frac{1}{8}B(A_2)^{ab}\frac{1}{4i}6[\Gamma_a,\Gamma_b]BP_{16}\Big)_\alpha^\delta\\
=\;& 4a_D\lambda_A^2\frac{i}{16\pi^2\epsilon}(\widetilde{16}_1\,\tilde{A}^3)^\alpha\,(F_m)_{\delta\epsilon}\,(\widetilde{16}_3)^\epsilon\,(\widetilde{10}_1)_m\Big(\frac{1}{8}(A_2)^{ab}\frac{1}{4i}(-6[\Gamma_a,\Gamma_b]^TP_{16})\Big)_\alpha^\delta\\
=\;& 4a_D\lambda_A^2\frac{i}{16\pi^2\epsilon}(\widetilde{16}_1\,\tilde{A}^3)^\alpha\,(F_m)_{\delta\epsilon}\,(\widetilde{16}_3)^\epsilon\,(\widetilde{10}_1)_m\Big(-\frac{6}{8}(A_2)^T\Big)_\alpha^\delta\\
=\;& -3a_D\lambda_A^2\frac{i}{16\pi^2\epsilon}\widetilde{16}_1\,\tilde{A}^3\,A_2\,\widetilde{10}_1\,\widetilde{16}_3
\end{aligned}
$$

APPENDIX D

FORMULAS FOR NUCLEON DECAY IN TERMS OF CHIRAL LAGRANGIAN FACTORS

Using the chiral Lagrangian techniques of ref. [38], the rates of nucleon decay are the following.

$$\begin{aligned}
\Gamma(p \to K^+\bar{\nu}_i) &= \frac{(m_p^2 - m_K^2)^2}{32\pi m_p^3 f_\pi^2} A_L^2 \left| [\beta C^{(us)(d\nu_i)} + \alpha C^{(\overline{us})(d\nu_i)}] \frac{2m_p}{3m_B} D \right. \\
&\quad \left. + [\beta C^{(ud)(s\nu_i)} + \alpha C^{(\overline{ud})(s\nu_i)}][1 + \frac{m_p}{3m_B}(D + 3F)] \right|^2 \\
\Gamma(p \to \pi^+\bar{\nu}_i) &= \frac{m_p}{32\pi f_\pi^2} A_L^2 \left| [\beta C^{(ud)(d\nu_i)} + \alpha C^{(\overline{ud})(d\nu_i)}](1 + D + F) \right|^2 \\
\Gamma(p \to \eta e_i^+) &= \frac{3(m_p^2 - m_\eta^2)^2}{64\pi f_\pi^2 m_p^3} A_L^2 \left\{ \left| \beta C^{(ud)(ue_i)}[1 + \frac{1}{3}(3F - D)] \right. \right. \\
&\quad \left. - \alpha C^{(\overline{ud})(ue_i)} \frac{1}{3}[1 - (3F - D)] \right|^2 \\
&\quad \left. + \left| \beta C^{(\overline{ud})(\overline{ue_i})}[1 + \frac{1}{3}(3F - D)] - \alpha C^{(ud)(\overline{ue_i})} \frac{1}{3}[1 - (3F - D)] \right|^2 \right\} \\
\Gamma(p \to K^0 e_i^+) &= \frac{(m_p^2 - m_K^2)^2}{32\pi f_\pi^2 m_p^3} A_L^2 \left\{ \left| \beta C^{(us)(ue_i)}[1 - \frac{m_p}{m_B}(D - F)] \right. \right. \\
&\quad \left. - \alpha C^{(\overline{us})(ue_i)}[1 + \frac{m_p}{m_B}(D - F)] \right|^2 \\
&\quad \left. + \left| \beta C^{(\overline{us})(\overline{ue_i})}[1 - \frac{m_p}{m_B}(D - F)] - \alpha C^{(us)(\overline{ue_i})}[1 + \frac{m_p}{m_B}(D - F) \right|^2 \right\} \\
\Gamma(p \to \pi^0 e_i^+) &= \frac{m_p}{64\pi f_\pi^2} A_L^2 \left\{ \left| [\beta C^{(ud)(ue_i)} + \alpha C^{(\overline{ud})(ue_i)}](1 + D + F) \right|^2 \right. \\
&\quad \left. + \left| [\beta C^{(\overline{ud})(\overline{ue_i})} + \alpha C^{(ud)(\overline{ue_i})}](1 + D + F) \right|^2 \right\} \\
\Gamma(n \to K^0\bar{\nu}_i) &= \frac{(m_n^2 - m_K^2)^2}{32\pi m_n^3 f_\pi^2} A_L^2 \left| \beta C^{(us)(d\nu_i)}(1 - \frac{m_n}{3m_B}(D - 3F)) \right.
\end{aligned}$$

$$
\begin{aligned}
& -\alpha C^{(\overline{us})(d\nu_i)}(1+\frac{m_n}{3m_B}(D-3F)) \\
& +(\beta C^{(ud)(s\nu_i)}+\alpha C^{(\overline{ud})(s\nu_i)})(1+\frac{m_n}{3m_B}(D+3F))\Big|^2 \\
\Gamma(n\to\pi^0\overline{\nu}_i) &= \frac{m_n^3}{64\pi f_\pi^2}A_L^2\left|\beta C^{(ud)(d\nu_i)}+\alpha C^{(\overline{ud})(d\nu_i)}\right|^2(1+D+F)^2 \\
\Gamma(n\to\eta\overline{\nu}_i) &= \frac{3(m_n^2-m_\eta^2)^2}{64\pi m_n^3 f_\pi^2}A_L^2\times \\
& \left|\beta C^{(ud)(d\nu_i)}(1+\frac{1}{3}(3F-D))-\alpha C^{(\overline{ud})(d\nu_i)}\frac{1}{3}(1+D-3F)\right|^2 \\
\Gamma(n\to\pi^-e_i^+) &= \frac{m_n}{32\pi f_\pi^2}A_L^2\{\left|\beta C^{(ud)(ue_i)}+\alpha C^{(\overline{ud})(ue_i)}\right|^2+ \\
& \left|\beta C^{(\overline{ud})(\overline{ue_i})}+\alpha C^{(ud)(\overline{ue_i})}\right|^2\}(1+D+F)^2
\end{aligned}
$$

where m_B is an average Baryon mass satisfying $m_B \approx m_\Sigma \approx m_\Lambda$ and all other notation follows [38][29]. Here, all coefficients of four-fermion operators are evaluated at M_Z. A_L takes into account renormalization from M_Z to 1 GeV, and is approximately equal to .22. [37]. These formulas reduce to the chiral Lagrangian formulas given in ref. [24] for $\beta \neq 0$ when $\alpha = 0$. In the calculations, we take $D = .81$, $F = .44$ [24], and $f_\pi = 139$ MeV [38].

[29] $C_{ijkl}^{(ud)(d\nu)} = C_{ijkl}^{(ud)(d\nu)[G]} + C_{ijkl}^{(ud)(d\nu)[W]}$, etc.

APPENDIX E

MASS MATRICES AND EFFECTIVE DETERMINANTS FOR MODEL 4(C)

Using eqn. (3.15) and the eqn. (C.22), the mass matrices for $W_{symmetry\,breaking}$ of model 4(c) can be calculated:

$$M_g = \begin{array}{c} \\ A_2 \\ \tilde{A} \\ S \\ S' \\ A_1 \\ A_1' \end{array} \begin{array}{c} \begin{array}{cccccc} A_2 & \tilde{A} & S & S' & A_1 & A_1' \end{array} \\ \begin{pmatrix} 0 & -\mathcal{S}_1 & 0 & 0 & 0 & 0 \\ -\mathcal{S}_1 & -2s & -2i\tilde{a} & -ia_1 & 0 & 0 \\ 0 & -2i\tilde{a} & 0 & \mathcal{S}_2 & 0 & -\frac{ia_1\mathcal{S}_3}{M} \\ 0 & -ia_1 & \mathcal{S}_2 & 2\mathcal{S}_3 & -i\tilde{a} & 0 \\ 0 & 0 & 0 & -i\tilde{a} & 0 & \frac{2s\mathcal{S}_3}{M} \\ 0 & 0 & -\frac{ia_1\mathcal{S}_3}{M} & 0 & \frac{2s\mathcal{S}_3}{M} & 0 \end{pmatrix} \end{array}$$

$$M_w = \begin{array}{c} \\ A_2 \\ \tilde{A} \\ S \\ S' \\ A_1 \\ A_1' \end{array} \begin{array}{c} \begin{array}{cccccc} A_2 & \tilde{A} & S & S' & A_1 & A_1' \end{array} \\ \begin{pmatrix} 0 & -\mathcal{S}_1 & 0 & 0 & 0 & 0 \\ -\mathcal{S}_1 & 3s & -2i\tilde{a} & 0 & 0 & 0 \\ 0 & -2i\tilde{a} & 0 & \mathcal{S}_2 & 0 & 0 \\ 0 & 0 & \mathcal{S}_2 & 2\mathcal{S}_3 & -i\tilde{a} & 0 \\ 0 & 0 & 0 & -i\tilde{a} & 0 & \frac{3s\mathcal{S}_3}{2M} \\ 0 & 0 & 0 & 0 & \frac{3s\mathcal{S}_3}{2M} & 0 \end{pmatrix} \end{array}$$

$$M_x = \begin{array}{c} \\ \lambda \\ A_2 \\ \tilde{A} \\ S \\ S' \\ A_1 \\ A_1' \end{array} \begin{array}{c} \begin{array}{ccccccc} \lambda & A_2 & \tilde{A} & S & S' & A_1 & A_1' \end{array} \\ \begin{pmatrix} 0 & \frac{5}{\sqrt{2}}ga_2^* & 0 & \frac{5}{\sqrt{2}}igs^* & 0 & \sqrt{2}ga_1^* & 0 \\ -\frac{5}{\sqrt{2}}ga_2^* & 0 & -\mathcal{S}_1 & 0 & 0 & 0 & -\frac{a_1\mathcal{S}_4}{2M} \\ 0 & -\mathcal{S}_1 & \frac{s}{2} & -2i\tilde{a} & -\frac{i}{2}a_1 & 0 & 0 \\ -\frac{5}{\sqrt{2}}igs^* & 0 & -2i\tilde{a} & 0 & \mathcal{S}_2 & 0 & -\frac{ia_1\mathcal{S}_3}{2M} \\ 0 & 0 & -\frac{i}{2}a_1 & \mathcal{S}_2 & 2\mathcal{S}_3 & -i\tilde{a} & 0 \\ -\sqrt{2}ga_1^* & 0 & 0 & 0 & -i\tilde{a} & 0 & \frac{5s\mathcal{S}_3}{4M} + \frac{5a_2\mathcal{S}_4}{4M} \\ 0 & \frac{a_1\mathcal{S}_4}{2M} & 0 & -\frac{ia_1\mathcal{S}_3}{2M} & 0 & \frac{5s\mathcal{S}_3}{4M} - \frac{5a_2\mathcal{S}_4}{4M} & 0 \end{pmatrix} \end{array}$$

$M_q =$

$$\begin{array}{c} \\ \lambda \\ \bar{\psi} \\ A_2 \\ \tilde{A} \\ S \\ S' \\ A_1 \\ A_1' \end{array} \begin{array}{c} \begin{array}{cccccccc} \lambda & \psi & A_2 & \tilde{A} & S & S' & A_1 & A_1' \end{array} \\ \begin{pmatrix} 0 & -gv^* & \frac{ga_2^*}{\sqrt{2}} & -2\sqrt{2}g\tilde{a}^* & \frac{5gs^*}{\sqrt{2}} & 0 & -\sqrt{2}ga_1^* & 0 \\ g\bar{v}^* & -\frac{a_2}{2} & -\frac{v}{\sqrt{2}} & 0 & 0 & 0 & 0 & 0 \\ -\frac{ga_2^*}{\sqrt{2}} & -\frac{\bar{v}}{\sqrt{2}} & 0 & \mathcal{S}_1 & 0 & 0 & 0 & \frac{a_1\mathcal{S}_4}{2M} \\ 2\sqrt{2}g\tilde{a}^* & 0 & \mathcal{S}_1 & -\frac{s}{2} & 0 & -\frac{a_1}{2} & 0 & 0 \\ -\frac{5gs^*}{\sqrt{2}} & 0 & 0 & 0 & 0 & \mathcal{S}_2 & 0 & -\frac{a_1\mathcal{S}_3}{2M} \\ 0 & 0 & 0 & -\frac{a_1}{2} & \mathcal{S}_2 & 2\mathcal{S}_3 & 0 & 0 \\ \sqrt{2}ga_1^* & 0 & 0 & 0 & 0 & 0 & 0 & \frac{a_2\mathcal{S}_4}{4M} - \frac{5s\mathcal{S}_3}{4M} \\ 0 & 0 & -\frac{a_1\mathcal{S}_4}{2M} & 0 & -\frac{a_1\mathcal{S}_3}{2M} & 0 & \frac{-a_2\mathcal{S}_4}{4M} - \frac{5s\mathcal{S}_3}{4M} & 0 \end{pmatrix} \end{array}$$

$$M_u = \begin{array}{c} \\ \lambda \\ \psi \\ A_2 \\ \tilde{A} \\ A_1 \\ A_1' \end{array} \begin{array}{c} \begin{array}{cccccc} \lambda & \bar{\psi} & A_2 & \tilde{A} & A_1 & A_1' \end{array} \\ \begin{pmatrix} 0 & -g\bar{v}^* & -2\sqrt{2}ga_2^* & -2\sqrt{2}g\tilde{a}^* & -2\sqrt{2}ga_1^* & 0 \\ gv^* & 2a_2 & -\frac{\bar{v}}{\sqrt{2}} & 0 & 0 & 0 \\ 2\sqrt{2}ga_2^* & -\frac{v}{\sqrt{2}} & 0 & \mathcal{S}_1 & 0 & \frac{a_1\mathcal{S}_4}{M} \\ 2\sqrt{2}g\tilde{a}^* & 0 & \mathcal{S}_1 & 2s & 0 & 0 \\ 2\sqrt{2}ga_1^* & 0 & 0 & 0 & 0 & -\frac{a_2\mathcal{S}_4}{M} \\ 0 & 0 & -\frac{a_1\mathcal{S}_4}{M} & 0 & \frac{a_2\mathcal{S}_4}{M} & 0 \end{pmatrix} \end{array}$$

$$M_e = \begin{array}{c} \\ \lambda \\ \psi \\ A_2 \\ \tilde{A} \\ A_1 \\ A_1' \end{array} \begin{array}{c} \begin{array}{cccccc} \lambda & \overline{\psi} & A_2 & \tilde{A} & A_1 & A_1' \end{array} \\ \begin{pmatrix} 0 & -g\overline{v}^* & 3\sqrt{2}ga_2^* & -2\sqrt{2}g\tilde{a}^* & 0 & 0 \\ gv^* & -3a_2 & -\frac{\overline{v}}{\sqrt{2}} & 0 & 0 & 0 \\ -3\sqrt{2}ga_2^* & -\frac{v}{\sqrt{2}} & 0 & \mathcal{S}_1 & 0 & 0 \\ 2\sqrt{2}g\tilde{a}^* & 0 & \mathcal{S}_1 & -3s & 0 & 0 \\ 0 & 0 & 0 & 0 & 0 & -\frac{3s\mathcal{S}_3}{2M} + \frac{3a_2\mathcal{S}_4}{2M} \\ 0 & 0 & 0 & 0 & -\frac{3s\mathcal{S}_3}{2M} - \frac{3a_2\mathcal{S}_4}{2M} & 0 \end{pmatrix} \end{array}$$

$$M_s = M_\sigma = \begin{array}{c} \\ S \\ S' \end{array} \begin{array}{c} \begin{array}{cc} S & S' \end{array} \\ \begin{pmatrix} 0 & \mathcal{S}_2 \\ \mathcal{S}_2 & 2\mathcal{S}_3 \end{pmatrix} \end{array}$$

Using $a_1, a_2, \tilde{a}, v, \overline{v}$, and $\mathcal{S}_4$ as independent variables, the effective determinants, defined in eqn. (3.9), are

$$\det' M_g = -\frac{4\,\tilde{a}^4\,{a_1}^6}{25\,{a_2}^2\,M^2}$$

$$\det' M_w = -\frac{36\,\tilde{a}^4\,{a_1}^6}{25\,{a_2}^2\,M^2}$$

$$\det' M_x = \frac{2\,\tilde{a}^4\,{a_1}^2\left(-100\,{a_1}^4 - 9\,{a_2}^2\,{\mathcal{S}_4}^2 + 100\,{a_2}^2\,{\mathcal{S}_4}^2\right)}{25\,{a_2}^3\,g^2\,M^2\,v\,\overline{v}}$$

$$\det' M_q = \frac{\tilde{a}^4\,{a_1}^2\left(-25\,{a_1}^4 + {a_2}^2\,{\mathcal{S}_4}^2\right)}{25\,{a_2}^2\,g^2\,M^2\,v\,\overline{v}}$$

$$\det' M_u = -\frac{{a_2}^2\,{\mathcal{S}_4}^2\,v\,\overline{v}}{16\,\tilde{a}^2\,g^2\,M^2}$$

$$\det' M_e = \frac{9\left({a_1}^4 - {a_2}^2\,{\mathcal{S}_4}^2\right)\,v\,\overline{v}}{64\,\tilde{a}^2\,g^2\,M^2}$$

$$\det' M_s = \det' M_\sigma = -\frac{256\,\tilde{a}^6\,{a_1}^2}{25\,{a_2}^2\,v^2\,\overline{v}^2}$$

APPENDIX F

RENORMALIZATION GROUP EQUATIONS BETWEEN THE PLANCK AND GUT SCALES

The relevant renormalization group equations for the superpotential given in eqn. (5.2) are as follows. All quantities are assumed to be real.

$$\frac{d\lambda_A}{dt} = \lambda_A \left(\frac{-63}{2} g^2 + 14\,\lambda_A{}^2 + 2\,\lambda_B{}^2 + 2\,\lambda_{N_3}{}^2 + \frac{45}{4}\,\gamma_1{}^2 + \frac{9}{2}\,\gamma_{10_1 A_1 10_2}{}^2 \right)$$

$$\frac{d\lambda_B}{dt} = \lambda_B \left(\frac{-63}{2} g^2 + 4\,\lambda_A{}^2 + \frac{9}{2}\,\lambda_B{}^2 + \frac{45}{8}\,\gamma_{\tilde{A}1}{}^2 + \frac{45}{8}\,\gamma_{\tilde{A}2}{}^2 + \frac{9}{2}\,\gamma_{10_1 A_1 10_2}{}^2 \right)$$

$$\begin{aligned} \frac{d\lambda_C}{dt} = \lambda_C \Big(& \frac{-255}{2} g^2 + 4\,\lambda_A{}^2 + 2\,\lambda_B{}^2 + \lambda_{N_1}{}^2 + \lambda_{N_2}{}^2 + 6\,\gamma_{S_1}{}^2 + \\ & 12\,\gamma_{\tilde{A}1}{}^2 + 12\,\gamma_{\tilde{A}2}{}^2 + \frac{45}{8}\,\gamma_2{}^2 + \frac{9}{2}\,\gamma_{10_1 A_1 10_2}{}^2 \Big) \end{aligned}$$

$$\begin{aligned} \frac{d\lambda_D}{dt} = \lambda_D \Big(& \frac{-191}{2} g^2 + 9\,\lambda_A{}^2 + 2\,\lambda_B{}^2 + \lambda_{N_1}{}^2 + \lambda_{N_3}{}^2 + 2\,\gamma_{\psi A_2 \bar{\psi}}{}^2 + \\ & 4\,\gamma_{S_1}{}^2 + 6\,\gamma_{\tilde{A}1}{}^2 + 6\,\gamma_{\tilde{A}2}{}^2 + \frac{45}{8}\,\gamma_1{}^2 + 2\,\gamma_2{}^2 + \frac{9}{2}\,\gamma_{10_1 A_1 10_2}{}^2 \Big) \end{aligned}$$

$$\begin{aligned} \frac{d\lambda_E}{dt} = \lambda_E \Big(& \frac{-127}{2} g^2 + 4\,\lambda_A{}^2 + 2\,\lambda_B{}^2 + 2\,\lambda_{N_2}{}^2 + \gamma_{S_1}{}^2 + \\ & 2\,\gamma_{\tilde{A}1}{}^2 + 2\,\gamma_{\tilde{A}2}{}^2 + 2\,\gamma_1{}^2 + \frac{45}{4}\,\gamma_2{}^2 + \frac{11}{2}\,\gamma_{10_1 A_1 10_2}{}^2 \Big) \end{aligned}$$

$$\frac{d\gamma_1}{dt} = \gamma_1 \left(\frac{-77}{2} g^2 + 5\,{\lambda_A}^2 + {\lambda_{N_3}}^2 + \frac{45}{8}\,{\gamma_{\tilde{A}1}}^2 + \frac{53}{4}\,{\gamma_1}^2 + {\gamma_{10_1 A_1 10_2}}^2\right)$$

$$\frac{d\gamma_2}{dt} = \gamma_2 \left(\frac{-77}{2} g^2 + {\lambda_{N_2}}^2 + 2\,{\gamma_{\psi A_2 \bar{\psi}}}^2 + {\gamma_{S_1}}^2 + \frac{45}{8}\,{\gamma_{\tilde{A}2}}^2 + \frac{53}{4}\,{\gamma_2}^2\right)$$

$$\frac{d\gamma_{\tilde{A}1}}{dt} = \gamma_{\tilde{A}1} \left(\frac{-77}{2} g^2 + \frac{5}{4}\,{\lambda_B}^2 + {\gamma_{S_1}}^2 + \frac{53}{4}\,{\gamma_{\tilde{A}1}}^2 + 2\,{\gamma_{\tilde{A}2}}^2 + \frac{45}{8}\,{\gamma_1}^2\right)$$

$$\frac{d\gamma_{\tilde{A}2}}{dt} = \gamma_{\tilde{A}2} \left(\frac{-77}{2} g^2 + \frac{5}{4}\,{\lambda_B}^2 + {\gamma_{S_1}}^2 + 2\,{\gamma_{\tilde{A}1}}^2 + \frac{53}{4}\,{\gamma_{\tilde{A}2}}^2 + \frac{45}{8}\,{\gamma_2}^2\right)$$

$$\frac{d\gamma_{10_1 A_1 10_2}}{dt} = \gamma_{10_1 A_1 10_2} \left(-34\,g^2 + 4\,{\lambda_A}^2 + 2\,{\lambda_B}^2 + 4\,{\gamma_*}^2 + 2\,{\gamma_1}^2 + 10\,{\gamma_{10_1 A_1 10_2}}^2\right)$$

$$\frac{d\gamma_*}{dt} = \gamma_* \left(-18\,g^2 + 28\,{\gamma_*}^2 + 9\,{\gamma_{10_1 A_1 10_2}}^2\right)$$

$$\frac{d\lambda_{N_1}}{dt} = \lambda_{N_1} \left(\frac{-45}{2} g^2 + 18\,{\lambda_{N_1}}^2 + {\lambda_{N_2}}^2 + {\lambda_{N_3}}^2 + \frac{45}{8}\,{\gamma_{\psi A_2 \bar{\psi}}}^2\right)$$

$$\frac{d\lambda_{N_2}}{dt} = \lambda_{N_2} \left(\frac{-45}{2} g^2 + {\lambda_{N_1}}^2 + 18\,{\lambda_{N_2}}^2 + {\lambda_{N_3}}^2 + \frac{45}{8}\,{\gamma_{\psi A_2 \bar{\psi}}}^2 + \frac{45}{8}\,{\gamma_2}^2\right)$$

$$\frac{d\lambda_{N_3}}{dt} = \lambda_{N_3} \left(\frac{-45}{2} g^2 + 5\,{\lambda_A}^2 + {\lambda_{N_1}}^2 + {\lambda_{N_2}}^2 + 18\,{\lambda_{N_3}}^2 + \frac{45}{8}\,{\gamma_{\psi A_2 \bar{\psi}}}^2 + \frac{45}{8}\,{\gamma_1}^2\right)$$

$$\frac{d\gamma_{\psi A_2 \bar{\psi}}}{dt} = \gamma_{\psi A_2 \bar{\psi}} \left(\frac{-77}{2} g^2 + {\lambda_{N_1}}^2 + {\lambda_{N_2}}^2 + {\lambda_{N_3}}^2 + \frac{53}{4}\,{\gamma_{\psi A_2 \bar{\psi}}}^2 + {\gamma_{S_1}}^2 + 2\,{\gamma_2}^2\right)$$

$$\frac{d\gamma_{S_1}}{dt} = \gamma_{S_1} \left(-32\,g^2 + 2\,{\gamma_{\psi A_2 \bar{\psi}}}^2 + 47\,{\gamma_{S_1}}^2 + 2\,{\gamma_{\tilde{A}1}}^2 + 2\,{\gamma_{\tilde{A}2}}^2 + 2\,{\gamma_2}^2\right)$$

$$\begin{aligned}\frac{da_A}{dt} = {} & 2\,\lambda_A \left(\frac{63}{2} g^2 m + 14\,a_A\,\lambda_A + 2\,a_B\,\lambda_B + 2\,a_{N_3}\,\lambda_{N_3} + \frac{45}{4}\,\alpha_1\,\gamma_1 + \frac{9}{2}\,\alpha_{10_1 A_1 10_2}\,\gamma_{10_1 A_1 10_2}\right) \\ & + a_A \left(\frac{-63}{2} g^2 + 14\,{\lambda_A}^2 + 2\,{\lambda_B}^2 + 2\,{\lambda_{N_3}}^2 + \frac{45}{4}\,{\gamma_1}^2 + \frac{9}{2}\,{\gamma_{10_1 A_1 10_2}}^2\right)\end{aligned}$$

$$\frac{da_B}{dt} = 2\lambda_B\left(\frac{63}{2}g^2 m + 4a_A\lambda_A + \frac{9}{2}a_B\lambda_B + \frac{45}{8}\alpha_{\tilde{A}1}\gamma_{\tilde{A}1} + \frac{45}{8}\alpha_{\tilde{A}2}\gamma_{\tilde{A}2} + \frac{9}{2}\alpha_{10_1A_110_2}\gamma_{10_1A_110_2}\right) + a_B\left(\frac{-63}{2}g^2 + 4{\lambda_A}^2 + \frac{9}{2}{\lambda_B}^2 + \frac{45}{8}{\gamma_{\tilde{A}1}}^2 + \frac{45}{8}{\gamma_{\tilde{A}2}}^2 + \frac{9}{2}{\gamma_{10_1A_110_2}}^2\right)$$

$$\frac{da_C}{dt} = 2\lambda_C\left(\frac{255}{2}g^2 m + 4a_A\lambda_A + 2a_B\lambda_B + a_{N_1}\lambda_{N_1} + a_{N_2}\lambda_{N_2} + 6\alpha_{S_1}\gamma_{S_1} + 12\alpha_{\tilde{A}1}\gamma_{\tilde{A}1} + 12\alpha_{\tilde{A}2}\gamma_{\tilde{A}2} + \frac{45}{8}\alpha_2\gamma_2 + \frac{9}{2}\alpha_{10_1A_110_2}\gamma_{10_1A_110_2}\right) + a_C\left(\frac{-255}{2}g^2 + 4{\lambda_A}^2 + 2{\lambda_B}^2 + {\lambda_{N_1}}^2 + {\lambda_{N_2}}^2 + 6{\gamma_{S_1}}^2 + 12{\gamma_{\tilde{A}1}}^2 + 12{\gamma_{\tilde{A}2}}^2 + \frac{45}{8}{\gamma_2}^2 + \frac{9}{2}{\gamma_{10_1A_110_2}}^2\right)$$

$$\frac{da_D}{dt} = 2\lambda_D\left(\frac{191}{2}g^2 m + 9a_A\lambda_A + 2a_B\lambda_B + a_{N_1}\lambda_{N_1} + a_{N_3}\lambda_{N_3} + 2\alpha_{\psi A_2\bar{\psi}}\gamma_{\psi A_2\bar{\psi}} + 4\alpha_{S_1}\gamma_{S_1} + 6\alpha_{\tilde{A}1}\gamma_{\tilde{A}1} + 6\alpha_{\tilde{A}2}\gamma_{\tilde{A}2} + \frac{45}{8}\alpha_1\gamma_1 + 2\alpha_2\gamma_2 + \frac{9}{2}\alpha_{10_1A_110_2}\gamma_{10_1A_110_2}\right) + a_D\left(\frac{-191}{2}g^2 + 9{\lambda_A}^2 + 2{\lambda_B}^2 + {\lambda_{N_1}}^2 + {\lambda_{N_3}}^2 + 2{\gamma_{\psi A_2\bar{\psi}}}^2 + 4{\gamma_{S_1}}^2 + 6{\gamma_{\tilde{A}1}}^2 + 6{\gamma_{\tilde{A}2}}^2 + \frac{45}{8}{\gamma_1}^2 + 2{\gamma_2}^2 + \frac{9}{2}{\gamma_{10_1A_110_2}}^2\right)$$

$$\frac{da_E}{dt} = 2\lambda_E\left(\frac{127}{2}g^2 m + 4a_A\lambda_A + 2a_B\lambda_B + 2a_{N_2}\lambda_{N_2} + \alpha_{S_1}\gamma_{S_1} + 2\alpha_{\tilde{A}1}\gamma_{\tilde{A}1} + 2\alpha_{\tilde{A}2}\gamma_{\tilde{A}2} + 2\alpha_1\gamma_1 + \frac{45}{4}\alpha_2\gamma_2 + \frac{11}{2}\alpha_{10_1A_110_2}\gamma_{10_1A_110_2}\right) + a_E\left(\frac{-127}{2}g^2 + 4{\lambda_A}^2 + 2{\lambda_B}^2 + 2{\lambda_{N_2}}^2 + {\gamma_{S_1}}^2 + 2{\gamma_{\tilde{A}1}}^2 + 2{\gamma_{\tilde{A}2}}^2 + 2{\gamma_1}^2 + \frac{45}{4}{\gamma_2}^2 + \frac{11}{2}{\gamma_{10_1A_110_2}}^2\right)$$

$$\frac{d\alpha_1}{dt} = 2\gamma_1\left(\frac{77}{2}g^2 m + 5a_A\lambda_A + a_{N_3}\lambda_{N_3} + \frac{45}{8}\alpha_{\tilde{A}1}\gamma_{\tilde{A}1} + \frac{53}{4}\alpha_1\gamma_1 + \alpha_{10_1A_110_2}\gamma_{10_1A_110_2}\right) + \alpha_1\left(\frac{-77}{2}g^2 + 5{\lambda_A}^2 + {\lambda_{N_3}}^2 + \frac{45}{8}{\gamma_{\tilde{A}1}}^2 + \frac{53}{4}{\gamma_1}^2 + {\gamma_{10_1A_110_2}}^2\right)$$

$$\frac{d\alpha_2}{dt} = 2\gamma_2\left(\frac{77}{2}g^2 m + a_{N_2}\lambda_{N_2} + 2\alpha_{\psi A_2\bar{\psi}}\gamma_{\psi A_2\bar{\psi}} + \alpha_{S_1}\gamma_{S_1} + \frac{45}{8}\alpha_{\tilde{A}2}\gamma_{\tilde{A}2} + \frac{53}{4}\alpha_2\gamma_2\right) + \alpha_2\left(\frac{-77}{2}g^2 + \lambda_{N_2}{}^2 + 2\gamma_{\psi A_2\bar{\psi}}{}^2 + \gamma_{S_1}{}^2 + \frac{45}{8}\gamma_{\tilde{A}2}{}^2 + \frac{53}{4}\gamma_2{}^2\right)$$

$$\frac{d\alpha_{\tilde{A}1}}{dt} = 2\gamma_{\tilde{A}1}\left(\frac{77}{2}g^2 m + \frac{5}{4}a_B\lambda_B + \alpha_{S_1}\gamma_{S_1} + \frac{53}{4}\alpha_{\tilde{A}1}\gamma_{\tilde{A}1} + 2\alpha_{\tilde{A}2}\gamma_{\tilde{A}2} + \frac{45}{8}\alpha_1\gamma_1\right) + \alpha_{\tilde{A}1}\left(\frac{-77}{2}g^2 + \frac{5}{4}\lambda_B{}^2 + \gamma_{S_1}{}^2 + \frac{53}{4}\gamma_{\tilde{A}1}{}^2 + 2\gamma_{\tilde{A}2}{}^2 + \frac{45}{8}\gamma_1{}^2\right)$$

$$\frac{d\alpha_{\tilde{A}2}}{dt} = 2\gamma_{\tilde{A}2}\left(\frac{77}{2}g^2 m + \frac{5}{4}a_B\lambda_B + \alpha_{S_1}\gamma_{S_1} + 2\alpha_{\tilde{A}1}\gamma_{\tilde{A}1} + \frac{53}{4}\alpha_{\tilde{A}2}\gamma_{\tilde{A}2} + \frac{45}{8}\alpha_2\gamma_2\right) + \alpha_{\tilde{A}2}\left(\frac{-77}{2}g^2 + \frac{5}{4}\lambda_B{}^2 + \gamma_{S_1}{}^2 + 2\gamma_{\tilde{A}1}{}^2 + \frac{53}{4}\gamma_{\tilde{A}2}{}^2 + \frac{45}{8}\gamma_2{}^2\right)$$

$$\frac{d\alpha_{10_1A_110_2}}{dt} = 2\gamma_{10_1A_110_2}\left(34g^2 m + 4a_A\lambda_A + 2a_B\lambda_B + 4\alpha_*\gamma_* + 2\alpha_1\gamma_1 + 10\alpha_{10_1A_110_2}\gamma_{10_1A_110_2}\right) + \alpha_{10_1A_110_2}\left(-34g^2 + 4\lambda_A{}^2 + 2\lambda_B{}^2 + 4\gamma_*{}^2 + 2\gamma_1{}^2 + 10\gamma_{10_1A_110_2}{}^2\right)$$

$$\frac{d\alpha_*}{dt} = 2\gamma_*\left(18g^2 m + 28\alpha_*\gamma_* + 9\alpha_{10_1A_110_2}\gamma_{10_1A_110_2}\right) + \alpha_*\left(-18g^2 + 28\gamma_*{}^2 + 9\gamma_{10_1A_110_2}{}^2\right)$$

$$\frac{da_{N_1}}{dt} = 2\lambda_{N_1}\left(\frac{45}{2}g^2 m + 18a_{N_1}\lambda_{N_1} + a_{N_2}\lambda_{N_2} + a_{N_3}\lambda_{N_3} + \frac{45}{8}\alpha_{\psi A_2\bar{\psi}}\gamma_{\psi A_2\bar{\psi}}\right) + a_{N_1}\left(\frac{-45}{2}g^2 + 18\lambda_{N_1}{}^2 + \lambda_{N_2}{}^2 + \lambda_{N_3}{}^2 + \frac{45}{8}\gamma_{\psi A_2\bar{\psi}}{}^2\right)$$

$$\frac{da_{N_2}}{dt} = 2\lambda_{N_2}\left(\frac{45}{2}g^2 m + a_{N_1}\lambda_{N_1} + 18\,a_{N_2}\lambda_{N_2} + a_{N_3}\lambda_{N_3} + \frac{45}{8}\alpha_{\psi A_2\bar{\psi}}\gamma_{\psi A_2\bar{\psi}} + \frac{45}{8}\alpha_2\gamma_2\right) + a_{N_2}\left(\frac{-45}{2}g^2 + {\lambda_{N_1}}^2 + 18\,{\lambda_{N_2}}^2 + {\lambda_{N_3}}^2 + \frac{45}{8}{\gamma_{\psi A_2\bar{\psi}}}^2 + \frac{45}{8}{\gamma_2}^2\right)$$

$$\frac{da_{N_3}}{dt} = 2\lambda_{N_3}\left(\frac{45}{2}g^2 m + 5\,a_A\lambda_A + a_{N_1}\lambda_{N_1} + a_{N_2}\lambda_{N_2} + 18\,a_{N_3}\lambda_{N_3} + \frac{45}{8}\alpha_{\psi A_2\bar{\psi}}\gamma_{\psi A_2\bar{\psi}} + \frac{45}{8}\alpha_1\gamma_1\right) + a_{N_3}\left(\frac{-45}{2}g^2 + 5\,{\lambda_A}^2 + {\lambda_{N_1}}^2 + {\lambda_{N_2}}^2 + 18\,{\lambda_{N_3}}^2 + \frac{45}{8}{\gamma_{\psi A_2\bar{\psi}}}^2 + \frac{45}{8}{\gamma_1}^2\right)$$

$$\frac{d\alpha_{\psi A_2\bar{\psi}}}{dt} = 2\gamma_{\psi A_2\bar{\psi}}\left(\frac{77}{2}g^2 m + a_{N_1}\lambda_{N_1} + a_{N_2}\lambda_{N_2} + a_{N_3}\lambda_{N_3} + \frac{53}{4}\alpha_{\psi A_2\bar{\psi}}\gamma_{\psi A_2\bar{\psi}} + \alpha_{S_1}\gamma_{S_1} + 2\,\alpha_2\gamma_2\right) + \alpha_{\psi A_2\bar{\psi}}\left(\frac{-77}{2}g^2 + {\lambda_{N_1}}^2 + {\lambda_{N_2}}^2 + {\lambda_{N_3}}^2 + \frac{53}{4}{\gamma_{\psi A_2\bar{\psi}}}^2 + {\gamma_{S_1}}^2 + 2\,{\gamma_2}^2\right)$$

$$\frac{d\alpha_{S_1}}{dt} = 2\gamma_{S_1}\left(32\,g^2 m + 2\,\alpha_{\psi A_2\bar{\psi}}\gamma_{\psi A_2\bar{\psi}} + 47\,\alpha_{S_1}\gamma_{S_1} + 2\,\alpha_{\tilde{A}1}\gamma_{\tilde{A}1} + 2\,\alpha_{\tilde{A}2}\gamma_{\tilde{A}2} + 2\,\alpha_2\gamma_2\right) + \alpha_{S_1}\left(-32\,g^2 + 2\,{\gamma_{\psi A_2\bar{\psi}}}^2 + 47\,{\gamma_{S_1}}^2 + 2\,{\gamma_{\tilde{A}1}}^2 + 2\,{\gamma_{\tilde{A}2}}^2 + 2\,{\gamma_2}^2\right)$$

$$\frac{da'_D}{dt} = 6\,a_D\,{\lambda_A}^2 + a'_D\left(\frac{-191}{2}g^2 + 9\,{\lambda_A}^2 + 2\,{\lambda_B}^2 + {\lambda_{N_1}}^2 + {\lambda_{N_3}}^2 + 2\,{\gamma_{\psi A_2\bar{\psi}}}^2 + 4\,{\gamma_{S_1}}^2 + 6\,{\gamma_{\tilde{A}1}}^2 + 6\,{\gamma_{\tilde{A}2}}^2 + \frac{45}{8}{\gamma_1}^2 + 2\,{\gamma_2}^2 + \frac{9}{2}{\gamma_{10_1A_110_2}}^2\right)$$

$$\frac{da'_C}{dt} = 3\,a_D\,\lambda_A\,\gamma_1 + a'_C\left(\frac{-205}{2}g^2 + {\lambda_{N_1}}^2 + 2\,{\gamma_{\psi A_2\bar{\psi}}}^2 + 4\,{\gamma_{S_1}}^2 + \frac{93}{8}{\gamma_{\tilde{A}1}}^2 + 6\,{\gamma_{\tilde{A}2}}^2 + \frac{61}{8}{\gamma_1}^2 + 2\,{\gamma_2}^2 + {\gamma_{10_1A_110_2}}^2\right)$$

$$\frac{da'_F}{dt} = 3\,a_D\,\lambda_A\,\lambda_D + a'_F\left(\frac{-319}{2}g^2 + 4\,{\lambda_A}^2 + 2\,{\lambda_B}^2 + 2\,{\lambda_{N_1}}^2 + 4\,{\gamma_{\psi A_2\bar{\psi}}}^2 + 8\,{\gamma_{S_1}}^2 + 12\,{\gamma_{\tilde{A}1}}^2 + 12\,{\gamma_{\tilde{A}2}}^2 + 4\,{\gamma_2}^2 + \frac{9}{2}{\gamma_{10_1A_110_2}}^2\right)$$

$$\frac{dm_{16_3}^2}{dt} = 10\,a_A{}^2 + 2\,a_{N_3}{}^2 + \frac{45}{4}\,\alpha_1{}^2 - 45\,g^2\,m^2$$
$$+10\left(m_{10_1}^2 + m_{16_3}^2\right)\lambda_A{}^2 + 2\left(m_{N_3}^2 + m_{\bar{\psi}}^2\right)\lambda_{N_3}{}^2 +$$
$$\frac{45}{4}\left(m_{A_1}^2 + m_{\bar{\psi}_1}^2\right)\gamma_1{}^2 + m_{16_3}^2\left(10\,\lambda_A{}^2 + 2\,\lambda_{N_3}{}^2 + \frac{45}{4}\,\gamma_1{}^2\right)$$

$$\frac{dm_{16_2}^2}{dt} = 2\,a_{N_2}{}^2 + \frac{45}{4}\,\alpha_2{}^2 - 45\,g^2\,m^2$$
$$+2\left(m_{N_2}^2 + m_{\bar{\psi}}^2\right)\lambda_{N_2}{}^2 + \frac{45}{4}\left(m_{A_2}^2 + m_{\bar{\psi}_2}^2\right)\gamma_2{}^2 + m_{16_2}^2\left(2\,\lambda_{N_2}{}^2 + \frac{45}{4}\,\gamma_2{}^2\right)$$

$$\frac{dm_{16_1}^2}{dt} = 2\,a_{N_1}{}^2 - 45\,g^2\,m^2 + 2\left(m_{N_1}^2 + m_{\bar{\psi}}^2\right)\lambda_{N_1}{}^2 + 2\,m_{16_1}^2\,\lambda_{N_1}{}^2$$

$$\frac{dm_{\psi_1}^2}{dt} = \frac{5}{2}\,a_B{}^2 + \frac{45}{4}\,\alpha_{\tilde{A}1}{}^2 - 45\,g^2\,m^2$$
$$+\frac{5}{2}\left(m_{\psi_2}^2 + m_{10_1}^2\right)\lambda_B{}^2 + \frac{45}{4}\left(m_{\tilde{A}}^2 + m_{\bar{\psi}_1}^2\right)\gamma_{\tilde{A}1}{}^2 +$$
$$m_{\psi_1}^2\left(\frac{5}{2}\,\lambda_B{}^2 + \frac{45}{4}\,\gamma_{\tilde{A}1}{}^2\right)$$

$$\frac{dm_{\psi_2}^2}{dt} = \frac{5}{2}\,a_B{}^2 + \frac{45}{4}\,\alpha_{\tilde{A}2}{}^2 - 45\,g^2\,m^2$$
$$+\frac{5}{2}\left(m_{\psi_1}^2 + m_{10_1}^2\right)\lambda_B{}^2 + \frac{45}{4}\left(m_{\tilde{A}}^2 + m_{\bar{\psi}_2}^2\right)\gamma_{\tilde{A}2}{}^2 +$$
$$m_{\psi_2}^2\left(\frac{5}{2}\,\lambda_B{}^2 + \frac{45}{4}\,\gamma_{\tilde{A}2}{}^2\right)$$

$$\frac{dm_{\bar{\psi}_1}^2}{dt} = \frac{45}{4}\,\alpha_{\tilde{A}1}{}^2 + \frac{45}{4}\,\alpha_1{}^2 - 45\,g^2\,m^2$$
$$+\frac{45}{4}\left(m_{\tilde{A}}^2 + m_{\psi_1}^2\right)\gamma_{\tilde{A}1}{}^2 + \frac{45}{4}\left(m_{A_1}^2 + m_{16_3}^2\right)\gamma_1{}^2 + m_{\bar{\psi}_1}^2\left(\frac{45}{4}\,\gamma_{\tilde{A}1}{}^2 + \frac{45}{4}\,\gamma_1{}^2\right)$$

$$\frac{dm_{\bar{\psi}_2}^2}{dt} = -45\,g^2\,m^2 + \frac{45}{4}\,\alpha_{\tilde{A}2}{}^2 + \frac{45}{4}\,\alpha_2{}^2 +$$
$$+$$
$$\frac{45}{4}\left(m_{\tilde{A}}^2 + m_{\psi_2}^2\right)\gamma_{\tilde{A}2}{}^2 + \frac{45}{4}\left(m_{A_2}^2 + m_{16_2}^2\right)\gamma_2{}^2 +$$
$$m_{\bar{\psi}_2}^2\left(\frac{45}{4}\,\gamma_{\tilde{A}2}{}^2 + \frac{45}{4}\,\gamma_2{}^2\right)$$

$$\frac{dm_{10_1}^2}{dt} = 8\,a_A{}^2 + 4\,a_B{}^2 + 9\,\alpha_{10_1 A_1 10_2}{}^2 - 36\,g^2\,m^2$$
$$+16\,m_{16_3}^2\,\lambda_A{}^2 + 4\left(m_{\psi_1}^2 + m_{\psi_2}^2\right)\lambda_B{}^2 + 9\left(m_{A_1}^2 + m_{10_2}^2\right)\gamma_{10_1 A_1 10_2}{}^2 +$$
$$m_{10_1}^2\left(8\,\lambda_A{}^2 + 4\,\lambda_B{}^2 + 9\,\gamma_{10_1 A_1 10_2}{}^2\right)$$

$$\frac{dm_{10_2}^2}{dt} = 8\,\alpha_*{}^2 + 9\,\alpha_{10_1 A_1 10_2}{}^2 - 36\,g^2\,m^2 +$$
$$8\left(m_*^2 + m_{10_2}^2\right)\gamma_*{}^2 + 9\left(m_{A_1}^2 + m_{10_1}^2\right)\gamma_{10_1 A_1 10_2}{}^2 + m_{10_2}^2\left(8\,\gamma_*{}^2 + 9\,\gamma_{10_1 A_1 10_2}{}^2\right)$$

$$\frac{dm_*^2}{dt} = 40\,\alpha_*{}^2 + 40\,m_*^2\,\gamma_*{}^2 + 80\,m_{10_2}^2\,\gamma_*{}^2$$

$$\frac{dm_{N_1}^2}{dt} = 32\,a_{N_1}{}^2 + 32\,m_{N_1}^2\,\lambda_{N_1}{}^2 + 32\left(m_{\bar{\psi}}^2 + m_{16_1}^2\right)\lambda_{N_1}{}^2$$

$$\frac{dm_{N_2}^2}{dt} = 32\,a_{N_2}{}^2 + 32\,m_{N_2}^2\,\lambda_{N_2}{}^2 + 32\left(m_{\bar{\psi}}^2 + m_{16_2}^2\right)\lambda_{N_2}{}^2$$

$$\frac{dm_{N_3}^2}{dt} = 32\,a_{N_3}{}^2 + 32\,m_{N_3}^2\,\lambda_{N_3}{}^2 + 32\left(m_{\bar{\psi}}^2 + m_{16_3}^2\right)\lambda_{N_3}{}^2$$

$$\frac{dm_{A_1}^2}{dt} = 4\,\alpha_1{}^2 + 2\,\alpha_{10_1 A_1 10_2}{}^2 - 64\,g^2\,m^2$$
$$+4\left(m_{\bar{\psi}_1}^2 + m_{16_3}^2\right)\gamma_1{}^2 + 2\left(m_{10_1}^2 + m_{10_2}^2\right)\gamma_{10_1 A_1 10_2}{}^2 +$$
$$m_{A_1}^2\left(4\,\gamma_1{}^2 + 2\,\gamma_{10_1 A_1 10_2}{}^2\right)$$

$$\frac{dm_{A_2}^2}{dt} = 4\,\alpha_{\psi A_2 \bar{\psi}}{}^2 + 2\,\alpha_{S_1}{}^2 + 4\,\alpha_2{}^2 - 64\,g^2\,m^2$$
$$+4\left(m_{\psi}^2 + m_{\bar{\psi}}^2\right)\gamma_{\psi A_2 \bar{\psi}}{}^2 + 2\left(m_{\tilde{A}}^2 + m_{S_1}^2\right)\gamma_{S_1}{}^2 +$$
$$4\left(m_{\bar{\psi}_2}^2 + m_{16_2}^2\right)\gamma_2{}^2 + m_{A_2}^2\left(4\,\gamma_{\psi A_2 \bar{\psi}}{}^2 + 2\,\gamma_{S_1}{}^2 + 4\,\gamma_2{}^2\right)$$

$$\frac{dm_{\tilde{A}}^2}{dt} = 2\,\alpha_{S_1}{}^2 + 4\,\alpha_{\tilde{A}1}{}^2 + 4\,\alpha_{\tilde{A}2}{}^2 - 64\,g^2\,m^2$$
$$+2\left(m_{A_2}^2 + m_{S_1}^2\right)\gamma_{S_1}{}^2 + 4\left(m_{\bar{\psi}_1}^2 + m_{\psi_1}^2\right)\gamma_{\tilde{A}1}{}^2 +$$
$$4\left(m_{\bar{\psi}_2}^2 + m_{\psi_2}^2\right)\gamma_{\tilde{A}2}{}^2 + m_{\tilde{A}}^2\left(2\,\gamma_{S_1}{}^2 + 4\,\gamma_{\tilde{A}1}{}^2 + 4\,\gamma_{\tilde{A}2}{}^2\right)$$

$$\frac{dm_{\bar{\psi}}^2}{dt} = \frac{45}{4}\alpha_{\psi A_2}\bar{\psi}^2 - 45\,g^2\,m^2 + \frac{45}{4}\,m_{\psi}^2\,\gamma_{\psi A_2}\bar{\psi}^2 + \frac{45}{4}\left(m_{A_2}^2 + m_{\bar{\psi}}^2\right)\gamma_{\psi A_2}\bar{\psi}^2$$

$$\frac{dm_{\bar{\psi}}^2}{dt} = 2\,a_{N_1}{}^2 + 2\,a_{N_2}{}^2 + 2\,a_{N_3}{}^2 + \frac{45}{4}\,\alpha_{\psi A_2}\bar{\psi}^2 - 45\,g^2\,m^2 + 2\left(m_{N_1}^2 + m_{16_1}^2\right)\lambda_{N_1}{}^2 + 2\left(m_{N_2}^2 + m_{16_2}^2\right)\lambda_{N_2}{}^2 + 2\left(m_{N_3}^2 + m_{16_3}^2\right)\lambda_{N_3}{}^2 + \frac{45}{4}\left(m_{A_2}^2 + m_{\bar{\psi}}^2\right)\gamma_{\psi A_2}\bar{\psi}^2 + m_{\bar{\psi}}^2\left(2\,\lambda_{N_1}{}^2 + 2\,\lambda_{N_2}{}^2 + 2\,\lambda_{N_3}{}^2 + \frac{45}{4}\,\gamma_{\psi A_2}\bar{\psi}^2\right)$$

$$\frac{dm_{S_1}^2}{dt} = 90\,\alpha_{S_1}{}^2 + 90\left(m_A^2 + m_{A_2}^2\right)\gamma_{S_1}{}^2 + 90\,m_{S_1}^2\,\gamma_{S_1}{}^2$$

APPENDIX G

PLANCK SCALE RENORMALIZATION GROUP BOUNDARY CONDITIONS FOR THE SCALAR MASSES

The matter states are assigned into E(6) representations as shown in Table G.1. The Planck scale boundary conditions for the scalar masses are

$$m_\Phi^2 = m_0^2 + U_\Phi m_H^2. \tag{G.1}$$

where Φ runs over all fields listed in Table G.1. U_Φ is the charge of field Φ under the U(1) subgroup of E(6) perpendicular to SO(10). For fields originating from a 27 representation of E(6), $U_\Phi = -2$ if Φ is a 10 representation of SO(10), and $U_\Phi = 1$ if it is a 16 representation. For fields originating from a 78 representation of E(6), $U_\Phi = 0$ for a 45 representation of SO(10); -3 for a 16; and 3 for a $\overline{16}$. [31]

field	originates from E(6) representation	field	originates from E(6) representation
16_1	27	16_2	$\overline{27}$
16_3	27	ψ	78
10_1	27	10_2	27
N_1	1	N_2	1
N_3	1	$\overline{\psi}$	$\overline{27}$
A_1	78	A_2	78
$\tilde{A}$	78	S_*	1
ψ_1	27	ψ_2	$\overline{27}$
$\overline{\psi}_1$	$\overline{27}$	$\overline{\psi}_2$	$\overline{27}$
S_1	1	S_2	1
S_3	1	S_4	1

Table G.1: Table showing the assignments of matter fields to E(6) representations.

BIBLIOGRAPHY

[1] S.L. Glashow, *Nucl. Phys.* **22** 579 (1961); A. Salam and J.C. Ward, *Phys. Lett.* **13** 168 (1964); S. Weinberg, *Phys. Rev. Lett.* **19** 1264 (1967).

[2] The Particle Data Group, *Phys. Rev.* **D54** 1, et seq. (1996).

[3] H. Georgi and S.L. Glashow, *Phys. Rev. Lett.* **32** 439 (1974).

[4] H. Georgi, H. Quinn, and S. Weinberg, *Phys. Rev. Lett.* **33** 451 (1974).

[5] M. Gell-Mann, P. Ramond, and R. Slansky, *Rev. Mod. Phys.* **50** 721 (1972); H. Georgi and S. Glashow, *Phys. Rev. Lett.* **32** 438 (1974); J. Pati and A. Salam, *Phys. Rev.* **D8** 1240 (1973).

[6] L.J. Hall, V.A. Kostelecky, and S. Raby, *Nucl. Phys.* **B267** 415 (1986).

[7] R. Barbieri and L.J. Hall, *Phys. Lett.* **B338** 212 (1994).

[8] R. Barbieri, L.J. Hall, and A. Strumia, *Nucl. Phys.* **B445** 219 (1995).

[9] G. Anderson, S. Dimopoulos, L.J. Hall, S. Raby, and G. Starkman, *Phys. Rev.* **D49** 3660 (1994).

[10] S. Dimopoulos, S. Raby, and F. Wilczek, *Phys. Rev.* **D24** 1681 (1981); S. Dimopoulos and H. Georgi, *Nucl. Phys.* **B193** 150 (1981).

[11] S. Dimopoulos and S. Raby, *Nucl. Phys.* **B192** 353 (1981); E. Witten, *Nucl. Phys.* **B185** 513 (1981); M. Dine, W. Fischler, and M. Srednicki, *Nucl. Phys.* **B189** 575 (1981).

[12] M.T. Grisaru, W. Siegel, and M. Roček, *Nucl. Phys.* **B159** 429 (1979).

[13] L. Girardello and M.T. Grisaru, *Nucl. Phys.* **B194** 419 (1984).

[14] See, e.g., R. Arnowitt and P. Nath, *Phys. Rev.* **D46** 3981 (1992).

[15] K. Inoue, A. Kakuto, H. Kamatsu, and S. Takeshita, *Prog. Theor. Phys.* **68** 927 (1982); L. Alvarez-Gaume, J. Polchinsky, and M.B. Wise, *Nucl. Phys.* **B221** 495 (1983); J. Ellis, J.S. Hagelin, D.V. Nanopoulos, and K. Tamvakis, *Phys. Lett.* **125B** 275 (1983); L.E. Ibañez and C. Lopez, *Nucl. Phys.* **B233** 545 (1984); L.E. Ibañez, C. Lopez, and C. Muños, *Nucl. Phys.* **B250** 218 (1985).

[16] M. Gell-Mann, P. Ramond, and R. Slansky, in *Supergravity* (ed. D.Z. Freeman and P. van Nieuwenhuizen) (North-Holland Pub. Co., Amsterdam, 1979).

[17] For reviews, see J.N. Bahcall and R.K. Ulrich, *Rev. Mod. Phys.* **60** 297 (1988); T.J. Bowles and V.N. Gavrin, *Annual Reviews of Nuclear Science* **43** 117 (1993); J.N. Bahcall, *Neutrino Astrophysics*, (Cambridge University Press, Cambridge, 1989).

[18] S. Dimopoulos and F. Wilczek, in *The Unity of the Fundamental Interactions*, Proceedings of the 19th Course of the International School of Subnuclear Physics, Erice, Italy, 1981 (ed. A. Zichichi) (Plenum, New York, 1983). For a recent discussion, see K.S. Babu and S.M. Barr, *Phys. Rev.* **D50** 3529 (1994).

[19] C.D. Froggatt and H.B. Nielsen, *Nucl. Phys.* **B147** 277 (1979).

[20] M. Carena, M. Oleckowski, S. Pokorski, and C.E.M. Wagner, *Nucl. Phys.* **B426** 269 (1994).

[21] L.J. Hall, R. Rattazzi, and U. Sarid, *Phys. Rev.* **D50** 7048 (1994); R. Hempfling, *Phys. Rev.* **D49** 6168 (1994).

[22] T. Blažek, S. Raby, and S. Pokorski, *Phys. Rev.* **D52** 4151 (1995).

[23] S. Weinberg, *Phys. Lett.* **91B** 51 (1980); L.J. Hall, *Nucl. Phys.* **B178** 75 (1981).

[24] J. Hisano, H. Murayama, and T. Yanagida, *Nucl. Phys.* **B402** 46 (1993).

[25] T. Blažek, M. Carena, S. Raby, and C. Wagner, in *Proceedings of the Fourth International Conference on Supersymmetries in Physics (SUSY96)*, College Park, Maryland, 1996 (ed. R.N. Mohapatra and A. Rasin) (Elsevier, Amsterdam, 1997) [*Nucl. Phys. Proc. Suppl.* **52A** 133 (1997)] (hep-ph/9608273); and "A Global χ^2 Analysis of Electroweak Data in SO(10) SUSY GUTs," OHSTPY-HEP-T-96-026 (hep-ph/9611217) (1996); T. Blažek and S. Raby, *Phys. Lett.* **B392** 371 (1997).

[26] L.J. Hall and S. Raby, *Phys. Rev.* **D51** 6524 (1995).

[27] S. Dimopoulos, S. Raby, and F. Wilczek, *Phys. Rev.* **D24** 1681 (1981); S. Dimopoulos and H. Georgi, *Nucl. Phys.* **B193** 150 (1981); L. Ibañez and G.G. Ross, *Phys. Lett.* **105B** 439 (1981); M.B. Einhorn and D.R.T. Jones, *Nucl. Phys.* **B196** 475 (1982); W.J. Marciano and G. Senjanovic, *Phys. Rev.* **D25** 3092 (1982). For

recent analyses, see P. Langacker and N. Polonsky, *Phys. Rev.* **D47** 4028 (1993); ibid., **D49** 1454 (1994); M. Carena, S. Pokorski, and C.E.M. Wagner, *Nucl. Phys.* **B406** 59 (1993).

[28] S. Dimopoulos, S. Raby, and F. Wilczek, *Phys. Lett.* **112B** 133 (1982); J. Ellis, D.V. Nanopoulos, and S. Rudaz, *Nucl. Phys.* **B202** 43 (1982). For recent analyses, see R. Arnowitt and P. Nath, *Phys. Rev.* **D49** 1479 (1994); J. Hisano, H. Murayama, and T. Yanagida, *Nucl. Phys.* **B402** 46 (1993); P. Langacker, in *In Celebration of the Discovery of the Neutrino*, Proceedings of the Benjamin Franklin Symposium, Philadelphia, Pennsylvania, 1992 (ed. C.E. Lane and R.I. Steinberg) (World Scientific, Singapore, 1993).

[29] H. Georgi, in *Particles and Fields — 1974*, Proceedings of the Williamsburg Meeting, AIP Conf. Proc. No. 23 (ed. C. Carlson) (AIP, New York, 1975); H. Fritzsch and P. Minkovski, *Ann. Phys.* **93** 193 (1975).

[30] S. Chaudhuri, S. Chung, and J.D. Lykken, in *Proceedings of the 2nd IFT Workshop on Yukawa Couplings and the Origins of Mass*, Gainesville, Florida, 1994; G. Cleaver, in *PASCOS 94*, Proceedings of the International Symposium on Particles, Strings, and Cosmology, Syracuse, New York, 1994 (ed. K. Wali) (World Scientific, Singapore, 1995).

[31] R. Slansky, *Physics Reports* **79** 1 (1981).

[32] See, S. Dimopoulos and H. Georgi, [27]; L.J. Hall, V.A. Kostelecky, and S. Raby, *Nucl. Phys.* **B267** 415 (1986); H. Georgi, *Phys. Lett.* **B169** 231 (1986); and S. Dimopoulos and A. Pomarol, *Phys. Lett.* **B353** 222 (1995).

[33] S. Weinberg, *Phys. Rev.* **D26** 287 (1982); N. Sakai and T. Yanagida, *Nucl. Phys.* **B197** 533 (1982).

[34] J. Ellis, J.S. Hagelin, D.V. Nanopoulos, and K. Tamvakis, *Phys. Lett.* **124B** 484 (1983); V.M. Belyaev and M.I. Vysotsky, *Phys. Lett.* **127B** 275 (1983); S. Chadha, G.D. Coughlan, M. Daniel, and G.G. Ross, *Phys. Lett.* **149B** 477 (1984).

[35] A.H. Chamseddine, R. Arnowitt, and P. Nath, *Phys. Rev. Lett.* **29** 970 (1982); R. Barbieri, S. Ferrara, and C.A. Savoy, *Phys. Lett.* **B119** 343 (1983); L.J. Hall, J. Lykken, and S. Weinberg, *Phys. Rev.* **D22** 2359 (1983); P. Nath, R. Arnowitt, and A.H. Chamseddine, *Nucl. Phys.* **B322** 121 (1983).

[36] S.P. Martin and M.T. Vaughn, *Phys Rev.* **D50** 2282 (1994).

[37] J. Ellis, D.V. Nanopoulos, and S. Rudaz, *Nucl. Phys.* **B202** 43 (1982).

[38] M. Claudson, M. Wise, and L.H. Hall, *Nucl. Phys.* **B195** 297 (1982); S. Chadha and M. Daniel, *Nucl. Phys.* **B229** 105 (1983).

[39] S.J. Brodsky, J. Ellis, J.S. Hagelin, and C. Sachradja, *Nucl. Phys.* **B238** 561 (1984).

[40] M.B. Gavela, S.F. King, C.T. Sachrajda, G. Martinelli, M.L. Paciello, and B. Taglienti, *Nucl. Phys.* **B312** 269 (1989).

[41] M.B. Gavela, S.F. King, C.T. Sachrajda, G. Martinelli, M.L. Paciello, and B. Taglienti, *Nucl. Phys.* **B312** 269 (1989); Y. Hara, S. Itoh, Y. Iwasaki, and T. Yoshie, *Phys. Rev.* **D34** 3399 (1986); S.J. Brodsky, J. Ellis, J.S. Hagelin, and C. Sachradja, *Nucl. Phys.* **B238** 561 (1984).

[42] Y. Hara, S. Itoh, Y. Iwasaki, and T. Yoshie, *Phys. Rev.* **D34** 3399 (1986).

[43] R. Arnowitt, A.H. Chamseddine, and P. Nath, *Phys. Rev.* **D32** 2348 (1985).

[44] R. Arnowitt and P. Nath, *Phys. Rev.* **D38** 1479 (1988).

[45] T. Goto, T. Nihei, and J. Arafune, *Phys. Rev.* **D52** 505 (1995).

[46] Y. Totsuka, in *Proceedings of the International Symposium on Underground Physics Experiments*, Toyko, Japan, 1990 (ed. K. Nakamura), Institute for Cosmic Ray Research report, ICRR-227-90-20 (1990).

[47] D.B. Cline, *Nucl. Instruments and Methods in Physics Research* **A327** 178 (1993).

[48] These results were also discussed by K.S. Babu and S.M. Barr, *Phys. Rev.* **D48** 5354 (1993).

[49] See, e.g., J.P. Derendinger, L. Ibañez, and H.P. Nilles, *Nucl. Phys.* **B267** 365 (1986).

[50] S. Dimopoulos and A. Pomarol, *Phys. Lett.* **B353** 222 (1995).

[51] T.P. Cheng and L.-F. Li, *Phys. Rev.* **D16** 1425 (1977); S.T. Petcov, *Sov. J. Nucl. Phys.* **25** 340 (1977); W. Marciano and H. Sandra, *Phys Lett.* **B67** 303 (1977); R. Shrock and B.W. Lee, *Phys. Rev.* **D16** 1445 (1977); T.P. Cheng and L.-F. Li, *Phys. Rev. Lett.* **45** 1908 (1980)

[52] R.D. Bolton, et al., *Phys. Rev.* **D38** 2077 (1988); The Particle Data Group, *Phys. Rev.* **D54** 1, et seq. (1996).

[53] S. Dimopoulos and D. Sutter, *Nucl. Phys.* **B452** 496 (1995).

[54] M. Drees, *Phys. Lett.* **B181** 279 (1986); J.S. Hagelin and S. Kelley, *Nucl. Phys.* **B342** 95 (1990); A.E. Faraggi, J.S. Hagelin, S. Kelley, and D.V. Nanopoulos, *Phys. Rev.* **D45** 3272 (1992).

[55] R. Rattazzi and U. Sarid, *Phys. Rev.* **D53** 1553 (1996).

[56] J. Hisano, T. Moroi, K. Tobe, and M. Yamaguchi, *Phys. Rev.* **D53** 2442 (1996).

[57] E.D. Commins, S.B. Ross, D. Demille, and B.C. Regan, *Phys. Rev.* **A50** 2960 (1994).

[58] M.E. Gomez and H. Goldberg, *Phys. Rev.* **D53** 5244 (1996).

[59] M. Cooper, et al., *Nucl. Instrum. and Meth.* **A303** 298 (1991); M. Cooper, et al., *ibid.* **A323** 198 (1992); M. Cooper, et al., *ibid.* **A372** 195 (1996).

[60] M. Dine, A.E. Nelson, and Y. Shirman, *Phys. Rev.* **D51** 1362 (1995); M. Dine, A.E. Nelson, Y. Nir, and Y. Shirman, *Phys. Rev.* **D53** 2658 (1996); S. Dimopoulos and S. Raby, *Nucl. Phys.* **B192** 353 (1981); M. Dine, W. Fishler, and M. Srednicki, *Nucl. Phys.* **B189** 575 (1981); M. Dine and W. Fishler, *Phys. Lett.* **B110** 227 (1982); M. Dine and M. Srednicki, *Nucl. Phys.* **B202** 238 (1982); L. Alvarez-Gaumé, M. Claudson, and M. Wise, *Nucl. Phys.* **B207** 96 (1982); C. Nappi and B. Ovrut, *Phys. Lett.* **B113** 175 (1982).

[61] S. Raby, OSU preprint OHSTPY-HEP-T-97-002 (hep-ph/9702299).

[62] J. Wess and J. Bagger, *Supersymmetry and Supergravity* (2d ed., Princeton University Press, Princeton, 1992).

[63] S. Bertolini, F. Borzumati, A. Masiero, and G. Ridolfi, *Nucl. Phys.* **B353** 591 (1991).

[64] H. Georgi, *Lie Algebras in Particle Physics* (Benjamin/Cummings Pub. Co., Reading, 1982).

[65] R. Barbieri, unpublished notes.

[66] R.N. Mohapatra and B. Sakita, *Phys. Rev.* **D21** 1062 (1980).